A POLARIZATION INTERFEROMETER FOR COHERENT OPTICAL IMAGE PROCESSING

by

Anthony Peter Lang, B.Sc., A.R.C.S.

April 1985

A Thesis submitted for the degree of Doctor of Philosophy of the University of London and for the Diploma of Membership of The Imperial College.

Physics Department
Imperial College
London SW7 2BZ

ABSTRACT

Conventional optical Fourier transform systems have speed advantages over digital processors. Unfortunately undiffracted light forms a very bright spot in the centre of the transform plane which corresponds to the mean or D.C. transmission level of the object transparency. This tends to mask the low spatial frequency information in the transform, and could damage video cameras and other detectors used to view the transform plane.

This thesis describes the design, construction and use of a high resolution polarization interferometer to reduce the intensity of this undiffracted light, resulting in improved detectability of low spatial frequency signals, and increased accuracy in the measurement of the relative strength of directionalities in the input transparency.

The system uses a pair of wedge prisms for alignment, a reversed Babinet compensator for phase control, and a variable ratio polarizing beamsplitter for setting the level to be subtracted.

The required tolerances are determined and all the adjustments are shown to be well within the accuracy needed. Results are presented for D.C. level subtraction applied to geological imagery, and also for a number of

other image subtraction experiments such as contrast reversal and differentiation.

ACKNOWLEDGEMENTS

Many thanks to all who have helped me, but especially:-

- to Dr R. W. Smith, Emeritus Professor W. T. Welford and many other colleagues of the Optics Section at Imperial College.

- To Mr C. V. Cooper for making the plane mirrors.

- To the staff of the main physics workshop for making some of the mounts (eventually!)

- To the Science and Engineering Research Council for financial support.

- And to Alison Begg, the typist, whose dedecated efforts, carful attention to de&ail and skilful wo?k transmuted a rouf ilegible skraul into a finished theesis.

CONTENTS

FIGURES

CHAPTER 1

PRELIMINARIES

1.1. Introduction

In the field of image processing, digital techniques currently offer the most versatility, but for some applications such as azimuthal or textural classification of images, coherent optical techniques offer faster processing speeds due to their parallel processing of two dimensional information. Thus, despite claims that optical image processing is a Cinderella who may never get to the ball (Harnett, Mountain and Barnett 1978) in some fields such as in the analysis of geological imagery, she arrived long ago, and midnight is still a long way off.

As far back as 1949, Barber published the results of analysing an aerial photograph of the sea to extract details of the wave directions and wavelengths. This work still goes on - Lessard, Welford and Zhang published similar results in 1981 using satellite imagery of sea waves.

Unfortunately, up until the early 1960's, researchers lacked a suitable high intensity, coherent light source, so most of the work on optical image processing tended to be theoretical. Some experimental work was performed but the

low light intensities available meant that long exposures were required - Harris (1964) published several photographs of diffraction patterns which required exposures of up to 1075 hours!

When the laser became available in the early 1960's, optical image processing began to be investigated experimentally, and enjoyed a boom until the mid 1970's when it lost ground to other topics.

Most of the work in the 1960's and early 1970's was performed in the geological sciences. For example, Bauer, Fontanel and Grau (1967) studied aerial photographs of glaciers and Heidecker and Supajanya (1975) studied the distribution of ground fractures in aerial photographs.

Geologically orientated review papers started to appear in the late 1960's such as Pincus and Dobrin (1966), Dobrin (1968) and McCullagh (1971) with more general review papers appearing in the 1970's (Birch 1972, Thompson 1975).

A high quality optical Fourier transform system was built at the Imperial College Optics Group, and several papers were published describing the results obtained. For example, Barnett et al (1976), Barnett and Harnett (1975), Harnett and Barnett (1977) and Harnett, Mountain and Barnett (1978). In the late 1970's research in the subject seemed to lose some of

its momentum, but the 1980's have seen a revival in optical image processing which seems set to carry on for many years yet.

It is often stated that the focal plane distribution in a coherent optical processor is the Fourier transform of the input transparency. This is true, but care must be taken in defining what is meant by "the input transparency" as will be demonstrated.

1.2. The basic theory of coherent optical image processing

In this section the basic principles of coherent optical image processing are described. They are based on the scalar diffraction theory of light (see for example Born and Wolf, 1959). Fuller accounts are given in the review articles by Vander Lugt (1968), Birch (1972) and Lee (1976) and also in the book by Yu (1983).

1.2.1. Basic diffraction theory

Suppose we have an object consisting of alternate opaque and transmitting bars of regular spacing d, and we illuminate it with a collimated (i.e. parallel) beam of coherent light. If we observe the light distribution a long way from the object we see a line of intense spots of light (see Fig. 1.1.) These occur when light waves from neighbouring transmitting regions are in phase and add up, i.e. when v is equal to an integral number of wavelengths. Hence for an intensity maximum in the observation plane:

$$d \sin(\theta) = n\lambda \qquad (1)$$

Where θ is the direction of the maximum relative to the axis when viewed from the object, λ is the wavelength of the light and n is an integer. If the object has an amplitude transmission which varies sinusoidally with position, then it can be shown that only 3 spots of light are seen in the observation plane corresponding to n=0, +1 and -1.

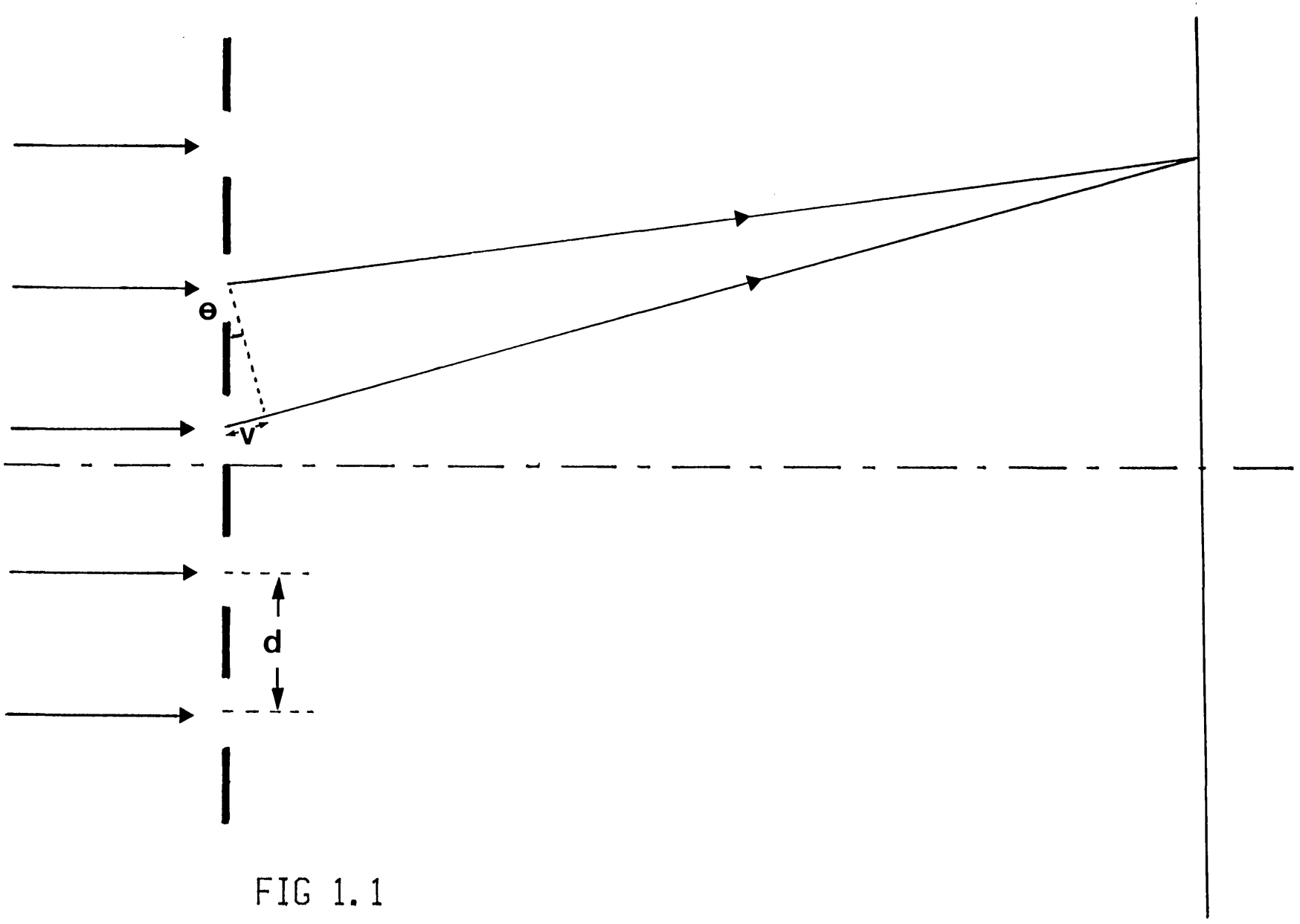

FIG 1.1
DIFFRACTION OF LIGHT BY A PERIODIC OBJECT

Now suppose we place a lens between the object and the observation plane such that the distances from the object to the lens and from the lens to the observation plane are equal to the front and back focal lengths of the lens respectively as in Fig. 1.2. Then the light reaching some point P in the observation plane O will have been diffracted at some angle θ corresponding to some spacing d in the object. The effect of the lens is thus to bring the diffraction pattern from infinity to the back focal plane of the lens.

Now supposing we define the amplitude transmission factor at some point x in the object by T(x), i.e. if a light wave of amplitude R falls on the transparency, the transmitted wave will have amplitude T(x).R. Then at some point x' in the observation plane, the light amplitude A(x') will be given by the sum of the contributions from each element δx of the object. Hence:

$$A(x') = \sum_{\substack{\text{over}\\ \text{the}\\ \text{object}\\ \text{aperture}}} R\ T(x)\ \delta x \cos \left(\begin{array}{l} \text{phase difference for light} \\ \text{from point x relative to} \\ \text{some arbitrary zero} \end{array} \right) \qquad (2)$$

The phase difference for light from point x is ϕ_x and is given by:

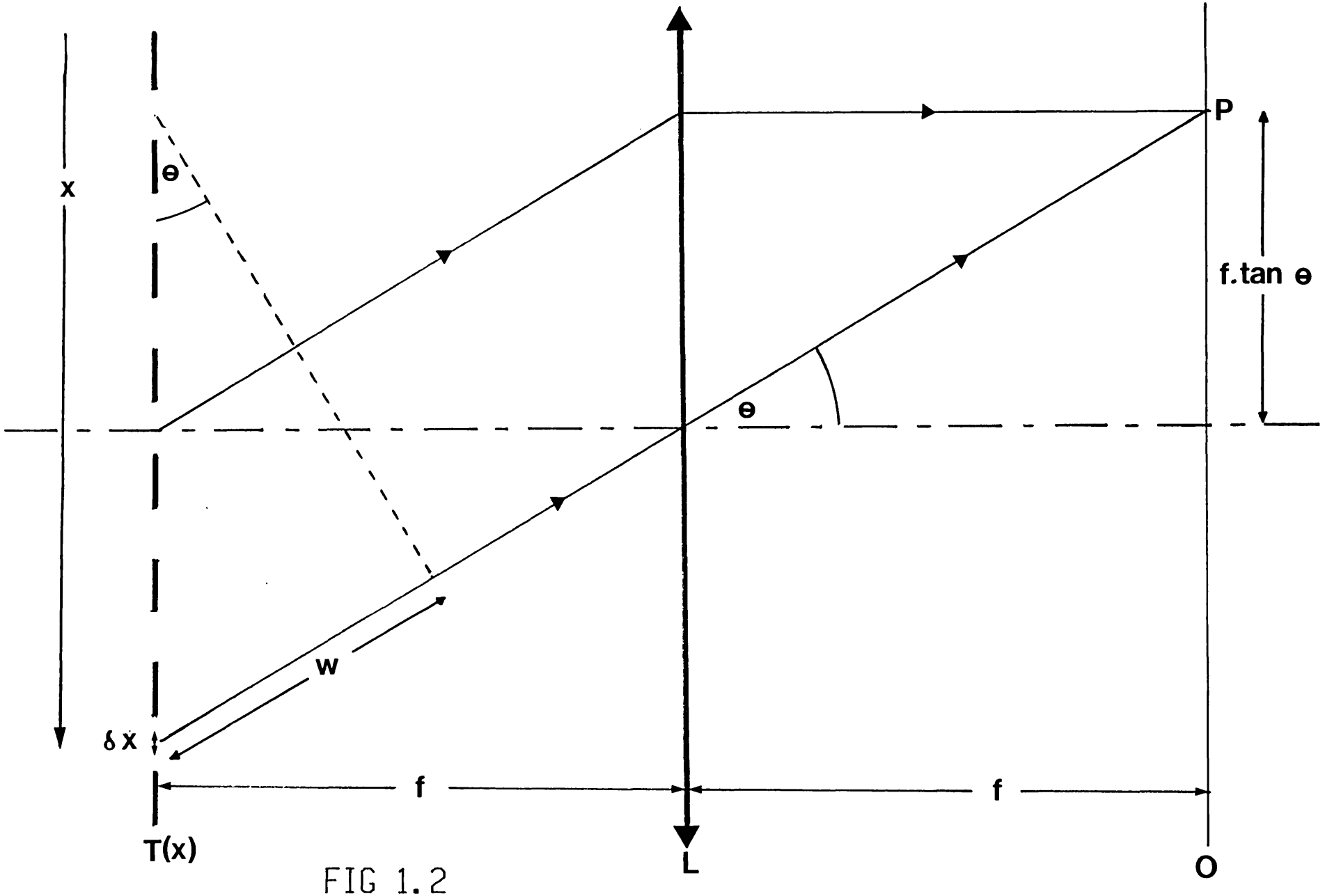

FIG 1.2
THE FOURIER TRANSFORM PROPERTY OF A LENS

$$\phi_x = \frac{2\pi}{\lambda} \left[\begin{array}{l} \text{path difference for light from point} \\ \text{x relative to some arbitrary zero} \end{array} \right] \qquad (3)$$

$$= \frac{2\pi w}{\lambda}$$

But we know that for a given object spacing d:

$$d \sin(\theta) = \lambda$$

Hence:

$$\sin(\theta) = \frac{\lambda}{d} = \frac{w}{x}$$

Therefore:

$$\phi_x = \frac{2\pi x}{d} = 2\pi xu$$

where u is the spatial frequency defined as 1/d

Therefore at point P in the observation plane:

$$A(x') = \sum_{\substack{\text{over} \\ \text{the} \\ \text{aperture}}} R\, T(x)\, \delta x \cos(2\pi xu) \qquad (4)$$

if we let $\delta x \to 0$, the sum becomes an integral,

$\delta x \to dx$, and equation 4 becomes:

$$A(x') = R \int_{\substack{\text{over}\\ \text{the}\\ \text{aperture}}} T(x) \cos(2\pi xu)\, dx \qquad (5)$$

A physical object may introduce other phase variations due to, for example, variations in film thickness for photographic transparencies. To allow for this we replace the cosine term with a complex exponential $e^{-2\pi ixu}$, remembering that the amplitude is represented by the real part of this. Therefore:

$$A(x') = R \int_{\substack{\text{over}\\ \text{the}\\ \text{aperture}}} T(x)\, e^{-2\pi ixu}\, dx \qquad (6)$$

This is a one dimensional Fourier transform relationship linking the object transmission T(x) with its diffraction pattern A(x').

Similarly in two dimensions we have:

$$A(x',y') = R \iint_{\substack{\text{over}\\ \text{the}\\ \text{aperture}}} T(x,y) e^{-2\pi i(xu+yv)} dx\, dy \qquad (7)$$

Where u and v are the spatial frequencies in the object, x

and y are the coordinates in the plane of the object and x' and y' are the coordinates in the observation plane.

Thus the light amplitude distribution in the back focal plane of the lens is the two dimensional Fourier transform of the amplitude transmission of the object in its front focal plane.

The full theory of this diffraction process, based on the Kirchhoff diffraction integral and described in standard texts such as Born and Wolf (1959), leads to essentially the same result as equation 7, but with a multiplying constant outside the integral. It should be noted that there are several different conventions regarding the mathematical forms of Fourier transforms with various factors of π outside the integral. All of the forms have the same basic properties but are not always exactly equivalent.

Now it is possible to consider any two dimensional object as being made up of an infinite number of superimposed sinusoidal gratings with different periods, orientations and amplitudes or "strengths". Each of these gratings produces three spots of light in the back focal plane of the lens with amplitudes proportional to the strength of the grating.

The object is a "continuum of gratings" so these spots merge into a continuous distribution - the Fourier transform

If the object has some dominant spatial frequency u, which diffracts light at an angle θ, then we will observe a bright spot at a distance $x' = f \tan(\theta)$ from the centre of the observation plane. Now $d \sin(\theta) = \lambda$ and θ is small, hence:

$$x' = \lambda f u$$

i.e. the distance of the spot of light from the centre of the observation plane is proportional to the inverse of the spacing of the corresponding grating. It is clear that the light is diffracted by the grating in a plane perpendicular to the grating lines. Therefore the bright spots of light in the observation plane will be in a line which is also orientated perpendicular to the grating lines.

If there is some direction in the object which is stronger or better represented than the others, then this will show up as a directionality in the focal plane distribution at right angles to that in the object.

If the object has some preferred spacing, then this will show up as a bright region at the corresponding distance from the centre of the focal plane.

If some of the regions of the focal plane are blocked with an absorbing screen, and the light passing through the other clear regions is collected by a second lens, then the image

formed by the second lens will be a modified form of the original object, with features of certain frequencies and/or directions removed. Hence it is possible to enhance certain features by suppressing everything else.

An everday analogy of this is the use of the tone controls or an equaliser in a hifi system to alter the distribution of the temporal frequencies in a signal, which can improve the clarity of poor quality signals.

1.2.2. Coherent optical image processing

The most common coherent optical processing layout is shown in Fig. 1.3.* A photographic transparency of amplitude transmission T(x,y) is placed in the front focal plane of a positive lens L, of focal length f, and illuminated by collimated, coherent light of wavelength λ and uniform amplitude R. Then from section 1.2.1. the amplitude distribution in the back focal plane, A(x',y'), is given by:

---

*There are other possible layouts. See for example Joxeux and Lowenthal, 1982

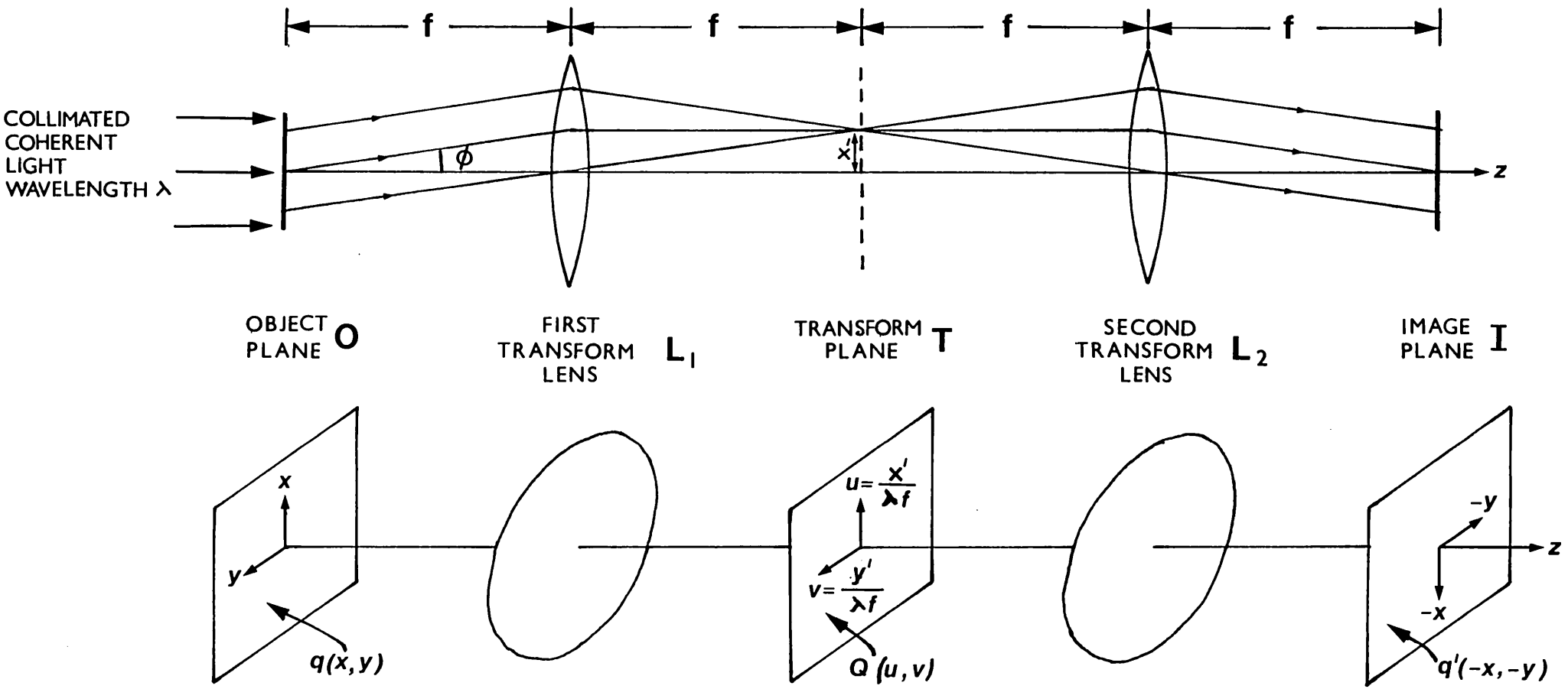

FIG 1.3
THE BASIC ARRANGEMENT OF A COHERENT OPTICAL FOURIER TRANSFORM SYSTEM

$$A(x',y') = CR \iint_{\substack{\text{over}\\ \text{the}\\ \text{aperture}}} T(x,y)e^{-2\pi i(ux+vy)}dx\ dy \qquad (8)$$

where C is a constant to allow for reflection, absorption etc by the lens. Henceforth in this thesis the back focal plane of the lens performing the optical Fourier transform will be called the transform plane, and the front focal plane of the lens will be called the object plane.

The actual spatial coordinates (x',y') in the transform plane are related to the spatial frequency coordinates (u,v) by:-

$$x' = \lambda f u$$
$$y' = \lambda f v \qquad (9)$$

Thus if we omit the constants outside the integral:

$$A(u,v) = \iint_{\substack{\text{over}\\ \text{the}\\ \text{aperture}}} T(x,y)e^{-2\pi i(ux+vy)}dx\ dy \qquad (10)$$

Henceforth in this thesis, this will be written as:

$$A(u,v) = \mathcal{F}\{T(x,y)\} \qquad (11)$$

where $\mathcal{F}$ represents the Fourier transform operation. If the purpose of the system is to modify the distribution of spatial frequencies in the image, it is then necessary to perform an inverse Fourier transform (represented by $\mathcal{F}^{-1}$) on A(u,v). In practice, a second lens, which is usually identical to the first, is used to perform a second optical Fourier transform. This is equivalent to an inverse Fourier transform plus a rotation by 180 degrees.

$$\mathcal{F}\{\mathcal{F}\{T(x,y)\}\} = T(-x,-y) \qquad (12)$$

Thus the output amplitude distribution is just an inverted image of the input amplitude distribution, but with a spatial frequency distribution modified by the transfer function of the system.

The photographic transparency will be bounded by some aperture and we represent this by:

$$T(x,y) = q(x,y) \cdot P(x,y) \qquad (13)$$

where q(x,y) represents the amplitude transmission of the transparency, and P(x,y) is the pupil function which has value of one inside the aperture, and zero everywhere else.

Usually optical image processing is performed using circular apertures where the pupil function $P_c(x,y)$ is defined by:

$$P_c(x,y) = 1 \qquad x^2+y^2<a^2$$
$$= 0 \qquad \text{elsewhere} \tag{14}$$

where a is the radius of the aperture.

When P(x,y) takes this form there are a number of names used for it in the literature, including the cylinder function, the top hat function, the circ function and the pill box function. This function is shown in Fig. 1.4.

If a photographic transparency is placed in the object plane of the optical Fourier transform system, a relatively large portion of the light passes through undiffracted. We represent this by splitting the object amplitude transmission into two parts:

$$T(x,y) = (q_o + q_1(x,y)) \cdot P_c(x,y) \tag{15}$$

where q_o represents the undiffracted or zero order component which is uniform across the aperture corresponding to the mean or DC amplitude transmission level of the object transparency and $q_1(x,y)$ represents the signal of interest which is superimposed on q_o.

Taking the Fourier transform of equation 15 and remembering that:

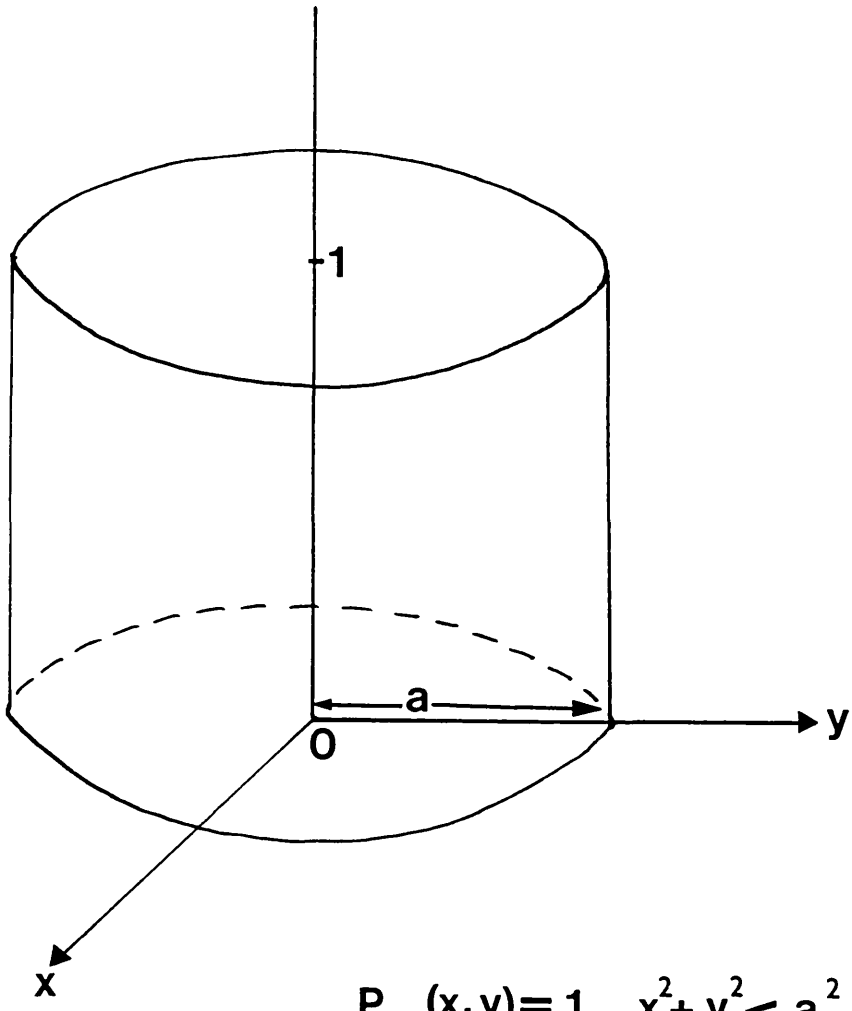

FIG 1.4

THE PUPIL FUNCTION

$$\mathcal{F}\{\text{constant}.f(x,y) + g(x,y)\} = \text{constant}.\,\mathcal{F}\{f(x,y)\} + \mathcal{F}\{g(x,y)\}$$

gives:

$$\mathcal{F}\{T(x,y)\} = q_o\,\mathcal{F}\{P_c(x,y)\} + \mathcal{F}\{q_1(x,y).P_c(x,y)\} \quad (16)$$

Now by the convolution theorem (see appendix 2) the last term in equation 16 can be split into two components convolved with one another.

Hence:

$$\mathcal{F}\{T(x,y)\} = q_o\,\mathcal{F}\{P_c(x,y)\} + \mathcal{F}\{q_1(x,y)\} \otimes \mathcal{F}\{P_c(x,y)\} \quad (17)$$

where $\otimes$ represents the convolution operation.

The Fourier transform of $P_c(x,y)$ is:

$$P_c(x,y) = 2\pi a^2 \frac{J_1(2\pi ra)}{2\pi ra} \quad (18)$$

where J_1 is a first order Bessel function of the first kind and $r = \sqrt{u^2+v^2}$ (see appendix 1)

Thus:

$$\mathcal{F}\{T(x,y)\} = 2\pi a^2 q_o \frac{J_1(2\pi ra)}{2\pi ra} + 2\pi a^2 \mathcal{F}\{q_1(x,y)\} \otimes \frac{J_1(2\pi ra)}{2\pi ra} \qquad (19)$$

All available detectors are sensitive to the intensity of the light, which is the square of the modulus of the amplitude. Thus the detected signal is:

$$\begin{aligned} I(u,v) = & \left| 2\pi a^2 q_o \frac{J_1(2\pi ra)}{2\pi ra} \right|^2 \\ & + \left(2\pi a^2 q_o \frac{J_1(2\pi ra)}{2\pi ra} \right) \cdot \left(2\pi a^2 \mathcal{F}\{q_1(x,y)\} \otimes \frac{J_1(2\pi ra)}{2\pi ra} \right)^* \\ & + \left(2\pi a^2 q_o \frac{J_1(2\pi ra)}{2\pi ra} \right)^* \cdot \left(2\pi a^2 \mathcal{F}\{q_1(x,y)\} \otimes \frac{J_1(2\pi ra)}{2\pi ra} \right) \\ & + \left| 2\pi a^2 \mathcal{F}\{q_1(x,y)\} \otimes \frac{J_1(2\pi ra)}{2\pi ra} \right|^2 \end{aligned} \qquad (20)$$

Where * represents the complex conjugate.

The first term of equation 20 only has significant values for a small region about the centre of the transform plane. The second and third terms of equation 20 both have

multiplying terms of the form $\frac{J_1(2\pi ra)}{2\pi ra}$. Thus these two terms also only have significant values near the centre of the transform plane.

The final term of equation 20 is the square of the modulus of the convolution of the Fourier transform of the signal of interest with the Bessel function term. The Bessel function term is usually of much smaller spatial extent than the Fourier transform of $q_1(x,y)$. Hence it leads to a limiting spatial resolution in the transform plane. This is unimportant for the current application.

For photographic transparencies, the magnitude of the zero order component q_o is usually much greater than the magnitude of the signal of interest $q_1(x,y)$. Thus the first three terms of equation 20 are usually much larger than the final term. On an optical Fourier transform system this leads to an intense region in the centre of the transform plane which can obscure low frequency signals of interest. The intensity can also be high enough to damage video cameras, photomultipliers and other detectors used in the transform plane.

An intensity distribution of the form $I(r) = \text{constant} \cdot \left(\frac{J_1(r)}{r}\right)^2$ is known as the Airy pattern (after Sir George Biddell Airy who first calculated the diffraction

pattern of a circular aperture). Diagrams of this pattern are usually normalised to a value of 1 in the centre. The value of $J_1(r)/r$ tends to $\frac{1}{2}$ as r tends to zero. Therefore the Airy pattern is usually plotted as $I(r) = \left(\frac{2J_1(r)}{r}\right)^2$. Computer plots of this are shown in Figs. 1.5. and 1.6. and a photograph of an actual Airy pattern is shown in Fig. 1.7.

1.2.3. Limiting resolution

For very high spatial frequencies in the object, light may be diffracted through an angle which is so large that it misses the lens. Hence there is a maximum spatial frequency which can be resolved by a perfect lens of $\frac{\phi_{max}}{\lambda}$ where ϕ_{max} is the maximum angle of diffraction for which light will pass through the lens, and λ is the wavelength. For a given focal length, the larger the lens, the greater the maximum spatial frequency which can be resolved. Very large lenses are difficult to design and build with high image quality and are also very expensive, but by placing the object transparency close to the lens on the same side as the transform plane, higher spatial frequencies may be collected at the expense of introducing a quadratic phase term, a magnification and other distortions into the transform plane distribution (see for example Joyeaux and Lowenthal, 1982). High quality concave mirrors can be made with large

FIG 1.5

THE AIRY PATTERN

$$I = \left(\frac{2J_1(r)}{r}\right)^2$$

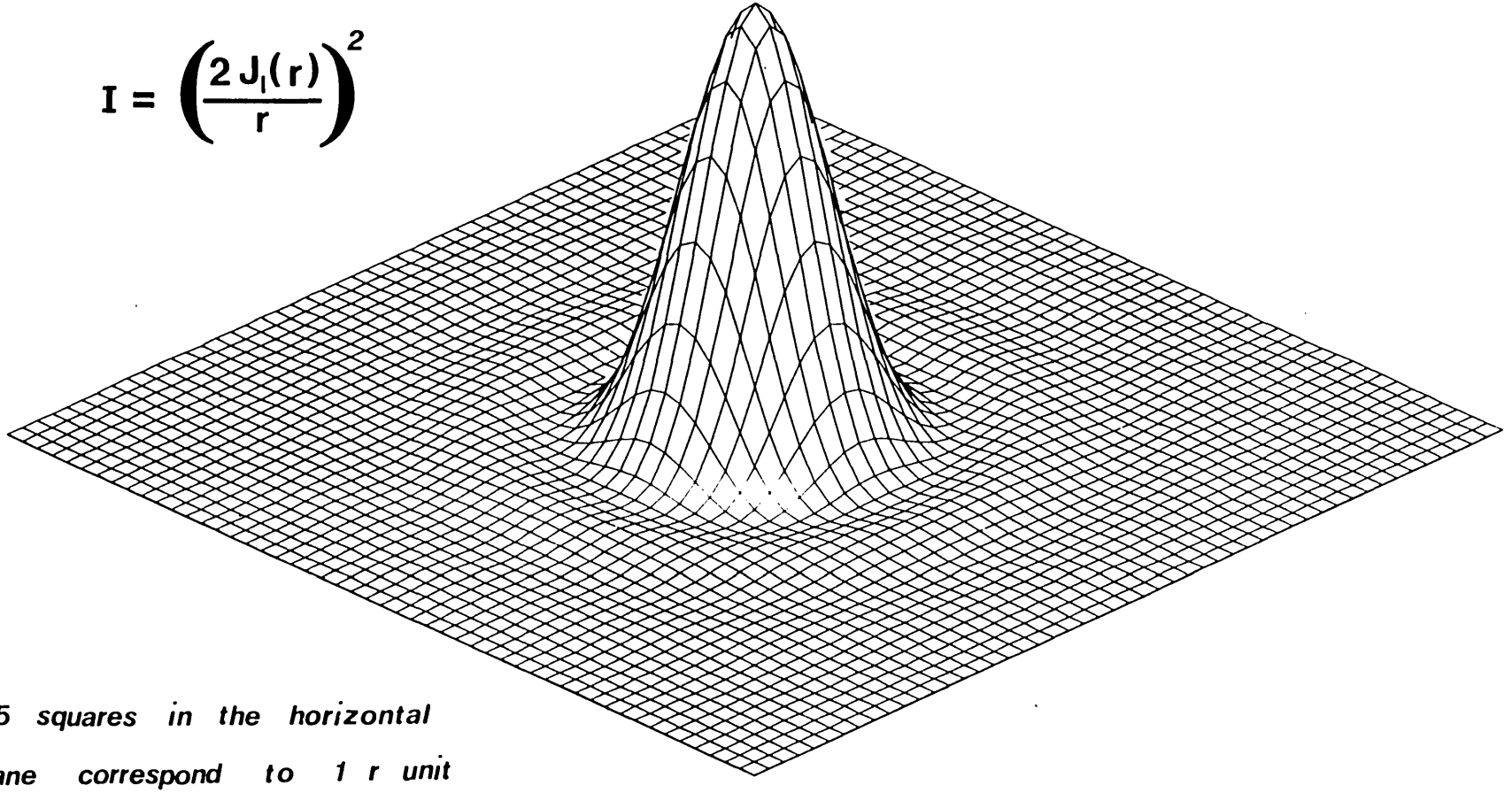

2·5 squares in the horizontal plane correspond to 1 r unit

Computed and plotted by M.W.L. Wheeler

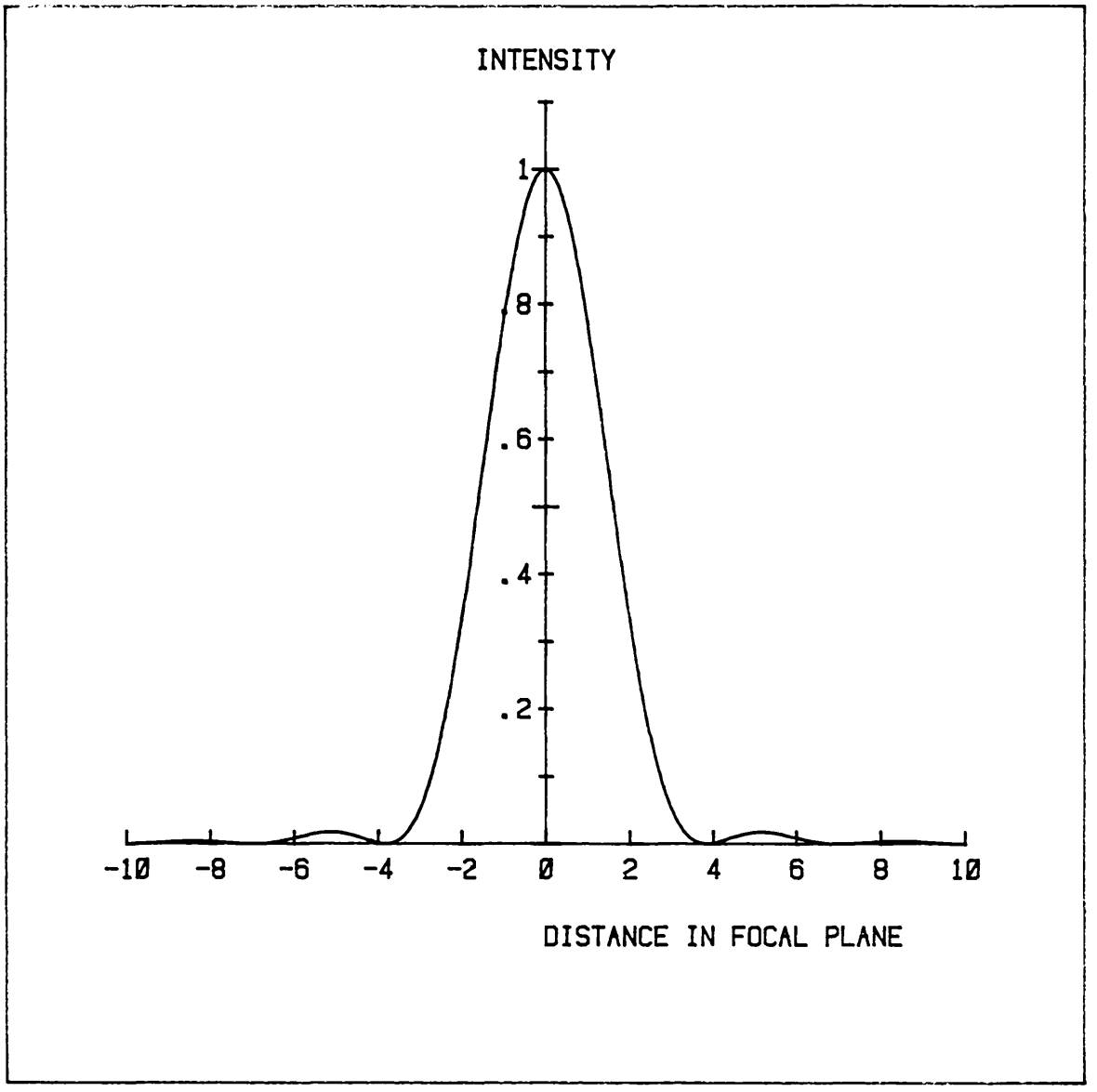

FIG 1.6

THE AIRY PATTERN - CROSS SECTION

FIG 1.7

THE AIRY PATTERN

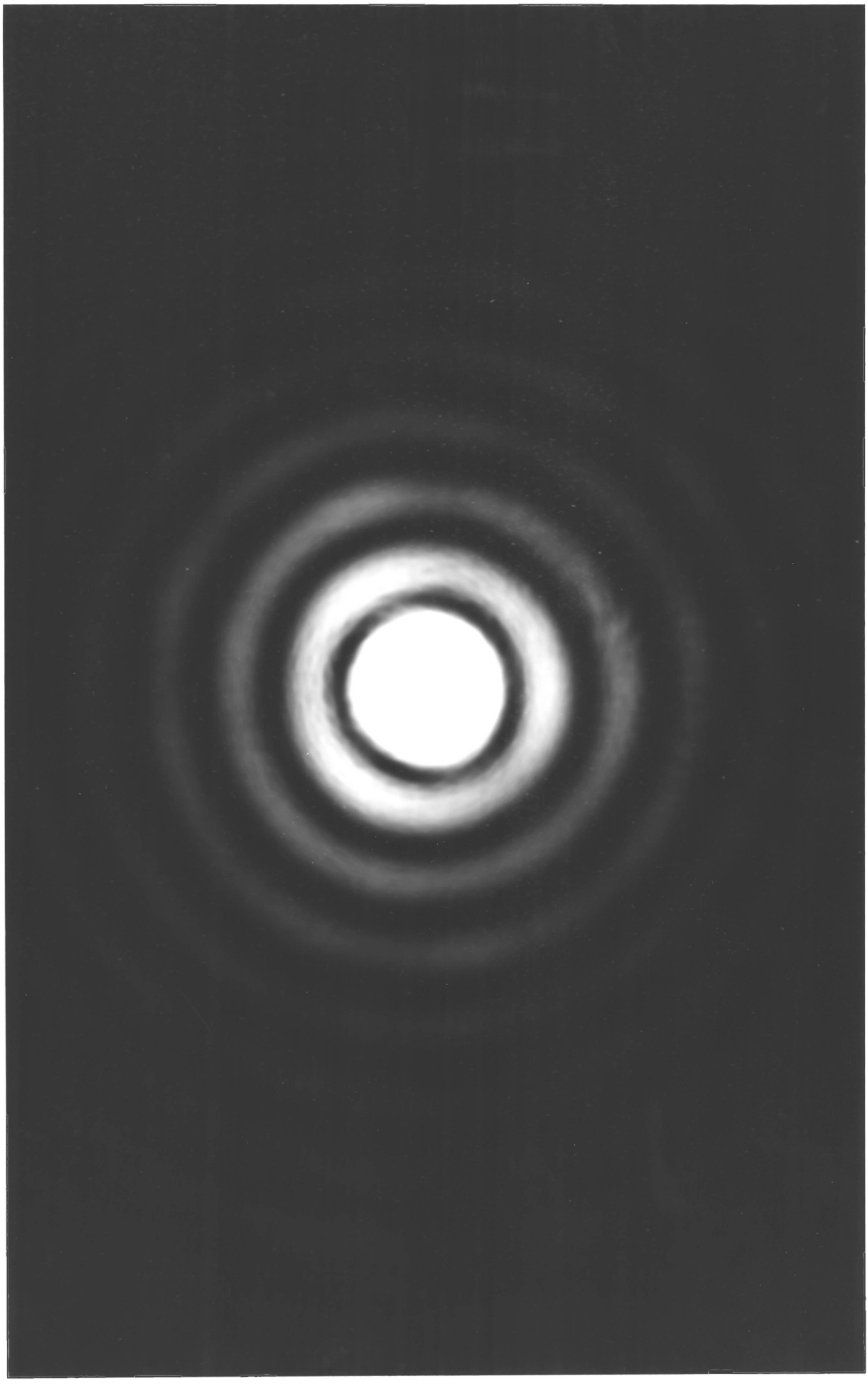

apertures and at least one mirror-based system has been reported (Nikolov, 1982).

A maximum spatial frequency of $\frac{\phi_{max}}{\lambda}$ is for a perfect lens with no aberrations and assuming that all of the light passing through the front face of the lens reaches the transform plane. A real lens will always have some residual aberration and there may be an aperture stop in the system. Both of these will reduce the maximum spatial frequency.

For example, the front focal plane of the lens used on the Imperial College optical Fourier transform bench is 182mm from the front lens surface which is 100mm in diameter. Thus the value of $\frac{\phi_{max}}{\lambda}$ for a 50mm object aperture is approximately 280 lines per mm at a wavelength of 488nm compared to 80 lines per mm which is the actual resolution achieved.

1.2.4. Liquid gates

On an interferometric scale, photographic film and plates are not very flat. Thickness variations across the film can be many wavelengths. In a normal optical Fourier transform system this leads to noise and distortion in the transform plane distribution. In an interferometer such as the one described in this thesis, it would result in a severe reduction in the efficiency of cancellation of the

undiffracted light. Therefore, these phase variations must be removed or reduced in magnitude.

The standard technique is to use a liquid gate. The photographic film or plate is placed between a pair of high quality optical flats and the spaces between them are filled with fluid of similar refractive index to the transparency. (see for example Berger and Harker 1966, Harburn and Ranniko 1971). This arrangement is effective in ironing out optical path differences, but it increases the cost and complexity of the system and tends to be messy and inconvenient to use. This is mainly due to convection currents and bubbles in the oil which take some time to settle. Therefore it is usually advisable to leave the unit to settle (preferably overnight) when it is first filled with oil, and for a few hours each time a new film or plate is inserted. With care, it is possible to change the film without too much disturbance to the oil, but unless the liquid gate contains a roll of film, its use tends to slow down the experiments.

A cheap holographic liquid gate has been reported (Kulkarni and Sen 1981) but the aberration correction was not as good as a unit with optical flats.

For some of the experiments described in this thesis, binary objects were used which were made from sheet metal.

These required no liquid gates. Since the compensating aperture was a binary object, only one liquid gate was required. Subtraction of two photographic images would require a second liquid gate.

The liquid gate constructed for use with this project consisted of an aluminium box with two optical flats held over apertures in the sides by metal frames as shown in Fig. 1.8. A metal slide with clips to hold the transparency in place was enclosed between the glass flats, and a metal lid over the top of the unit minimised contamination by airborne dust. The unit was sealed with rubber o-rings whose elasticity allowed the tilt of the windows to be adjusted.

The windows were aligned parallel to each other by inserting the empty unit into a laser interferometer and fluffing out the fringes in the reflections from their inner faces.

The fluid used was Dow Corning type 710 silicone fluid from BDH Chemical Ltd. Fig. 1.9. in a photograph of the finished unit.

OPTICAL FLATS - F1 AND F2

TRANSPARENCY - T

O RINGS - O

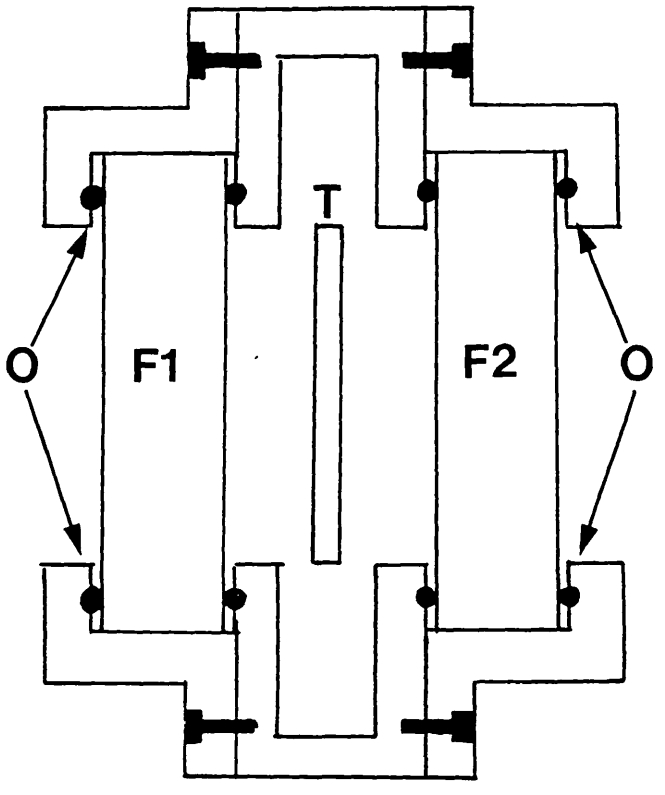

FIG 1.8

SCHEMATIC PLAN OF THE LIQUID GATE

FIG 1.9

THE LIQUID GATE

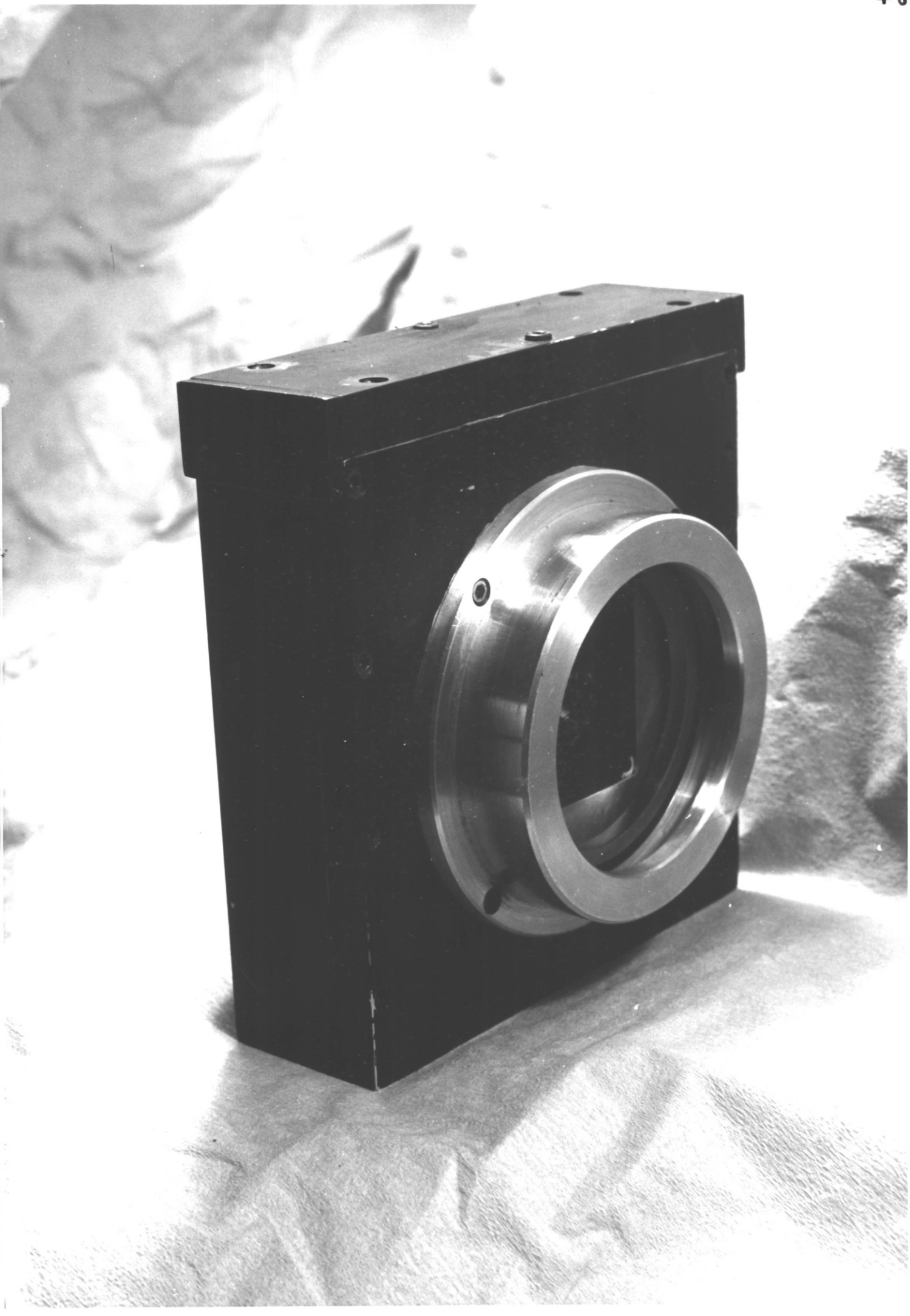

1.3. A practical example of the problems caused by undiffracted light

An experiment was carried out on behalf of the Geography Department of the University of Keele. They wanted a measure of the directionalities in a number of 35mm photographic negatives, taken on a scanning electron microscope, of various sedimentary rock samples.

Two film strips were provided. One in which the dominant spatial frequencies appeared (by visual inspection) to be around 4 or more lines per mm, and one in which the dominant spatial frequencies appeared to be lower - around one line per mm or less. Examples of these photographs, one from each film, are shown in Figs. 1.10. and 1.11. The overall magnification in these photographic prints is approximately 1000 times.

The films were analysed on the Imperial College coherent optical processor (described by Barnett, Harnett, Welford and Wynne, 1976 and in the Ph.D. thesis of P. R. Harnett)

A rotating sector disc with an aperture of wedge angle 5 degrees was placed in the magnified transform plane with a photomultiplier behind it, so as to measure the angular distribution of light in the transform plane. Over the range of intensities encountered, the photomultiplier

FIG 1.10

A TYPICAL SCANNING ELECTRON MICROSCOPE PHOTOGRAPH OF A SEDIMENTARY ROCK SAMPLE

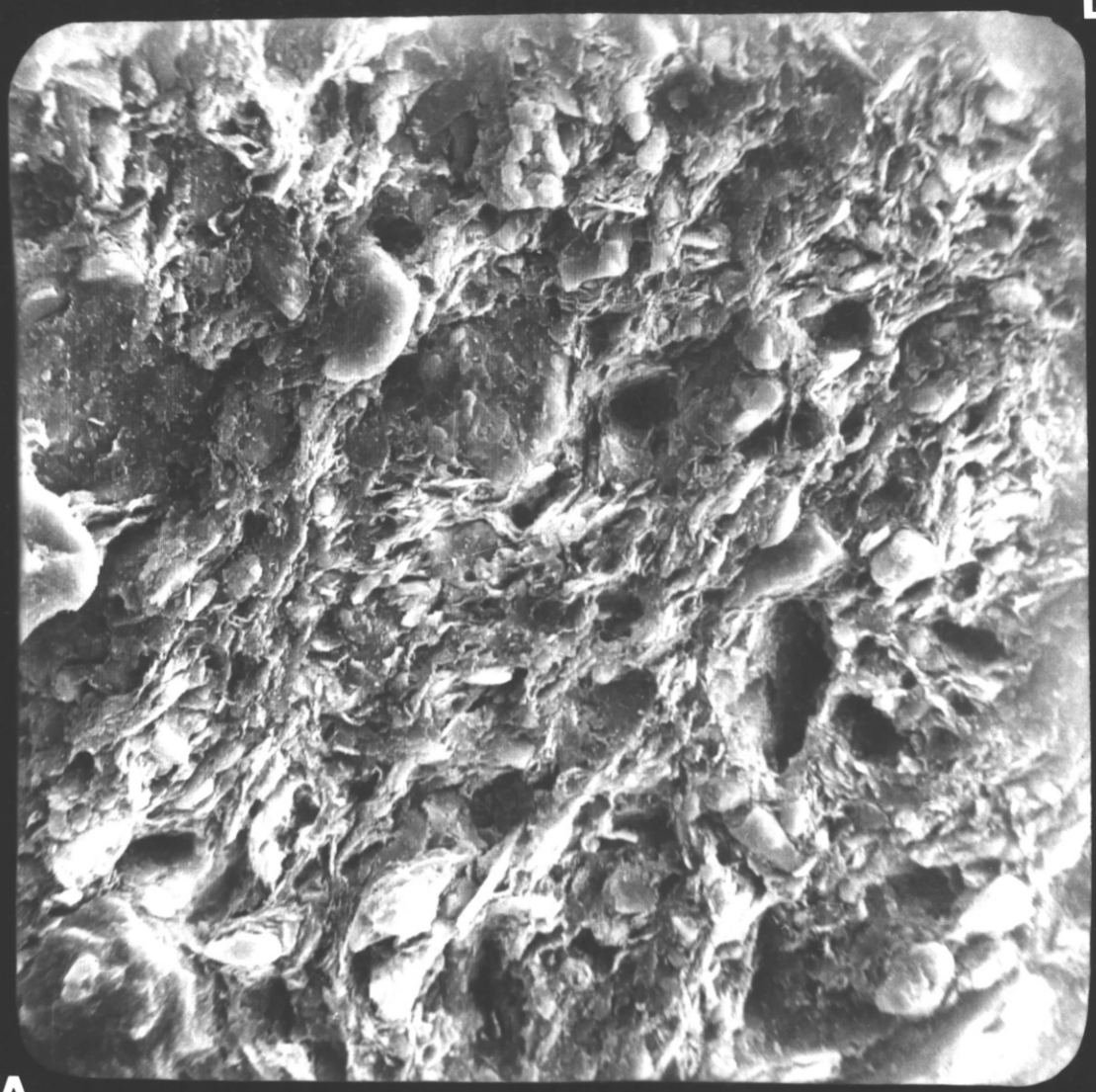
B
A

FIG 1.11

ANOTHER SCANNING ELECTRON MICROSCOPE PHOTOGRAPH WITH LOWER AVERAGE SPATIAL FREQUENCY THAN FIG 1.10

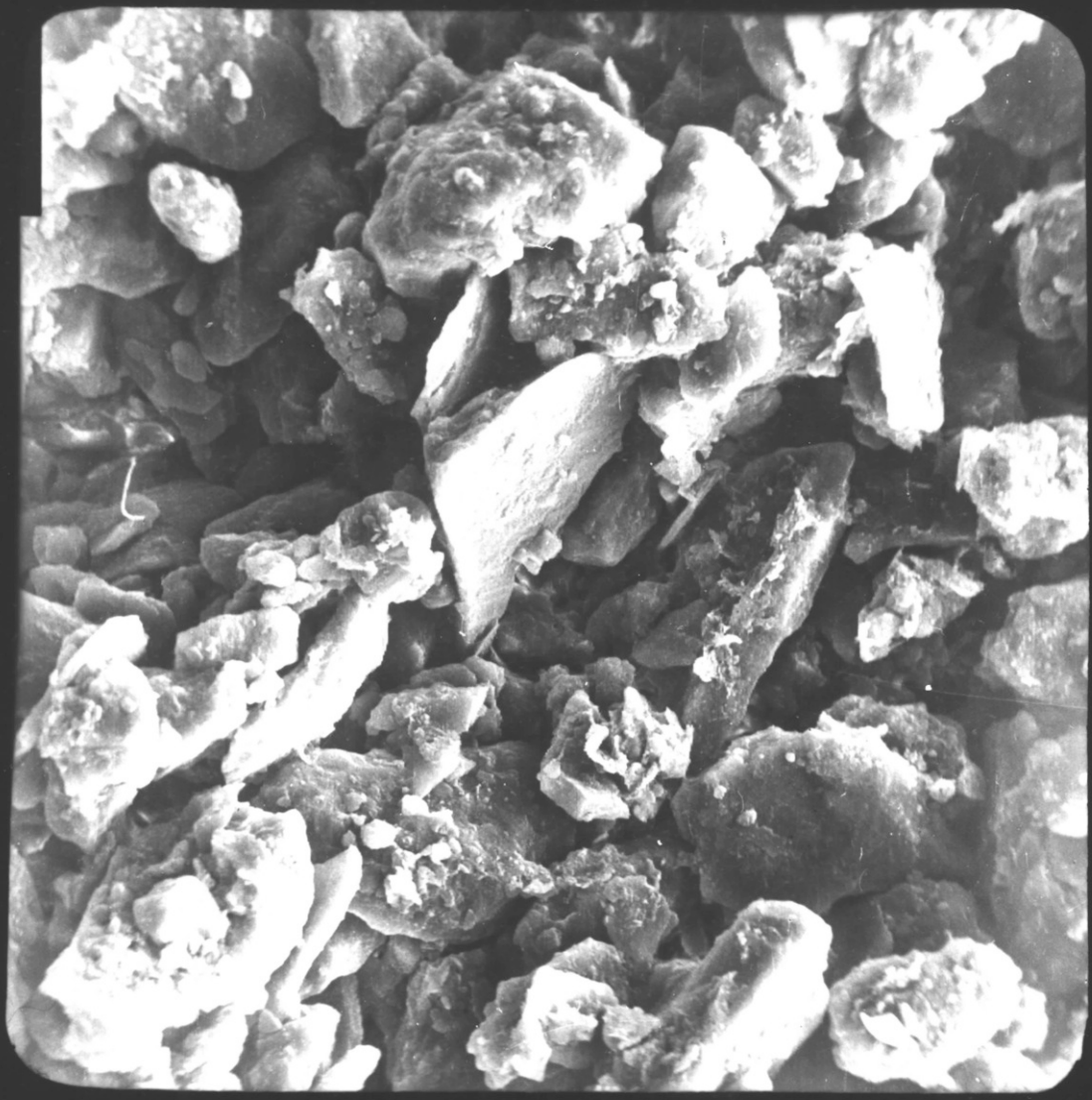

output signal is proportional the light intensity falling on its photocathode. Therefore for a given sector position, the output signal will be proportional to the intensity integrated over the sector.

Unfortunately, there was a slight irregularity in the sensitivities of different parts of the photocathode which was reported and measured by the instruments first user, P. R. Harnett (1980). This would lead to an angular bias in the results of scanning the optical transforms with the sector disc. Luckily, there is a symmetry in these irregularities, so that if we substitute the average of each diametrically opposite pair of readings for both members of the pair, the angular bias is reduced to about $\pm\frac{3}{4}$ of a per cent which is tolerable.

The intense central Airy pattern of the transform could damage the photomultiplier, so this was blocked off with the head of a small watchmaker's screw.

The result of these experiments are shown in Figs. 1.12. and 1.13.

On all the polar graphs in this thesis, the numbers on the radial scale correspond to the output signal from the photomultiplier. This depends on the operating voltage of the photomultiplier, the laser power and the losses in the

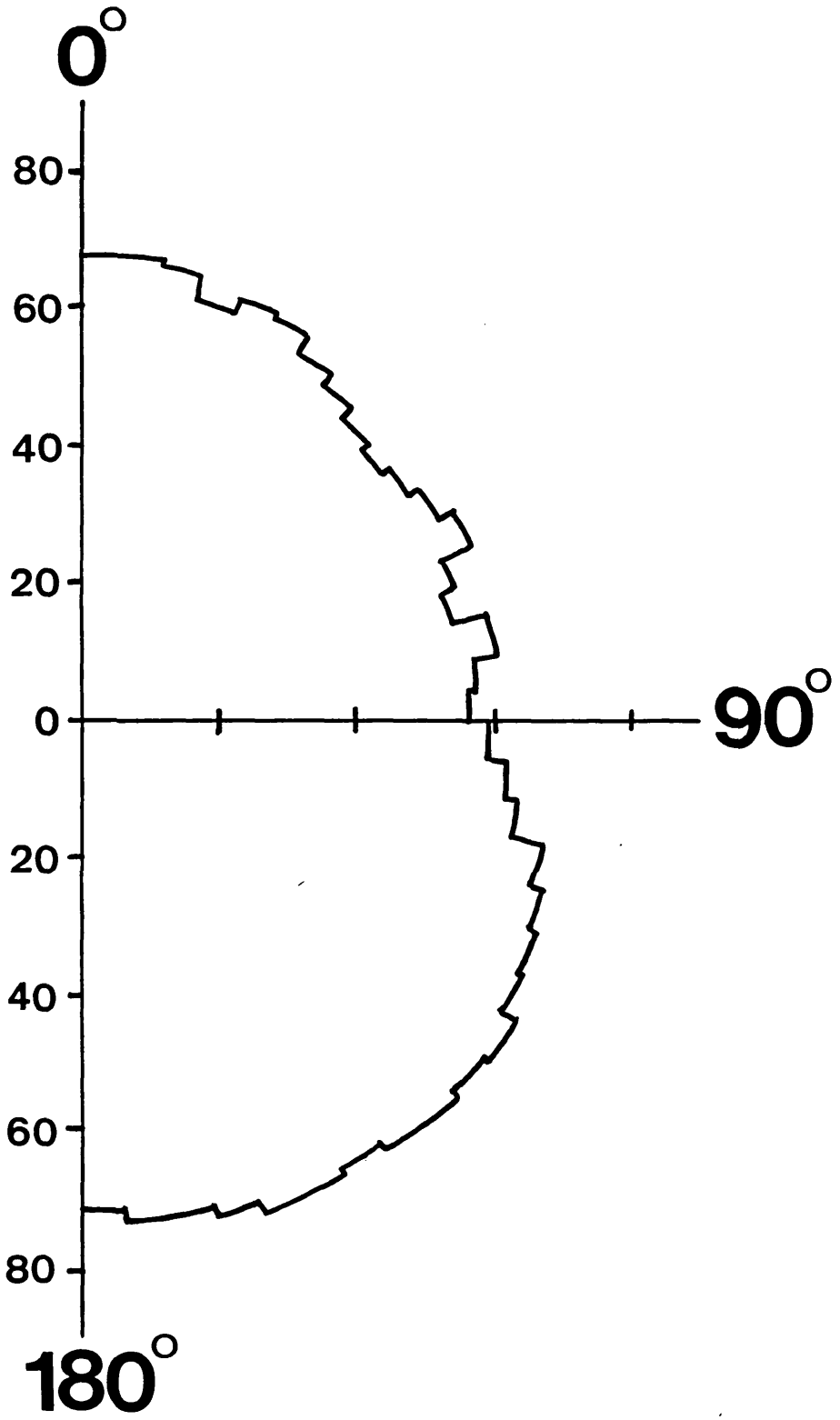

FIG 1.12

THE RESULT OF SCANNING THE OPTICAL FOURIER TRANSFORM OF FIG 1.10 WITH A ROTATING SECTOR DISC

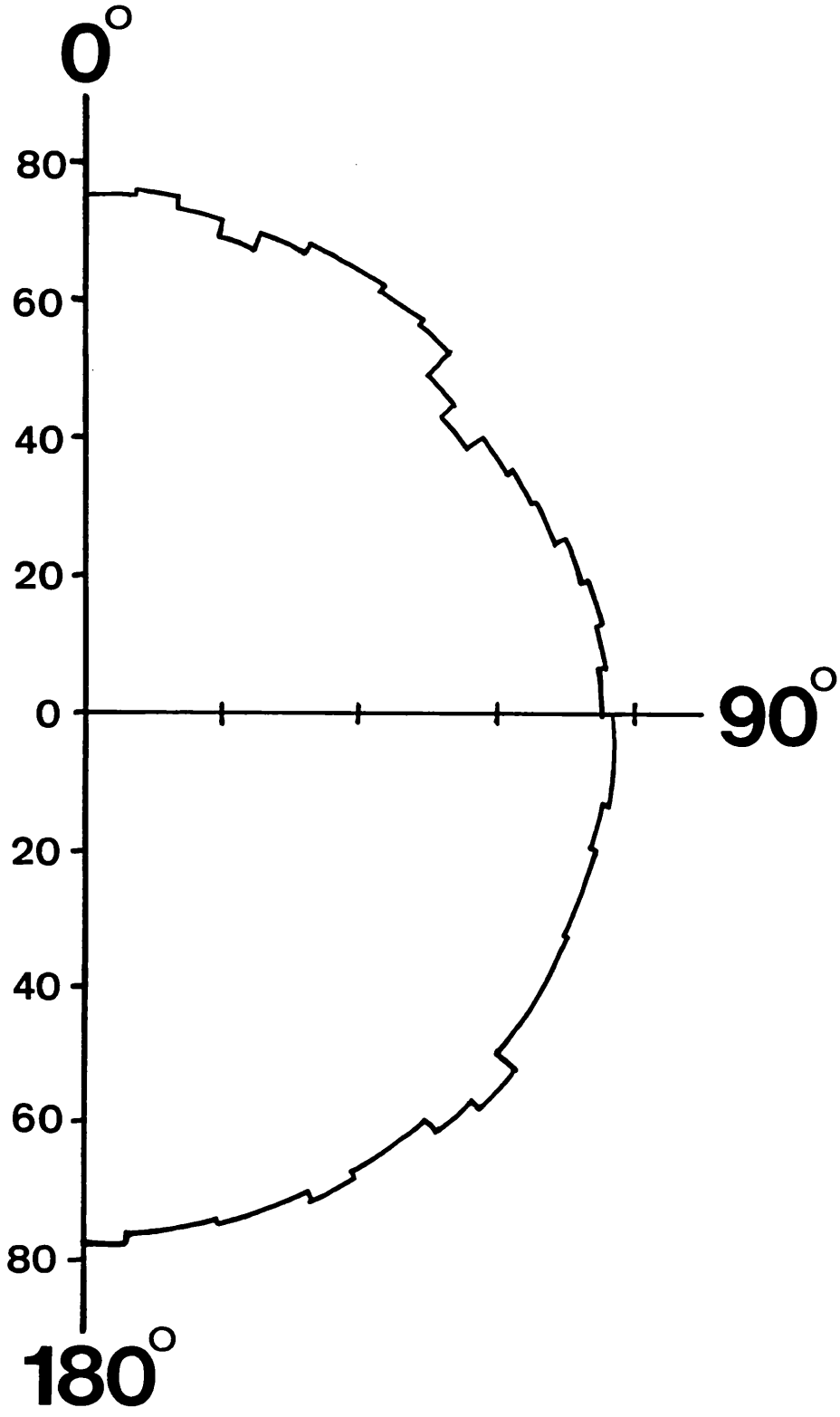

FIG 1.13

THE RESULT OF SCANNING THE OPTICAL FOURIER TRANSFORM OF FIG 1.11 WITH A ROTATING SECTOR DISC

system. Therefore the numbers are, to a certain extent, arbitrary. The system was set up to collect light diffracted by spatial frequencies from 0.2 to 8 lines per mm. Fig. 1.12. shows the results obtained by scanning the optical Fourier transform of Fig. 1.10. There is a directionality present, roughly in the direction A-B, which matches that expected from a visual inspection, but the rings of the Airy pattern have added quite a strong D.C. term. This takes the form of a circle on a polar graph. Directional variations in the light distribution produce a varying signal superimposed on this circle.

A numerical representation of the strength of the directionality in Fig. 1.12. is given by the ratio of the maximum to the minimum signal. In this case the ratio is 1.40.

Fig. 1.13. shows the results obtained by analysing the optical Fourier transform of Fig. 1.11. The expected directionality does not show up well on the results due to the relatively large contribution from the undiffracted light. The maximum to minimum intensity ratio for Fig. 1.13. is 1.24.

Similar problems would occur in the optical Fourier analysis of any photographs where the average spatial frequency is low.

To get a true idea of the relative strengths of any directionalities which may be present in photographs such as these, the central intense Airy pattern must either be removed or changed to a less obtrusive form.

1.4. Previous work

The problem of removing the undiffracted light in the transform plane has been tackled by several researchers with varying degrees of success.

The first group to work on the problem were Stark et al (1969). They used a π phase step placed so as to introduce a π phase difference between the light passing through the two halves of the aperture. This modifies the diffraction pattern to give a pattern whose intensity is zero along a line through its centre, parallel to the edge of the phase step, at the expense of a slight reduction in resolution in this direction. For two dimensional inputs a more complex system must be used. Stark et al suggest the use of a contoured aperture in which the amplitude distribution of the light incident on the transparency is made non-uniform by the addition of an absorbing filter with contoured transmission. This was followed by Pernick et al (1970) who considered the use of gaussian, lorentzian and exponential contours and concluded that the detectability of low spatial frequencies is improved by their use. Unfortunately this does not remove the undiffracted light but just changes its distribution to one with a wider central peak, but no rings surrounding it.

Removal of the undiffracted light requires interferometric cancellation. This involves the coherent superposition of the diffraction patterns of the input aperture and a compensating aperture of the same size as the limiting aperture of the input transparency, and whose transmission is equal to the D.C. transmission level of the input transparency. A π phase charge is introduced between the two beams so that the D.C. level is cancelled out leaving only the signal of interest. Felstead (1971) suggested that the D.C. level could be removed from one dimensional inputs by using an aperture in two halves, with the signal in one half and the other half clear except for a π phase retardation plate. This is similar to the method of Stark et al. For two dimensional signals he suggests the use of a Mach Zehnder interferometer, but points out that this would be almost impossible to adjust and maintain in the zero fringe position.

Fink (1972) used a Smith polarization interferometer to successfully remove the D.C. level from what appeared to be an input object consisting of some combination of geometrical shapes, but this method used imaging through prisms which severely limits the resolution and introduces aberrations. Also the dimensions involved meant that the system could not readily be adapted for use on the existing Imperial College Fourier transform bench.

Therefore a different form of interferometer needs to be built.

1.5. Requirements for D.C. removal

1.5.1. The basic idea of interferometric cancellation

Equation 15 stated that the transmission T(x,y) of a photographic transparency can be written as:

$$T(x,y) = (q_o + q_1(x,y))\ P_c(x,y)$$

where q_o is the zero order component which is uniform across the aperture and $q_1(x,y)$ is the signal of interest.

Removal of the q_o term requires the addition of another term of the form $-q_o P_c(x,y)$ i.e. a plane wave with the same limiting aperture as the transparency and propagating in exactly the same direction with a phase difference between the two terms of 180 degrees.

If this is done then the transform plane amplitude distribution will be the Fourier transform of $q_1(x,y).P_c(x,y)$ which is given by the second term of equation 19, i.e. :

$$\mathcal{F}\left\{q_1(x,y)\ P_c(x,y)\right\} = 2\pi a^2\, \mathcal{F}\left\{q_1(x,y)\right\} \otimes \frac{J_1(2\pi ra)}{2\pi ra}$$

1.5.2. Resolution requirements

At this stage it is useful to ask how accurately the relative alignment, phase difference and relative amplitudes

of the beams have to be set to result in the reduction of the intensity of the undiffracted light by a given factor. Calculations were performed on a Hewlett Packard HP85 computer to find the intensity distributions for combinations of two Airy patterns with various relative amplitudes, phase differences and separations.

The light distribution in the focal plane along a line joining the centres of the two patterns I(x) is given by:

$$I(x) = \left| \frac{C2J_1(x)}{x} + \frac{D2J_1(x-\Delta)}{(x-\Delta)} \cdot e^{i\phi} \right|^2 \qquad (21)$$

where C and D are the amplitudes at the centres of the two patterns, ϕ is the phase difference between them and Δ is their separation.

The intensity maxima will lie along this line and will occur when $\frac{dI(x)}{dx} = 0$

Performing this differentiation produces a formidable looking equation which, as Δ, ϕ and x may not be small, cannot readily be simplified. Therefore it was decided to take the "easy way out" and to find the maxima by numerical methods.

For relatively small values of x, $J_1(x)$ is given by:

$$J_1(x) = \tfrac{1}{2}x - \frac{(\tfrac{1}{2}x)^3}{1^2 2} + \frac{(\tfrac{1}{2}x)^5}{1^2 2^2 3} - \ldots . \qquad (22)$$

(see Dwight 807.21 page 191)

The results of these calculations are shown in the following pages. In all of the focal plane distributions, the focal plane distance is plotted in units of x where the intensity of each pattern is constant $\left(2\,\frac{J_1(x)}{x}\right)^2$

The separations chosen were in fractions of the Rayleigh resolution unit which is defined as the separation when the central peak of one pattern falls on the first zero of the other. It is often used to define the two point resolution limit for optical systems with incoherent light, but strictly speaking it does not apply to coherent light. It has been used in these calculations as it is a unit of convenient size which scales with the system aperture.

The final interferometer was designed to have one fixed beam, and one steerable beam. To make the plots of intensity against distance in the focal plane correspond to this, one Airy pattern was centred at a position of 0 on the horizontal axis, with a phase of 0 and a maximum amplitude of 1, whilst the position, relative phase, and relative amplitude of the other pattern were adjusted.

(a) Relative alignment requirements

Both patterns were set to peak amplitudes of 1 with a phase difference of 180 degrees between them. Fig. 1.14. shows the intensity distributions for separations between the Airy pattern centres of 1.0, 0.5 and 0.3 Rayleigh resolution units. As expected, the maximum intensity drops as the separation decreases, with the separation of the two maxima slightly greater than the separation of the centres of the two individual patterns.

The pattern for a separation of 1.0 Rayleigh resolution units has been published in several references (such as Ghatak and Thyagarajan 1978) and this acts as a check on the accuracy of the program.

Fig. 1.15 shows the maximum intensity plotted against separation. From this it can be seen that to obtain a reduction in peak intensity by a factor of 50, the separation needs to be approximately 0.1 Rayleigh resolution units.

(b) Phase requirements

Both patterns were set to peak intensities of 1 with a separation of 0.1 Rayleigh resolution units. Fig. 1.16 shows the results for phase differences of 180, 175 and 170 degrees. The maximum intensity does not change much between

the first two patterns and even at a phase difference of 170 degrees, the maximum intensity has only increased by about 50 per cent over the 180 degrees case. Fig. 1.17 shows the maximum intensity plotted against phase difference. From this it can be seen that to obtain a reduction in intensity of 50 times needs a phase difference of approximately 180±5 degrees.

(c) Amplitude requirements

With the two patterns set to a separation of 0.1 Rayleigh resolution units and a phase difference of 180 degrees, Fig. 1.18 shows the intensity distribution when one pattern has a maximum amplitude of 1.0 and the other pattern has maximum amplitudes of 1.0, 0.95 and 0.90. Fig. 1.19 shows the maximum intensity of the largest peak plotted against the relative amplitude of the second pattern, showing that to achieve a reduction in peak intensity by a factor of 50 requires the amplitudes of the two patterns to be matched to within approximately two per cent.

Summary of resolution requirements

The calculated results presented so far in this section represent slightly unreal situations as they assume that one or two of the three parameters (relative alignment, phase difference and relative amplitude) can be set to exactly the

desired values. Hence a reduction in the maximum intensity by a factor of 50 times is a little optimistic. If we allow all three parameters to differ from the desired values by the amounts suggested by the calculations in this section, we obtain the intensity distribution shown in Fig. 1.20. This has a reduction in the maximum intensity by a factor of approximately 40 times, which would be an acceptable value for this project. Therefore we may summarise the resolution requirement of the interferometer as follows:-

(a) Relative alignment

The two Airy patterns in the transform plane should have a separation of not more than 0.1 Rayleigh resolution units. For the existing system at Imperial College, with an aperture of 25mm and a lens focal length of 700mm, this corresponds to a tilt between the wavefronts of 0.5 arc seconds.

(b) Phase difference

The phase difference should be approximately 180±5 degrees.

(c) Relative amplitude

The amplitude of the beams should be the same to within approximately 2 per cent.

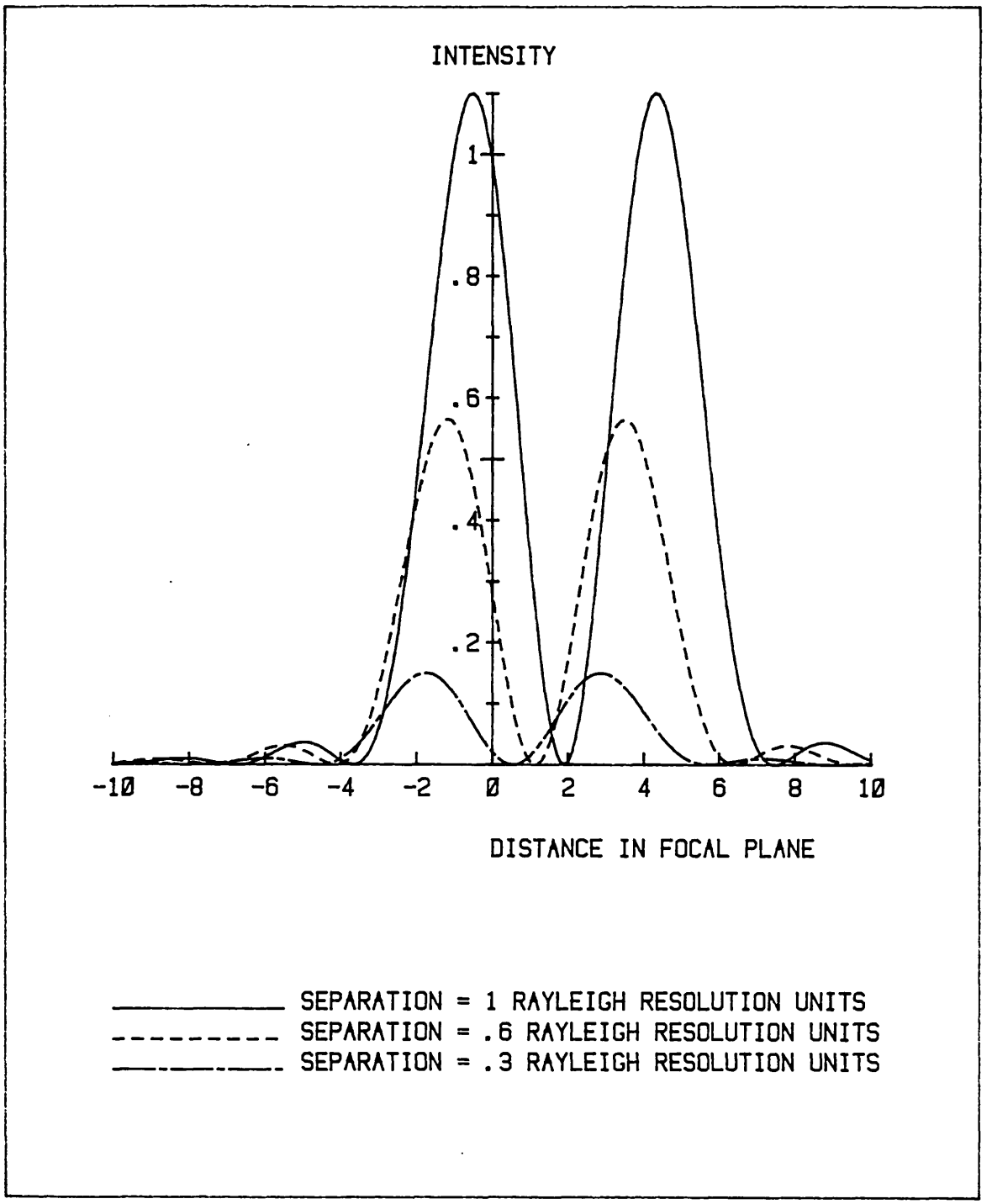

FIG 1.14

COMPUTED INTENSITY DISTRIBUTIONS FOR A PAIR ØF AIRY PATTERNS WITH THE SAME AMPLITUDES, A PHASE DIFFERENCE OF 18Ø DEGREES AND THREE DIFFERENT SEPARATIONS

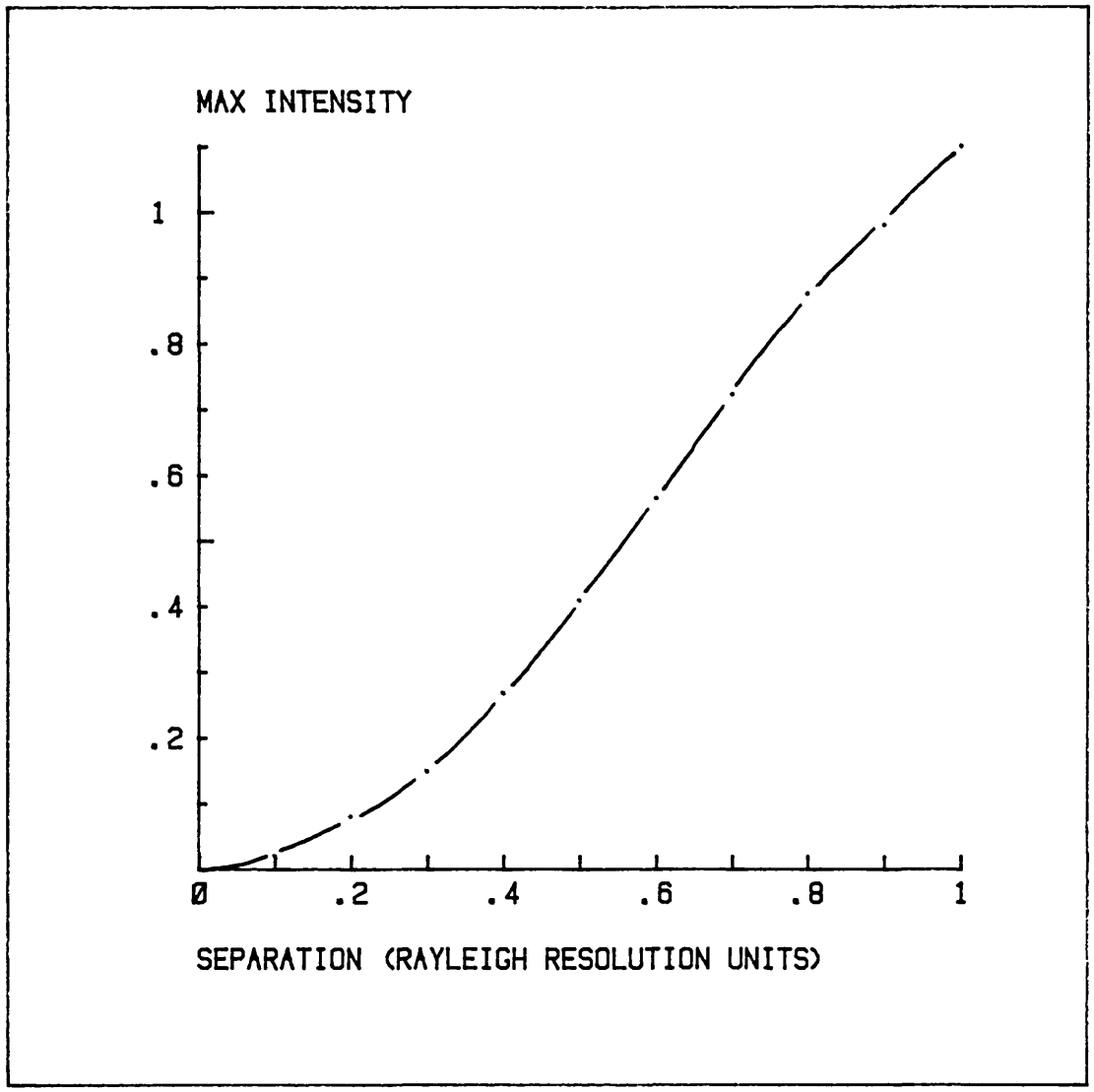

FIG 1.15

COMPUTED MAXIMUM INTENSITY FOR A PAIR OF AIRY PATTERNS WITH THE SAME AMPLITUDES AND A PHASE DIFFERENCE OF 180 DEGREES PLOTTED AGAINST THEIR SEPARATION

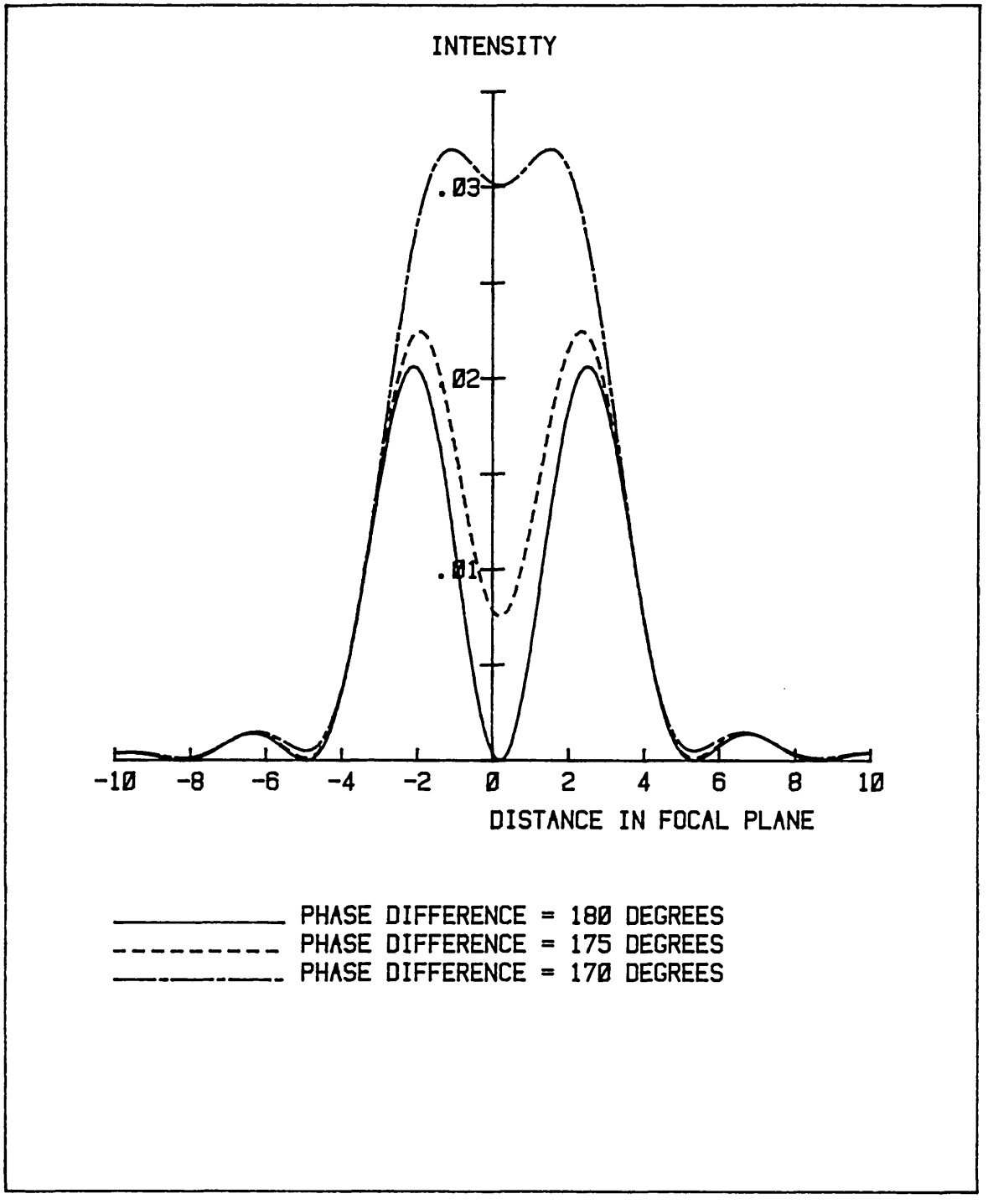

FIG 1.16

COMPUTED INTENSITY DISTRIBUTIONS FOR A PAIR OF AIRY PATTERNS WITH THE SAME AMPLITUDES, A SEPARATION OF 0.1 RAYLEIGH RESOLUTION UNITS AND THREE DIFFERENT PHASE DIFFERENCES

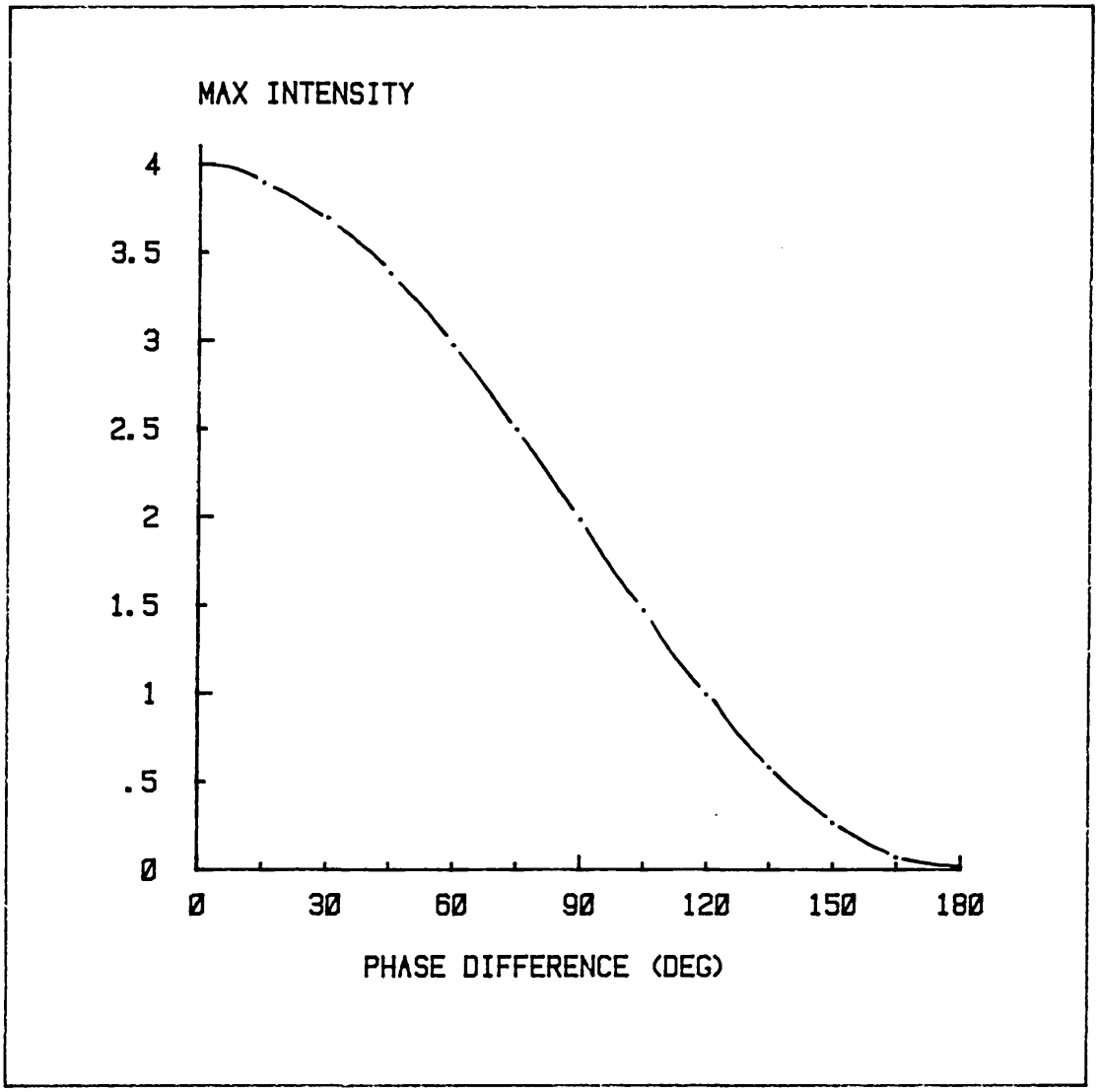

FIG 1.17

COMPUTED MAXIMUM INTENSITY FOR A PAIR OF AIRY PATTERNS WITH THE SAME AMPLITUDES AND A SEPARATION OF 0.1 RAYLEIGH RESOLUTION UNITS PLOTTED AGAINST THEIR PHASE DIFFERENCE

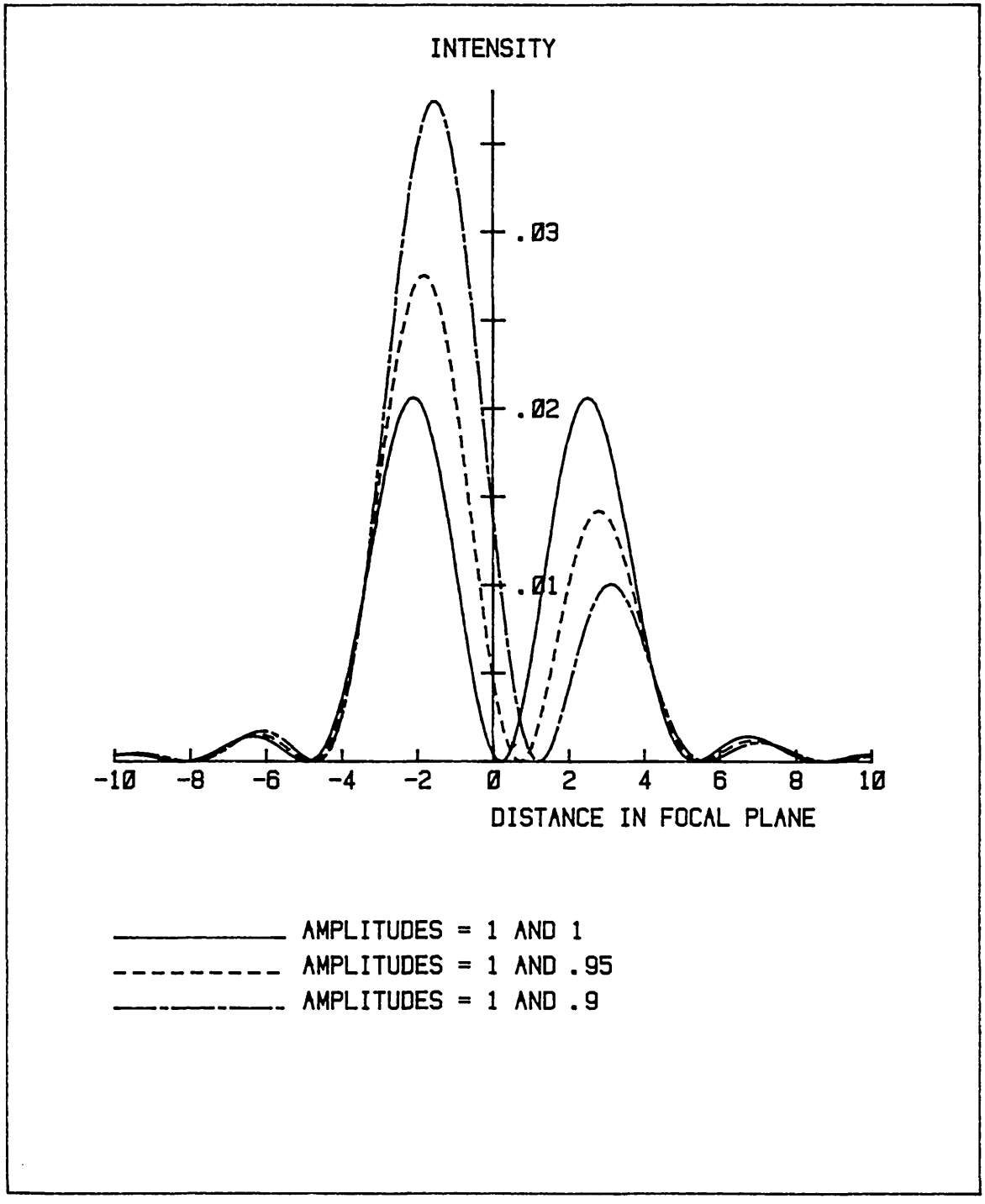

FIG 1.18

COMPUTED INTENSITY DISTRIBUTIONS FOR A PAIR OF AIRY PATTERNS WITH A SEPARATION OF Ø.1 RAYLEIGH RESOLUTION UNITS, A PHASE DIFFERENCE OF 18Ø DEGREES AND THREE DIFFERENT RELATIVE AMPLITUDES

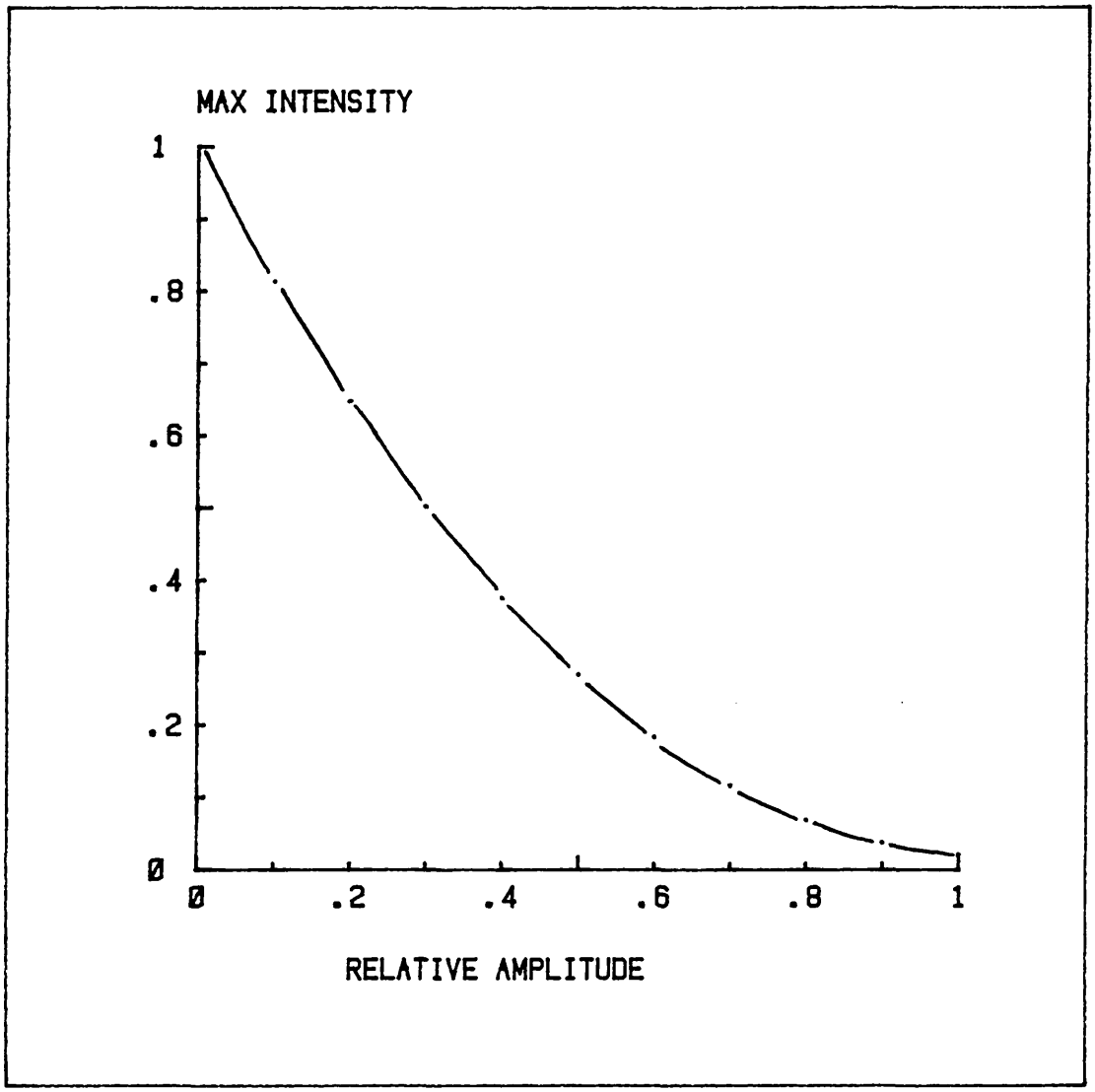

FIG 1.19

COMPUTED MAXIMUM INTENSITY FOR A PAIR OF AIRY PATTERNS WITH A SEPARATION OF Ø.1 RAYLEIGH RESOLUTION UNITS AND A PHASE DIFFERENCE OF 18Ø DEGREES PLOTTED AGAINST THEIR RELATIVE AMPLITUDES

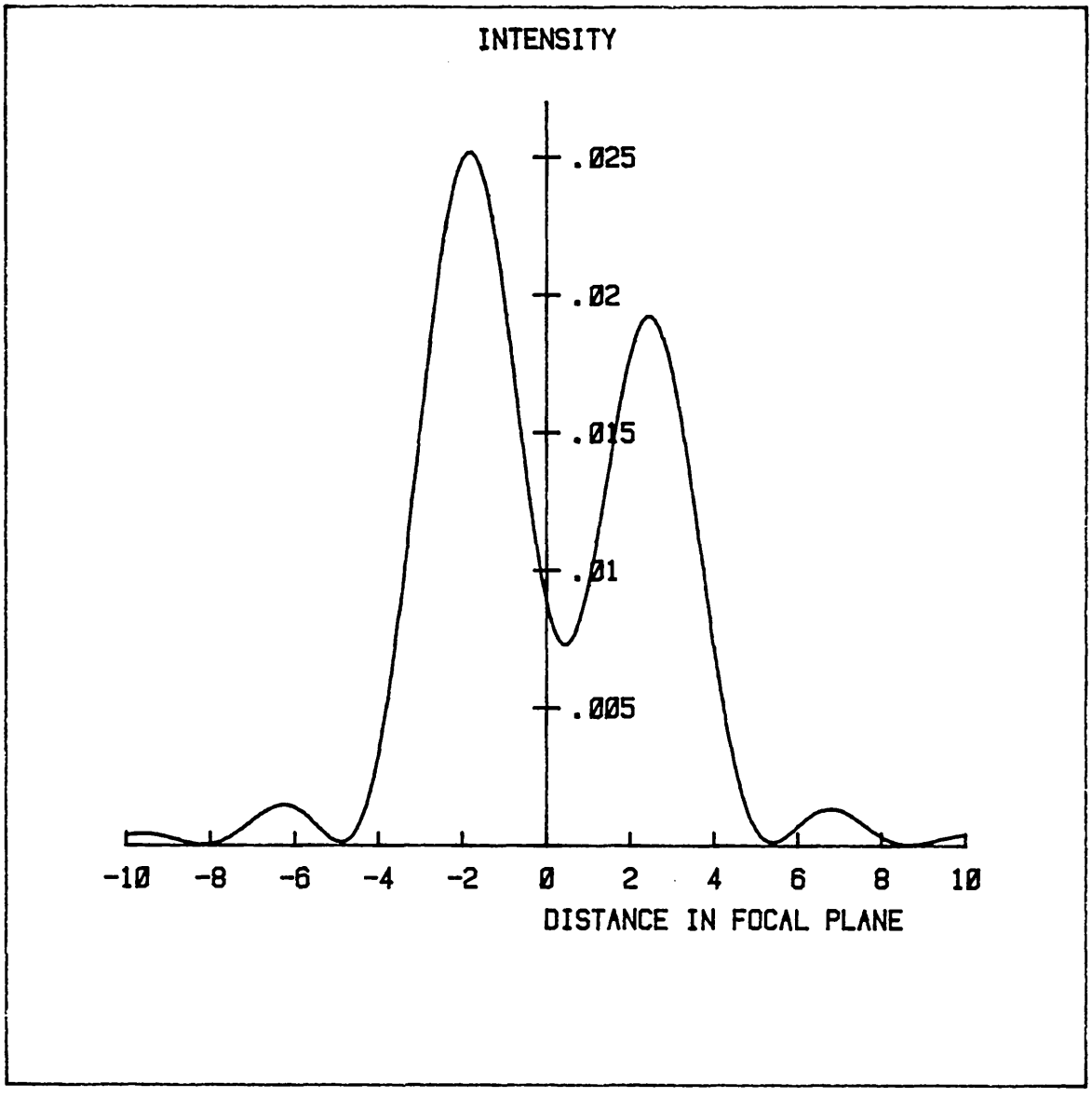

FIG 1.20

COMPUTED FOCAL PLANE INTENSITY DISTRIBUTION AT THE RESOLUTION LIMIT OF THE INTERFEROMETER

1.5.3. Aberrations

If the beams are aberrated, the form of the Airy patterns will change. In general, light will be redistributed away from the central peaks, and into the first few rings, but provided the aberrations are not too severe (see below) the patterns will be similar to the unaberrated ones (for computer plots of Airy patterns with various aberrations see the M.Sc. report of R. Belleby 1981). If both beams have the same aberrations, the patterns will have identical distortions and will still cancel but this is unlikely.

If the aberrations are different in the two beams, then partial cancellation will occur, the degree of which depending on the magnitude and form of the aberrations.
If the aberrations are small, quite good cancellation of the central peak could be achieved by adjusting the relative amplitudes of the beams, but only at the expense of reduced cancellation efficiency in the rings.
The Strehl tolerance for the maximum intensity of the diffraction pattern to drop by 20 per cent is for the aberration of the wavefront to be approximately $\pm\lambda/14$.

This could be compensated for by adjusting the relative amplitudes of the patterns. For this application the important thing is the difference in the two diffraction patterns, so $\lambda/14$ may be taken as a rough estimate of the

difference tolerance between the two wavefronts.

CHAPTER 2

THE INTERFEROMETER

2.1. Methods of achieving the required resolutions

2.1.1. Alignment methods

There are many ways to deflect a beam of light, but very few are capable of providing the required resolution at an acceptable cost. The usual method is to reflect the beam off a plane mirror in an adjustable holder. This is just capable of achieving high enough resolution, but only with very large and expensive mounts. Another disadvantage is that if the mirror wobbles by a small angle, the beam is deflected by twice that angle leading to possible stability problems. Electro-optic and acousto optic deflectors have limited resolution and require high voltage supplies and control electronics.

Prism devices can offer high resolution and compact mounts, but the usual designs suffer from a number of disadvantages. The first design, due to De (1955) uses a narrow angle wedge prism to deflect the light beam. By rotating the prism, the beam can be steered with an accuracy of around one arc second.

The second design mentioned by De and described by Marshall (1980) uses a pair of oppositely rotating wedge prisms to steer the beam anywhere within a cone of angular radius approximately twice the prism wedge angle.

Both of these designs suffer from the disadvantages that the relationships between beam deviation and prism movements are very non linear. A variable shear is introduced as well as a deflection and the sensitivities, which are fixed by the prism wedge angles are limited by manufacturing tolerances to around one arc second.

Immersing the prisms in a bath filled with fluid of refractive index slightly different to that of the glass would give higher resolution but requires high optical quality windows and introduces problems due to convection currents in the oil and difficulties in controlling the prism movements.

These resolutions are not high enough, so it was decided to use a new type of prism beam steering device (Lang 1983, after an idea by W. T. Welford).

2.1.2. Theory of the new beam steering device

Consider a single wedge prism near minimum deviation. If the prism wedge angle is 2A, its refractive index is n and

the angle of incidence at minimum deviation is I_o, then:

$$\text{Sin } (I_o) = n \text{ Sin } (A) \qquad (23)$$

If this prism is turned through a small angle α, away from minimum deviation, then it can be shown that the deviation increases by:

$$\frac{(n^2-1) \text{ Sin } (I_o) \alpha^2}{n^2 \cos^2(A) \cos (I_o)} \quad \text{(see appendix 4)} \qquad (24)$$

Now suppose two prisms with the same refractive indices and wedge angles are placed almost antiparallel as in Fig. 2.1, with a small constant tilt between them of β.

The second prism produces a deviation of:

$$- \frac{(n^2-1) \text{ Sin}(I_o) (\alpha-\beta)^2}{n^2 \cos^2(A) \cos(I_o)} \qquad (25)$$

Hence the total deviation is:

$$\frac{(n^2-1) \sin(I_o) 2\beta\alpha}{n^2 \cos^2(A) \cos(I_o)} + \text{ constant} \qquad (26)$$

i.e. linear in α, with sensitivity proportional to β.

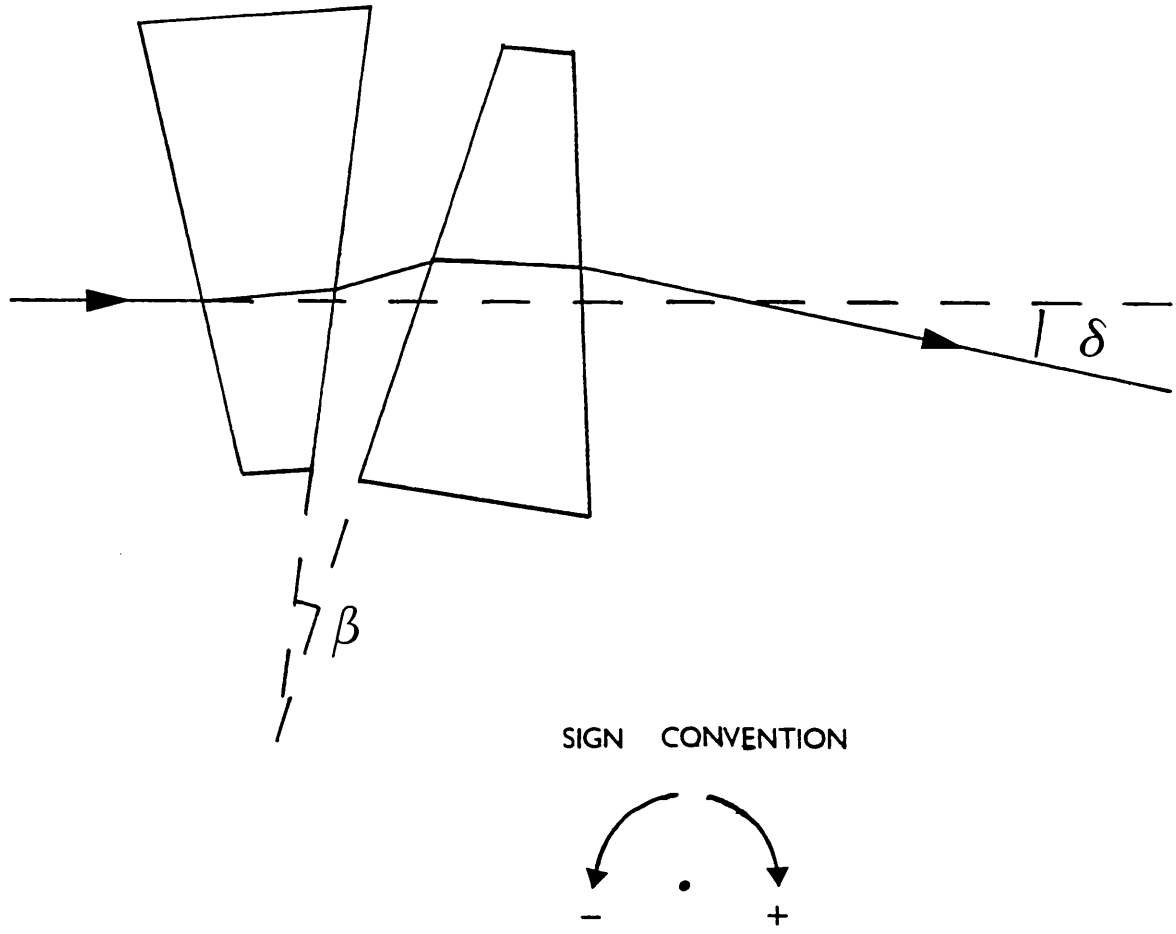

FIG 2.1

SCHEMATIC DIAGRAM OF THE BEAM STEERING DEVICE

The properties of the device were calculated using an accurate computer ray trace through the prisms. The results are described in the following few pages.

Fig. 2.2 shows the effect of reversing the tilt between the prism, i.e. replacing β by $-\beta$. As expected, the result is a change in the sign of the deviation, with very little effect on the shape of the curve.

The magnitude of the slope of the linear part of the curve plotted against the angle between the prisms is shown in Fig. 2.3 confirming that the deviation is proportional to β.

Plotting a similar graph of the magnitude of the slope against the prism wedge angle (Fig. 2.4.) shows that the deviation is also proportional to α.

Fig. 2.5 shows the magnitude of the slope plotted against the prism refractive index. This appears roughly linear but this is due to the limited range of indices used. In fact the slope is proportional to $\left(\frac{n^2-1}{n^2} \right)$. The small ripples on this curve are an artifact of the plotter.

These results, along with other computer plots, show that equation 26 is valid for several orders of magnitude of wedge angle and tilt between the prisms, and for all

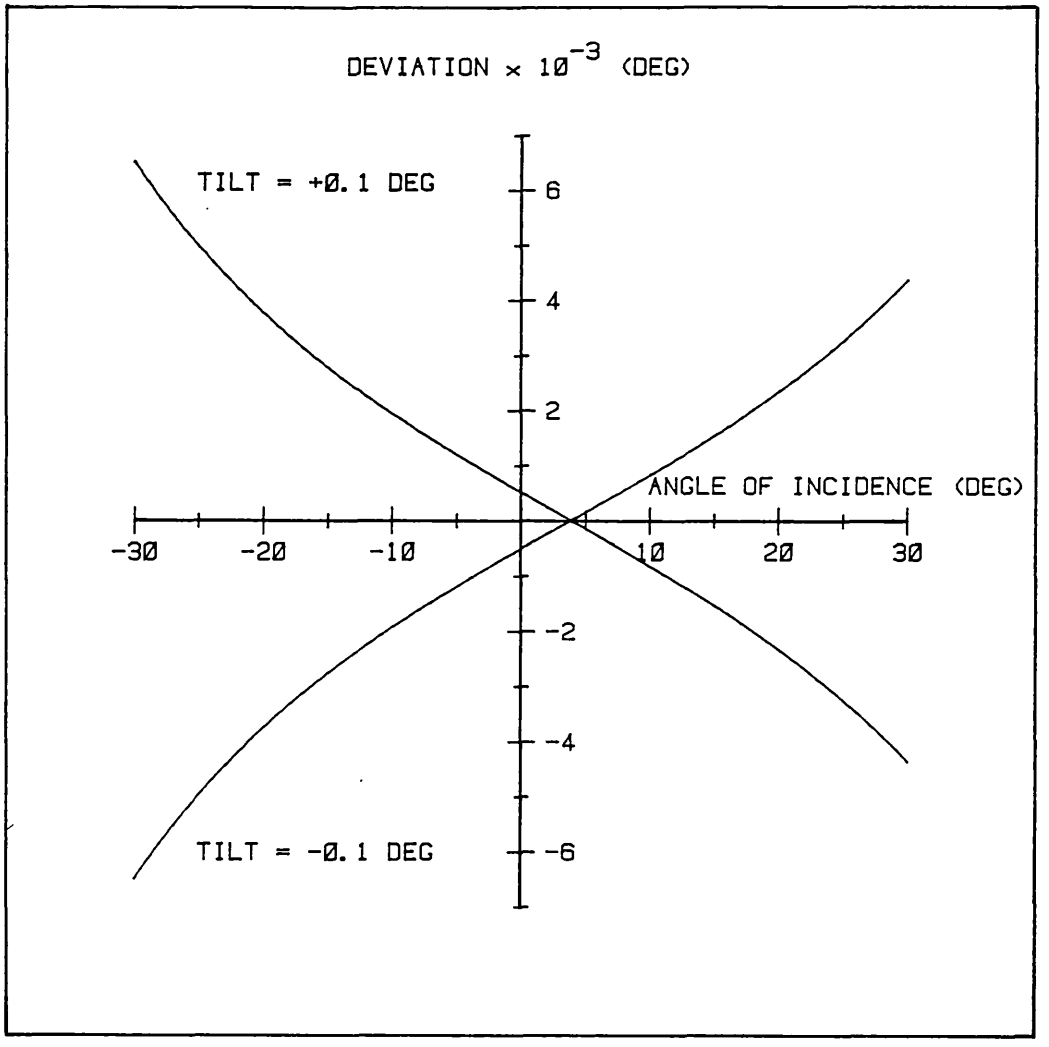

FIG 2.2

THEORETICAL RESULTS FOR 5 DEGREE PRISMS OF REFRACTIVE INDEX 1.52 WITH TILTS BETWEEN THEM OF +/- 0.1 DEGREES

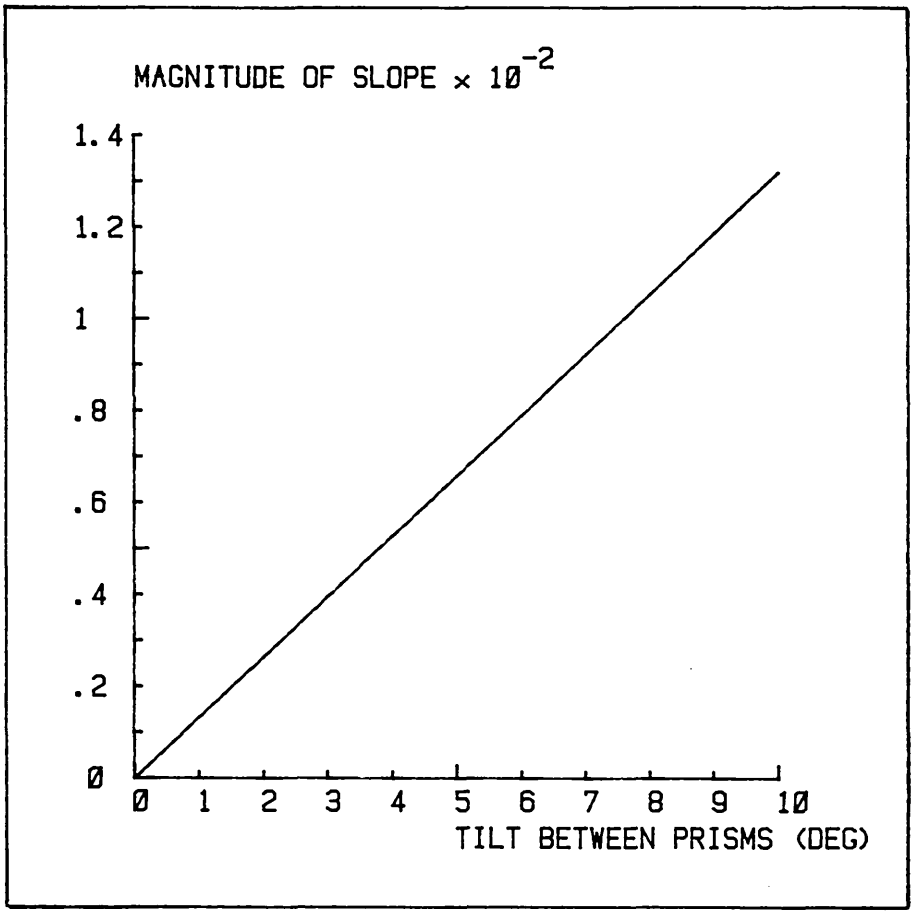

FIG 2.3

SLOPE OF LINEAR PART OF CURVE VS TILT BETWEEN PRISMS FOR PRISMS WITH WEDGE ANGLES OF 5 DEGREES AND REFRACTIVE INDEX 1.52

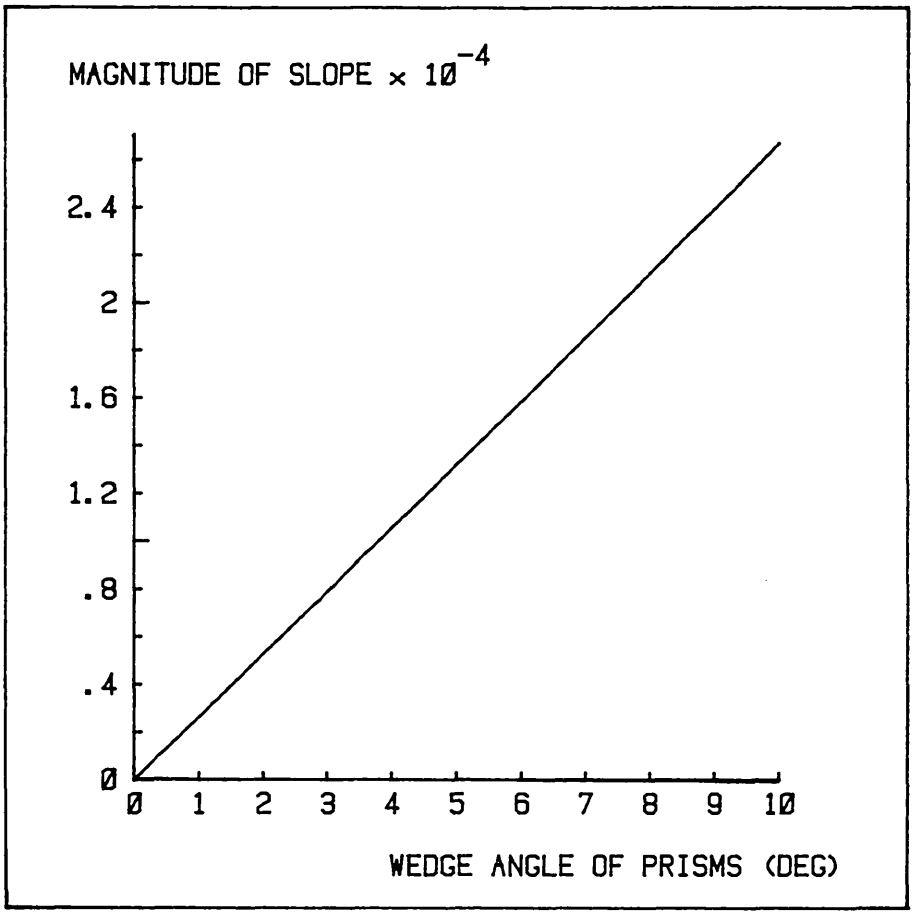

FIG 2.4

SLOPE OF LINEAR PART OF CURVE VS WEDGE ANGLE FOR PRISMS OF REFRACTIVE INDEX 1.52 WITH A TILT BETWEEN THEM OF 0.1 DEGREES

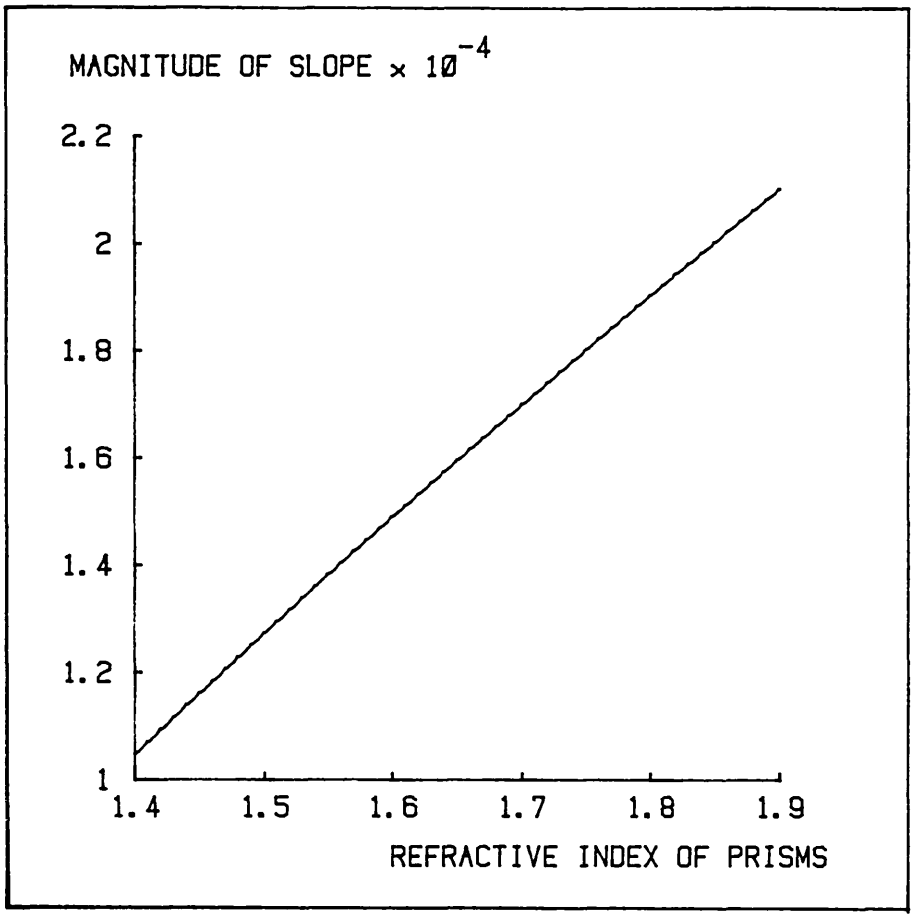

FIG 2.5

SLOPE OF LINEAR PART OF CURVE VS REFRACTIVE INDEX OF PRISMS FOR PRISMS WITH WEDGE ANGLES OF 5 DEGREES AND A TILT BETWEEN THEM OF Ø.1 DEGREES

currently possible refractive indices. The curves are linear to within about ±5 per cent over a range of incidence angles of approximately ±20 degrees.

Up until now, it has been assumed that the prisms are identical, but in practice, the wedge angles will be slightly different, and it is useful to ask what effect the difference has on the curves.

For a constant tilt and identical refractive indices, Fig. 2.6. shows that a small difference in the wedge angles shifts the curves relative to the axes, but with very little change in their shapes.

If the difference in the prism wedge angles is such that it is greater than about 1/40 of the tilt between them, then the curves become distorted as shown in Fig. 2.7. For some applications this may be unimportant, but if linearity between prism movements and beam deviation is required, then the prisms must be accurately matched.

2.1.3. Experimental results for the beam device

The device was constructed using $5^{o}48'$ prisms of BK7 optical glass (refractive index at 632.8nm = 1.515), matched to 10 seconds of arc. The seemingly odd wedge angle was a result of the low tolerance required. Any prisms of approximately

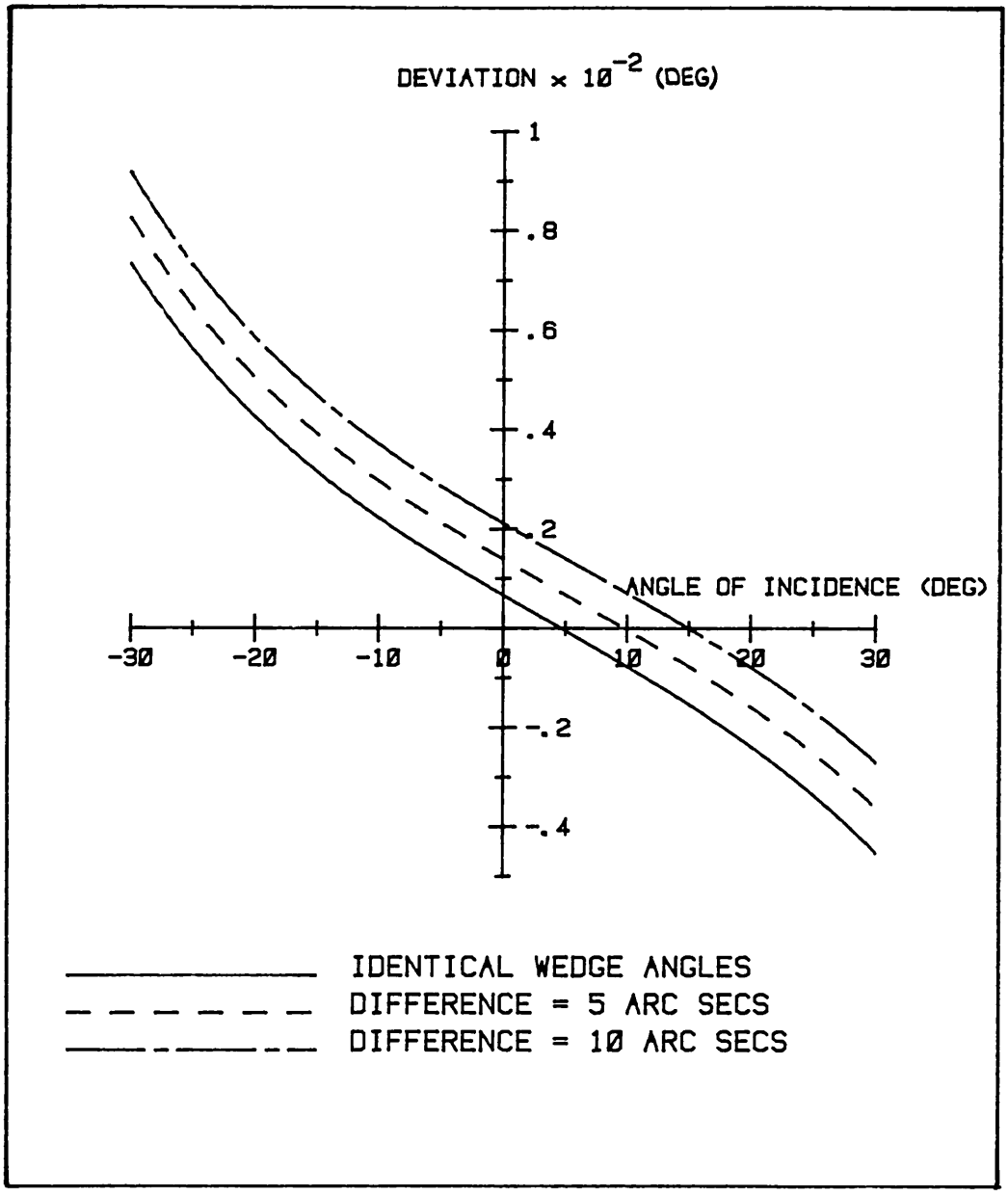

FIG 2.6

THE EFFECT OF THE DIFFERENCE IN THE WEDGE ANGLES FOR 6 DEGREE PRISMS WITH REFRACTIVE INDEX 1.52 AND A TILT BETWEEN THEM OF 0.09 DEGREES

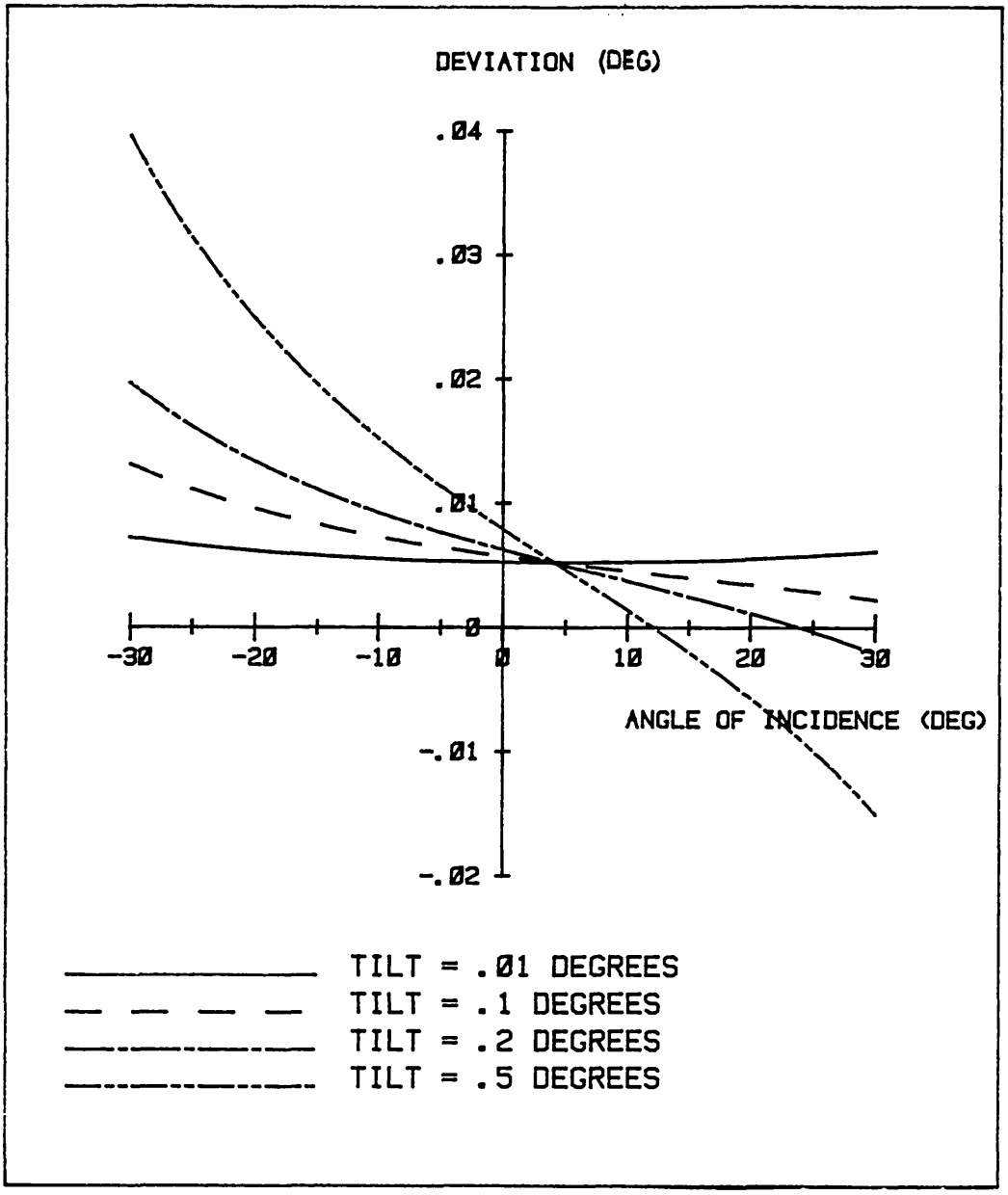

FIG 2.7

THE EFFECT OF FOUR DIFFERENT TILTS WITH PRISMS OF WEDGE ANGLES 5.00 AND 5.01 DEGREES

6 degrees wedge angle would give a suitable range and resolution, provided they were accurately matched.

The prisms were antireflection coated with a broad band coating optimised for a wavelength of 488nm - the wavelength to be used in the interferometer. The large range of incidence angles meant that the more efficient V coats would be unsuitable as they are designed for only one incidence angle.

Fig. 2.8 shows the experimental arrangement. Light from a helium-neon laser (λ=632.8nm) was expanded and collimated by an auto collimator and then passed through the prisms onto a plane mirror in an adjustable mount. After a second pass through the prisms, the deviation relative to the original beam is, to within approximately half a per cent, twice the deviation produced by a single pass.

The resulting deviation was then measured using the auto collimator with an accuracy of approximately 0.2 arc seconds.

As the anti reflection coatings were optimised for a wavelength of 488nm (blue) the reflections of the red helium neon laser light were bright enough to allow the use of these for setting the prisms to the correct orientation and tilt. This was performed by observing the reflections from

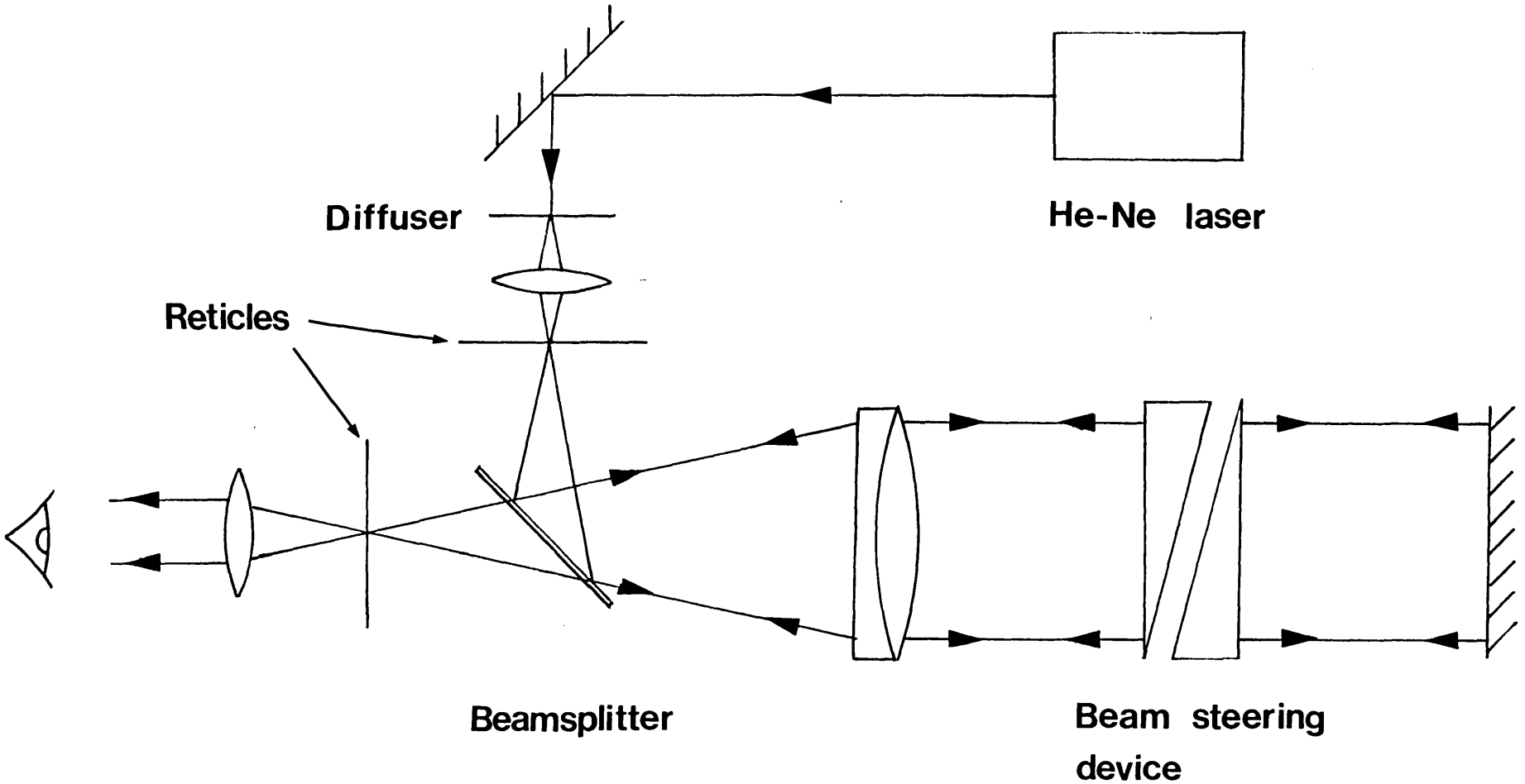

FIG 2.8
EXPERIMENTAL ARRANGEMENT USED TO TEST THE BEAM STEERING DEVICE

the four faces allowing for the slightly different angles of refraction for the various beams.

Fig. 2.9 shows the experimental and theoretical results for a tilt of 0.5 degrees showing a good agreement between the theoretical curve (full line) and the experimental results (crosses).

The reduction ratio here is about 950 to 1, which, coupled with rotating mounts of 5 arc minutes resolution gives a deviation resolution of approximately 0.3 arc seconds.

This reduction ratio could be increased still further by reducing the tilt, with the limit being set by the difference in the wedge angles. The limit with these prisms would be a reduction ratio of approximately 4000 times.

The rotating mounts had fairly small, metal control knobs. To increase the sensitivity large rubber bungs were fixed onto these knobs.

The finished beam steering device is shown in Fig. 2.10.

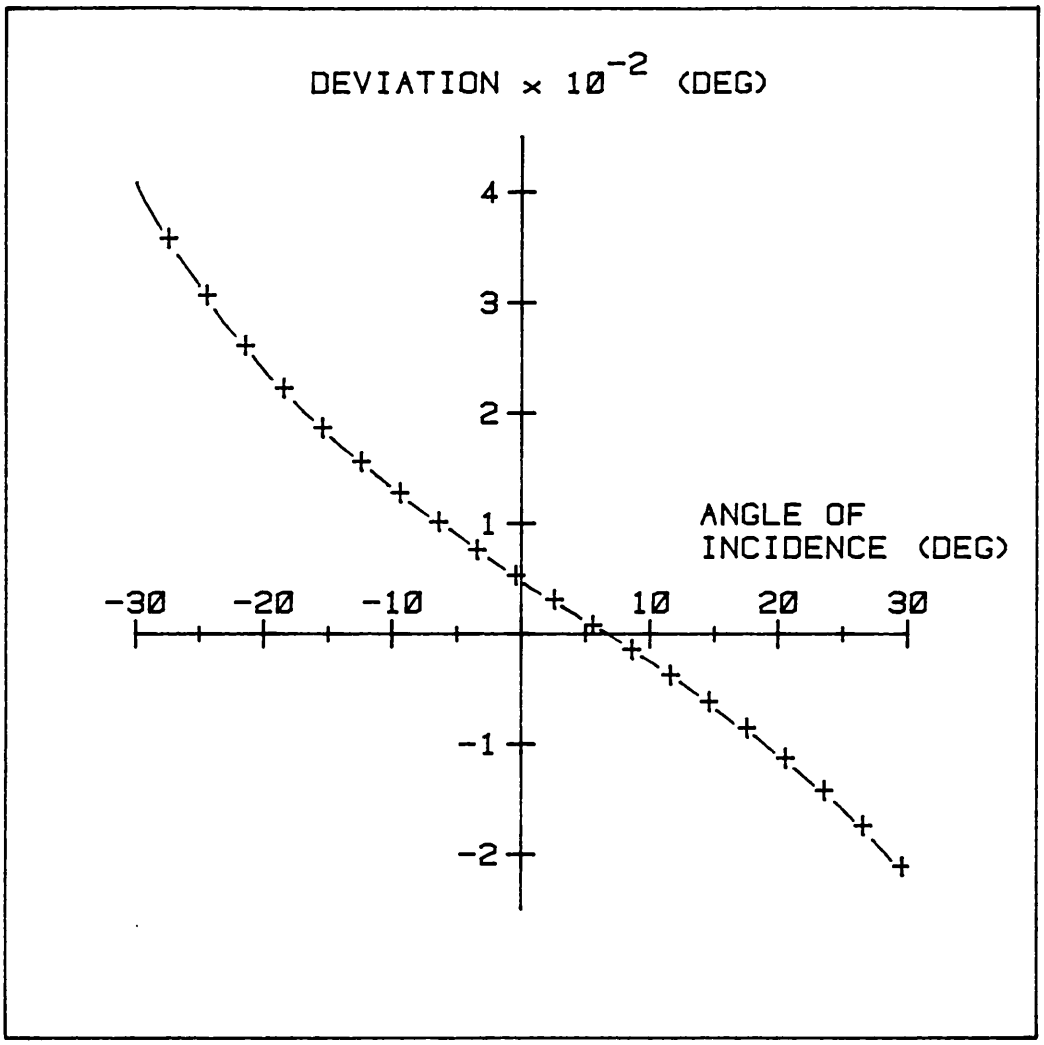

FIG 2.9

EXPERIMENTAL RESULTS FOR THE BEAM STEERING PRISMS.

PRISM WEDGE ANGLES = 5.8 DEGREES MATCHED TO 10 ARC SECONDS

REFRACTIVE INDEX OF PRISMS = 1.515

TILT BETWEEN PRISMS = 0.5 DEGREES

THE SOLID LINE IS THE THEORETICAL RESULT AND THE CROSSES ARE THE EXPERIMENTAL VALUES

FIG 2.10

THE BEAM STEERING DEVICE

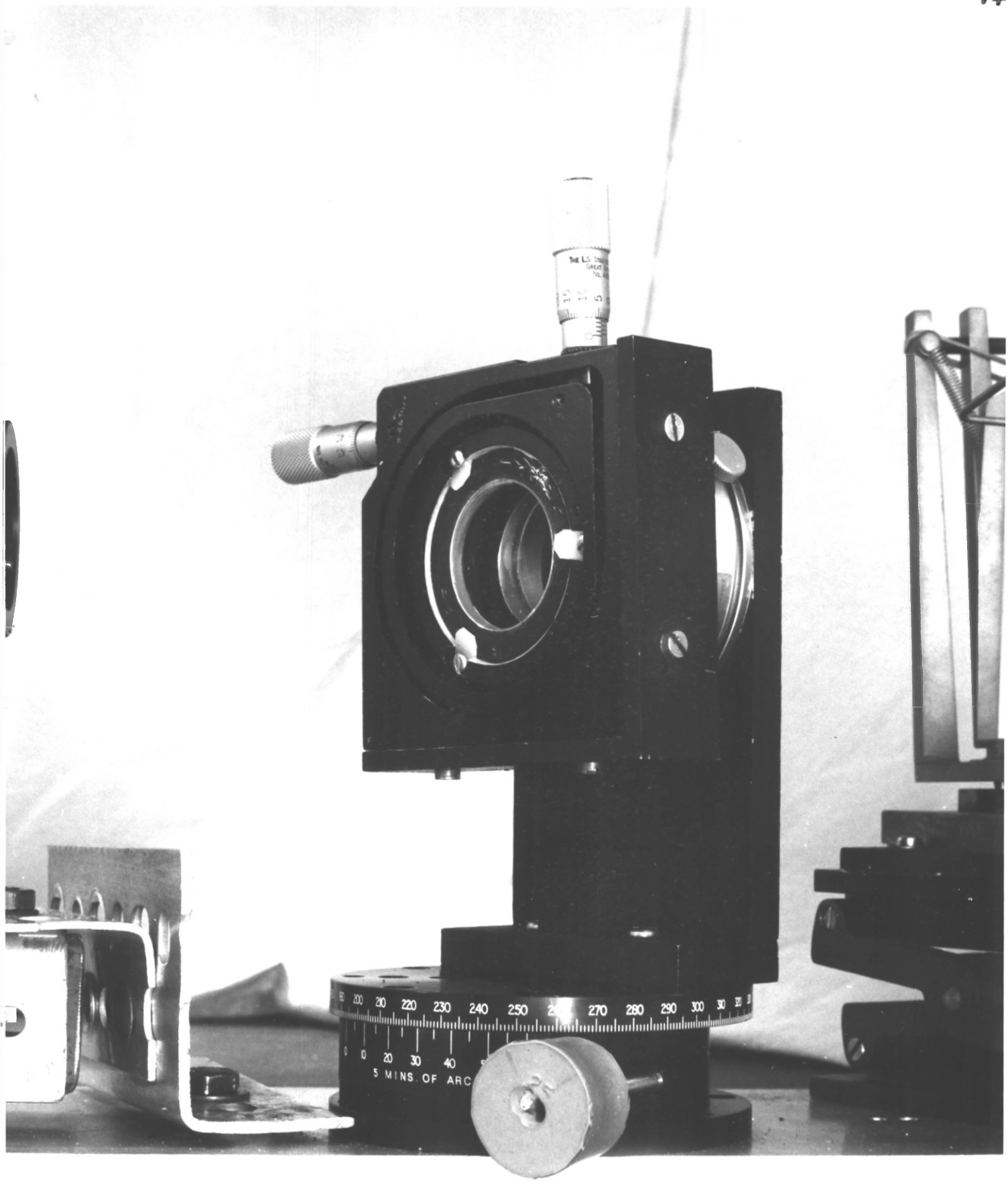
5 MINS. OF ARC

2.1.4. Stability

There was no observable drift of the beam in use, and due to the large reduction ratio, the device is not very sensitive to vibration. To test the long term stability, it was set to a known deviation and left in the laboratory with the usual amounts of noise, vibration and temperature variations. After one week the deviation was checked and, within the accuracy of the auto collimator it was found to be unchanged.

2.1.5. Other properties of the device

The device has two other properties which need to be considered. Namely a sideways shift and phase change of the beam as the prisms are rotated. The sideways shift is of a few mm, but this can be almost eliminated by passing the beam through the prisms twice in opposite directions. The phase change will be several thousand radians. This will be unimportant for many applications and for this interferometer it just means that it is necessary to align the beams first and adjust the phase difference afterwards.

Details of the beam steering device have been published (Lang, 1983), a copy of which is bound at the back of this thesis.

2.1.6. Phase Control

Controlling the phase difference between the two light beams at the output of a two beam interferometer is equivalent to controlling the optical path difference between the two arms of the instrument. This can be achieved in several ways, the most obvious of which is to move one mirror back and forth perpendicularly to one of the beams. Mechanical translation devices are limited in stability and resolution (around 1μm resolution for a differential micrometer) and reduction mechanisms such as levers can only improve the resolution by a small factor (perhaps 10 or so).

Piezoelectric translation devices are capable of resolutions down to about one nanometer (Spanner and Marth, 1983), but they are expensive and are claimed to have a tendancy to drift over a period of a few minutes. Rotating a plane parallel plate of glass in the light beam by a small angle could possibly provide the required phase resolution but a high degree of parallelism is required for the plate, and the rotation introduces a variable shear which could be inconvenient. The third method is to use a gas cell with variable gas pressure and hence variable refractive index.

All of the above methods suffer from a number of disadvantages. Firstly, only one beam of the

interferometer passes through the device. So all of the optical components need to be of full interferometric quality and are therefore expensive. Secondly, in the case of piezoelectric devices and gas cells a lot of bulky and expensive equipment is required outside the interferometer to control them.

These methods will work with many types of interferometers, however, when polarization interferometers are used other, and often more convenient, methods are available. These methods are based on the fact that the two beams are identified by their orthogonal polarization states and hence may be manipulated independently of each other outside the interferometer. This is most readily achieved using a variable retarder (such as a uniform field compensator or electro optic cell) prior to the beams being separated by a polarizing beam splitter or after they have been recombined. This method has several advantages:- The optical components need not be of full interferometric quality as only the difference in the way the device treats the two polarization states is important. Stability is less of a problem as the mirrors in the interferometer can be rigidly fixed, and as the phase control device is outside of the interferometer, the latter can be made more compact.

Because of these advantages, it was decided that the interferometer to be used for this project should be of the polarization type. Dyson (1970) mentions the use of variable retarders for phase control in two beam interferometers, but he places the retarder after the interferometer so that the beams have been recombined, and the relatively small aperture of the device (usually around 10mm diameter) severely limits the field of view. This project required an interferometer with an aperture of around 25mm diameter, so it was decided to place the variable retarder in the laser beam before the two polarization states are separated by the polarizing beam splitter.

2.1.7. Experimental test of the phase control method

A reversed Babinet compensator (Jerrard, 1951) was used for this project as it was already available, but any type of uniform field compensator could have been used (see Jerrard, 1948). Fig. 2.11 is a photograph of the device*. If electronic control was required, an electro optic retarder such as a Kerr or Pockels cell without polarizers could have been used.

---

* Manufactured by the Precision Tool and Instrument Co. (PTI Ltd), Liss, Hants. Catalogue No. 2331

FIG 2.11

THE VARIABLE RETARDER

- A REVERSED BABINET COMPENSATOR

Firstly, the retarder needs to be calibrated, as described by Jerrard (1953) (see Appendix 3 for details). Calibration of the device to be used gave a resolution of (0.1688 ± 0.0004) x 2π radians per mm travel of the micrometer, at a wavelength of 488nm.

To test the principle of the method of phase control the interferometer shown in Fig. 2.12 was set up. Plane polarized light from the laser passes through a half wave plate to rotate the plane of polarization so that, combined with a calcite wedge, it acts as a variable ratio beamsplitter. A phase difference is introduced by the compensator before the polarization states are separated by the calcite wedge. The beams then pass through a Mach Zehnder interferometer with two cardboard baffles to block off the two unwanted beams. After being recombined, the beams pass through a linear polarizer (polaroid) to make the fringes visible. A 35μm pinhole selects a small region of the fringe pattern and the light passing through it is detected by a photomultiplier.

The interferometer was operated with an unexpanded laser beam. At first, it might seem obvious to magnify the fringe pattern at the output before detection, so as to increase the resolution, but doing this would decrease the amount of light passing through the pinhole, and

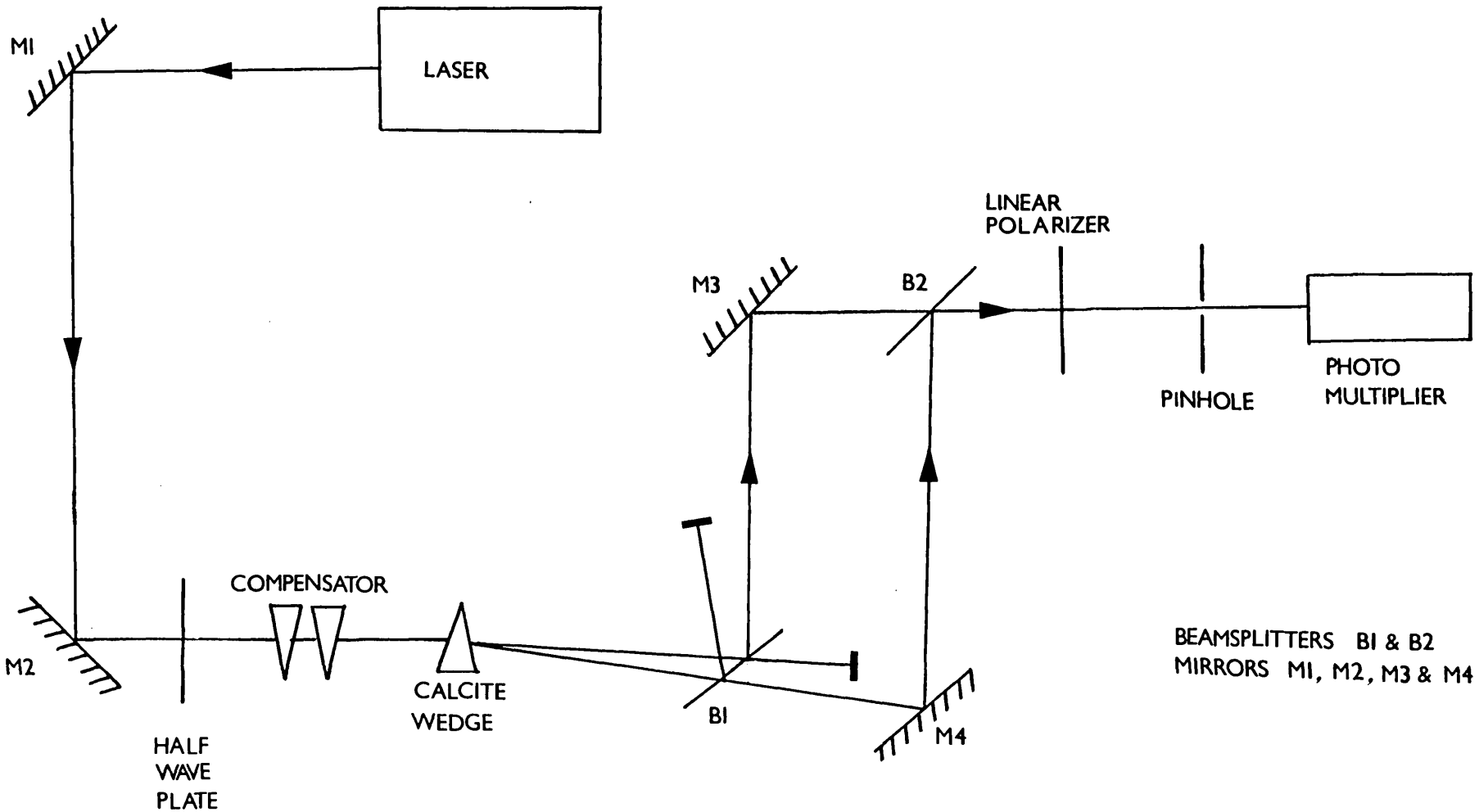

FIG 2.12
EXPERIMENTAL ARRANGEMENT USED TO TEST THE METHOD OF PHASE CONTROL

since the laser was operating at a fairly high output level, the pinhole would have to be made larger by a similar factor to get the same output signal from the detector.

The inteferometer was adjusted to give straight fringes across the output of approximately 2mm spacing. The compensator setting was then slowly changed and the fringes moved across the pinhole due to the changing phase difference between the two beams. Fig. 2.13 shows the photomultiplier output signal which, over the range of intensities encountered, is proportional to the detected intensity, plotted against the compensator setting. This is approximately a plot of fringe profile and has approximately the form of a sine curve, as shown by the sine curve fitted to the data. The curve does not go down to zero due to a number of factors.
The main reason is probably due to an intensity mismatch between the two beams, but the finite pinhole size, scattered light and stray light due to reflection all make contributions to the background signal. There is a certain amount of scatter in the data points about the sine curve due to small vibrations in the system and as the result of using an elderly photomultiplier with a low intensity signal.

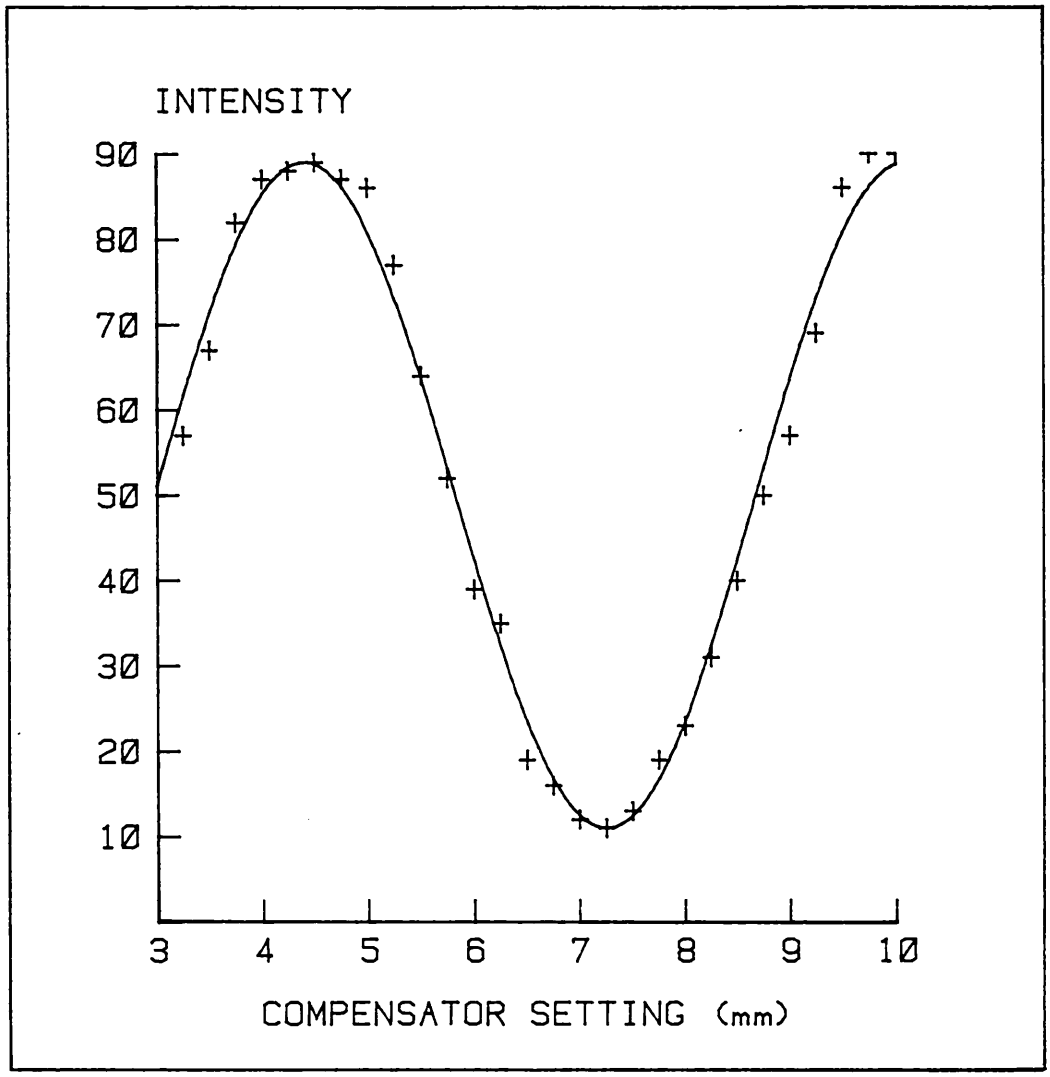

FIG 2.13

PHOTOMULTIPLIER OUTPUT FOR THE PHASE CONTROL TEST

The period of the sine curve suggests a slightly different calibration result to that of the full calibration described in Appendix 3. This is due to a slight drift of the Mach Zehnder interferometer used for the test, during the collection of one set of results.

Allowing for these equipment limitations, these results suggest that the required phase resolution of approximately ±5 degrees is achievable.

2.1.8. Amplitude control

There are many ways of controlling the relative amplitudes of the light beams in a two beam interferometer. In many cases one of the most convenient is to use a variable ratio beamsplitter. This can take several forms, the most common of which is a glass plate with a beamsplitter coating whose reflection coefficient varies with position. An adjustable mount provides control of the beam amplitudes. Bertani et al (1983) describe a beamsplitter based on frustrated total internal reflection which may be better for many applications.

If polarization division is being used, the simplest method of achieving such a beamsplitter is to use a

linearly polarized light source, followed by a half wave plate and a polarizing beamsplitter such as a birefringent prism (see for example Ball, 1982). The half wave plate rotates the plane of polarization and hence changes the relative amplitudes of the two orthogonal polarization components separated by the prisms. Ordinary small rotating mounts would give amplitude control of around $\frac{1}{4}$ of a per cent which is high enough for this application.

2.1.9. Half wave plates

There are two main types of high quality half wave plates. Multiple order plates have a retardation of (n x 360) + 180 degrees where n is an integer, i.e. a whole number of waves plus half a wave. Single order plates are made from two multiple order plates sandwiched together so that the whole wave retardations cancel leaving a total retardation of only 180 degrees. Single order plates are less sensitive to tilting and thermal expansion than multiple order plates, but they are much more expensive due to their being more difficult to manufacture.

With care, the multiple order plates meet the requirements for this project and so this type was chosen.

2.2 The final form of the interferometer

2.2.1 The components

Once the methods for controlling the various parameters of the light beams had been decided upon, the next problem was to decide on the types of components to use and the layout of the interferometer. The system was to be built to use the Fourier transform lenses and other equipment described by Harnett (1980), which imposed a number of limitations on the dimensions of the instrument.

All of the possible arrangements of the interferometer have a number of features in common. These are:- a laser light source followed by a half wave plate and a variable retarder for control of the relative amplitudes and phase difference, a polarizing beamsplitter to separate the two orthogonally polarized beams, and a second beamsplitter to recombine the beams after they have passed through the object and the compensating aperture. Somewhere prior to the object and compensating aperture, both beams must be expanded to greater than 25mm diameter, the polarization state in one arm of the interferometer must be converted to match that in the other arm to enable destructive interference to take place when the beams are recombined, and the beam steering device must be added to steer one beam.

The various possible layouts for the interferometer fall

into two groups. The first group uses a beam expander between the variable retarder and the polarizing beamsplitter. This eliminates problems due to beam expander aberrations as both beams are expanded by the same optical components. However, the aperture of the beam steering device must be larger than the object aperture to allow for vignetting at large angles of incidence. Also the second half wave plate and the polarizing beamsplitter must both have apertures at least as large as the object aperture. The only large aperture polarizing beamsplitters currently available are of the thin film type (see for example Banning 1947 and Buchman et al 1971), which have low efficiency compared to the birefringent types. These features would also make the interferometer extremely expensive and although expense may not be a major factor in a high quality system, the available funds for this project were limited.

In the other group of possible layouts most of the manipulations of the light are performed on unexpanded laser beams, expanding them just prior to passing through the object transparency and compensating aperture. In this case the optical and mechanical components need not be very large and the polarizing beamsplitter can be a birefringent prism (see for example Shurcliff 1962, Vats and Miles 1977 and Machewirth 1979). Because of these advantages it was decided to use this type of layout.

Most commercially available birefringent beamsplitters are made from two prisms cemented together. A simpler and cheaper design is to use a wedge of birefringent material. This can introduce an angular separation between the two orthogonally polarized beams of several degrees, but both beams will be deviated by a large angle, although this is unimportant for the current application. The prism chosen was a calcite wedge of apex angle 30 degrees which produced an angular separation between the beams of approximately 10 degrees.

After the beams have passed through the transparency and compensating aperture, they have to be recombined. A non polarizing beamsplitter is best for this as it provides a second output beam to use as an aid for alignment of the interferometer.

The beamsplitter used was 60mm diameter, made of BK7 optical glass, with a 50% dielectric coating on its front surface and a single layer magnesium fluoride anti-reflection coating on its back surface. The surfaces were flat to $\lambda/10$ over 60mm.

A single layer magnesium fluoride anti-reflection coating has a lower reflection coefficient for the p polarization than for the s polarization (see the table below), so the output beams of the interferometer were

chosen to be p polarized.

Intensity reflection coefficient of the back surface of the beamsplitter

		Uncoated	Coated with a single layer MgF_2
Polarization	S	0.097	0.037
	P	0.0094	0.00092

The main problem with this type of layout is that a pair of beam expanders are required whose aberrations match to within approximately $\lambda/15$. There are three main ways to expand a laser beam, the most obvious of which is to use lenses in the form of a telescope. Unfortunately, lenses of the required quality were not available with reasonable size and cost.

The second way is to use prisms (see for example Hammer, 1982). These are normally used to produce beams with elliptical cross sections, but by using two such devices it is possible to produce beams with circular cross sections. To use this method several high quality prisms would be required for each beam, and stability of the device could be a problem.

The third way is to use paraboloidal mirrors. These

are available with high quality surfaces at reasonable cost, and so this method of beam expansion was chosen.

A summary of the layout is shown in Fig. 2.14. Light from the laser passes through a half wave plate, a variable retarder and a calcite wedge to provide amplitude and phase control. One of the beams emerging from the calcite wedge passes through a second half wave plate to rotate the plane of polarization by 90 degrees and enable the beams to destructively interfere when they are recombined.

The other beam passes through the beam steering prisms. Both beams are expanded using microscope objectives and a paraboloidal mirror and one beam then passes through the input transparency, in a liquid gate to eliminate phase irregularities, whilst the other beam passes through the compensating aperture. The beams are then recombined by a non polarizing beamsplitter before passing through the Fourier transform lens which forms the final output.

2.2.2. Fixing the optical components into their mounts

Most commercially available mounts use some form of clamp to hold the optical components in place. This is convenient

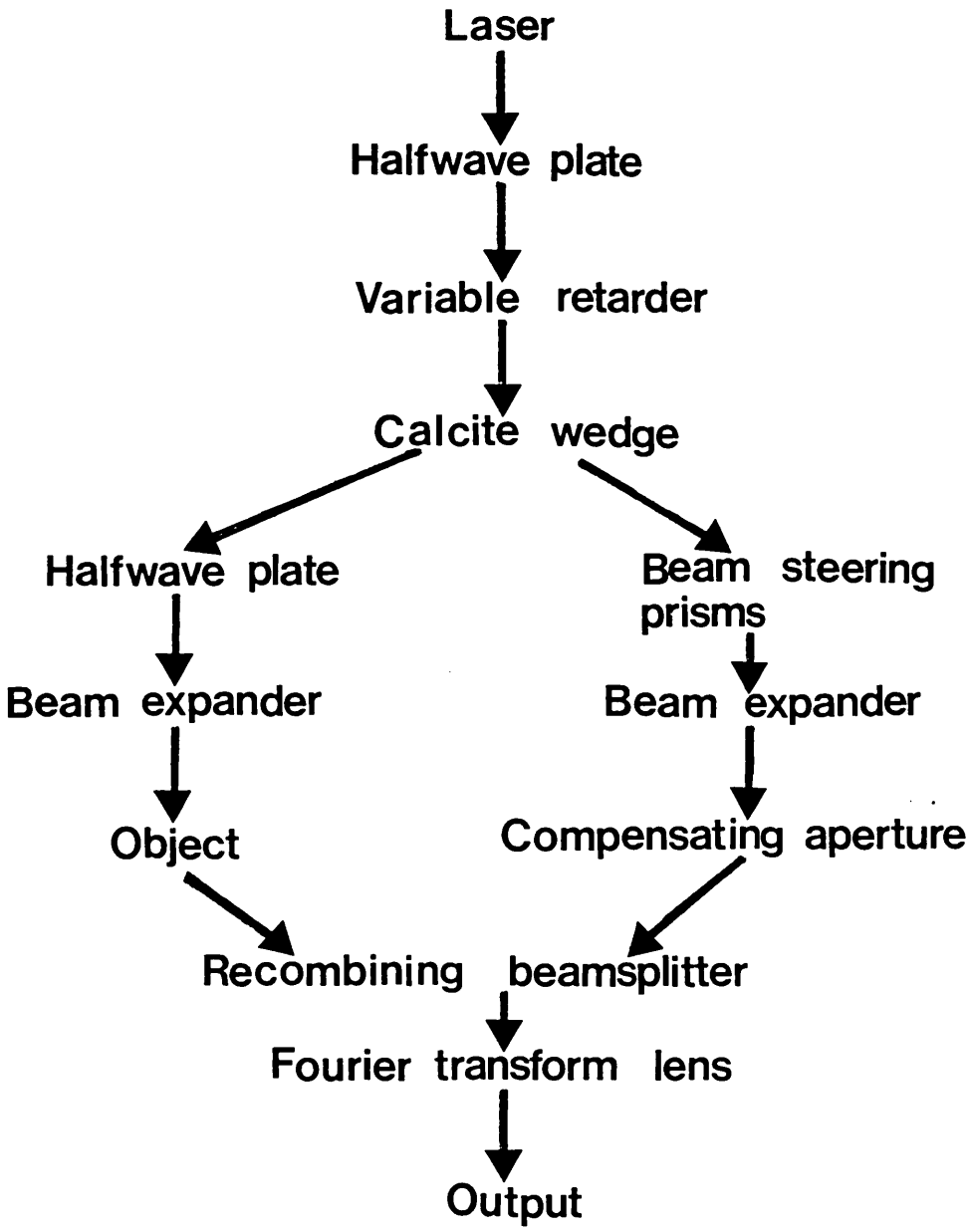

FIG 2.14

SCHEMATIC LAYOUT OF THE INTERFEROMETER

and allows for rapid changing of the components but the clamps are liable to distort the optical surfaces.

The components of the interferometer need to fixed rigidly into their mounts, but allowances have to be made for the differential thermal expansion between the glass and the metal surround, which could also distort the components.

It was considered that the best solution was to glue the components into their mounts using a slightly elastic cement to allow for any stresses. The best cement found by earlier workers at the Imperial College Optics Group was Scotchweld E.C. - 2216 B/A (Carnell et al, 1974). This is a two part cement which mixes to form a grey viscous paste that cures at room temperature. Sufficient rigidity to hold the component in place is achieved within about 6 hours of mixing, but about 7 days (at 24^{o}C) are required for it to obtain its full strength The fully cured cement retains a slight elasticity which takes up the differential expansion between the glass and its mount. For a glass component a gap of 100μm per 50mm glass diameter produces negligible stress on the glass, so all of the mounts allowed for gaps of this size.

2.2.3. Effects of the environment

All components distort under the influence of external stresses. In an interferometer, movements of the components, air currents and temperature gradients can all have a very large effect on the interference patterns and part of the 'art' of interferometry is to reduce these effects to an acceptable level.

There are many ways of achieving this (see for example Dyson, 1965 and 1968) with varying degrees of success. Methods of reducing the effects of the major types of disturbances will now be considered.

(a) Air currents

Probably the best way to reduce air currents is to cover all the light paths and isolate them from the outside world, leaving as little open space around the optics as possible. Usually this is done by making a cover large enough to go over the whole instrument, but this still leaves room for air to circulate inside the cover. It was considered to be better for this application to build the cover in several parts. Each part formed a tunnel enclosing the apparatus and light paths, but leaving as little open space for air to circulate as possible. The covers were made from expanded polystyrene which also provided some thermal insulation.

The laser used on the Imperial College spatial filtering bench is a Lexel air cooled argon ion laser. This puts out a jet of hot air which had to be deflected away from the apparatus with large sheets of card.

(b) Temperature gradients

This was not considered to be a major problem, provided the hot air from the laser was deflected away from the interferometer, and time was allowed for the room temperature to stabilize.

(c) Vibration and movement of the inferometer

This is a major problem with nearly all interferometers and can be approached from two directions. Namely to reduce the amount of movement of the optical components or to make the effects of any movements on the final fringe pattern as small as possible.

The former method generally requires the interferometer to be very solidly built, and using mounts with as few degrees of freedom of movement as possible, whilst still leaving enough adjustments for alignment purposes. Movements due to thermal expansions can be greatly reduced by using materials with low thermal expansion coefficients

such as Invar and Zerodur, but these materials tend to be expensive.

Most of the components to be used for this interferometer required an optical axis 65mm above the base plate. Unfortunately, the paraboloidal mirror and beam steering prisms required a higher optical axis. Therefore it was decided to raise the other components above the main bench on a metal plate, bolted onto a heavy milling machine table. The weight of the unit provided sufficient friction to make bolting it to the main bench unnecessary.

To try and isolate the interferometer from vibration transmitted through the building, the main optical table was supported by partially inflated motorcycle inner tubes.

Reducing the sensitivity of the output fringes to movements of the optical components is a more difficult task. One way is to use the same optical components for both beams. Thus any small movements of the components will affect both beams equally and the output fringe pattern will be unchanged. Several of the components on this interferometer were of this type. Another way is to use optical components which are insensitive to small movements. Probably the best known of this type of component is the retroreflector, consisting of either three plane mirrors at right angles to one

another, or a corner cube prism. These are immune to the effects of small angular movements, and interferometers in which they are used instead of plane mirrors tend to be very stable (see for example Dyson, 1965).

In this interferometer, the light beams must only pass through the transparency and compensating aperture once. So to prevent overlap of the incoming and outgoing beams at the retroreflector, and to allow space for mechanical mounts, replacing mirrors by retroreflectors would require components with apertures of about three or more times the required beam diameter. Also, retroreflectors can change the polarization state of light passing through them. Therefore the idea of using retroreflectors was abandoned. The prism beam steering device was very insensitive to the effects of vibration and required quite a large knock to produce a noticeable effect on the interferometer output fringes.

2.2.4. The layout

Once all of the components and their mounts had been chosen the next thing was to decide on the exact layout of the device. There were two main constraints. Firstly the path lengths had to be kept as small as possible to reduce the effects of air currents. Secondly, the coherence length of the laser was only a few cm, so the optical path lengths

needed to be approximately equal for the two beams.

Before construction the layout was planned using cardboard cutouts of the optical and mechanical components with thin thread to represent the light beams. This method was fairly accurate, and when the device was asembled only small position adjustments were required.

The final layout is shown in Fig. 2.15. Light from the argon ion laser (λ = 488nm) passes through the first half wave plate to control the relative amplitudes of the two orthogonal polarization states. The reversed Babinet compensator introduces a controllable phase difference between the two polarization states which are then separated by the calcite wedge. An aluminised prism separates the beams still further. One beam is double passed through the beam steering prisms using a beam-splitter and mirror. The other beam passes through the second half wave plate to rotate its plane of polarization by 90 degrees and enable destructive interference to take place when the beams are recombined.

Both beams are then expanded by the spatial filter units which each consist of a 10x microscope objective and a 5μm pinhole. Two mirrors with a slight angle between them direct the beams onto a paraboloidal mirror. This

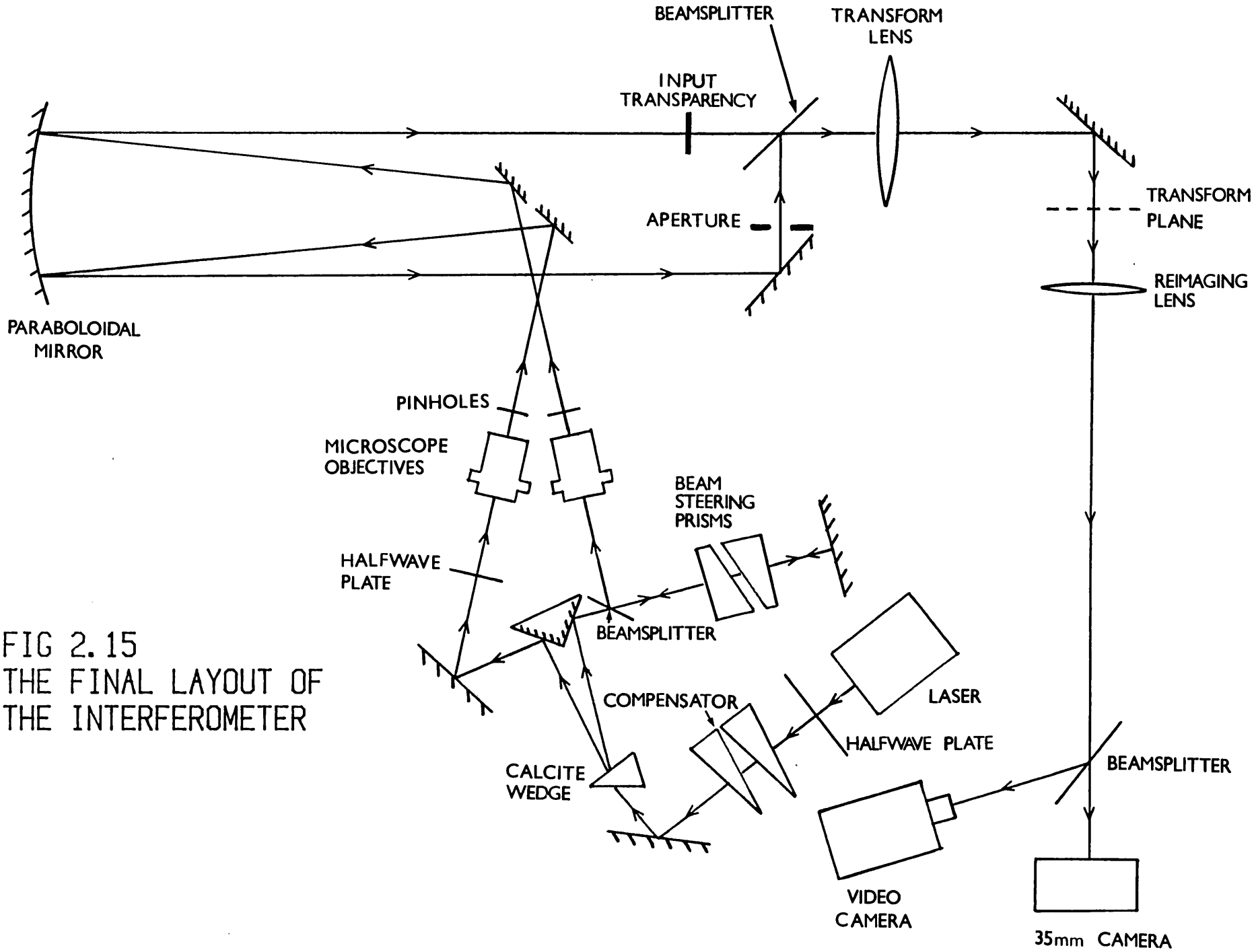

FIG 2.15
THE FINAL LAYOUT OF
THE INTERFEROMETER

collimates the beams and directs them back towards the transform lens. One beam passes through the input transparency in a liquid gate whilst the other is deflected by a mirror and through the clear aperture. The beams are then recombined by a beamsplitter and pass through the transform lens to form the Fourier transform distribution in the transform plane via a plane mirror. A second lens reimages and magnifies the transform plane distribution onto the film plane of a 35mm camera. A beamsplitter directs some of this light into a video camera used for alignment purposes.

Several views of the interferometer are shown in Figs. 2.16 to 2.19.

FIG 2.16

THE MAIN SECTION OF THE INTERFEROMETER

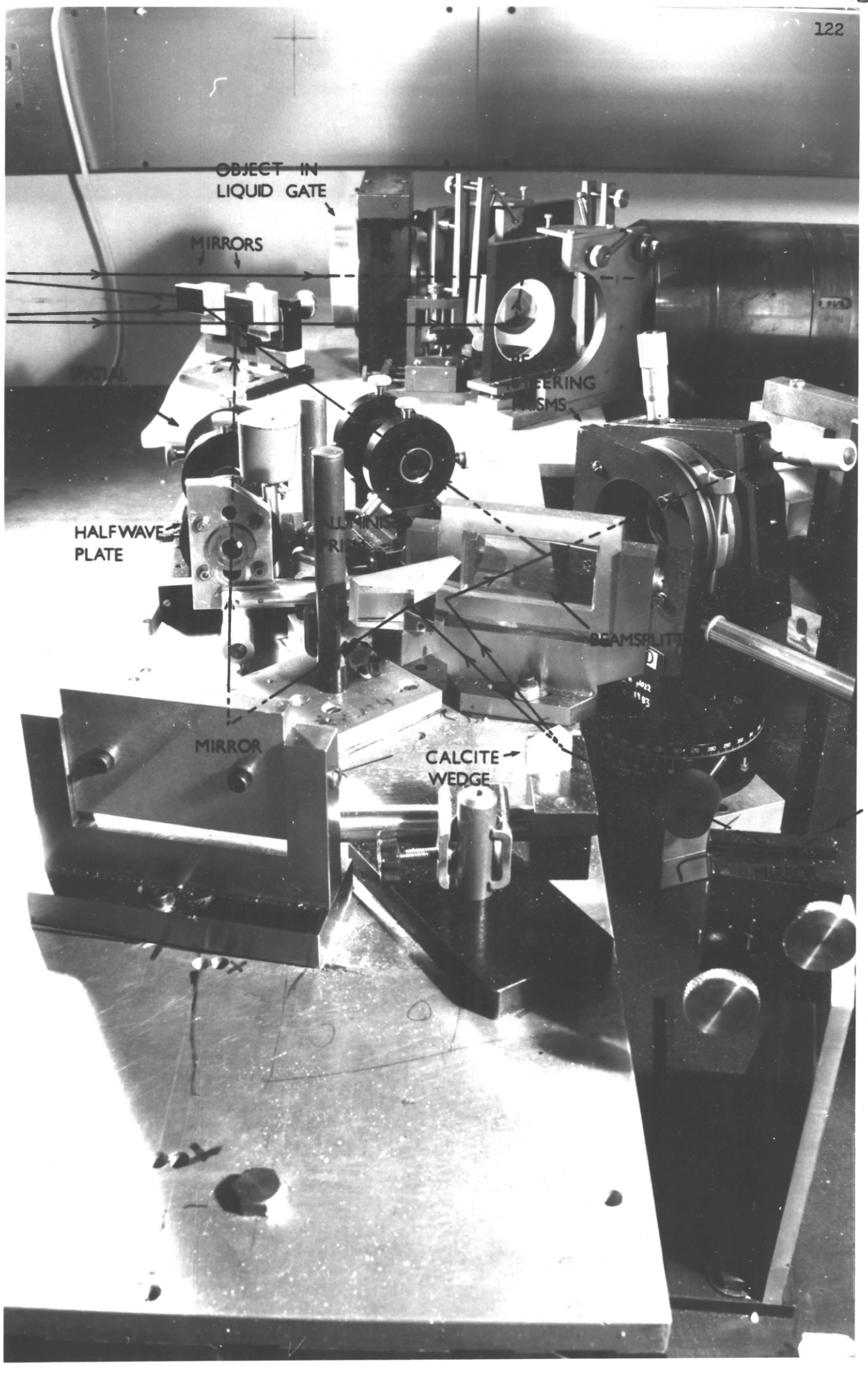
122
OBJECT IN
LIQUID GATE
MIRRORS
HALFWAVE
PLATE
MIRROR
CALCITE
WEDGE

FIG 2.17

THE SPATIAL FILTER UNITS AND THE SECOND HALF WAVE PLATE

0 1 2 3 4 5
MECHS
SEY 62514
GREY

FIG 2.18

THE PARABOLOIDAL MIRROR

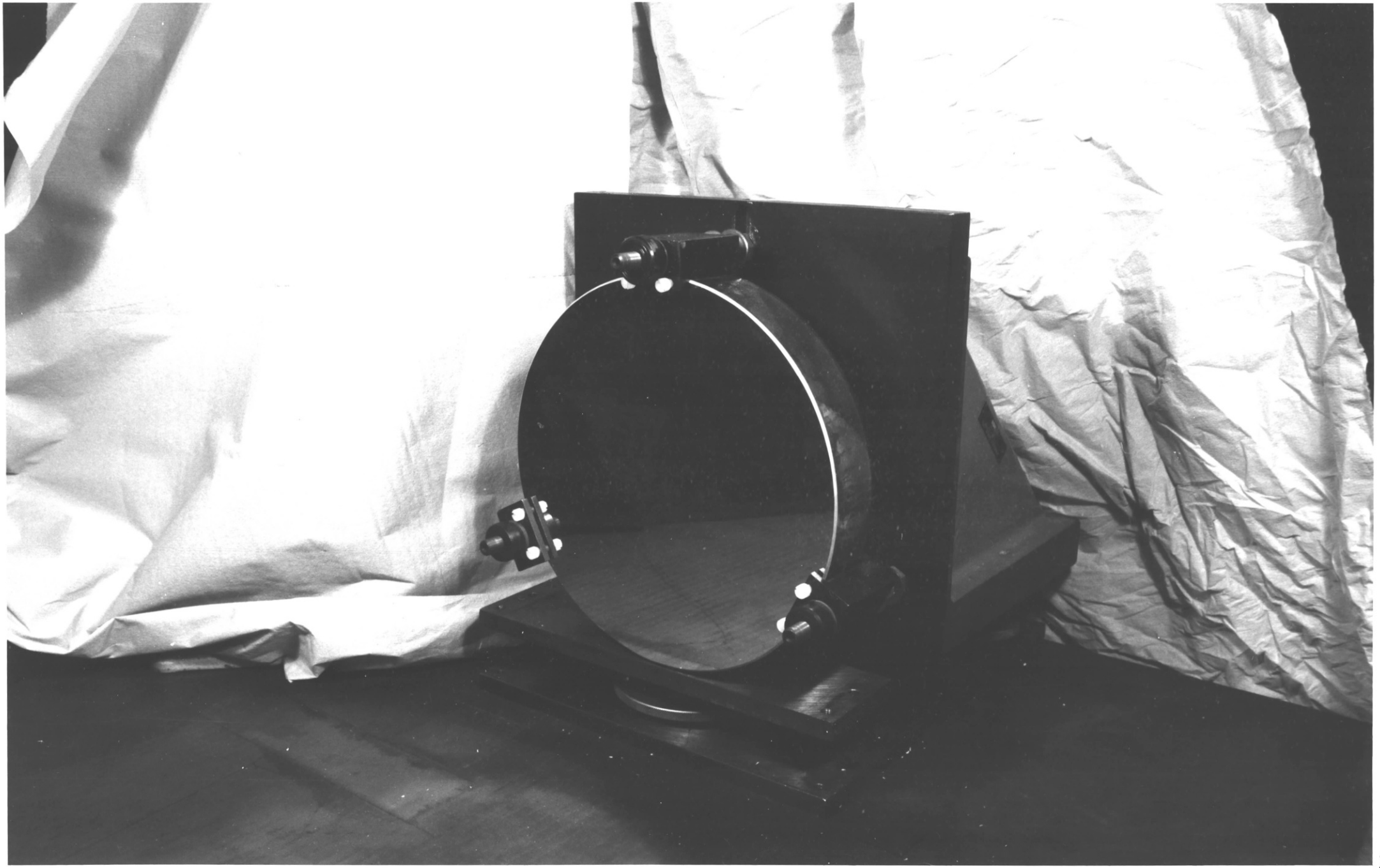

FIG 2.19

THE LIQUID GATE, COMPENSATING APERTURE, RECOMBINING BEAMSPLITTER AND TRANSFORM LENS

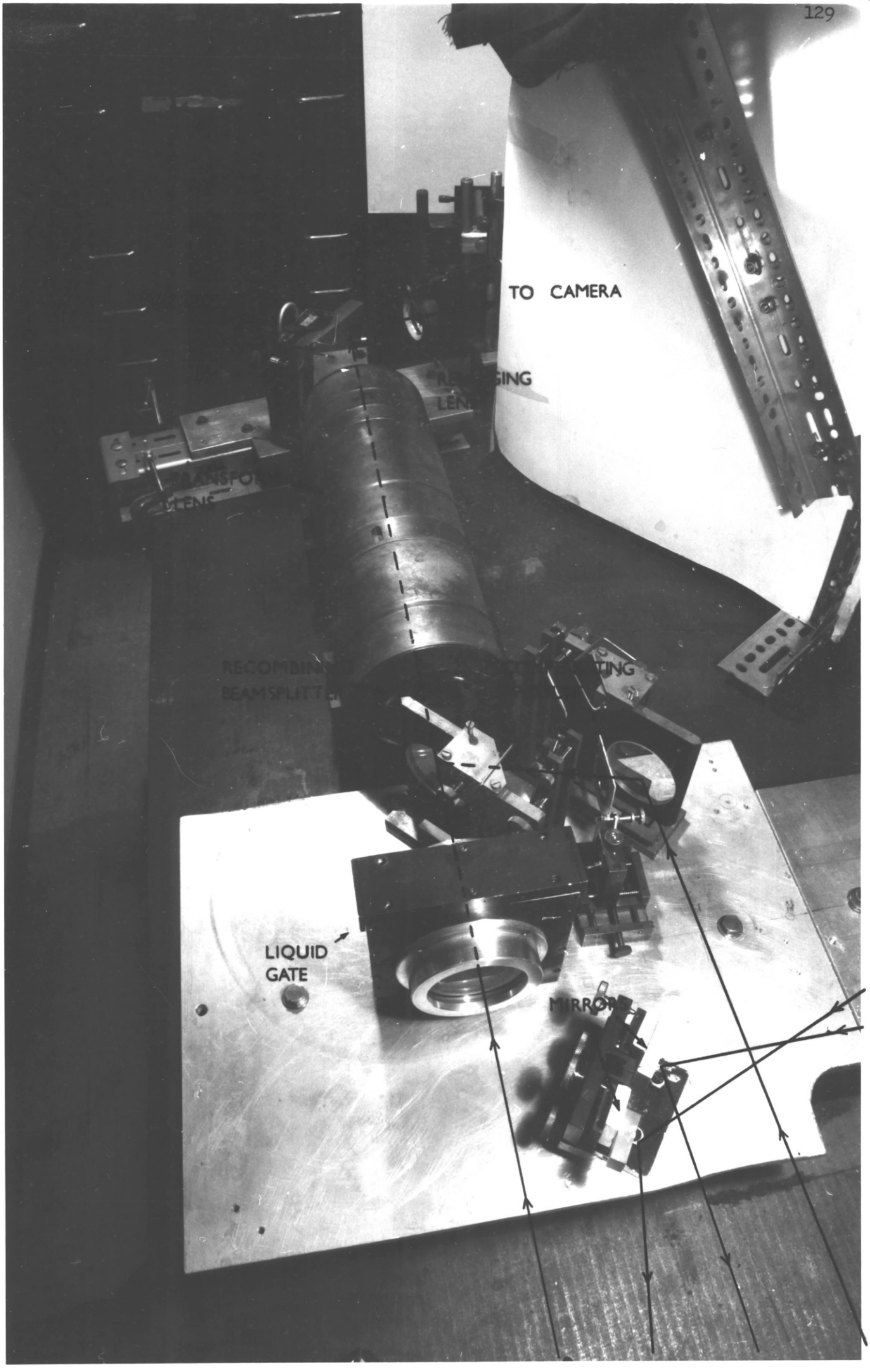
TO CAMERA
LIQUID
GATE

CHAPTER 3

USING THE INTERFEROMETER

3.1. Measuring the state of adjustment of the inteferometer

Once the interferometer had been assembled, and the required adjustment resolutions had been achieved, methods had to be found to monitor the relative amplitudes, phases and alignment of the two beams.

Measuring tilts between plane wavefronts of around half an arc second with a 25mm aperture poses a number of problems as the fringe spacing is about 200mm, although observation of the fringes could be used for rough alignment and techniques using electronic detectors could possibly be used for fine tuning.

A simpler technique is to look at the light distribution in the transform plane. This will consist of two overlapping Airy patterns, with their separation proportional to the tilt between the wavefronts.

Computer calculations were performed to calculate the transform plane distributions for a range of separations relative phases and relative amplitudes for the two Airy patterns. The calculated intensity distributions are plotted so that the area of each square represents the modulus of the amplitude at its centre.

To summarise the results, for separations of about one Rayleigh resolution unit, or less, there are wedge shaped regions of low intensity at right angles to the axis of separation of the two Airy pattern centres. The angle of this wedge tends to increase as the separation decreases, and the distance of the wedge axis from the middle of the pattern roughly indicates the phase difference between the two Airy patterns.

To test these results experimentally, a Mach Zehnder inteferometer was adjusted to give an output consisting of straight tilt fringes. A pinhole aperture was then placed in the fringes, resulting in two Airy patterns in the far field. The phase difference between the Airy patterns is determined by the phase difference between the two beams forming the tilt fringes at the pinhole position, and their separation is determined by the tilt between the wavefronts.

The pinholes available proved to have slight departures from perfectly circular apertures which tended to distort the resulting patterns. Therefore the experimental results shown were taken using the final interferometer and larger apertures. However, the early results suggested that the method worked.

Fig. 3.1 shows the computed light distribution for two Airy patterns with a separation of one Rayleigh resolution unit and a phase difference of 180 degrees.

Figs. 3.2 and 3.3 show the computed results when the separation of the patterns are 0.5 and 0.3 Rayleigh resolution units respectively, still with a phase difference of 180 degrees.

Figs. 3.4 to 3.6 show the experimental results of combining two Airy patterns with the same amplitudes, a phase difference of 180 degrees and three different separations. For relatively large separations the resulting pattern has several lines of bright spots radiating outwards from the centre in a similar way to the interference pattern of two coherent point sources, although with different relative intensities and spacings (Fig. 3.4). As the separation decreases these lines disappear and are replaced by a wedge shaped regions of low intensity (Fig. 3.5) which get wider as the separation decreases further (Fig. 3.6).

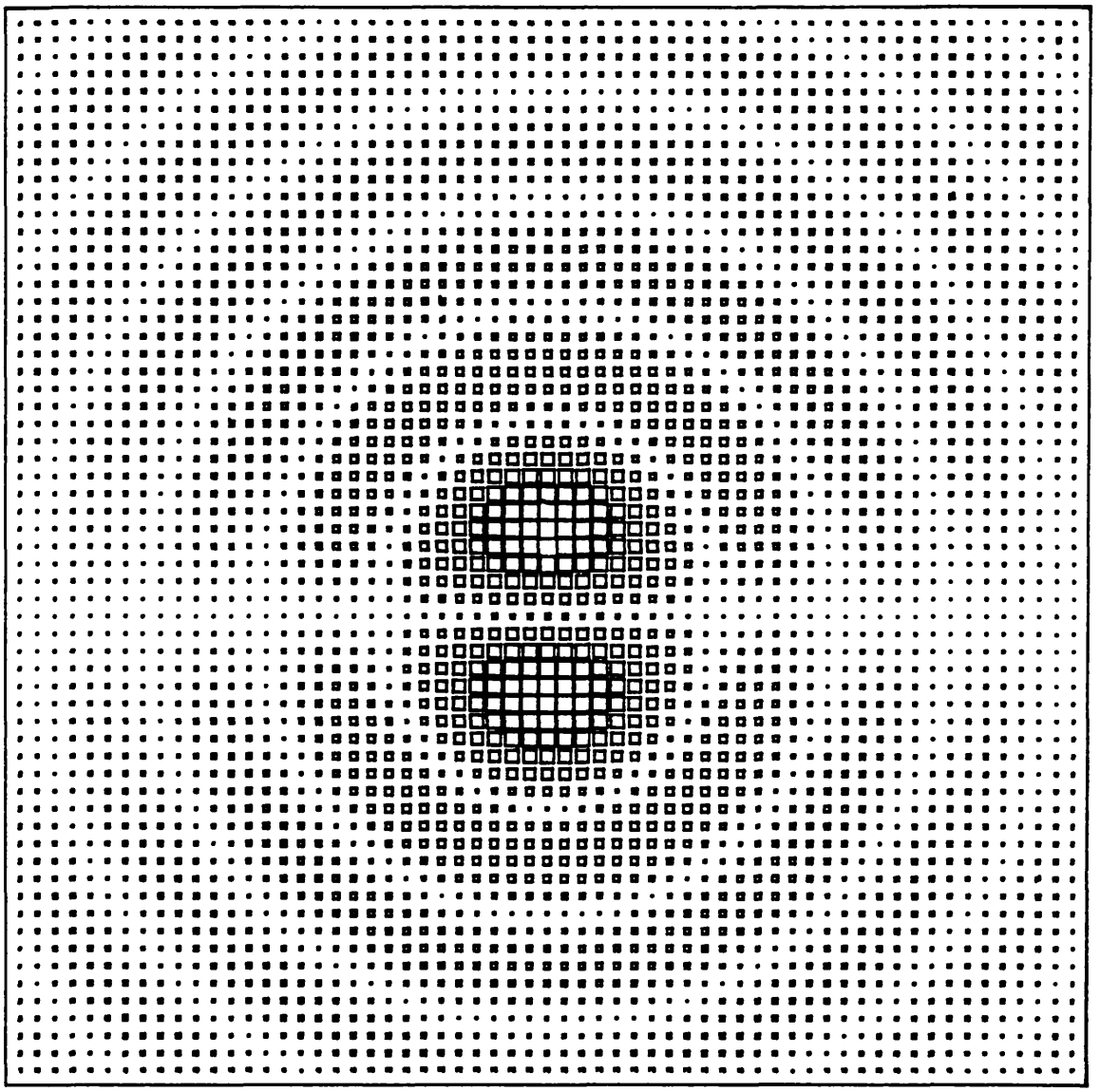

FIG 3.1

COMPUTED TWO DIMENSIONAL INTENSITY DISTRIBUTION FOR TWO AIRY PATTERNS WITH A SEPARATION OF 1 RAYLEIGH RESOLUTION UNIT AND A PHASE DIFFERENCE OF 180 DEGREES

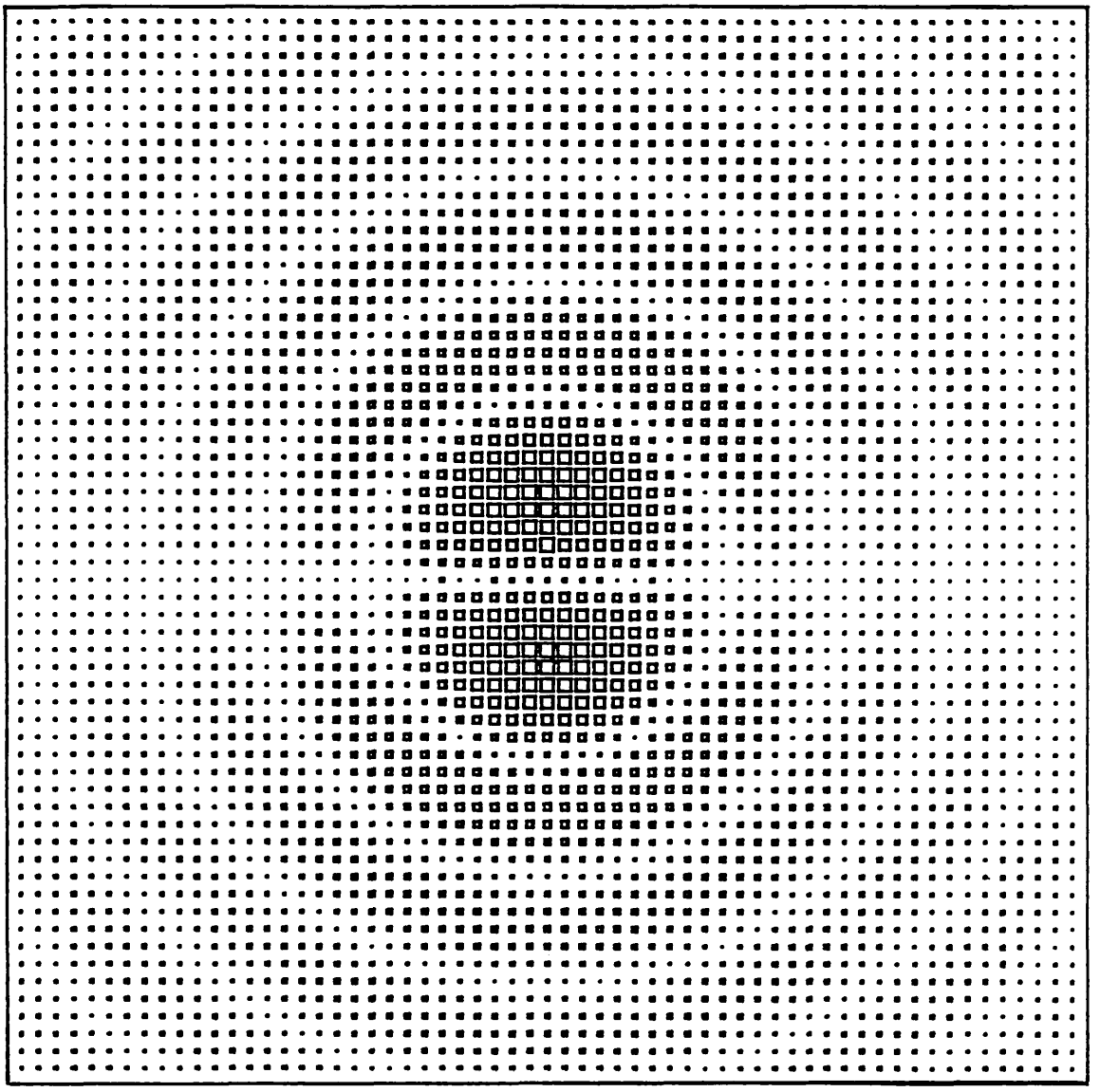

FIG 3.2

COMPUTED TWO DIMENSIONAL INTENSITY DISTRIBUTION FOR TWO AIRY PATTERNS WITH A SEPARATION OF Ø.5 RAYLEIGH RESOLUTION UNITS AND A PHASE DIFFERENCE OF 18Ø DEGREES

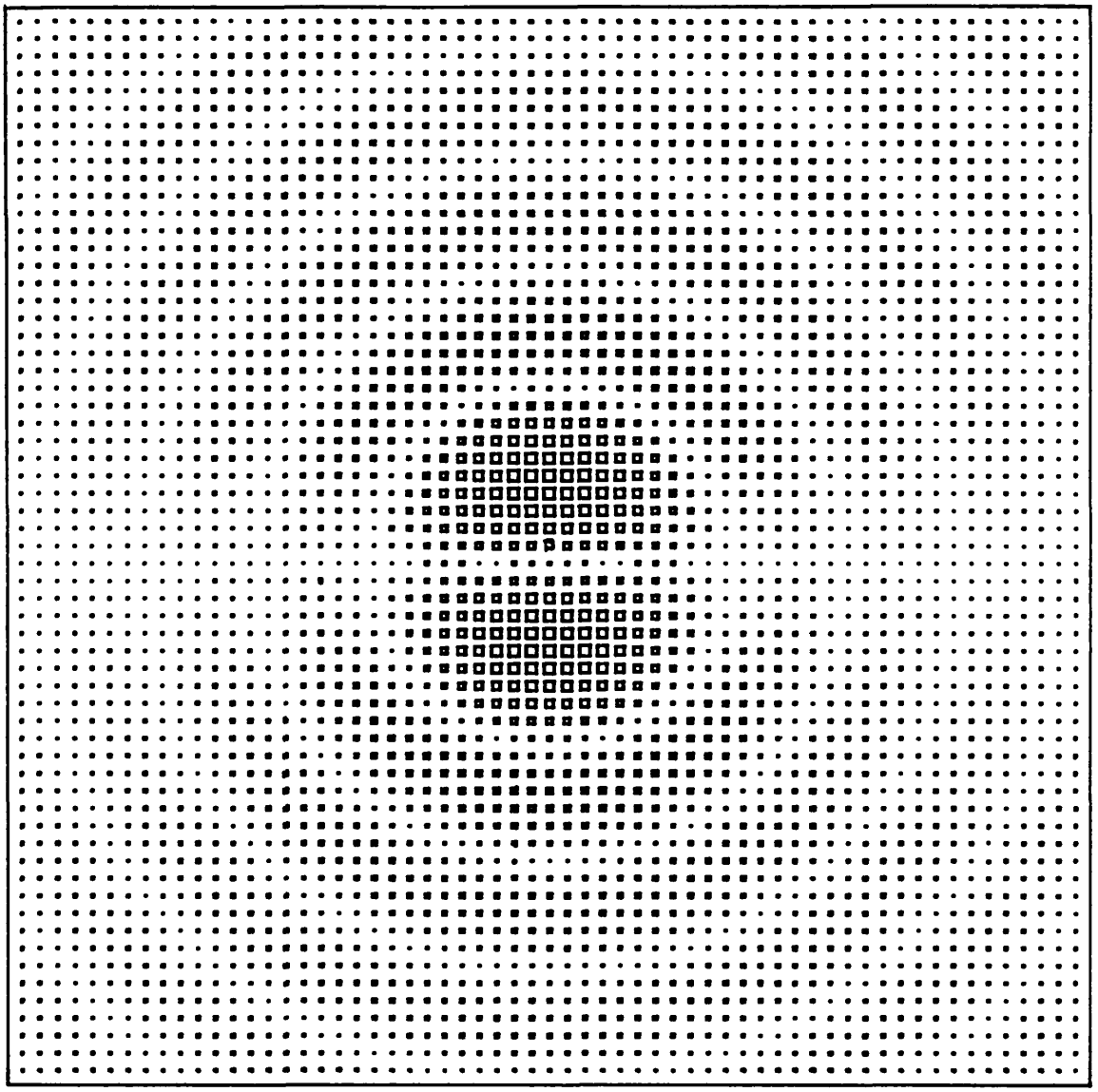

FIG 3.3

COMPUTED TWO DIMENSIONAL INTENSITY DISTRIBUTION FOR TWO AIRY PATTERNS WITH A SEPARATION OF Ø.3 RAYLEIGH RESOLUTION UNITS AND A PHASE DIFFERENCE OF 18Ø DEGREES

FIG 3.4

THE EXPERIMENTAL RESULT OF COMBINING TWO AIRY PATTERNS WITH A SEPARATION OF APPROXIMATELY 3.8 RAYLEIGH RESOLUTION UNITS AND A PHASE DIFFERENCE OF APPROXIMATELY 180 DEGREES

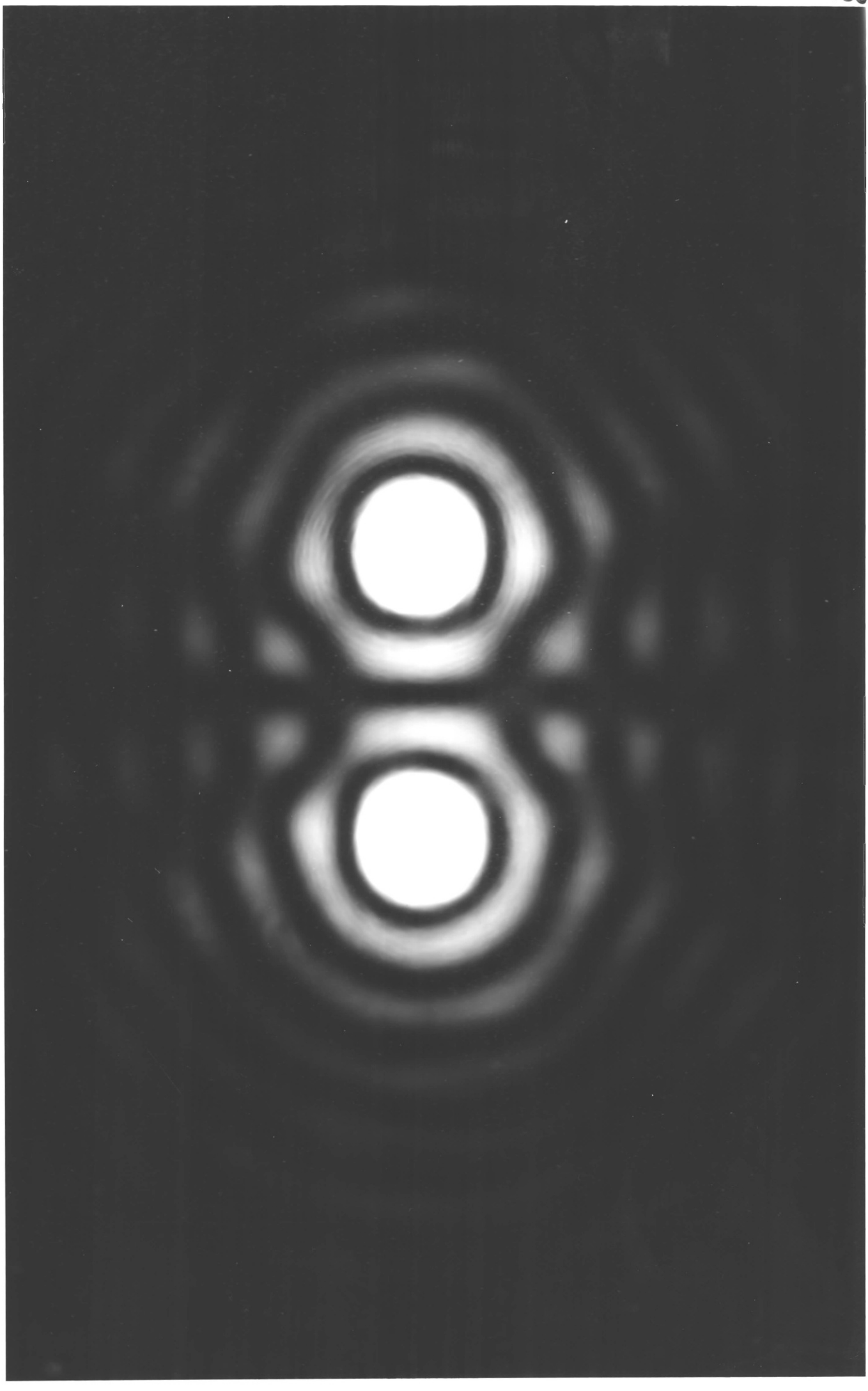

FIG 3.5

THE EXPERIMENTAL RESULT OF COMBINING TWO AIRY PATTERNS WITH A SEPARATION OF APPROXIMATELY 1.7 RAYLEIGH RESOLUTION UNITS AND A PHASE DIFFERENCE OF APPROXIMATELY 180 DEGREES

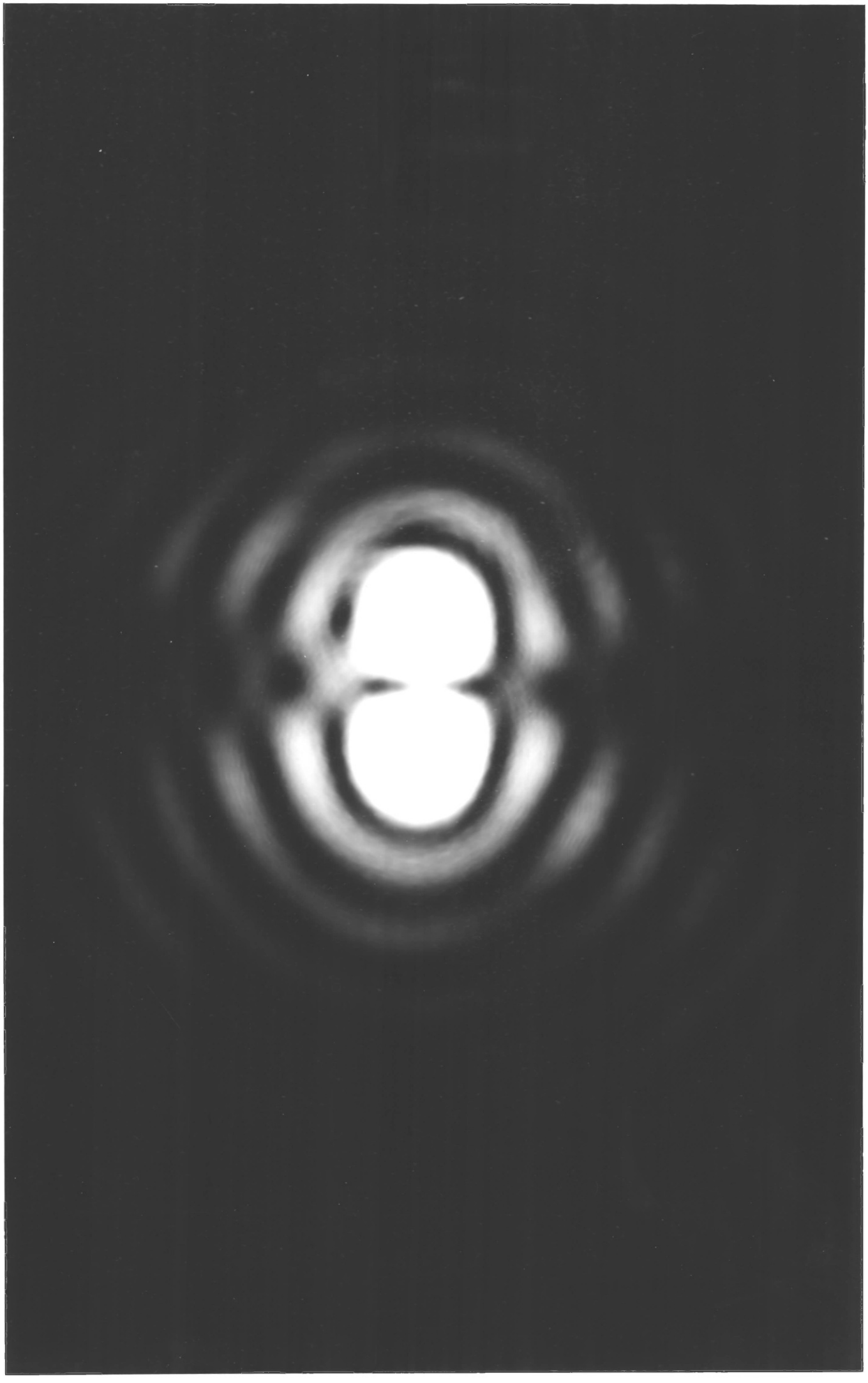

FIG 3.6

THE EXPERIMENTAL RESULT OF COMBINING TWO AIRY PATTERNS WITH A SEPARATION OF APPROXIMATELY 1 RAYLEIGH RESOLUTION UNIT AND A PHASE DIFFERENCE OF APPROXIMATELY 180 DEGREES

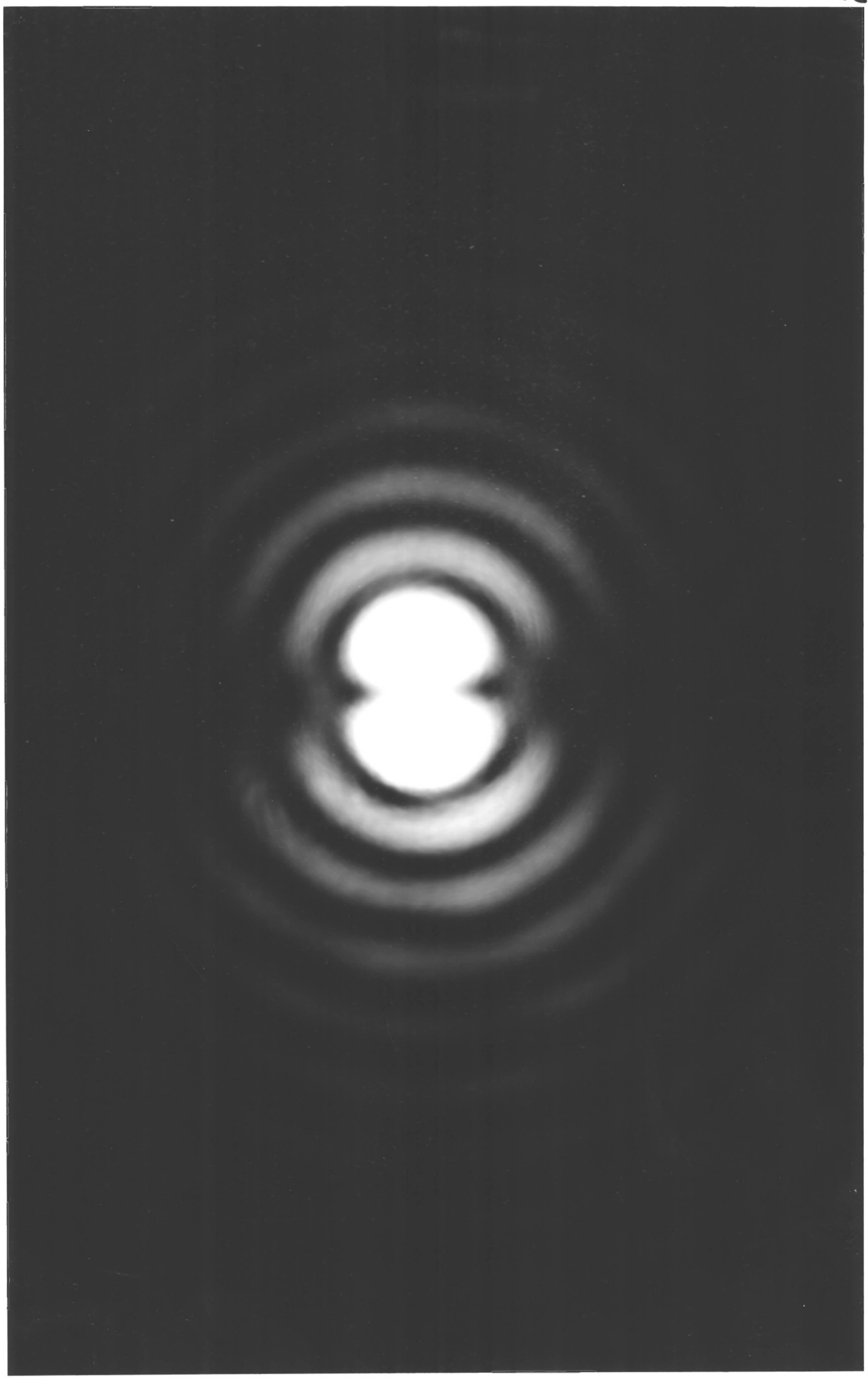

If the two patterns are in phase, the dark wedge shaped region is replaced by a bright region as shown in Fig. 3.7 (this pattern is for the same separation as in Fig. 3.5). If the phase difference between the patterns takes some value other than 0 or 180 degrees, then the wedge shaped regions still appear, but their axis is displaced towards one pattern.

Fig. 3.8 shows the computed light distribution for a separation of 0.1 Rayleigh resolution units and a phase difference of 135 degrees.

FIG 3.7

THE EXPERIMENTAL RESULT OF COMBINING TWO AIRY PATTERNS WITH A SEPARATION OF APPROXIMATELY 1.7 RAYLEIGH RESOLUTION UNITS AND A PHASE DIFFERENCE OF APPROXIMATELY ZERO

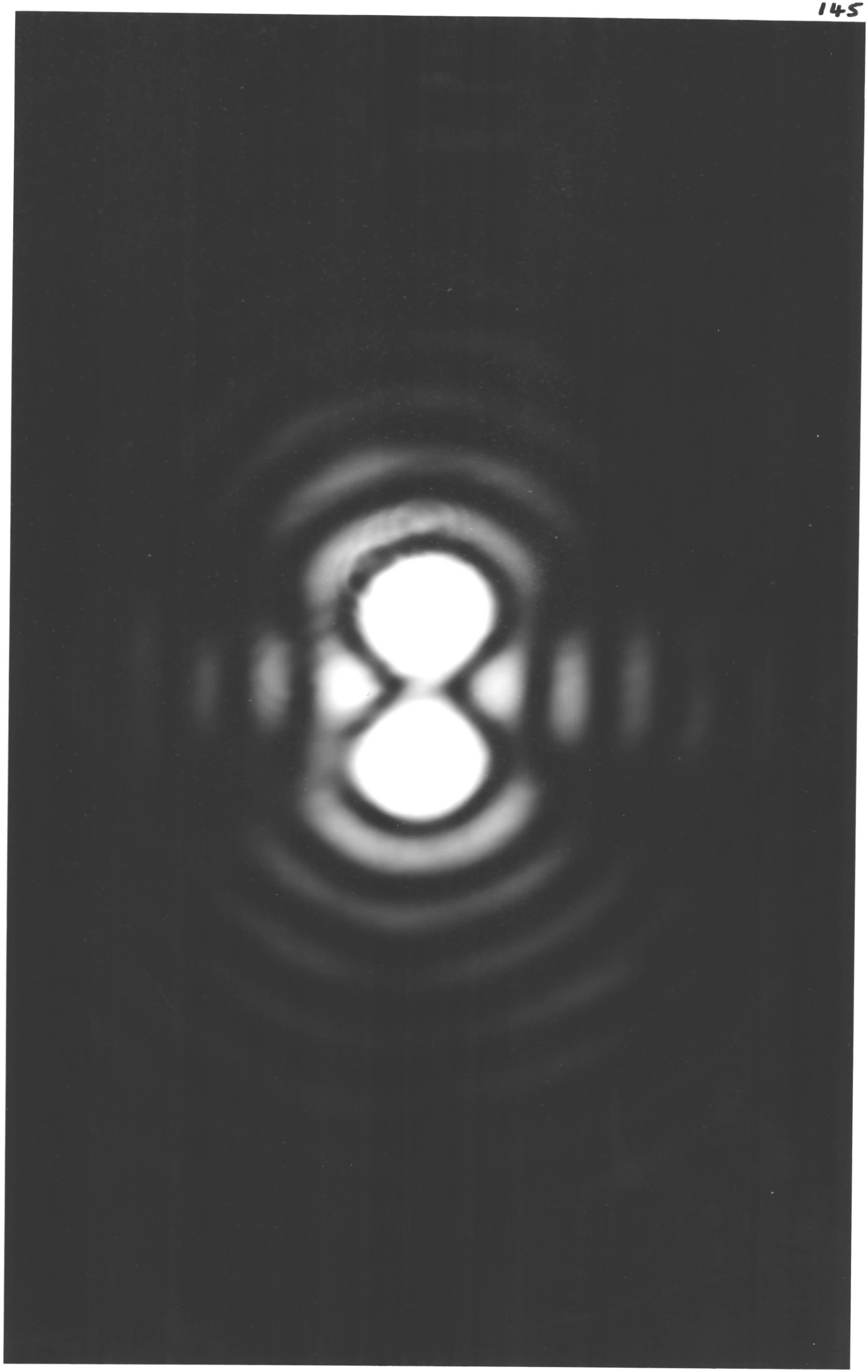

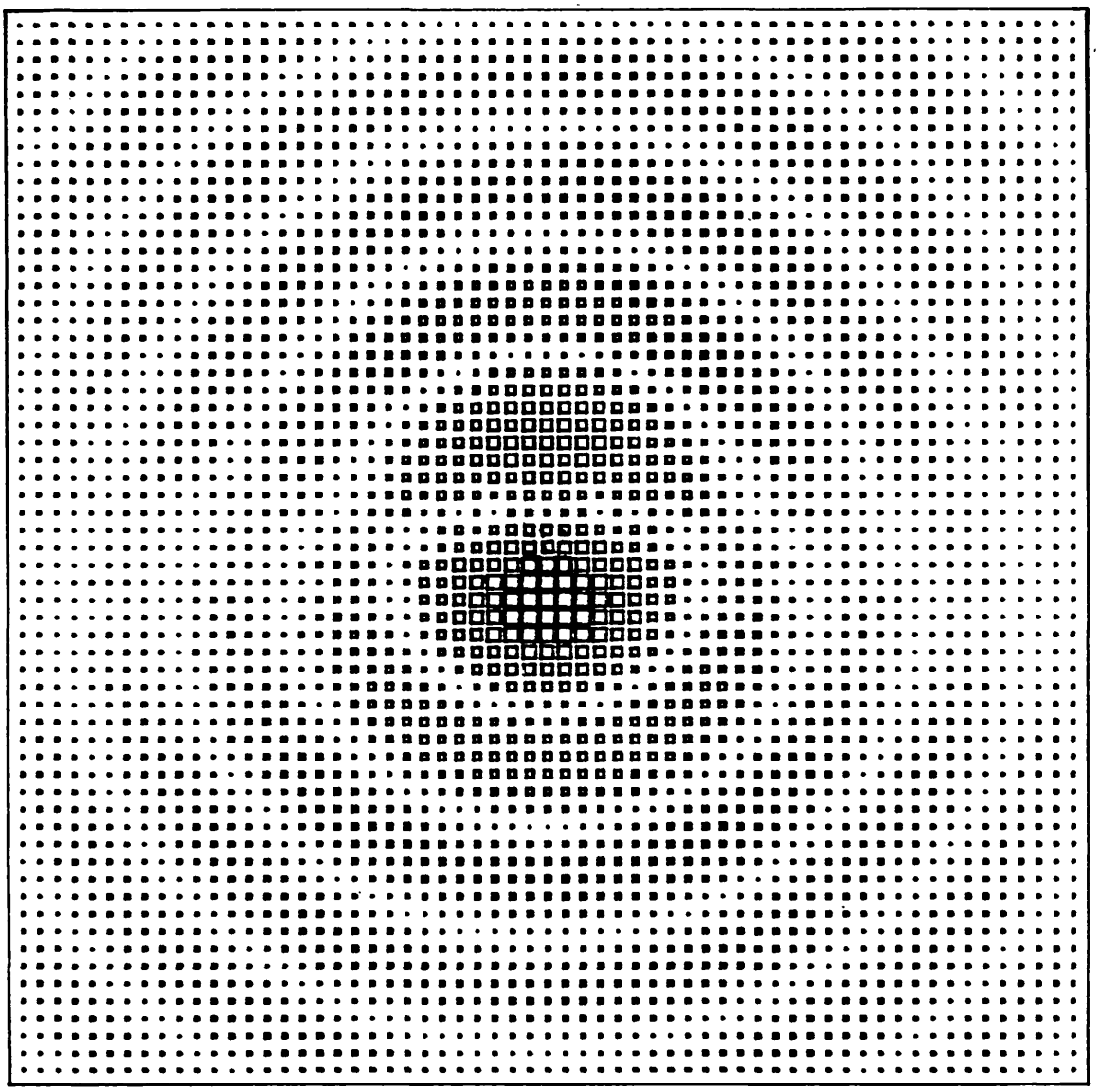

FIG 3.8

COMPUTED TWO DIMENSIONAL INTENSITY DISTRIBUTION FOR TWO AIRY PATTERNS WITH A SEPARATION OF Ø.1 RAYLEIGH RESOLUTION UNITS AND A PHASE DIFFERENCE OF 135 DEGREES

NOTE THAT THE SIZES OF THE SQUARES HAVE BEEN INCREASED TO SHOW THE RINGS MORE CLEARLY

If the two beams entering the Fourier transform lens do not overlap exactly, then there are additional fringes due to a tilt between the wavefronts when they converge in the transform plane.

To put this more mathematically, the two identical apertures, slightly displaced from one another, are equivalent to one aperture convolved with a pair of delta functions, whose separation is that of the two apertures.

By the convolution theorem, the Fourier transform of this is the Fourier transform of one aperture (i.e. the Airy Pattern) multiplied by the Fourier transform of a pair of delta functions (i.e. cosine fringes). In this case the transform plane distribution is as shown in Fig. 3.9. The fringes are eliminated by adjusting the position of the compensating aperture using small translation stages.

In use it was found to be convenient to observe the transform plane distribution using a video camera. A density slicer between the camera and the TV monitor enabled the structure of the pattern to be made much clearer. Figs. 3.10 and 3.11 show the processed output for two different pattern separations. Fig. 3.12 shows the results when one patern is substantially more intense than the other. The radiating lines of spots are just detectable, but are nowhere near as obvious as when the patterns have

FIG 3.9

THE EXPERIMENTAL TRANSFORM PLANE INTENSITY DISTRIBUTION WHEN THE TWO APERTURES DO NOT EXACTLY COINCIDE

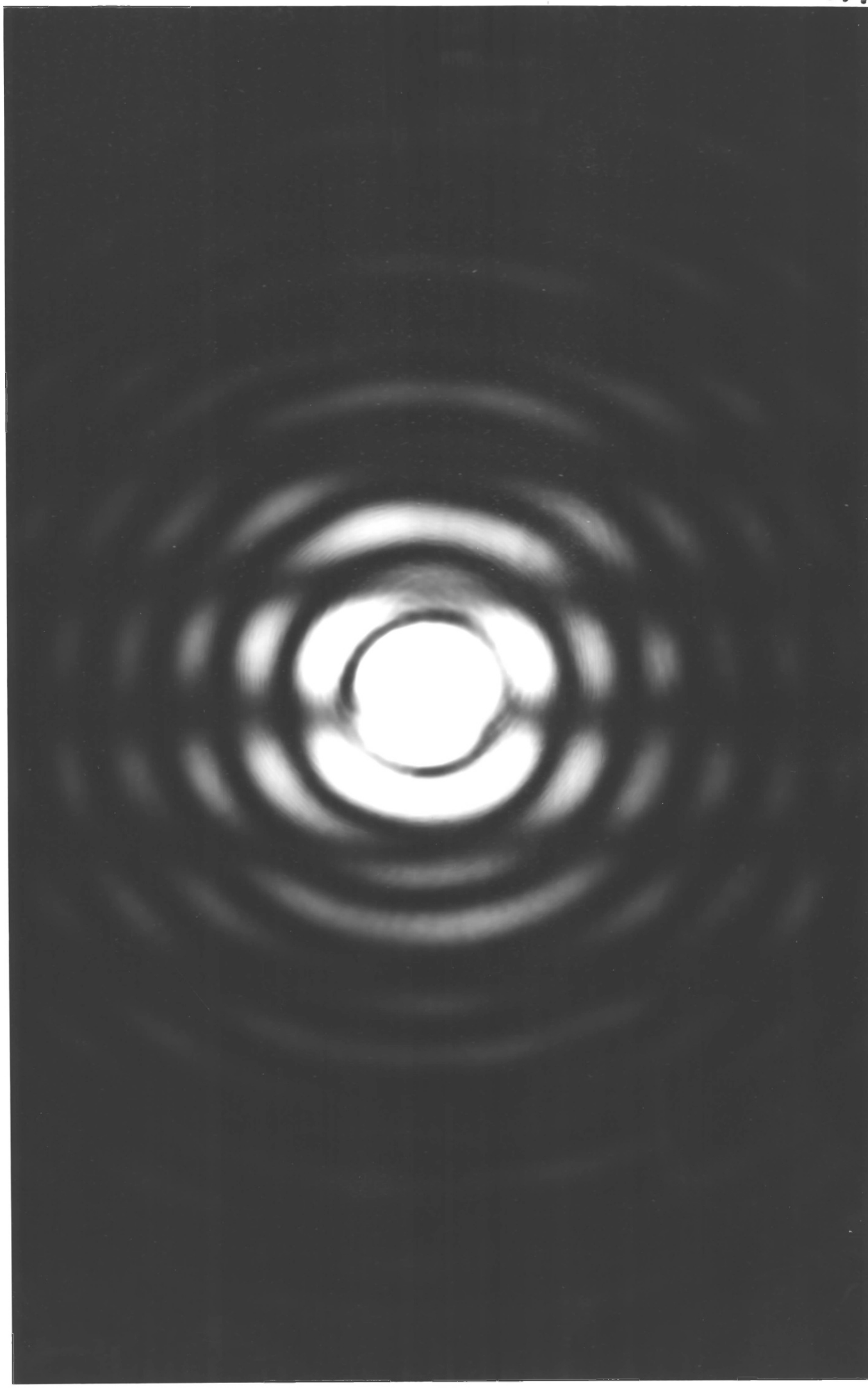

FIG 3.10

VIDEO PROCESSED VERSION OF THE INTENSITY DISTRIBUTION SHOWN IN FIG 3.7

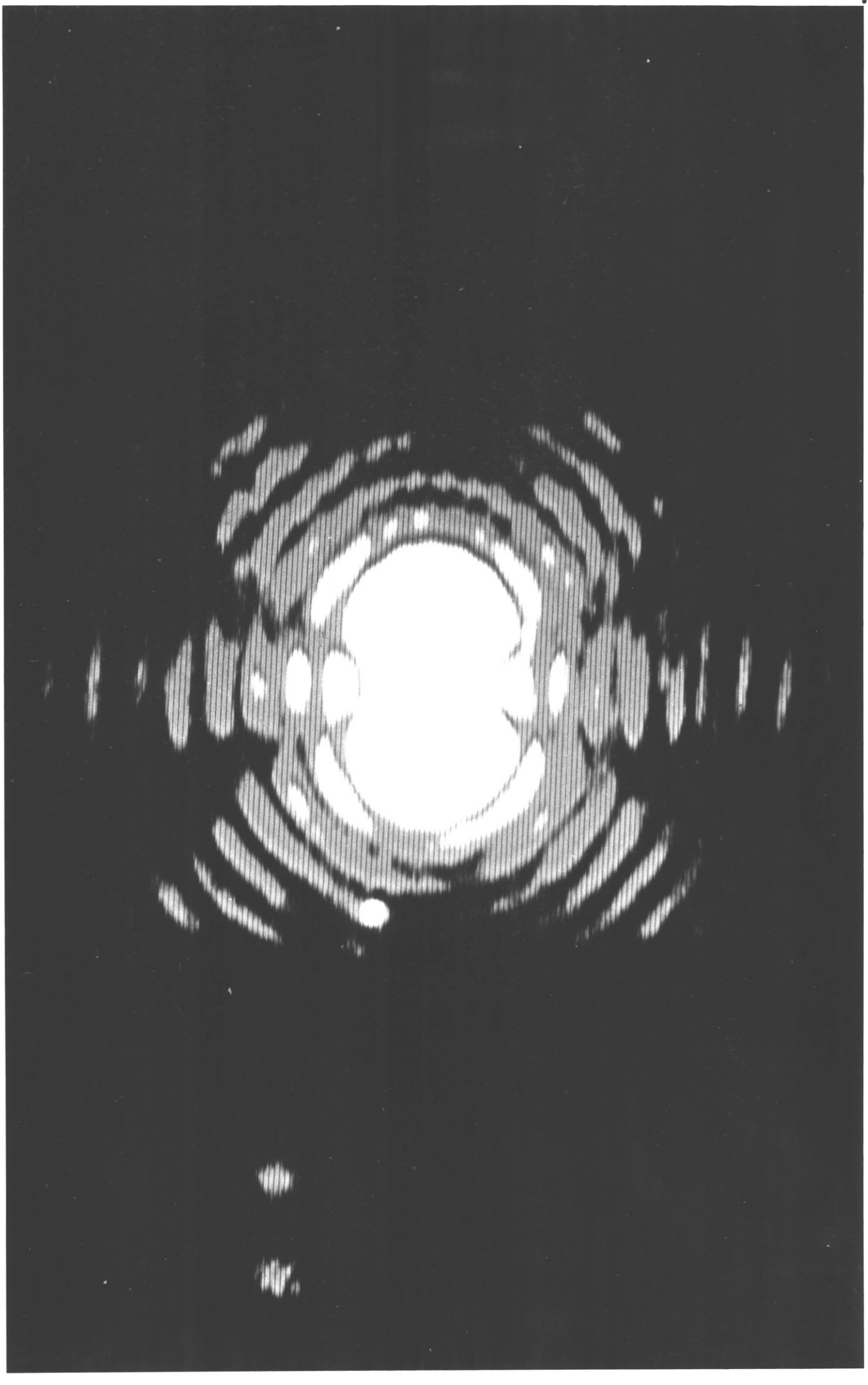

FIG 3.11

VIDEO PROCESSED VERSION OF THE INTENSITY DISTRIBUTION SHOWN IN FIG 3.4

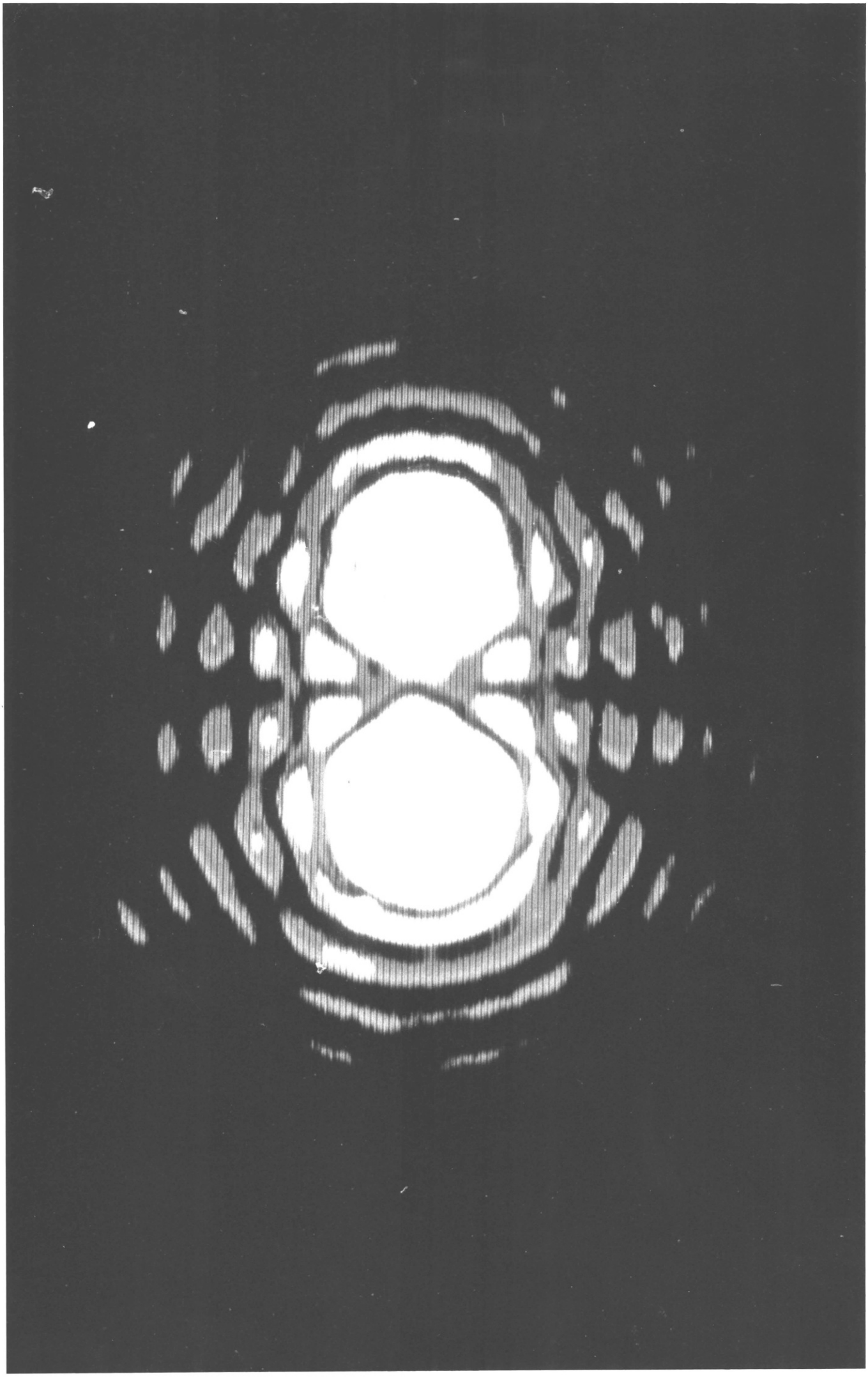

FIG 3.12

VIDEO PROCESSED TRANSFORM PLANE DISTRIBUTION WHEN THE BEAMS HAVE DIFFERENT AMPLITUDES

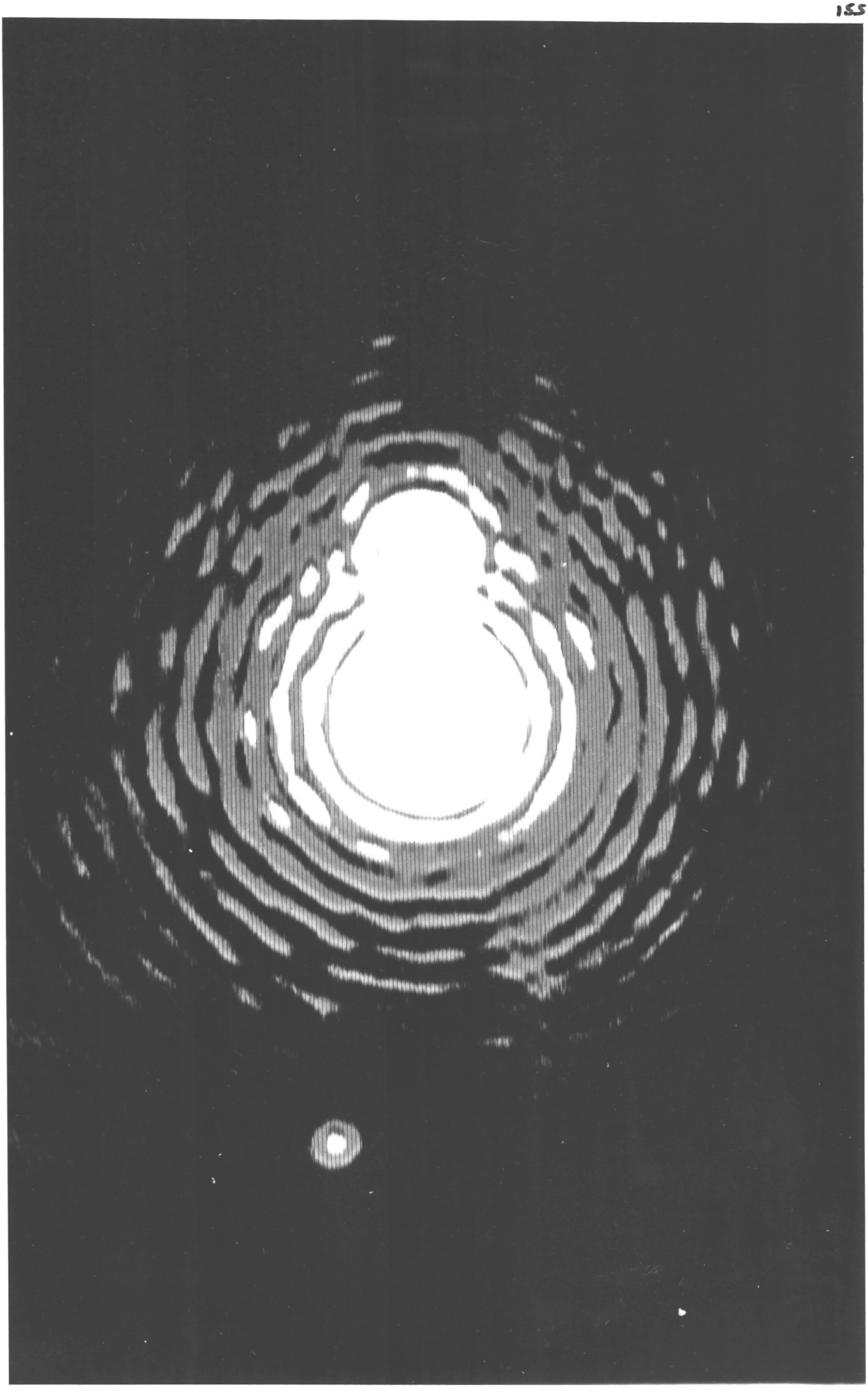

equal intensities. The photographic prints in this thesis have a magnification of approximately three times compared to the TV screen image. These patterns were large enough to be seen from the other side of the main optical table, thus making alignment of the instrument much easier. (The small spot on some of these photographs is due to a defect in the TV camera tube).

To measure the relative amplitudes of the two patterns, each beam was blocked off in turn, and the intensity of the other beam was measured with a photocell and a digital voltmeter.

The video system was also found to be useful for observing the transform plane distribution for photographic inputs. A typical video processed transform (that of Fig. 1.10) is shown in Fig. 3.13.

FIG 3.13

VIDEO PROCESSED OPTICAL FOURIER TRANSFORM

OF FIG 1.10

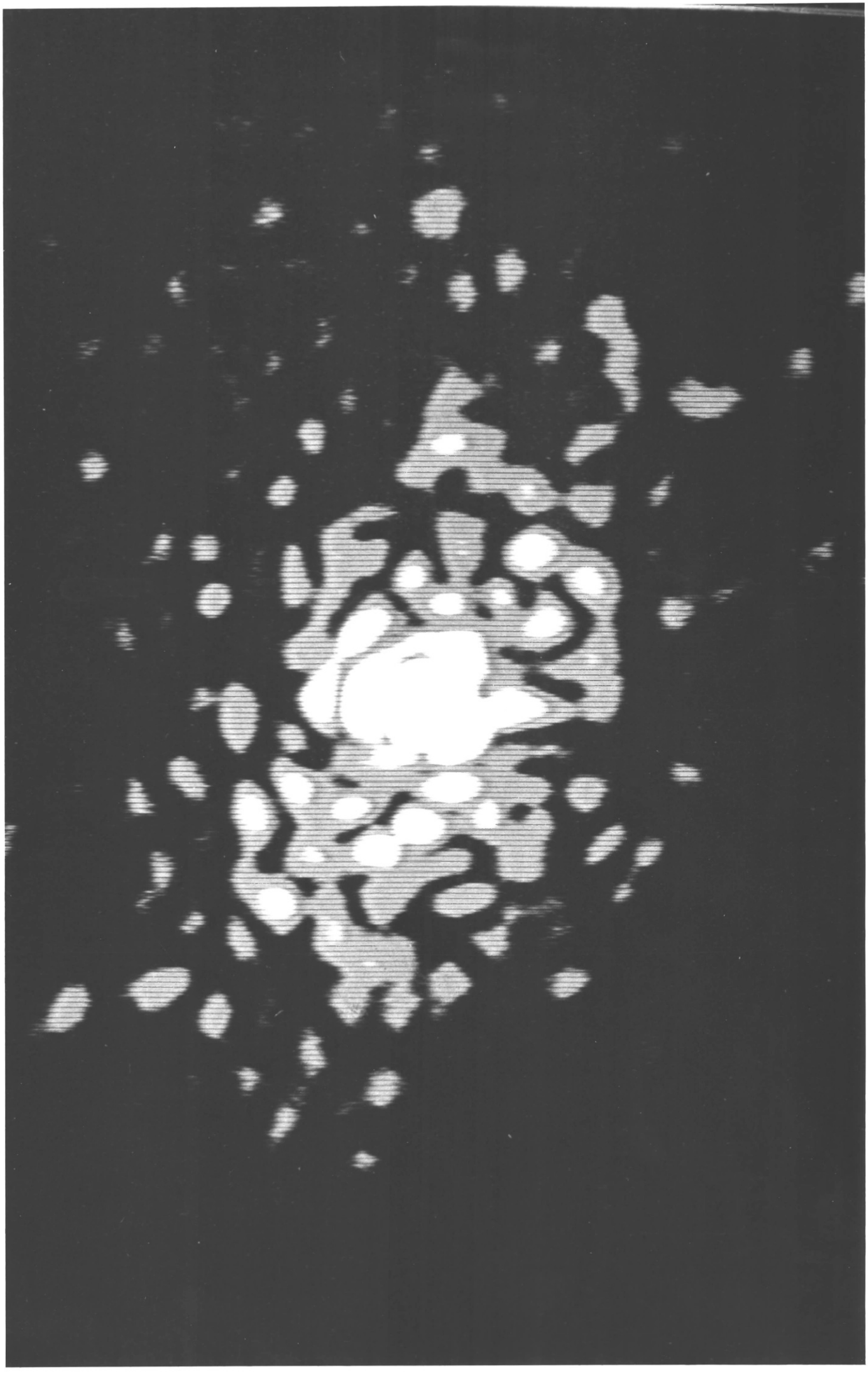

3.2. The alignment procedure

To align the interferometer, the following procedure was followed

(1) Align the light beams roughly by eye

(2) Equalise the beam intensities by blocking each beam of the interferometer in turn and measuring the intensity of the remaining Airy pattern with a photocell and digital voltmeter.

(3) Use the recombining beamsplitter to align the beams more accurately whilst observing the fringe pattern in the second pair of beams emerging from the recombining beamsplitter.

(4) Fine tune the alignment using the beam steering prisms whilst observing the transform plane distribution on the video monitor, adjusting the pinhole position if necessary.

(5) Adjust the phase difference to 180 degrees using the variable retarder whilst still observing the transform plane distribution on the video monitor.

(6) Finally, make small adjustments to the relative alignment, phase difference and relative amplitude so as to minimise the central intensity of the pattern.

CHAPTER 4

EXPERIMENTAL RESULTS

4.1. Output fringes

Once the interferometer had been assembled and aligned, it was adjusted to produce tilt fringes at the output so as to judge the final wavefront quality. Typical output fringes are shown in Fig. 4.1, which shows that the difference between the wavefronts is approximately $\lambda/15$ over the aperture of approximatelv 25mm diameter. Thus the required wavefront quality has been achieved.

4.2. Experimental subtraction of two Airy patterns

To judge the cancellation efficiency of the interferometer, it was necessary to measure the intensity distribution along a line through the centre of the Fourier plane. There ae two ways to approach this. One method is to photograph the Fourier plane distribution and then measure the density variations across the negative on a densitometer. This only gives an approximation to the original intensity distribution, as the density of photographic materials does not (usually) show a perfectly linear relationship with the original incident intensity.

FIG 4.1

OUTPUT FRINGES OF THE INTERFEROMETER WITH CLEAR CIRCULAR APERTURES IN BOTH BEAMS

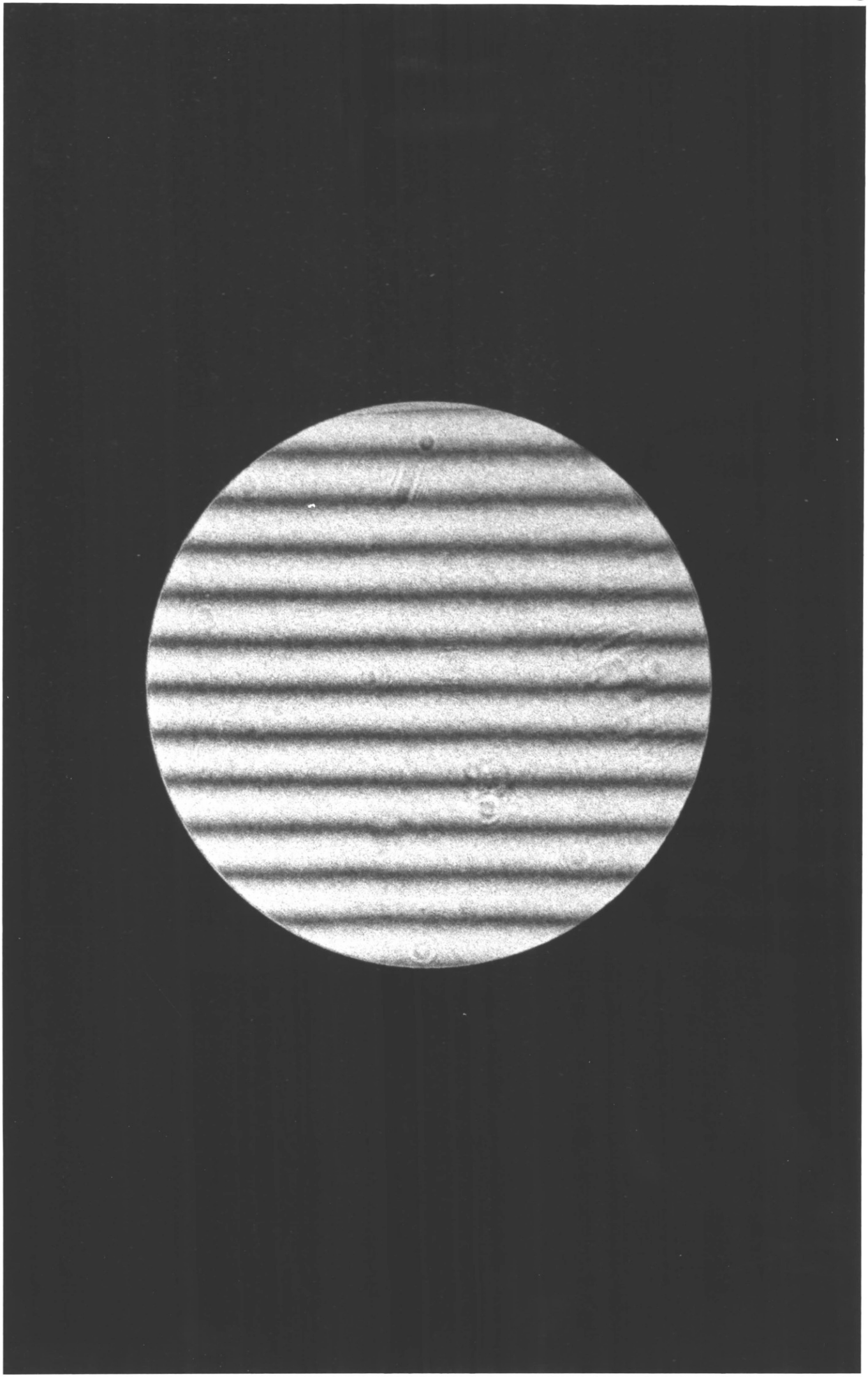

A more accurate method is to measure the intensity distribution by scanning a detector across the Fourier plane.

A 35μm pinhole was fixed in front of photomultiplier which was then mounted on a translatable table in the second transform plane formed by the re-imaging lens. To measure its position, a dial indicator was placed with the end of its probe in contact with the photomultiplier housing.

With the compensating beam of the interferometer blocked and a clear, circular aperture in the other beam, the position of the pinhole was adjusted until it was in the centre of the transform plane - corresponding to maximum output signal from the photomultiplier.

The pinhole was then scanned across the transform plane several times to check whether there was any backlash or wobble in the motion which would lead to the pinhole not passing through the centre of the transform plane. None was found to a tolerance of 0.01mm in the pinhole position.

A second circular aperture, identical to the first was placed in the compensating arm of the interferometer, which was then adjusted to give the most efficient cancellation.

The pinhole was scanned across the transform plane in steps of 1/20mm and at each position the intensities of one pattern and the combination of the two patterns were measured by alternately blocking and unblocking the compensating beam.

Fig. 4.2 shows the results obtained when only one Airy pattern is present. The form is very similar to the theoretical one suggesting a good quality input beam. When both patterns are present, and the interferometer is adjusted to produce maximum cancellation efficiency, the result is Fig 4.3 which shows a peak intensity reduction by a factor of approximately 30 times. The difference between this and the calculated value of approximately 40 times is due to the residual aberration of the instrument which was ignored in the calculations.

On a linear intensity scale, the range of intensities in the light distribution mean that it is difficult to see much detail away from the centre. The detail is shown much more clearly if the results are plotted with a logarithmic scale on the intensity axis as in Figs. 4.4 and 4.5. This also shows up the slight asymmetry in the pattern with the peaks on one side being slightly more intense than those on the other.

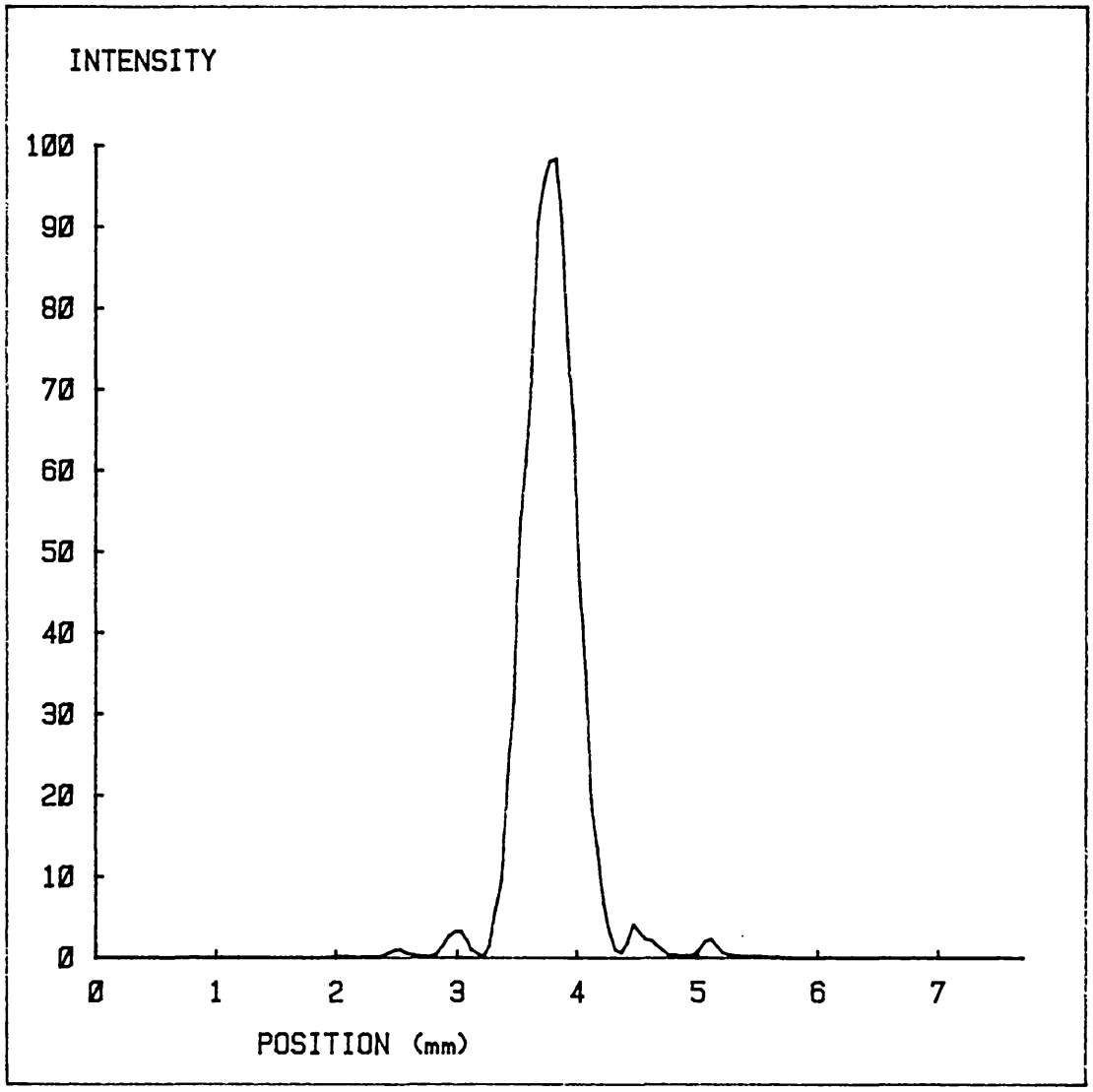

FIG 4.2

INTENSITY DISTRIBUTION THROUGH THE CENTRE OF THE MAGNIFIED TRANSFORM PLANE WITH A CLEAR CIRCULAR APERTURE IN THE OBJECT PLANE AND THE COMPENSATING ARM OF THE INTERFEROMETER BLOCKED

LINEAR INTENSITY SCALE

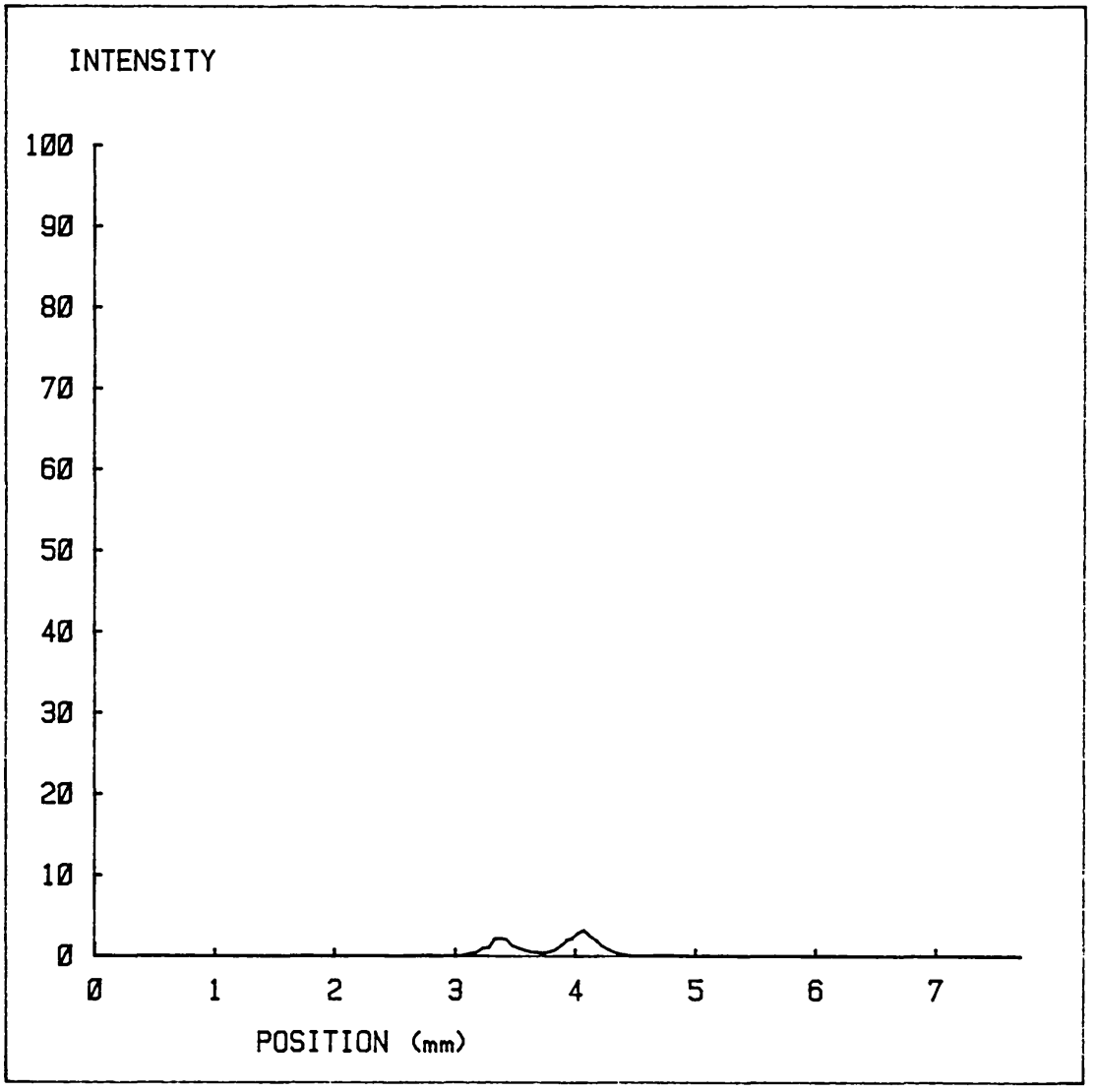

FIG 4.3

INTENSITY DISTRIBUTION THROUGH THE CENTRE OF THE MAGNIFIED TRANSFORM PLANE WITH IDENTICAL CLEAR CIRCULAR APERTURES IN BOTH ARMS OF THE INTERFEROMETER WHICH WAS ADJUSTED TO GIVE MAXIMUM CANCELLATION LINEAR INTENSITY SCALE

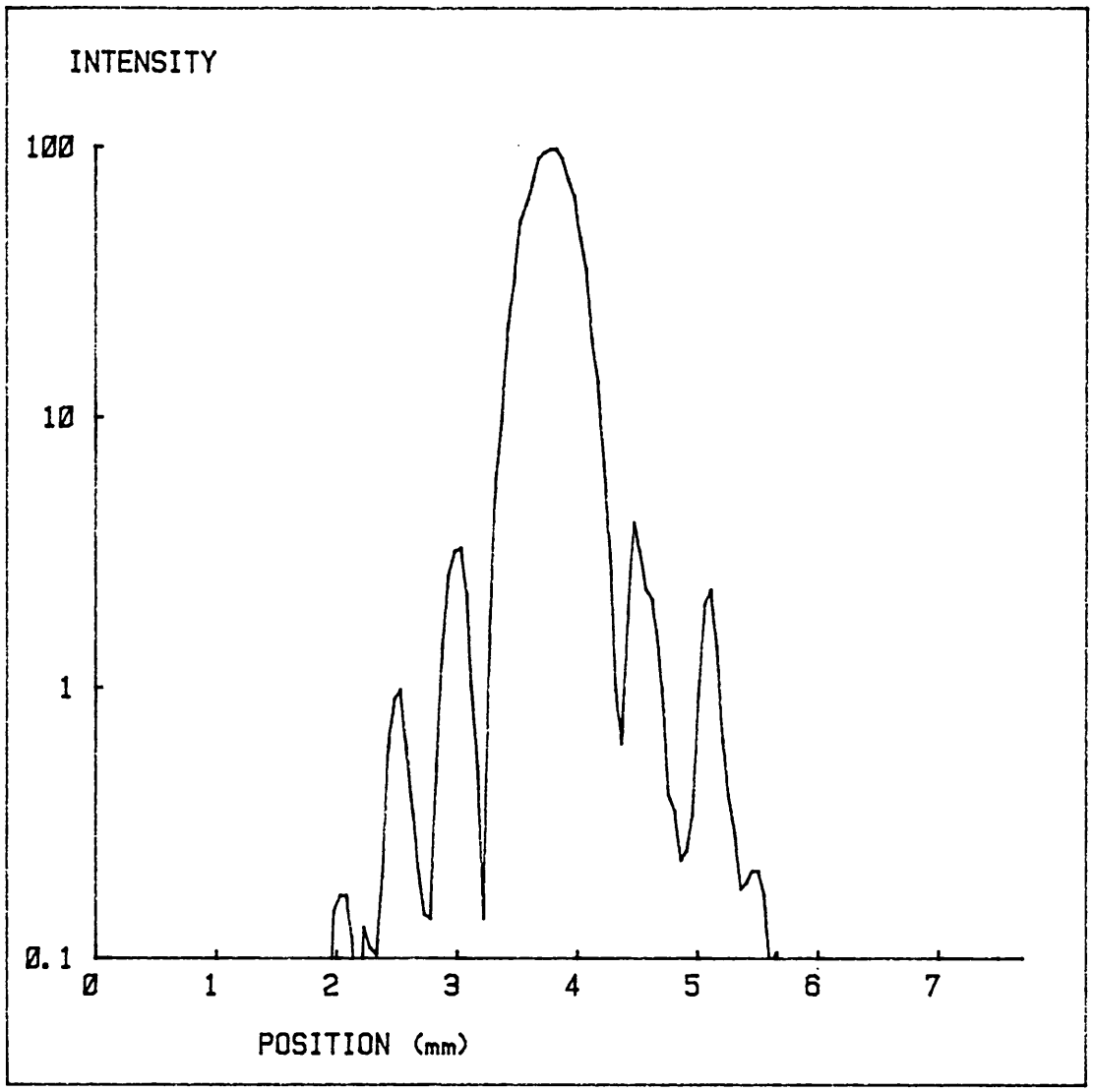

FIG 4.4

INTENSITY DISTRIBUTION THROUGH THE CENTRE OF THE MAGNIFIED TRANSFORM PLANE WITH A CLEAR CIRCULAR APERTURE IN THE OBJECT PLANE AND THE COMPENSATING ARM OF THE INTERFEROMETER BLOCKED

LOGARITHMIC INTENSITY SCALE

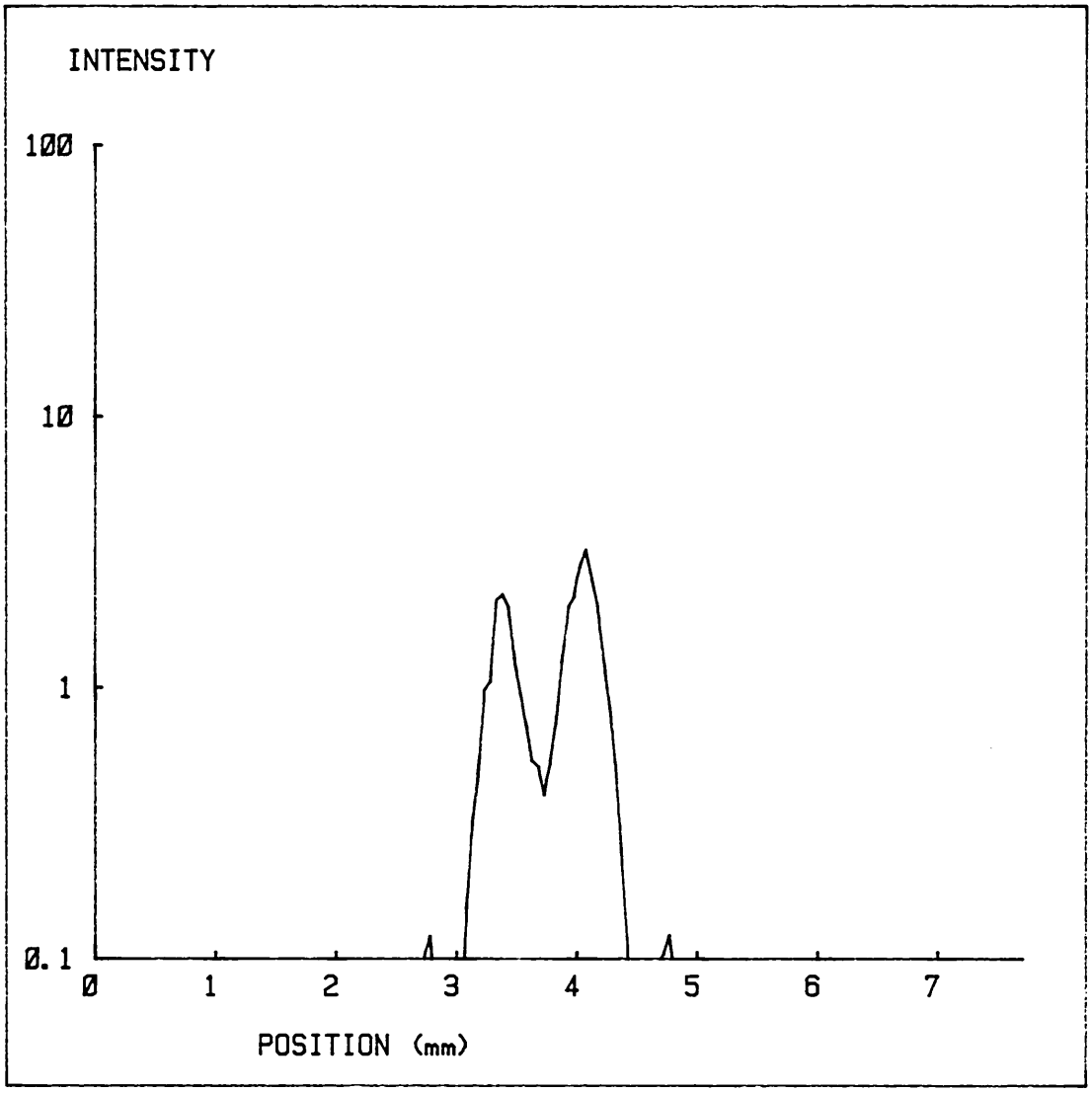

FIG 4.5

INTENSITY DISTRIBUTION THROUGH THE CENTRE OF THE MAGNIFIED TRANSFORM PLANE WITH IDENTICAL CLEAR CIRCULAR APERTURES IN BOTH ARMS OF THE INTERFEROMETER WHICH WAS ADJUSTED TO GIVE MAXIMUM CANCELLATION LOGARITHMIC INTENSITY SCALE

4.3. Subtraction of undiffracted light with photographic inputs

Two photographic negatives were chosen for study. Prints of these were shown earlier in Fig. 1.10 and Fig. 1.11. They are both views of sedimentary rock samples from under the North Sea, taken on a scanning electron microscope. For use on the Fourier transform system the negatives were sandwiched together with a circular aperture cut from 1mm thick aluminium sheet, and immersed in a liquid gate to reduce phase irregularities.

A visual inspection of the negatives suggests that there are preferred directions in both of the negatives, with dominant spatial frequencies of about 4 lines per mm in Fig. 1.10 and about 1 line per mm in Fig. 1.11.

Optical Fourier transforms of the two negatives are shown in Figs. 4.6 and 4.7. Due to the very large range of intensities in the transform plane distributions, it is impossible to show the central and outer regions of the transform on the same photograph. If the film is exposed for the outer regions the central region is vastly over-exposed, whereas if the film is exposed for the central region, the outer regions do not register on the film.

FIG 4.6

THE OPTICAL FOURIER TRANSFORM OF FIG 1.10

WITH THE UNDIFFRACTED LIGHT PRESENT

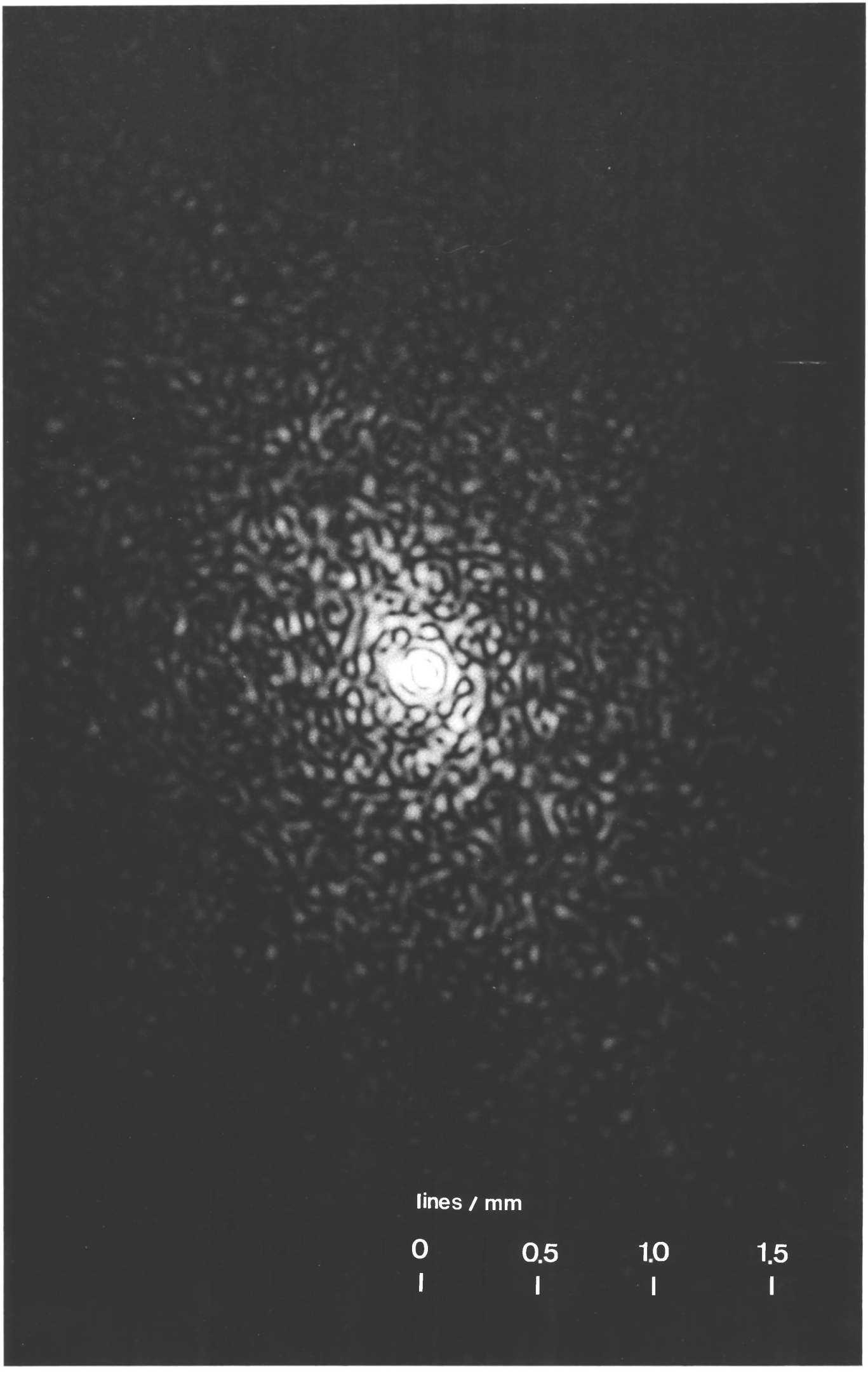
lines / mm
0
0.5
1.0
1.5

FIG 4.7

THE OPTICAL FOURIER TRANSFORM OF FIG 1.11

WITH THE UNDIFFRACTED LIGHT PRESENT

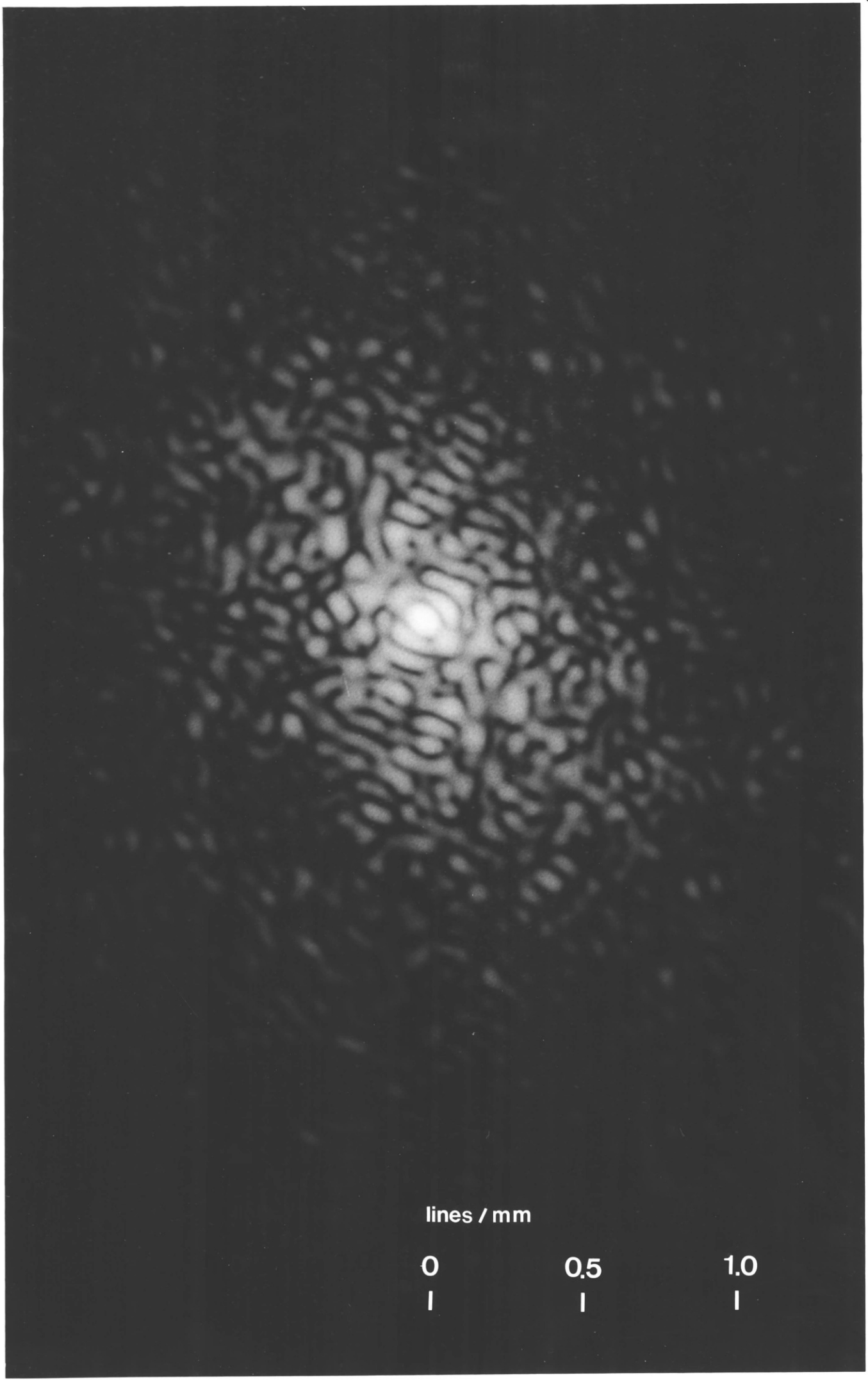
lines / mm
0
0.5
1.0

The exposures here were chosen to show the central part of the transform, and were of about ½ to 10 seconds on Ilford HP5 film rated at ASA500.

Fig. 4.6 is the optical Fourier transform of Fig. 1.10. The transform appears to be roughly elliptical with axes in the ratio 2 to 1 indicating a directionality in the original input transparency at right angles to the major axis of the ellipse.

Fig. 4.7 is the optical Fourier transform of Fig. 1.11. This also has an elliptical shape, with axes in the ratio of just under 2 to 1, but at low spatial frequencies the transform appears to be more circular.

When the interferometer is adjusted to reduce the intensity of the undiffracted light as much as possible. The resulting transform plane distributions are shown in Figs. 4.8 and 4.10. Fig. 4.8 is the optical Fourier transform of Fig. 1.10 with the intensity of the undiffracted light reduced by a factor of approximately 30 times. The central region now has a similar appearance to the region just outside the centre , suggesting that once the intensity of the undiffracted light is reduced to an acceptable level, we see some of the structure due to very low frequency inputs - although some of the light in this region is due to residual

undiffracted light, and there is a fair amount of laser speckle present.

A scan of this transform plane distribution with the rotating sector disc results in Fig. 4.9. The polar plot of the measured intensity is roughly an ellipse with a ratio of maximum to minimum signal of approximately 2.1 to 1. This is very close to the value of 2 to 1 estimated for Fig. 4.6 and larger than the ratio of 1.4 to 1 found for the transform when the undiffracted light was present, but partially blocked with a DC stop. This suggests that Fig. 4.9 is a realistic representation of the directionalities present in Fig. 1.10.

Using the interferometer to reduce the undiffracted light intensity for the optical Fourier transform of Fig. 1.11 results in Fig. 4.10. This also has a central intensity reduction of approximately 30 times. This suggests that the cancellation efficiency of the interferometer is not strongly object dependant. Analysing this optical transform with the rotating sector disc results in Fig. 4.11. The directionality here is not as apparent as in Fig. 4.9. The ratio of maximum to minimum signal is approximately 1.4 to 1 compared to a ratio of 1.24 to 1 when the undiffracted light is present but partially blocked with a DC stop.

FIG 4.8

THE OPTICAL FOURIER TRANSFORM OF FIG 1.10 WITH THE INTENSITY OF THE UNDIFFRACTED LIGHT REDUCED BY A FACTOR OF APPROXIMATELY 30 TIMES

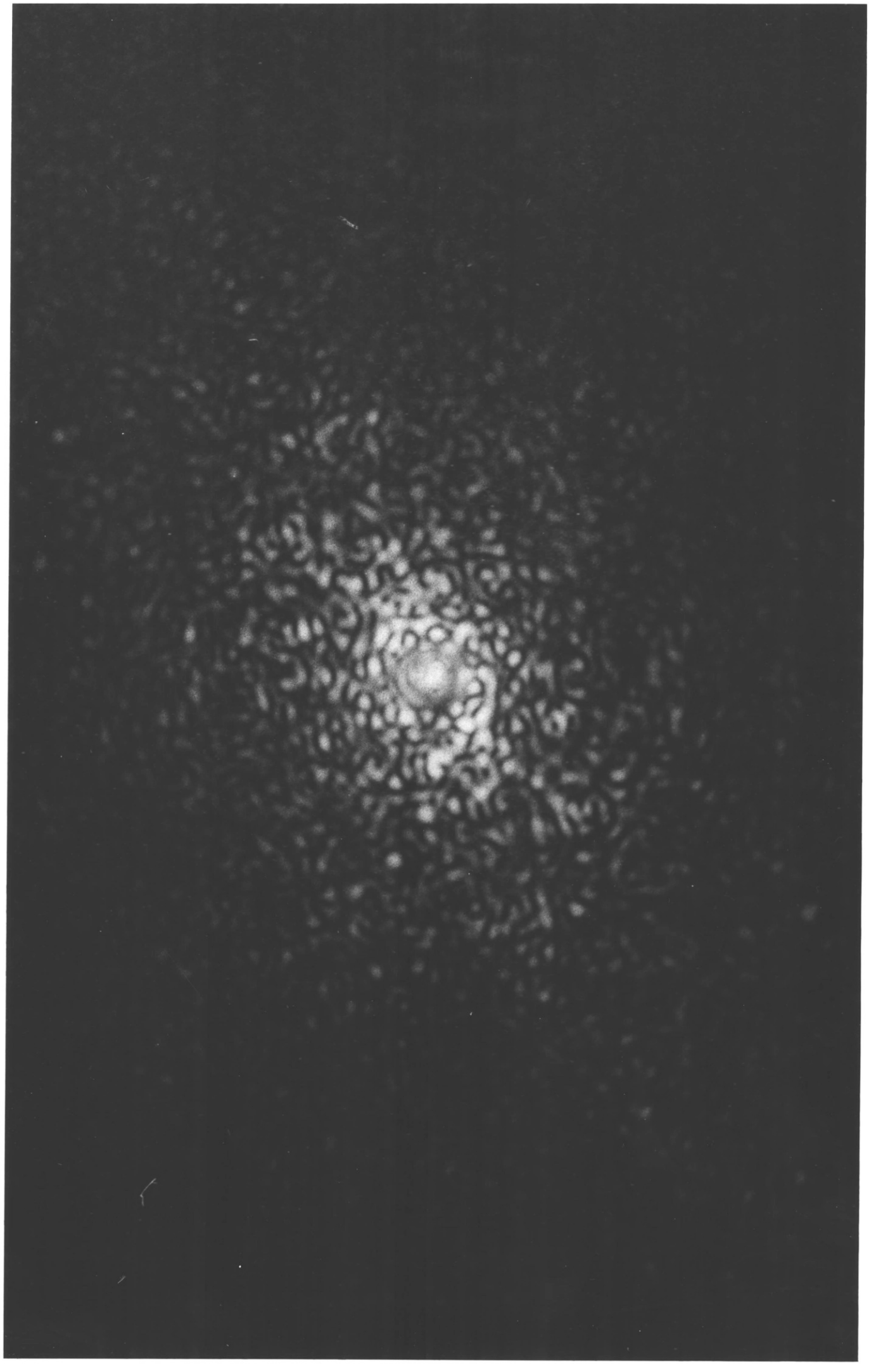

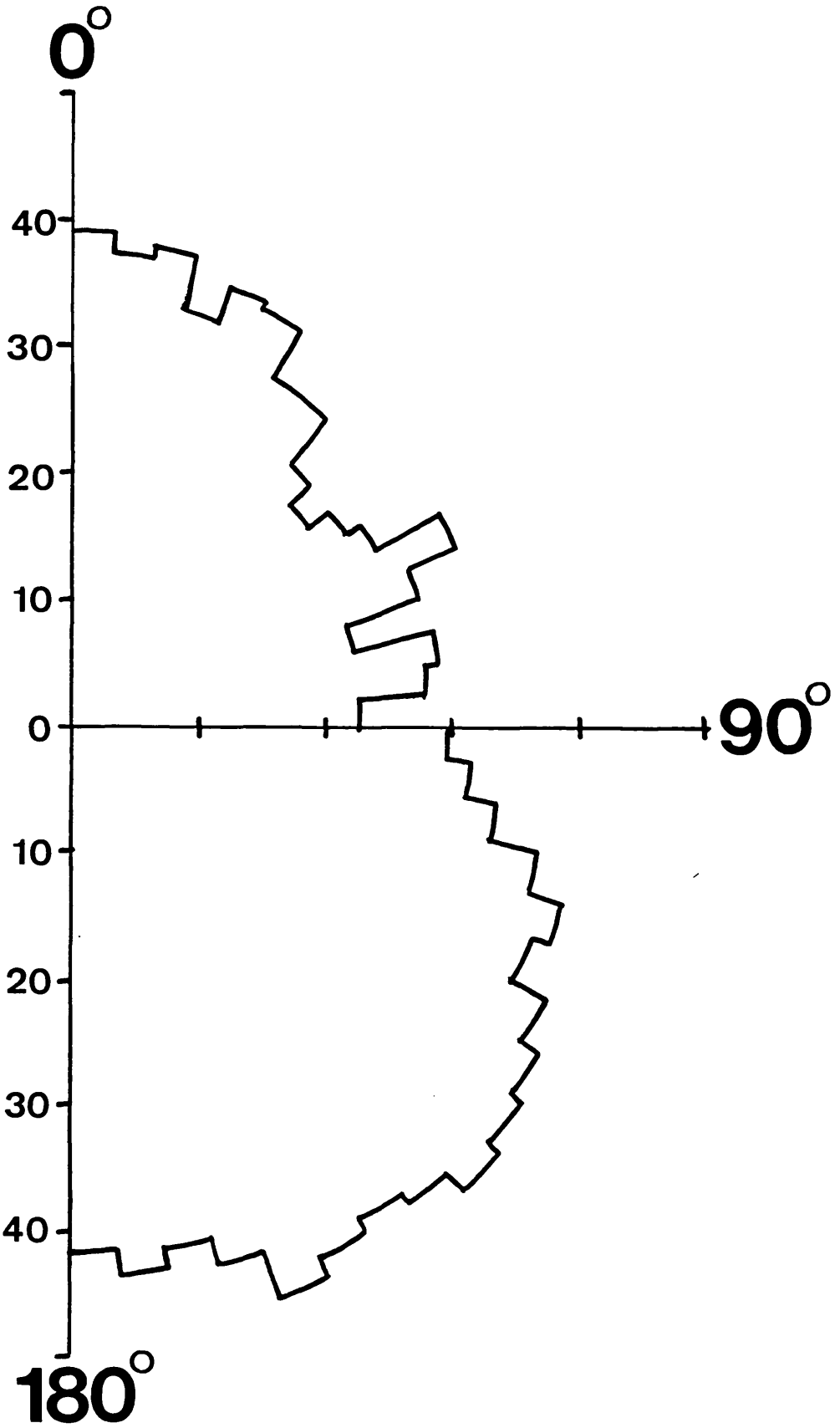

FIG 4.9

THE RESULT OF SCANNING THE INTENSITY DISTRIBUTION SHOWN IN FIG 4.8 WITH A ROTATING SECTOR DISC

FIG 4.10

THE OPTICAL FOURIER TRANSFORM OF FIG 1.11 WITH THE INTENSITY OF THE UNDIFFRACTED LIGHT REDUCED BY A FACTOR OF APPROXIMATELY 30 TIMES

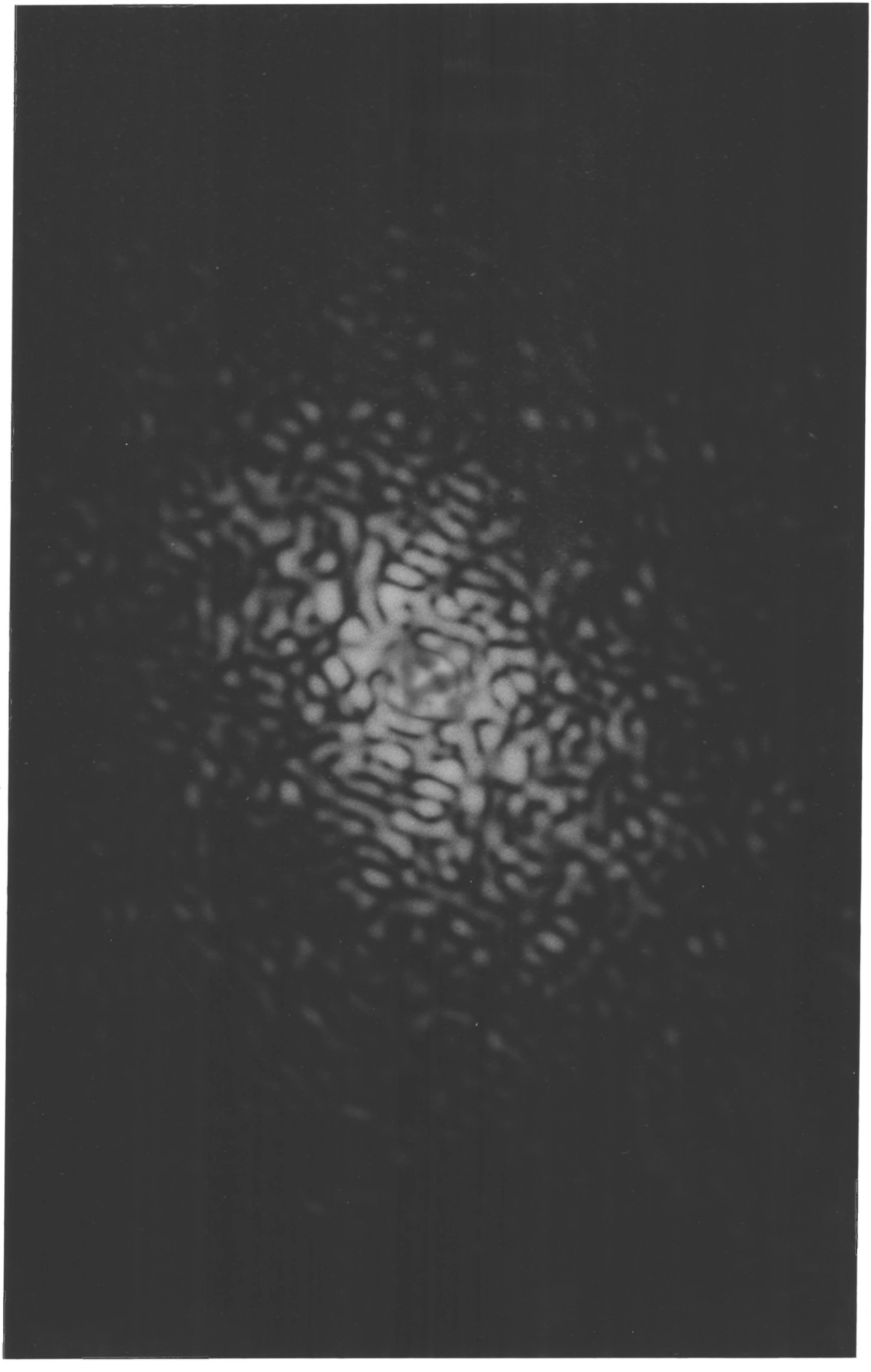

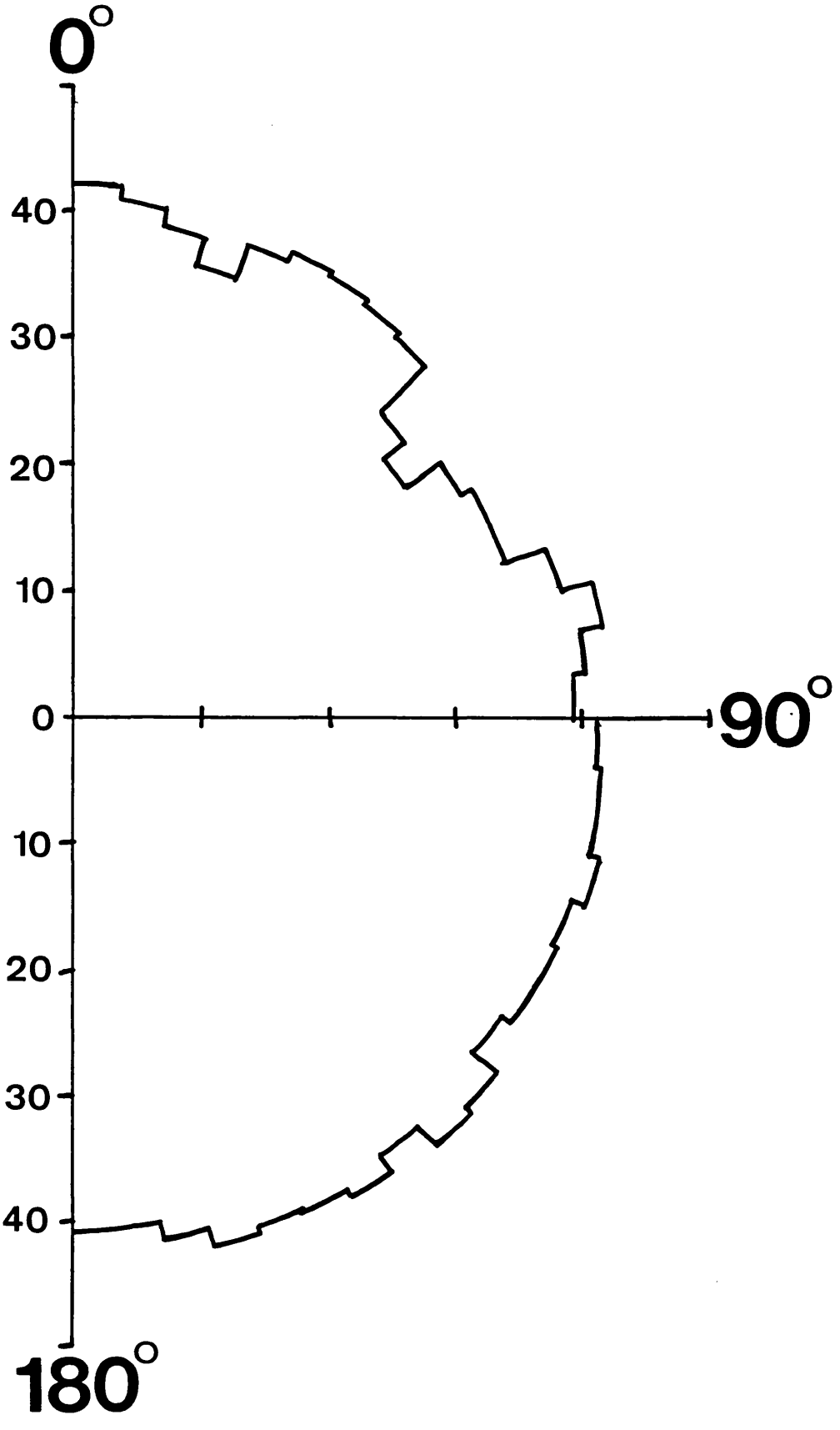

FIG 4.11

THE RESULT OF SCANNING THE INTENSITY DISTRIBUTION SHOWN IN FIG 4.1Ø WITH A ROTATING SECTOR DISC

In Fig. 4.7 the low spatial frequency regions have less angular variations than, and are more intense than the higher spatial frequency regions. The sector disc integrates the intensity over a range of spatial frequencies, hence the maximum to minimum signal ratio is less than expected.

There is a dip in intensity at an angle of about 130 degrees which seems to correlate with a lack of features at an angle of about 40 degrees in the original object.

With the negative of Fig. 1.10 in the input plane, the interferometer was adjusted to give maximum reduction in the intensity of the undiffracted light. The photomultiplier and pinhole were then scanned across the center of the transform plane as before. At each position the intensity was measured twice - once with the compensating arm of the interferometer blocked, and once with both beams present.

Fig. 4.12 shows the measured intensity distribution through the centre of the transform plane when the compensating beam is blocked. When both beams are present and the intensity of the undiffracted light is reduced by as much as possible, the intensity distribution is as shown in Fig. 4.13.

Once again, the large range of intensities present in the transform plane mean that the low intensity regions do not

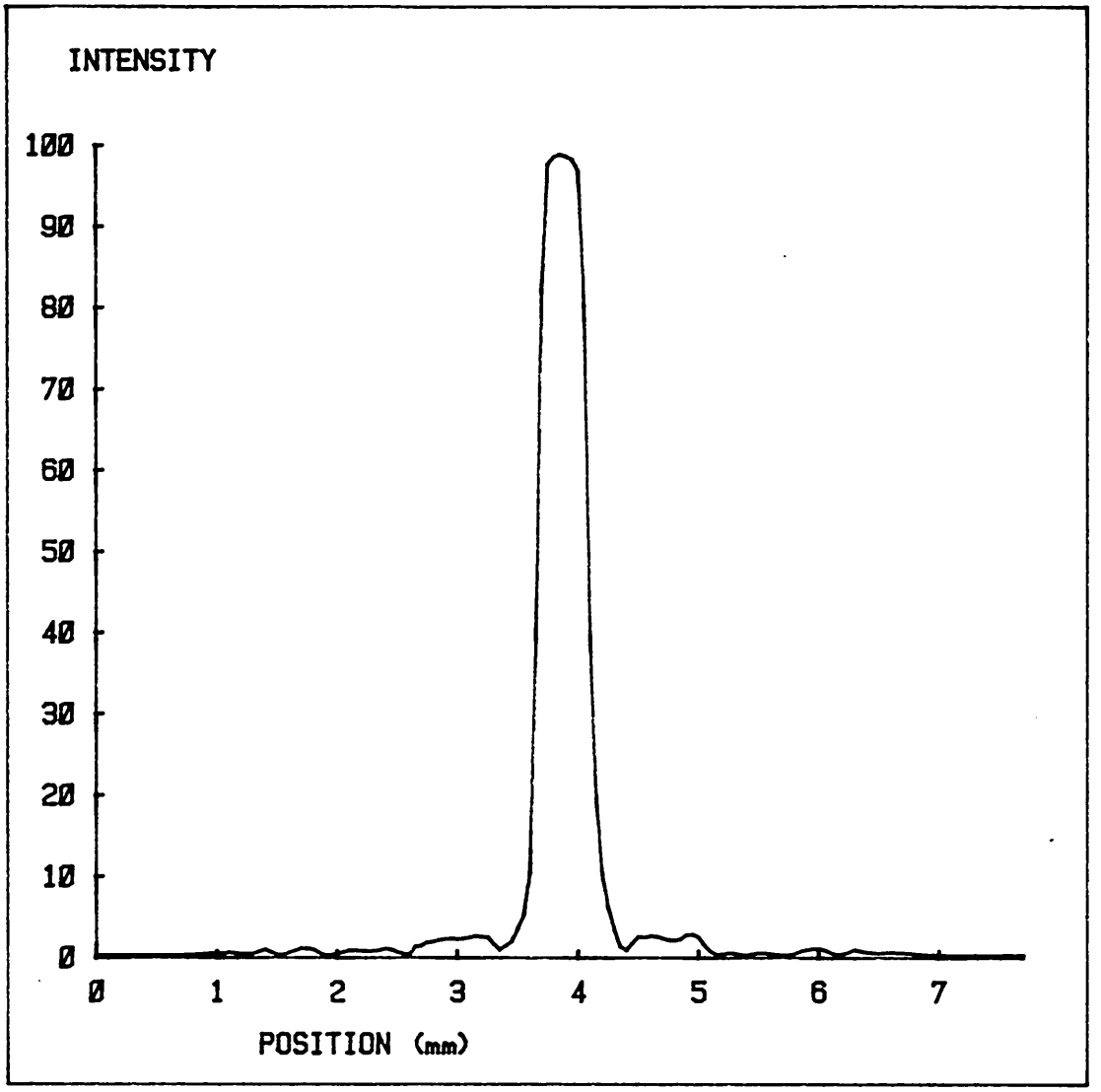

FIG 4.12

INTENSITY DISTRIBUTION THROUGH THE CENTRE OF FIG 4.8

LINEAR INTENSITY SCALE

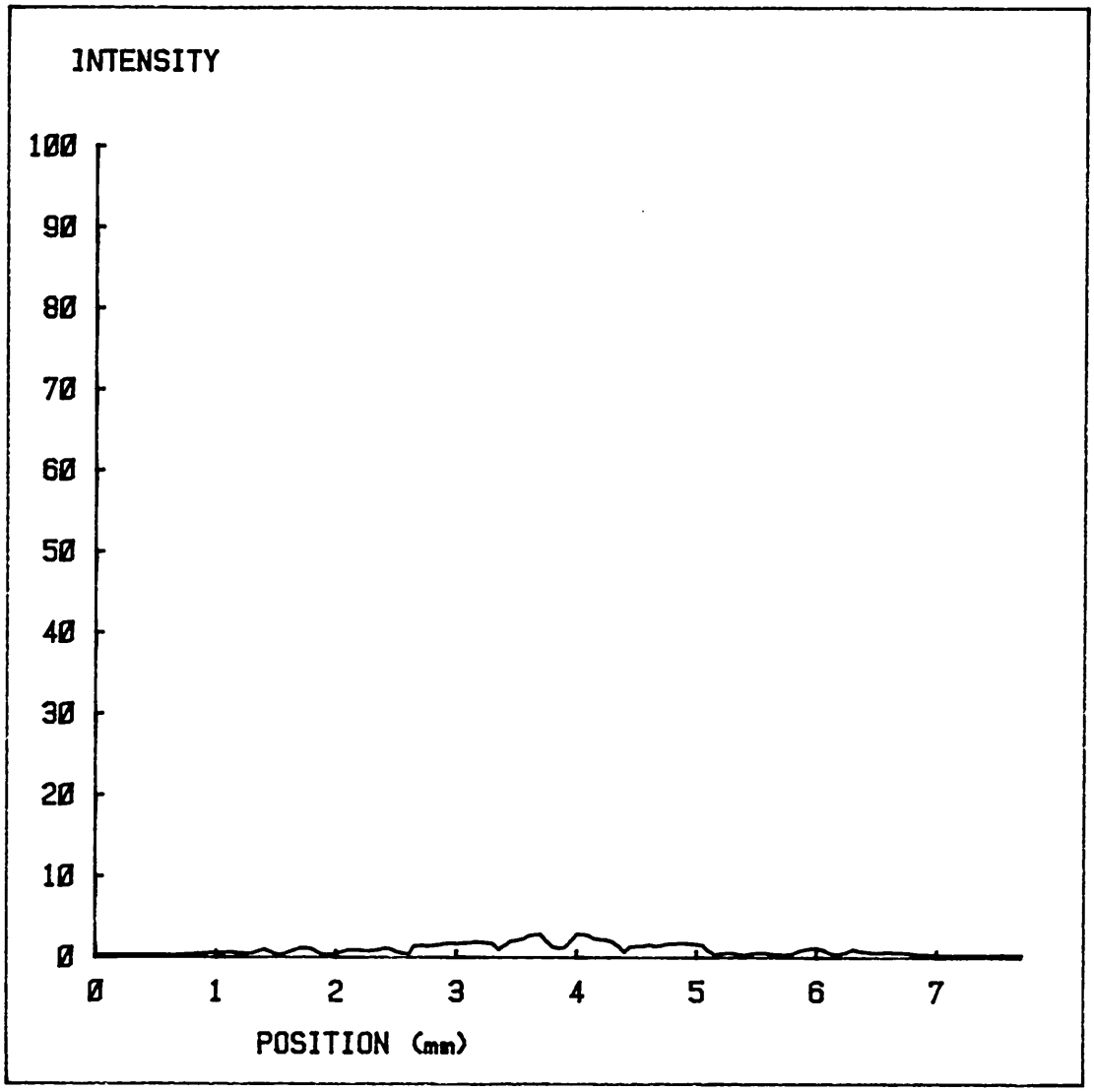

FIG 4.13

INTENSITY DISTRIBUTION THROUGH THE CENTRE OF FIG 4.10

LINEAR INTENSITY SCALE

show up well, so these distributions are plotted with a logarithmic intensity scale in Figs. 4.14 and 4.15.

When studying the photographs of the optical Fourier transforms in Figs. 4.6 to 4.10, the speckle pattern can be seen to be approximately 180 degrees symmetrical, as is to be expected, but with slight small-scale asymmetries due to irregularities and defects in the system. This symmetry is also shown in Figs. 4.14 and 4.15 where the intensity distribution is roughly the same as both sides of the centre of the transform plane.

If the undiffracted light is totally removed, the exact centre of the transform plane should have zero intensity. The intensity does in fact dip at the centre, but not to zero indicating incomplete cancellation.

Fig. 4.16 is a photograph of the photomultiplier and pinhole, mounted on the translation stage in the magnified transform plane. The photomultiplier was the one previously used with the rotating sector disc.

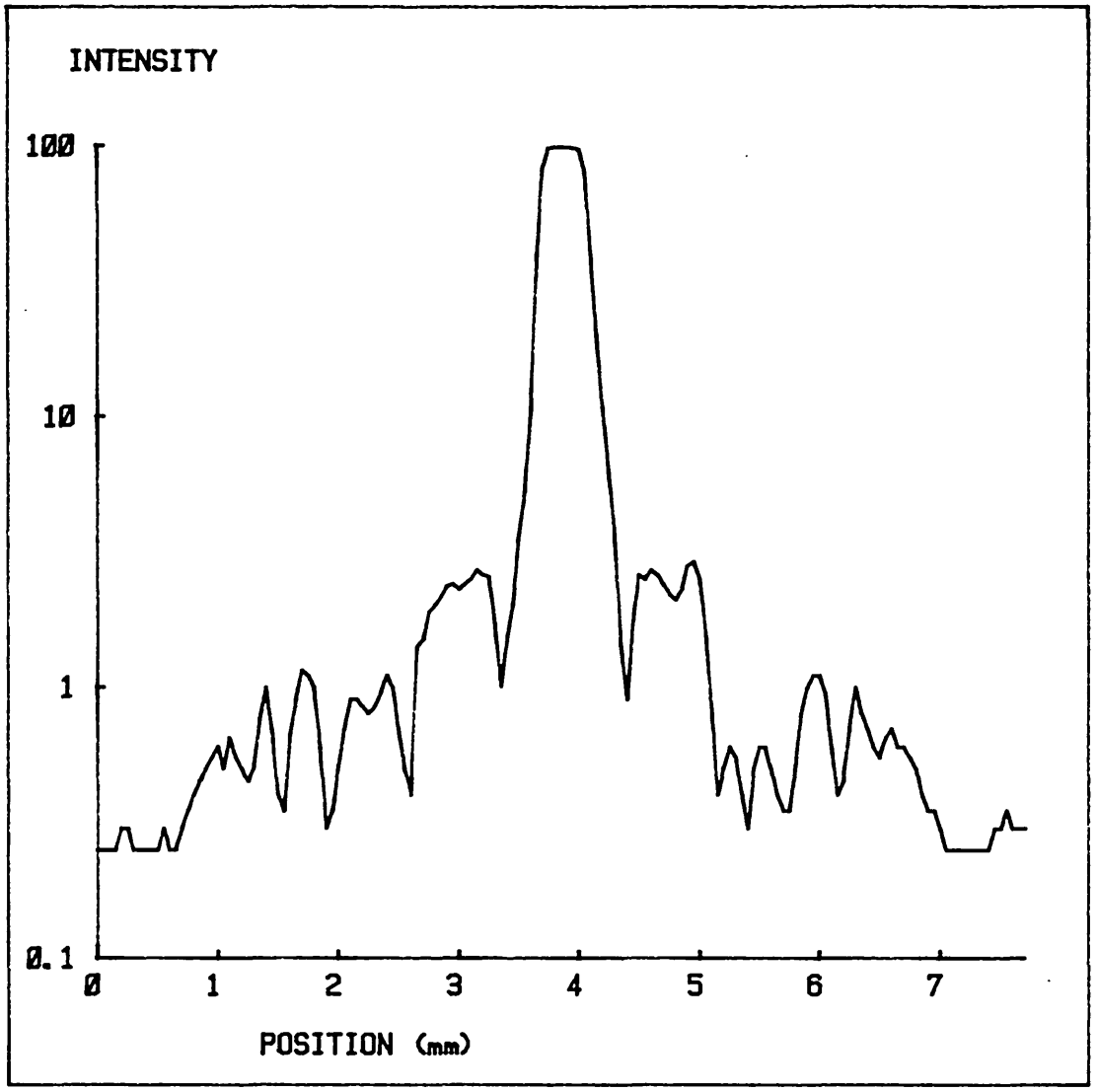

FIG 4.14

INTENSITY DISTRIBUTION THROUGH THE CENTRE OF FIG 4.8

LOGARITHMIC INTENSITY SCALE

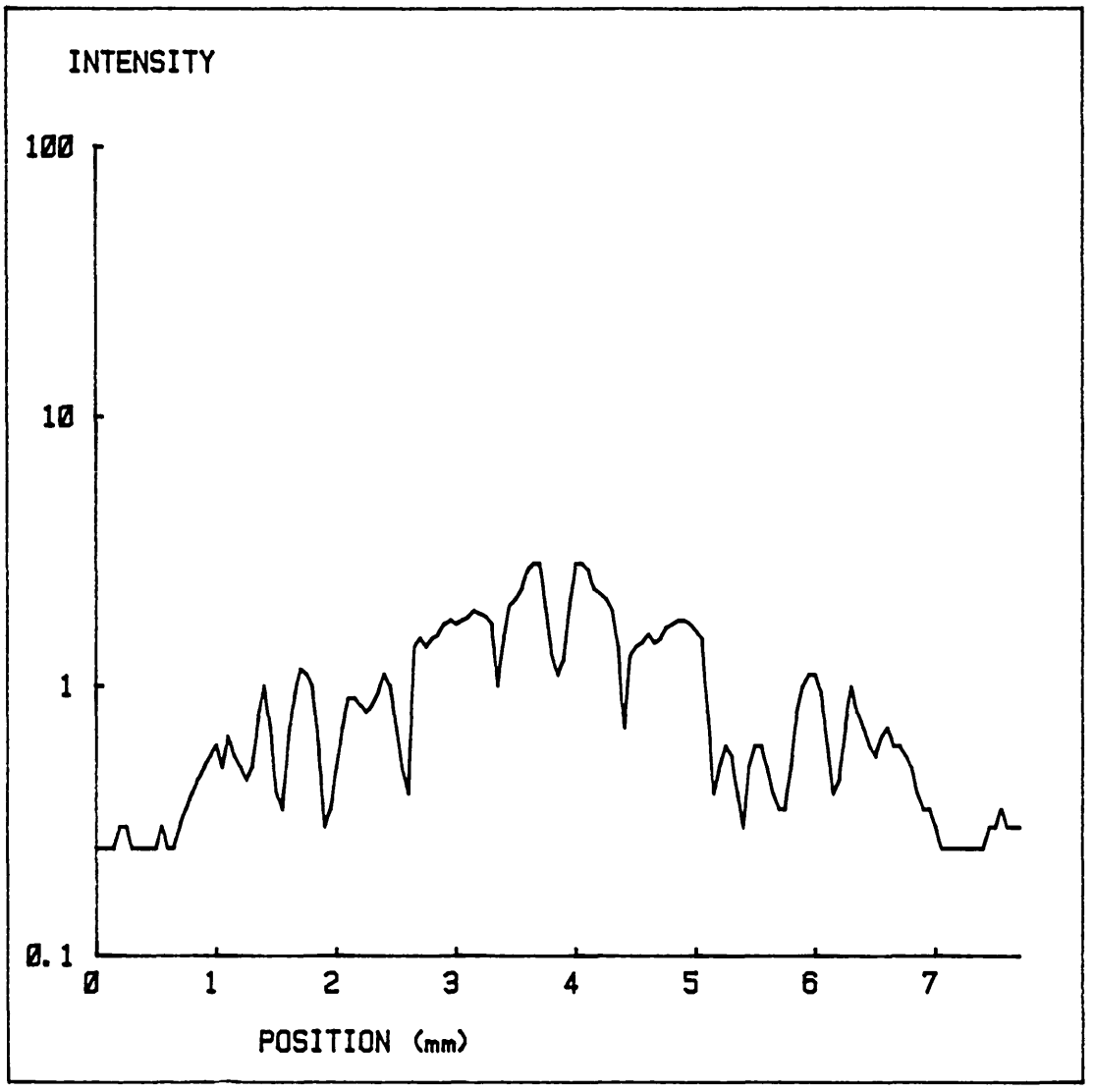

FIG 4.15

INTENSITY DISTRIBUTION THROUGH THE CENTRE OF FIG 4.10

LOGARITHMIC INTENSITY SCALE

FIG 4.16

THE PINHOLE AND PHOTOMULTIPLIER ASSEMBLY

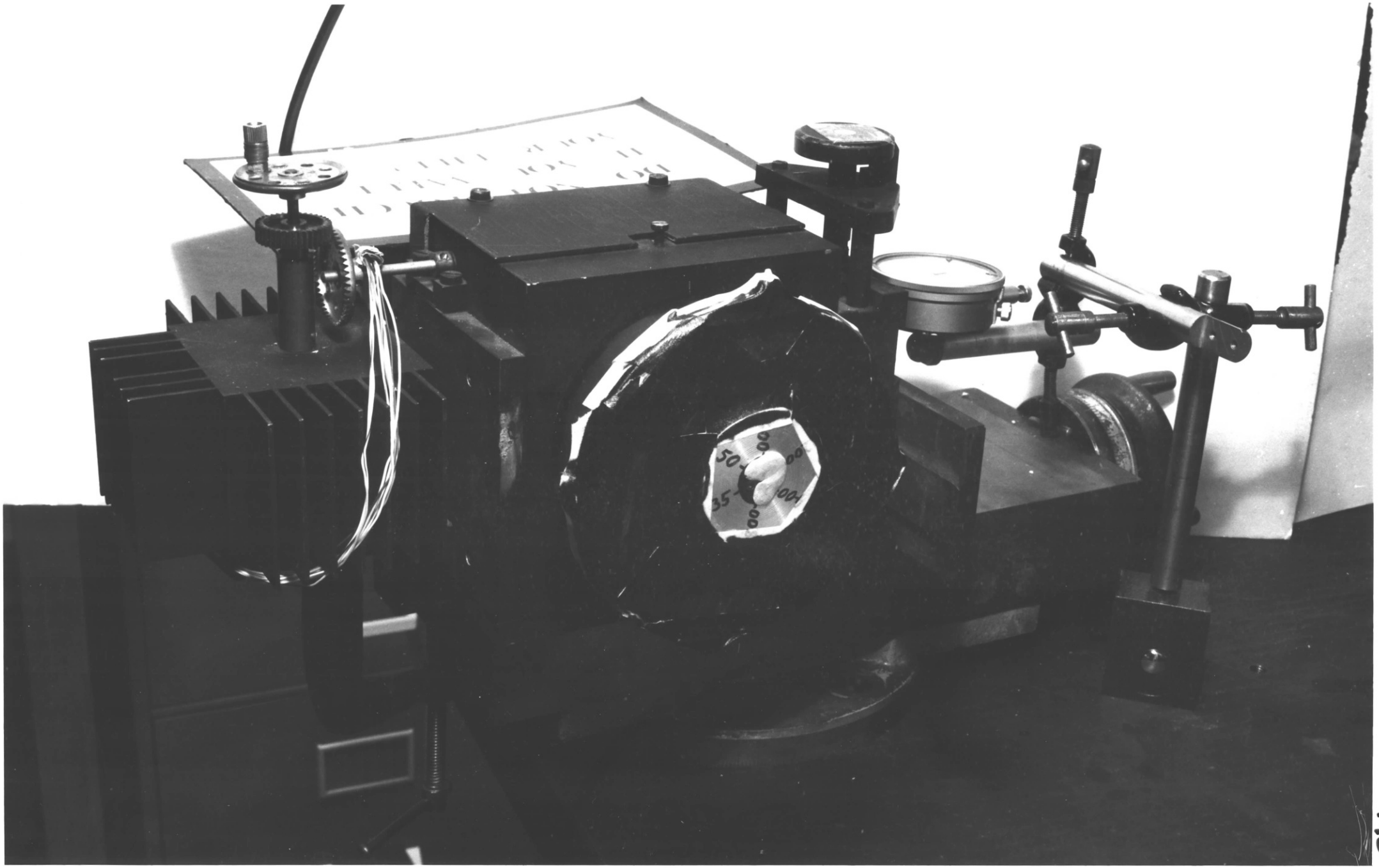
50
35

4.4. Contrast control and reversal

By subtracting a suitable amount of the DC light, an image can be produced with different contrast to that of the original object. For example, suppose we have an object whose amplitude transmission is a square wave as in Fig. 4.17i.

If the DC level is left unchanged, then assuming that the spatial frequency of the object is low enough for the blurring effects due to the finite size of the point spread function to be negligible (see appendix 2), the output image intensity of some optical system used to view the object will be as in Fig. 4.17ii, i.e. the square of the modulus of the amplitude distribution. If we subtract a DC level equal to the peak amplitude transmission of the object, then the output amplitude distribution will be as in Fig. 4.17iii. Squaring this gives Fig. 4.17iv which has reversed contrast compared to the original object.

If we subtract a DC level equal to half the peak amplitude transmission of the object, then we get an output amplitude as shown in Fig. 4.17v leading to the output intensity shown in Fig. 4.17vi, i.e. zero contrast.

Suppose we now use a continuous tone input transparency, represented by the amplitude distribution shown in Fig. 4.18i.

Partially subtracting the DC level results in the amplitude distribution shown in Fig. 4.18ii. Note that whereas before the amplitudes were all positive, in some of the regions they are now negative.

The intensity distribution (Fig. 4.18iv) is the square of the modulus of the amplitude distribution. Thus we see that the effect is similar to contrast reversal in regions where the amplitude was originally less than the subtracted DC amplitude and approximately normal contrast over the rest of the image.

To demonstrate this experimentally, the contrast was reversed for an input consisting of a wire grid in a circular frame (Fig. 4.19). The contrast reversed version is shown in Fig. 4.20.

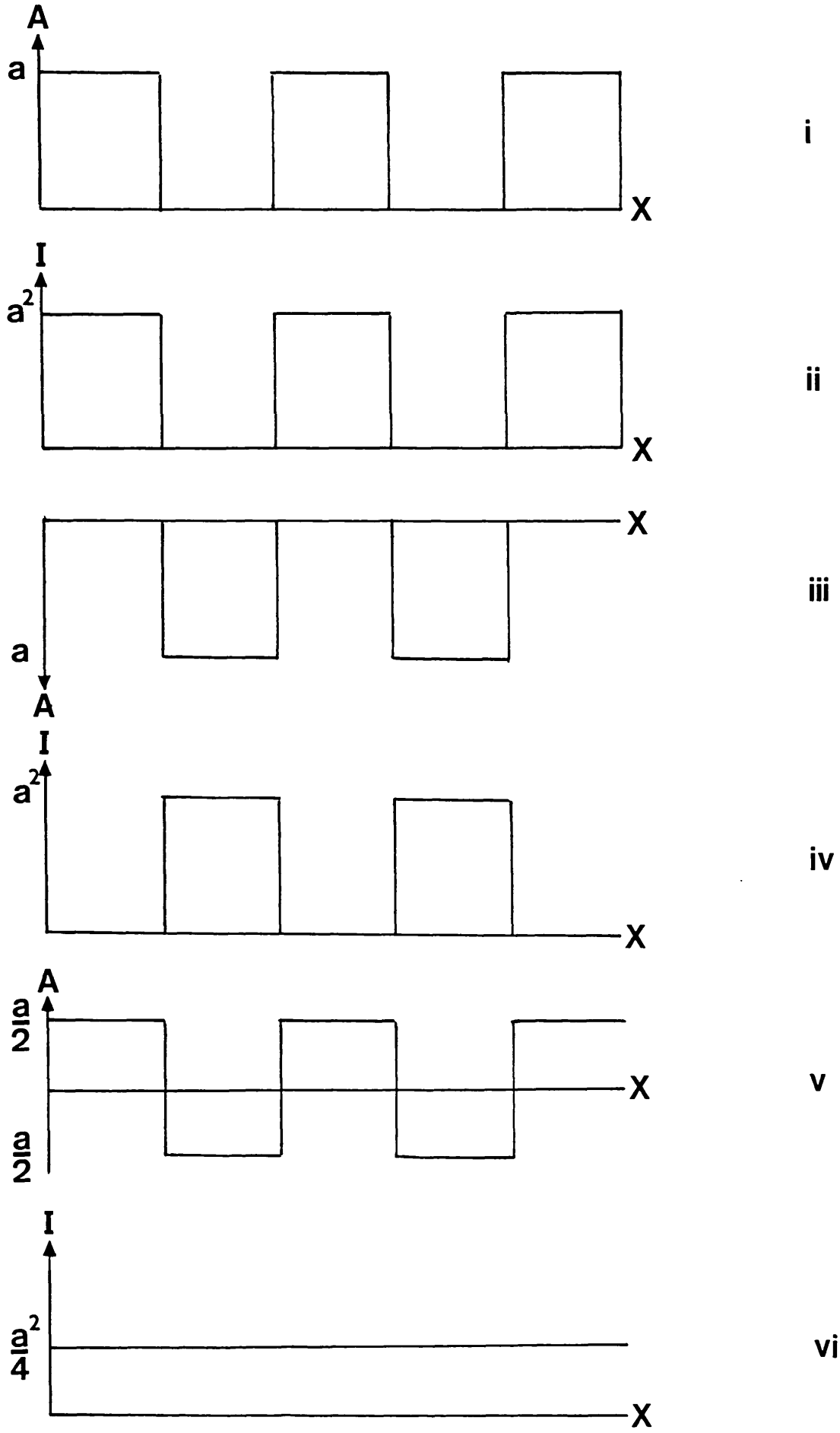

FIG 4.17

THE THEORY OF CONTRAST REVERSAL WITH A BINARY OBJECT

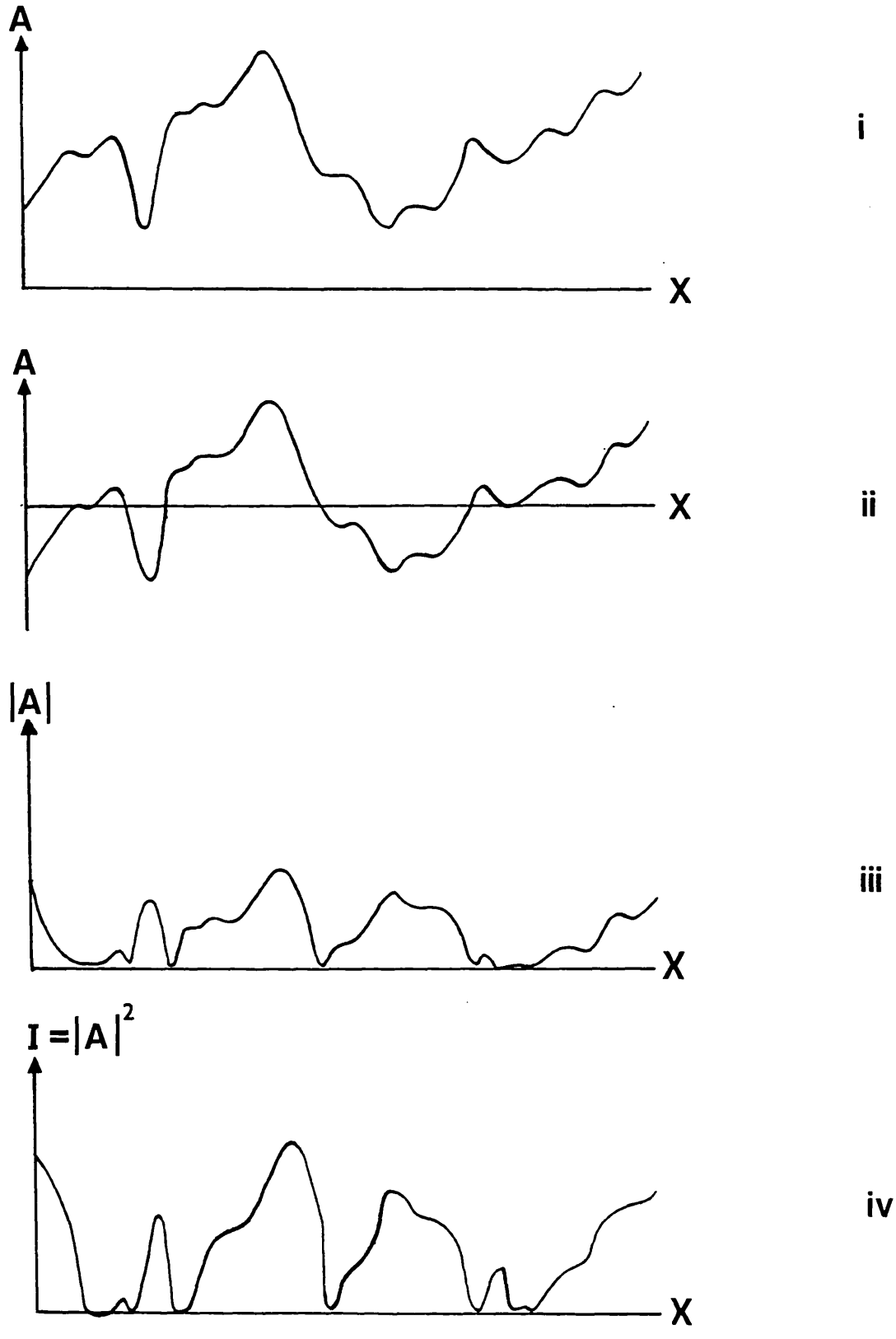

FIG 4.18

THE THEORY OF "LOCALISED CONTRAST REVERSAL" WITH A CONTINUOUS TONE OBJECT

FIG 4.19

GRID WITH NORMAL CONTRAST

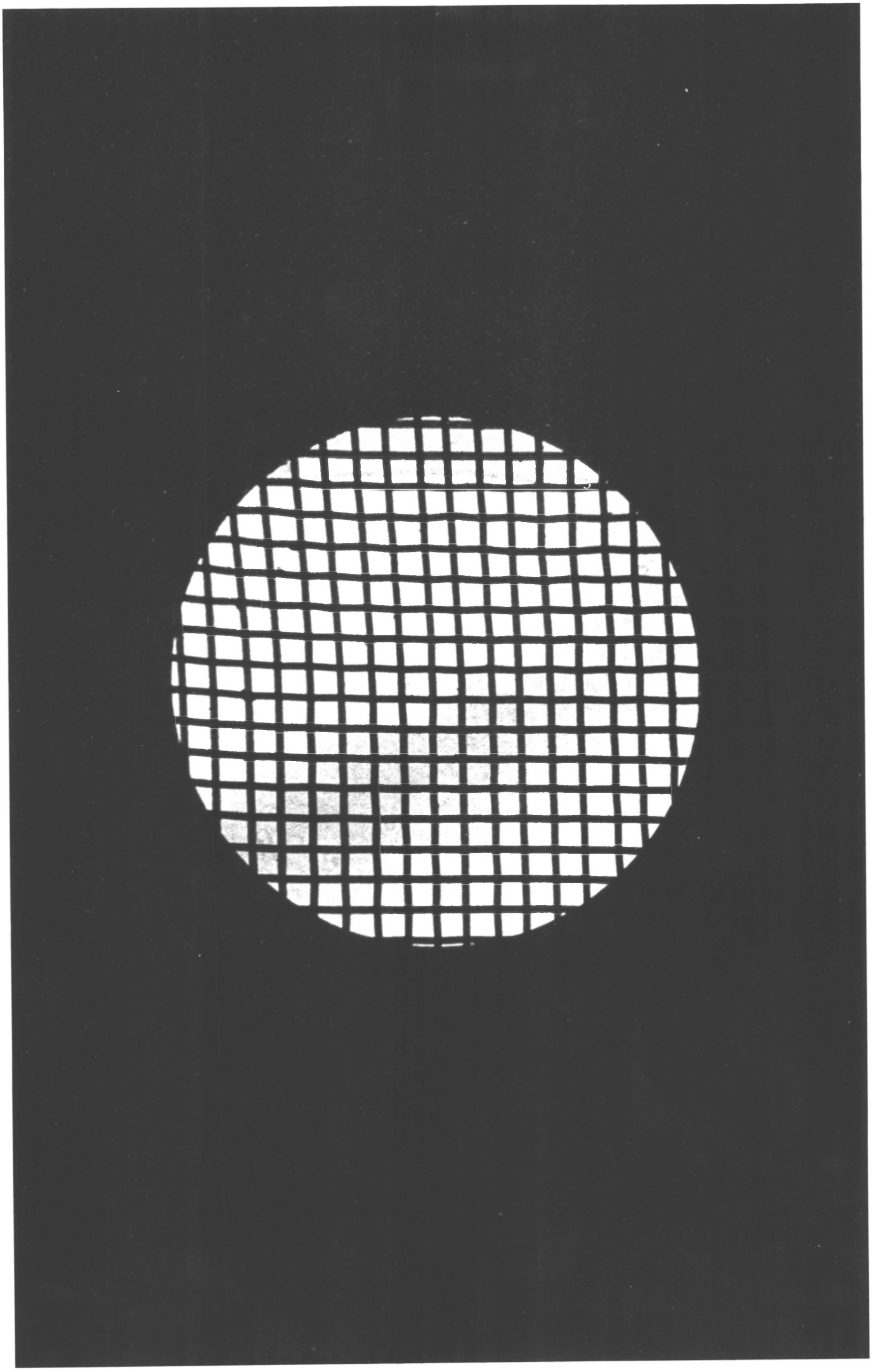

FIG 4.20

GRID WITH REVERSED CONTRAST

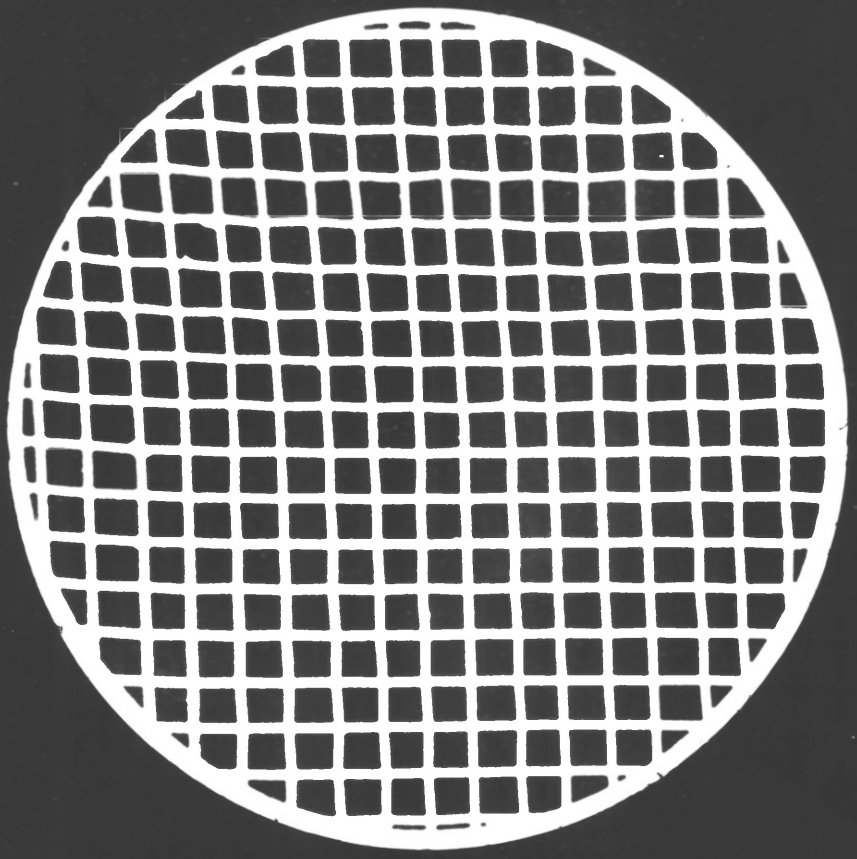

4.5. Differentiation

An approximation to the differential expression $\frac{df(x,y)}{dx}$ is given by

$$\frac{d\ f(x,y)}{dx} \simeq \frac{f(x+\Delta x,y) - f(x,y)}{\Delta x} \qquad (27)$$

where Δx is a small increment in x.

Hence, if we have two identical light distributions f(x,y) centred at (x,y) and (x+Δx,y), then subtracting one from the other will result in approximate differentiation of the input with respect to x.

As only one liquid gate was available, this had to be tested using binary objects with completely clear apertures.

An example would be the differentiation of a circle. In this case a pair of circular apertures are used, and the experimental results are shown in Fig. 4.21.

FIG 4.21

DIFFERENTIATION OF A CIRCULAR APERTURE

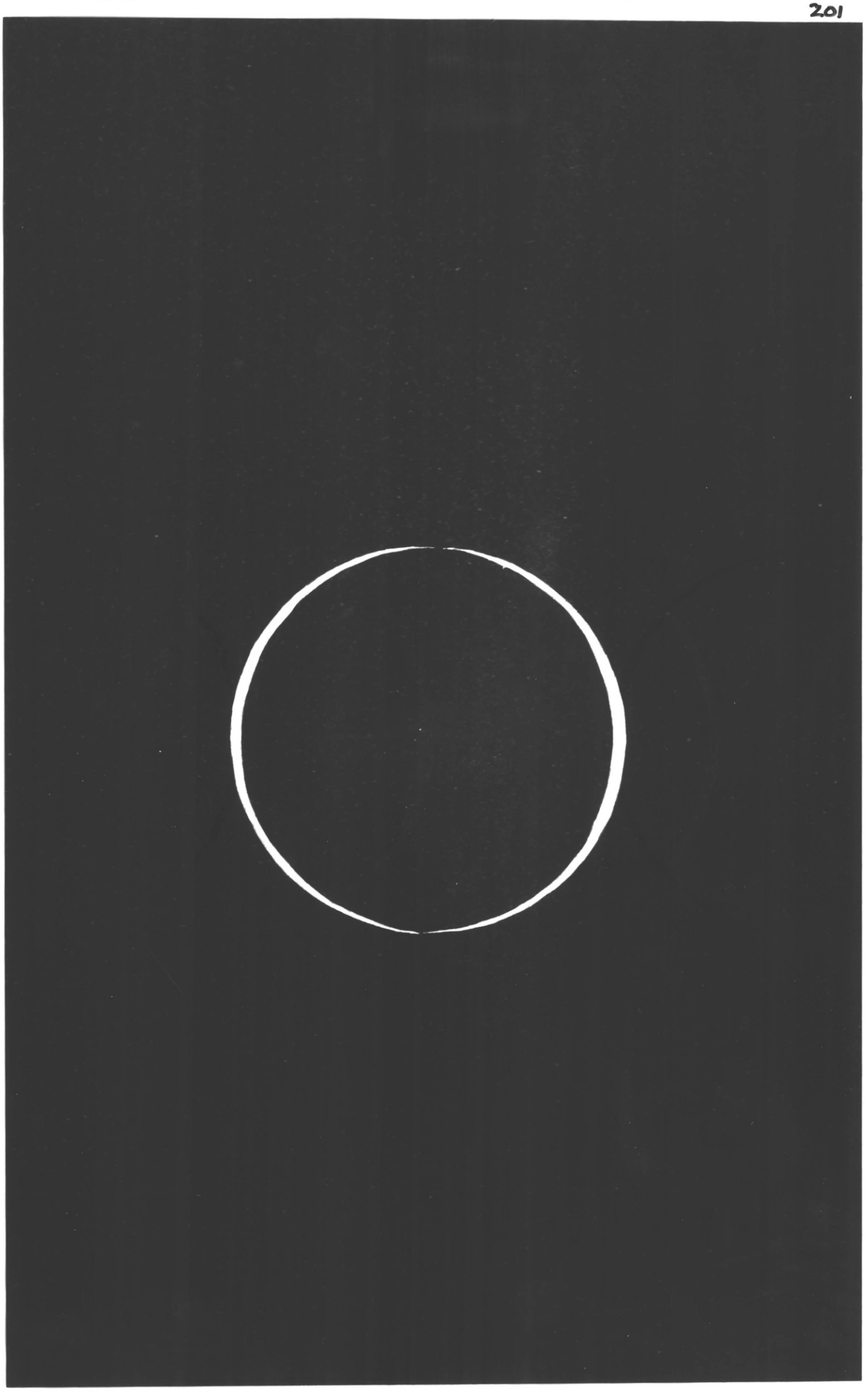

CHAPTER 5

SUMMARY AND CONCLUSIONS

This thesis is concerned with the reduction in the intensity of the undiffracted light in an optical Fourier transform system. After a brief history of the subject of coherent optical image processing, it was shown that there is a Fourier transform relationship linking the amplitude distribution in the back focal plane of a positive lens to the amplitude transmission of a transparency placed in its front focal plane and illuminated by collimated, coherent light. The main useful feature of this relationship is that if the transparency has some directions or spacings which are stronger or better represented than the others, then this will show up as bright regions in the transform plane.

If the input transparency is recorded on photographic film, a relatively large portion of the light passes through it undiffracted. This undiffracted light is focused by the lens to form a very intense region in the centre of the transform plane.

The effects of this undiffracted light on the optical Fourier analysis of geological imagery were described, and it was suggested that the measurements made of the relative strengths of the directionalities present in the input

transparency were biased by the contribution of the undiffracted light. It was concluded that these measurements would be made more accurate by either reducing the intensity of this undiffracted light or by changing its distribution to a less obtrusive form.

The relatively high intensity of the undiffracted light could also damage detectors used in the transform plane.

Previous work on this topic was then reviewed. There were three approaches: (a) The placing of a π phase plate over half the aperture or (b) the use of apertures with amplitude transmission that drop smoothly from a maximum at the centre to zero at the perimeter, both of which modified the form of the pattern due to the undiffracted light and (c) interferometric cancellation which reduces its intensity. It was concluded that for two dimensional inputs, the only viable method is interferometric cancellation, but previous methods of this type were limited in aperture and resolution and could not be readily adapted for use on the existing Imperial College Fourier transform bench.

There are three main parameters of the light beam which had to be considered:- the relative alignment of the beams, their phase difference and their relative amplitudes. Computer calculations showed that to achieve a reduction in the intensity of the undiffracted light by a factor of 40

times, assuming unaberrated beams, requires a phase difference of 180±5 degrees, beam amplitudes matched to within approximately 2 per cent and the beams aligned so that the separation of the corresponding Airy patterns in the transform plane is approximately one tenth of the radius of the central disc of each pattern or less. With the Imperial College system this corresponds to a tilt between the wavefronts of approximately half an arc second.

In Chapter 2, the detailed design of an interferometer to be used to reduce the intensity of the undiffracted light was considered. Controlling the relative alignment of the beams requires a stable beam steering method with high resolution and of the many methods available it was concluded that the most suitable was the use of a prism beam steering device. Previously reported designs suffered from a number of disadvantages. To overcome these a new type of prism device was constructed consisting of a pair of accurately matched wedge prisms, arranged almost antiparallel, with a small tilt between them. It was shown that there is an approximately linear relationship between the angle of rotation of the prisms and the beam deviation and that the sensitivity of the device could be changed over several orders of magnitude by changing the tilt between the prisms.

The interferometer was chosen to be of the polarization type as this would allow convenient and highly accurate control

of the phase difference and relative amplitude of the beams. In such an instrument the two beams are identified by their orthogonal polarization states and hence may be manipulated independently outside the interferometer. A variable retarder such as a uniform field compensator can be used to control the phase difference between the beams, and a half wave plate combined with a polarizing beamsplitter can be used as a variable ratio beamsplitter for controlling the relative amplitudes of the beams. This method of phase control was tested using a reversed Babinet compensator, and within the limitations set by the apparatus, it was concluded that the required resolution was achievable.

The procedure for aligning the interferometer was described in Chapter 3. With a tilt between the wavefronts of half an arc second, the fringe spacing at the output of the interferometer is approximately 200mm. Therefore these fringes could not be used to monitor the relative alignment of the beams. A more accurate method is to observe the transform plane intensity distribution which consists of two overlapping Airy patterns.

Computer simulations showed that for separations of approximately the radius of the central disc of one pattern or less, there is a wedge shaped region of low intensity whose wedge angle and position enable the relative alignment and phase difference of the beams to be estimated. Several

experimental examples were presented to show that these simulations were correct.

The use of a closed circuit video system with a density slicer was found to be extremely useful for viewing the transform plane.

Experimental results obtained using the interferometer were presented in Chapter 4. The required aberration tolerance for the instrument was that the wavefronts should match to within approximately $\lambda/14$. The output fringes obtained showed that this had been achieved.

Measurements of the intensity distribution along a line through the centre of the transform plane, with clear circular apertures in both arms of the interferometer showed that the maximum intensity of the undiffracted light had been reduced by a factor of approximately 30 times. Repeating these measurements with a photographic transparency in the object plane also resulted in a reduction in the intensity of the undiffracted light by a factor of approximately 30 times, suggesting that the cancellation efficiency of the interferometer is not strongly object dependent.

Measurements of the angular distribution of the light in the optical Fourier transforms of the geological transparencies

considered earlier led to the conclusion that reducing the intensity of the undiffracted light gives accurate values for the relative strengths of the directionalities present in the transparencies. Some detail is visible within the central region of the optical Fourier transform which was previously obscured by the undiffracted light and it was concluded that this detail was mainly due to very low frequency features in the input transparency.

Other optical image processing operations were discussed and it was shown experimentally that contrast reversal and differentiation of binary objects were possible.

The original aim of this project was to remove or reduce the intensity of the undiffracted light in the centre of the transform plane, and to obtain accurate measurements of the relative strengths of directionalities present in photographic transparencies with low average spatial frequencies. This has been achieved. Also detectors used in the transform plane when the undiffracted light intensity is reduced are less likely to be damaged.

A summary of this project was presented at the Optics '84 Conference at the University of Keele in September 1984, and a paper based on this presentation is to be published in the February 1985 issue of Optica Acta.

At the time of binding of this thesis, the offprints of this paper were not available, so a copy of the publishers proof print has been bound at the back of this thesis.

APPENDIX 1

THE FOURIER TRANSFORM OF A CIRCULAR APERTURE

The Fourier transform of a circular aperture

To find the Fourier transform of a circular aperture, we start with the Fourier transform equation from section 1.2.2.:

$$\{P_c(x,y)\} = \iint_{\substack{\text{over}\\ \text{the}\\ \text{aperture}}} P_c(x,y)e^{-2\pi i(ux+vy)}dxdy \qquad (A.1.1)$$

where x and y are the spatial coordinates, u and v are the spatial frequency coordinates and $P_c(x,y)$ represents the aperture. To evaluate this integral we first make a few simplifications. The system is circularly symmetric, so we only need to calculate the pattern in the u direction. To simplify matters further we switch to polar coordinates by setting

$$x = \rho \cos\theta \qquad (A.1.2)$$

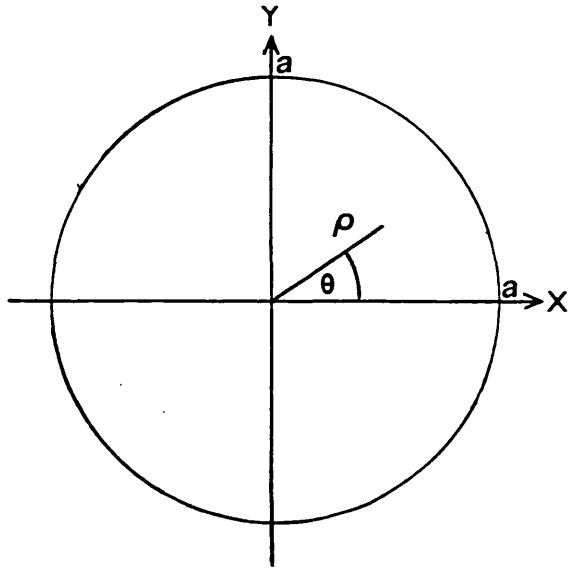

so the integral becomes:

$$\mathcal{F}\{P_c(x,y)\} = \int_0^a \int_{-\pi}^{+\pi} e^{-2\pi i\rho u\cos\theta}\rho d\rho d\theta \qquad (A.1.3)$$

Abramowitz and Stegun (1965) equation 9.1.21 is:

$$J_o(t) = \frac{1}{\pi}\int_0^{\pi} e^{it\cos\theta}d\theta \qquad (A.1.4)$$

where $J_o(t)$ is a zero order Bessel function of the first kind. Therefore the θ part of the integral becomes:

$$2\pi\ J_o(2\pi\rho u) \qquad (A.1.5)$$

The minus sign disappears as $J_o(t)$ is an even function. Therefore:

$$\mathcal{F}\{P_c(x,y)\} = 2\pi\int_0^a \rho J_o(2\pi\rho u)\ d\rho \qquad (A.1.6)$$

to simplify this we put:

$$\sigma = 2\pi\rho u \qquad (A.1.7)$$

$$\text{hence } \rho d\rho = \frac{\sigma d\sigma}{(2\pi u)^2} \qquad (A.1.8)$$

and hence:

$$\mathcal{F}\{P_c(x,y)\} = \frac{2\pi}{(2\pi u)^2} \int_0^a \sigma J_o(\sigma) d\sigma \qquad \text{(A.1.9)}$$

Abramowitz and Stegun (1965) equation 9.1.30 is:

$$\sigma J_o(\sigma) = \frac{d}{d\sigma} \sigma J_1(\sigma) \qquad \text{(A.1.10)}$$

where $J_1(\sigma)$ is a first order Bessel function of the first kind. Therefore:

$$\int_0^a \sigma J_o(\sigma) d\sigma = \left[\sigma J_1(\sigma) \right]_0^a \qquad \text{(A.1.11)}$$

Hence:

$$\mathcal{F}\{P_c(x,y)\} = \frac{2\pi}{(2\pi u)^2} 2\pi a u J_1(2\pi a u) \qquad \text{(A.1.12)}$$

Therefore:

$$\mathcal{F}\{P_c(x,y)\} = 2\pi a^2 \frac{J_1(2\pi a u)}{(2\pi a u)} \qquad \text{(A.1.13)}$$

As the system is circularly symmetric, we can replace u by $r = \sqrt{u^2+v^2}$

Therefore:

$$\mathcal{F}\{P_c(x,y)\} = 2\pi a^2 \frac{J_1(2\pi ra)}{2\pi ra} \qquad \text{(A.1.14)}$$

This is equation 18 from section 1.2.2.

On an optical Fourier transform system as shown in Fig. 1.3, the actual spatial coordinate in the transform plane is given by $x' = \lambda f u$. Therefore if a clear circular aperture of radius a is placed in the object plane and the incident illumination has amplitude R, the transform plane amplitude distribution is given by

$$A(r) = R\, 2\pi a^2 \frac{J_1(2\pi ax'/\lambda f)}{(2\pi ax'/\lambda f)}$$

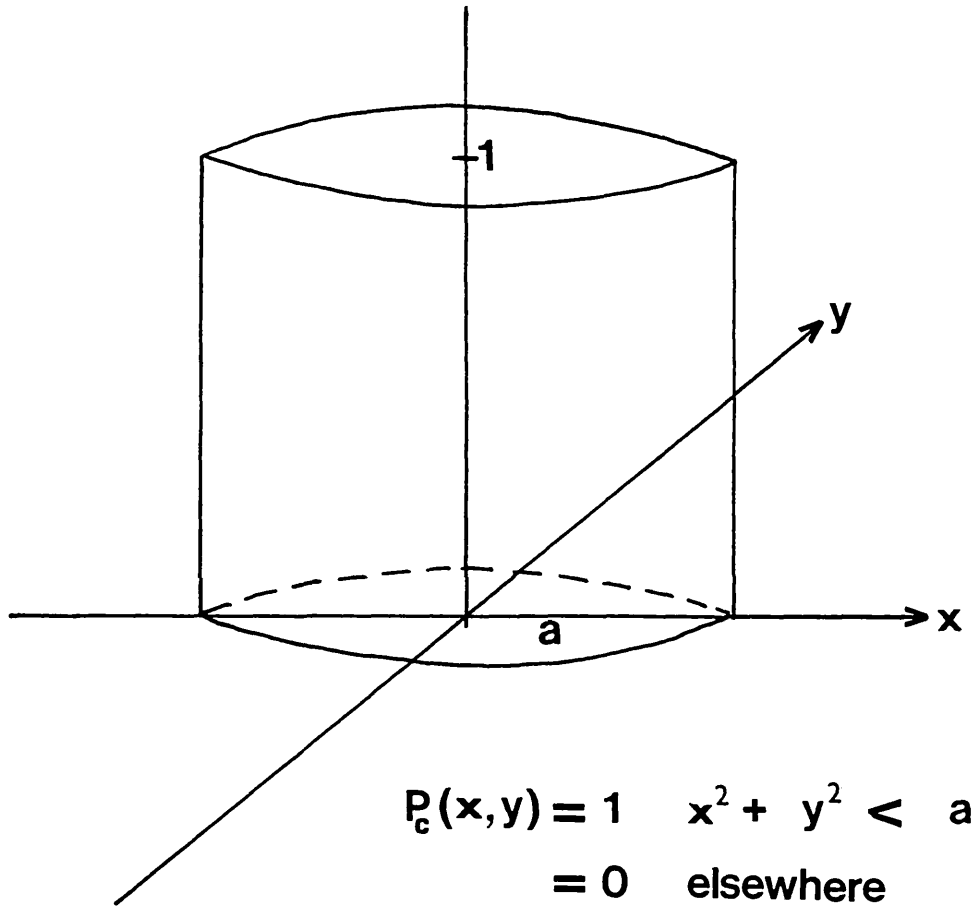

$$P_c(x,y) = 1 \quad x^2 + y^2 < a^2$$
$$= 0 \quad \text{elsewhere}$$

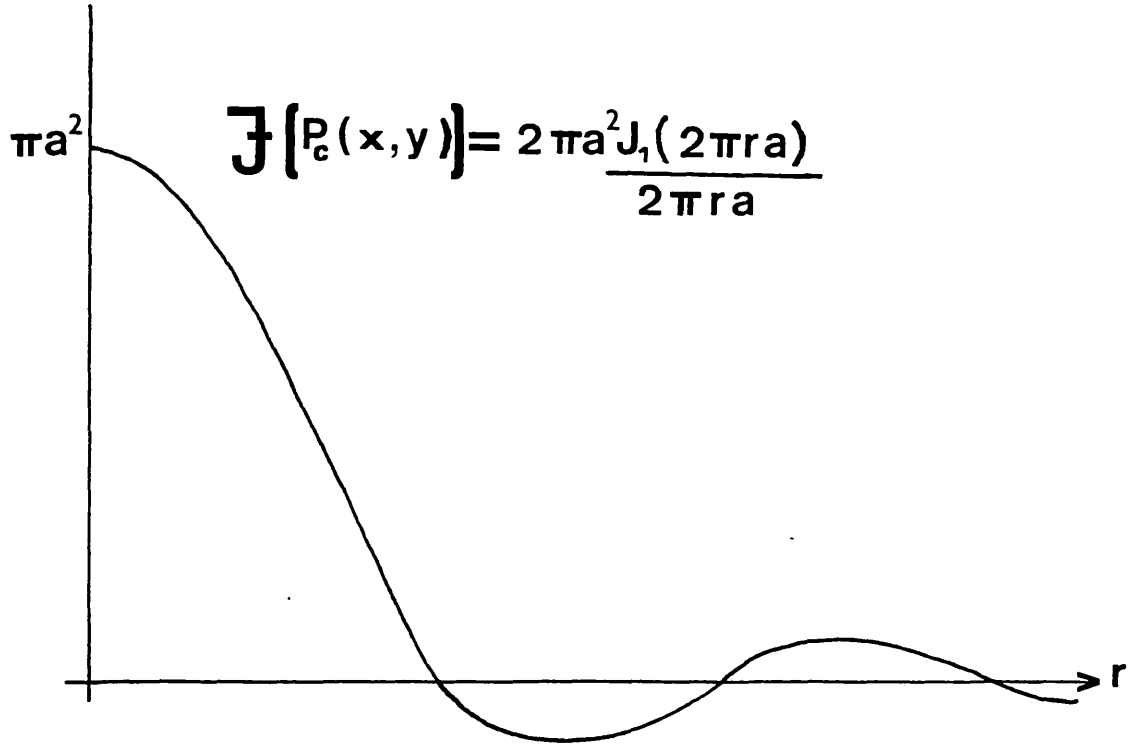

$$\mathcal{F}[P_c(x,y)] = 2\pi a^2 \frac{J_1(2\pi r a)}{2\pi r a}$$

FIG A.1.1

THE CIRCULAR APERTURE AND ITS FOURIER TRANSFORM

APPENDIX 2

CONVOLUTION

The convolution theorem

Suppose we have two functions g(x) and f(x) whose Fourier transforms G(u) and F(u) are given by:

$$G(u) = \int_{-\infty}^{+\infty} g(x) e^{-2\pi iux} dx \qquad \text{(A.2.1)}$$

and

$$F(u) = \int_{-\infty}^{+\infty} f(x) e^{-2\pi iux} dx \qquad \text{(A.2.2)}$$

The Fourier transform of the product g(x).f(x) is given by:

$$H(u) = \int_{-\infty}^{+\infty} g(x).f(x) e^{-2\pi iux} dx \qquad \text{(A.2.3)}$$

Expressing f(x) in terms of its Fourier transform gives:

$$H(u) = \int_{-\infty}^{+\infty} g(x)\ e^{-2\pi iux} dx \left(\int_{-\infty}^{\infty} F(u')\ e^{+2\pi iu'x} du' \right) dx \qquad \text{(A.2.4)}$$

where u' is a dummy variable.

Reversing the order of the integration gives:

$$H(u) = \int_{-\infty}^{+\infty} F(u') \left[\int_{-\infty}^{+\infty} g(x)\ e^{-2\pi i (u-u')x} dx \right] du' \qquad (A.2.5)$$

Therefore:

$$H(u) = \int_{-\infty}^{+\infty} F(u')\ G(u-u')du' \qquad (A.2.6)$$

Expressions of this form are known as convolution integrals and are denoted in this thesis by the symbol $\otimes$ so:

$$\int_{-\infty}^{+\infty} F(u')\ G(u-u')du' = F(u) \otimes G(u) \qquad (A.2.7)$$

is the convolution of F(u) with G(u)

Several other symbols are often used to represent the convolution operation instead of $\otimes$, notably @ and *.

Using the previous notation:

$$\mathcal{F}\{g(x).f(x)\} = F(u) \otimes G(u)$$
$$= G(u) \otimes F(u)$$

The meaning of convolution

Convolution operations can be considered in the following way. Supose we have two functions F(u) and G(u) which we will arbitrarily choose to have the forms shown in Figs. A2.i. and A2.ii. Using the equation for H(u) we see that we have to consider the product function F(u').G(u-u'). Now G(-u') is simply the function G(u) reversed and plotted against u' rather than u (Fig. A2.iv). G(u-u') is this function shifted along the u' axis by an amount +u (Fig.A2.v). F(u') is the same function as F(u) but plotted against u' rather than u (Fig. A2.vi). So F(u').G(u-u') is the function shown in Fig. A2.vii.

The value of H(u) is the integral of this product function with respect to u' over the range of u' from $-\infty$ to $+\infty$ i.e. the area under the product function curve. (Fig. A2.viii). As u changes, one pattern "slides over" the other resulting in a continuously changing value for H(u). Note that for values of u where there is no overlap, H(u) is zero. Hence, in general, the width of H(u) is equal to the sum of the widths of F(u) and G(u).

The effect of convolution is one of blurring in which each discrete point of the curve of the function F(u) is replaced by a blur of the shape of the reversed curve of the function G(u). The convolution H(u) is the function given by the

super position of all these blurred points. Processes like this occur all over physics.

In practice we often find that the width of one curve is much less than that of the other. For example the point spread function of a lens is usually much smaller than the image produced by the lens. Thus the result of the convolution is a blurring of the fine detail in the image.

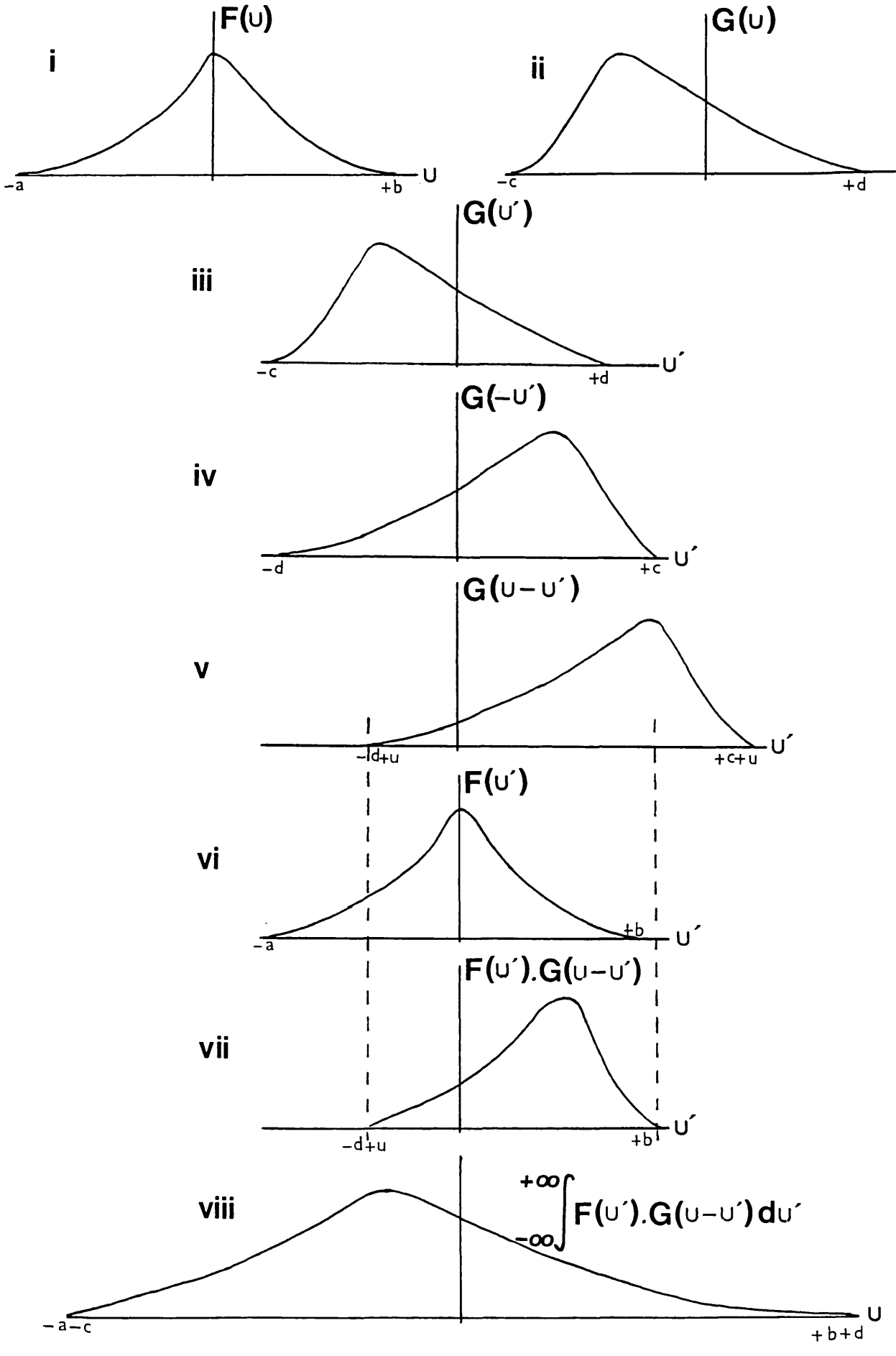

FIG A.2.1

A GRAPHICAL REPRESENTATION OF CONVOLUTION

APPENDIX 3

VARIABLE RETARDERS AND THEIR CALIBRATION

Variable retarders and their calibration

If two coherent, monochromatic waves, linearly polarized in planes perpendicular to one another are combined, the result is in general elliptically polarized.

If the electric fields of the two beams are represented by:-

$$E^1_x = a \cos (wt-\alpha) \qquad E^2_y = b \cos (wt-\beta)$$

$$E^1_y = 0 \qquad E^2_x = 0$$

where a and b are the wave amplitudes, w is the angular frequency, and α and β are the phases of the two waves relative to some arbitrary zero.

Then the elliptically polarized beam will have the components:-

$$E^e_x = a \cos (wt-\alpha)$$

$$E^e_y = b \cos (wt-\beta)$$

It is often necessary to measure the phase difference $\delta=(\alpha-\beta)$ in such a beam of elliptically polarized light. The instruments used for these measurements are called optical compensators and are in fact, variable retarders. Some,

such as the Babinet compensator, have retardations which vary linearly over the field of view, whilst others, such as the Soleil and reversed Babinet compensators have uniform retardation over the field of view. The various types are described by Jerrard (1948).

The normal method of use is to pass the light of unknown phase difference δ through the compensator, which is adjusted until linearly polarized light emerges.

At this point, an observer looking through a suitably orientated linear polarizer sees a uniformly dark field of view. See Fig. A.3.1.

The phase difference between the polarization components of the original light can then be calculated from the compensator settings.

In general, commercially available compensators are claimed (by the manufacturers) to have resolutions of between $\lambda/100$ and $\lambda/3000$ in the visible (depending on the type). Although it has also been claimed (Dyson 1970) that the linearity of path difference with motion of the crystal prisms often leaves something to be desired.

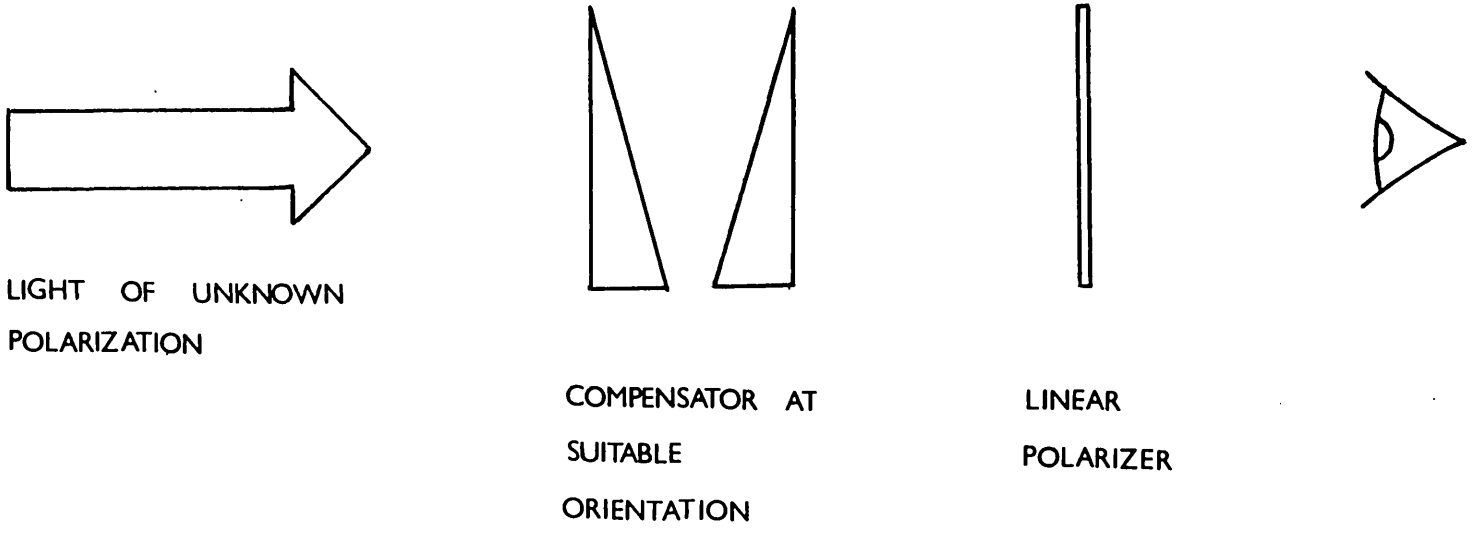

FIG A.3.1
THE USUAL METHOD OF USING AN OPTICAL COMPENSATOR

Variations between different compensators mean that each one should be individually calibrated for the wavelength in use. Unfortunately, the sensitivity of the eye is such that the position of minimum intensity is difficult to locate with high accuracy. Therefore many compensators include a half shadow plate (Jerrard 1951), which usually takes the form of a mica plate of small retardation covering half the field of view.

This enables the compensator to be adjusted to give equal intensities in the two halves of the field of view, i.e. the retardations in the two halves are equally spaced about the setting for linearly polarized output light.
The eye is much more sensitive to variation in intensity when it has two areas side by side to compare with each other.

Calibration

Before use, the compensator needs to be calibrated for the wavelength at which it is to be used. The method (due to Jerrard 1953) is as follows.

(a) Without half shadow plate

The compensator is placed between crossed polarizers in azimuth 45^{o} as in Fig. A3.2. The compensator is set to one

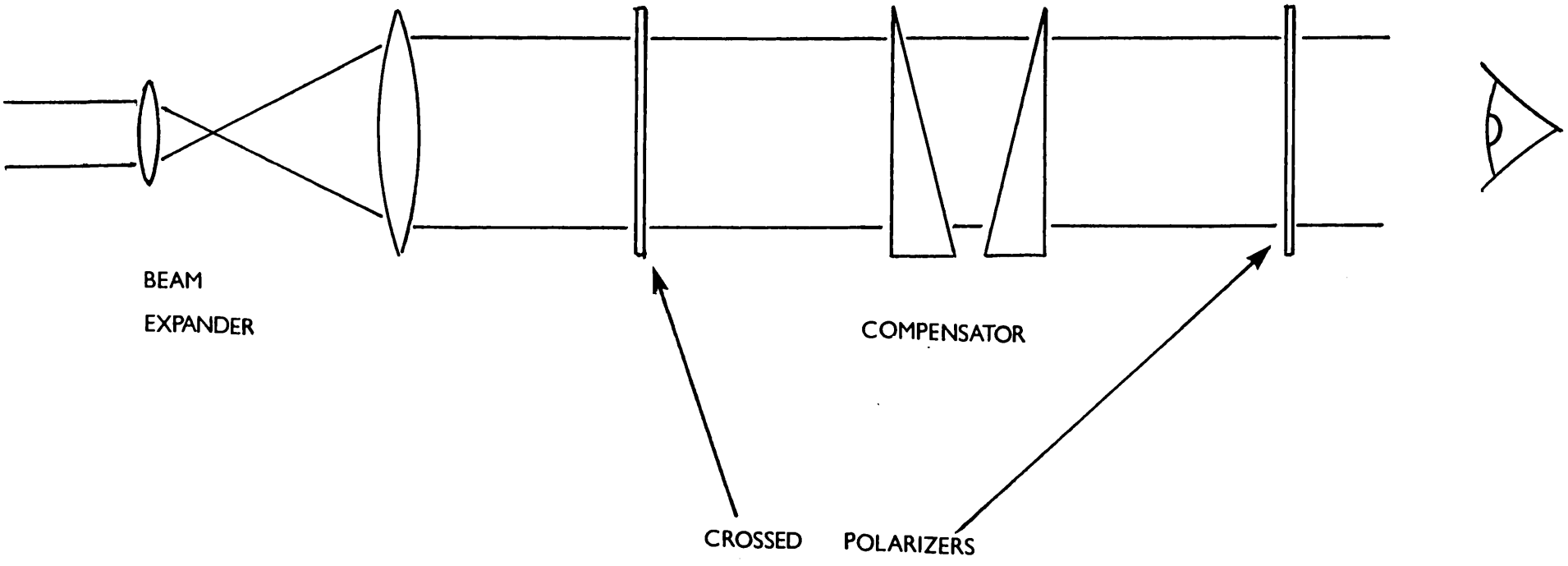

FIG A.3.2
THE APPARATUS USED TO CALIBRATE AN OPTICAL COMPENSATOR

end of its range of adjustment, and with monochromnatic light passing through, its setting is adjusted until a dark field of view is obtained and the drum reading is noted.

The drum is now turned until the next dark field of view occurs and the reading is noted again. This is repeated until the drum reaches the other end of its traverse and a graph is plotted of extinction number against drum reading. This should be a straight line, the slope of which gives the phase difference per drum division.

Due to the low sensitivity of the eye to low intensity light sources the whole process should be repeated for compensator azimuths of 135°, 225° and 315° and an average result calculated.

(b) With half shadow plate

If the half shadow plate has a retardation η and is at an azimuth h, then for the two halves of the field of view to be equally bright, the phase difference ψ of the compensator must satisfy:

$$\tan(\psi) = \sin(2h)\ \tan(\eta/2)$$ (Jerrard 1951)

but as η is small, this may be written:

$$\psi = \sin(2h)\ \eta/2$$

For any given value of η, there is an optimum value of h which gives maximum sensitivity. This azimuth can be calculated if the properties of the eye are ignored, but in practice it is best found by trial.

The apparatus used is the same as before, with the compensator between crossed polarizers.

The compensator and half shadow plate are rotated separately until the whole field of view is dark. The compensator alone is then rotated through 45^{o} so that the compensator and half shadow plate are in azimuth 45^{o} and 0^{o} respectively, measured from the transmission azimuth of the first polarizer.

The compensator drum is then rotated until the whole field of view is dark again, and the drum reading is noted. The half shadow plate is now rotated by 10^{o} and the compensator is adjusted to give equal intensities in the two halves of the field of view. This reading is noted, the match is destroyed by changing the compensator setting and a new reading is taken.

This process of destroying and restoring the match is repeated at least 6 times and from these readings the mean

and variation from the mean are calculated. This is repeated for half shadow azimuth of 20°, 30° and so on at 10° intervals throughout its range of rotation.

A graph is now plotted of mean drum reading against half shadow azimuth. Since the drum readings are proportional to the phase difference ψ, this should be a sine curve.

The azimuth h_o for which the variation from the mean is a minimum is the most favourable azimuth for the observer under these conditions.

Finally, the half shadow plate is set in azimuth h_o and the same procedure as in the case without the half shadow plate is followed, except that the adjustments are made to give equal intensity in both halves of the field of view rather than to darkness. A graph of match number against drum reading is plotted, the slope of which gives the phase difference per drum reading.

Calibration of the device used for this project

The compensator used was of the reversed Babinet type with a half shadow plate as shown schematically in Fig. A3.3. This has the disadvantage that there is a slight deviation of the beam (around $\frac{1}{2}$ degree), but since there are only 4 surfaces

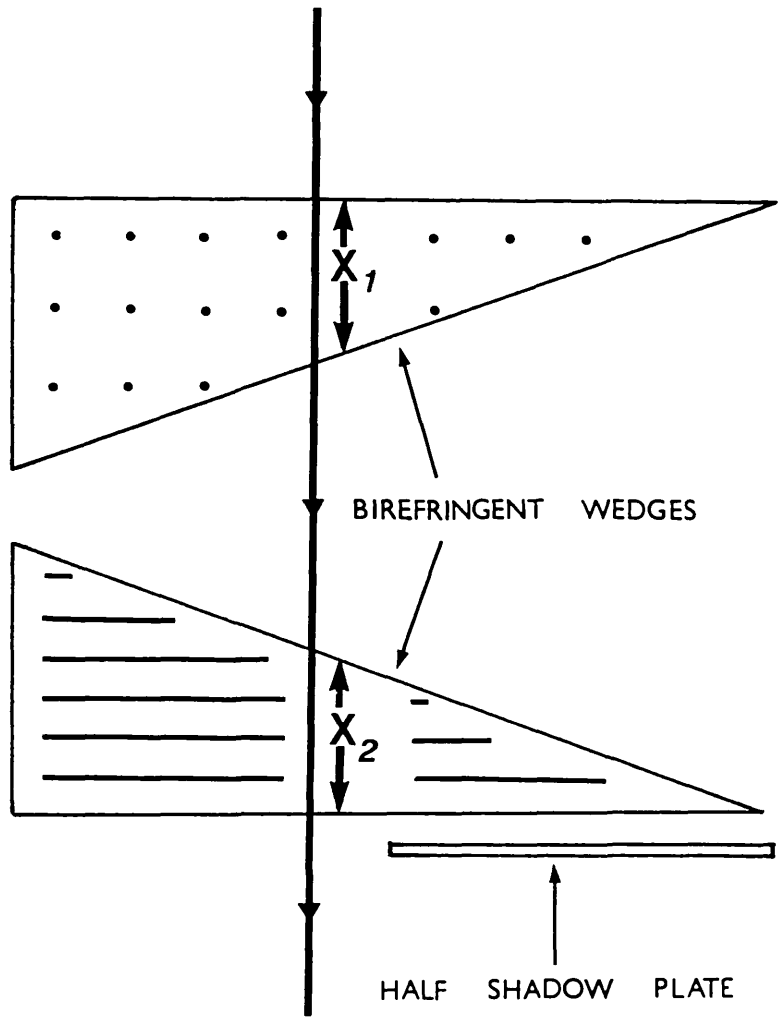

FIG A.3.3

THE REVERSED BABINET COMPENSATOR

to polish, it is easier to manufacture than some other types.

Fig. 2.12 is a photograph of the actual device used. The test arrangement is shown in Fig. A3.4. Light from an Argon ion laser (λ = 488nm) was expanded and collimated with a microscope objective and a paraboloidal mirror. An uncoated beamsplitter reduced the intensity to a comfortable one for viewing. The compensator was placed between crossed polaroid sheets and the output light was observed on a ground glass screen.

Results of the first part of the calibration are shown in Fig. A3.5. There was very little difference between the variation from the mean for different azimuths, with perhaps a slight decrease at approximately 126°. So this was chosen as the "most favourable azimuth".

Results from the second part of the calibration are shown in Fig. A3.6 and give a resolution of (0.1688 ± 0.0004) x 2π radians per mm at a wavelength of 488nm.

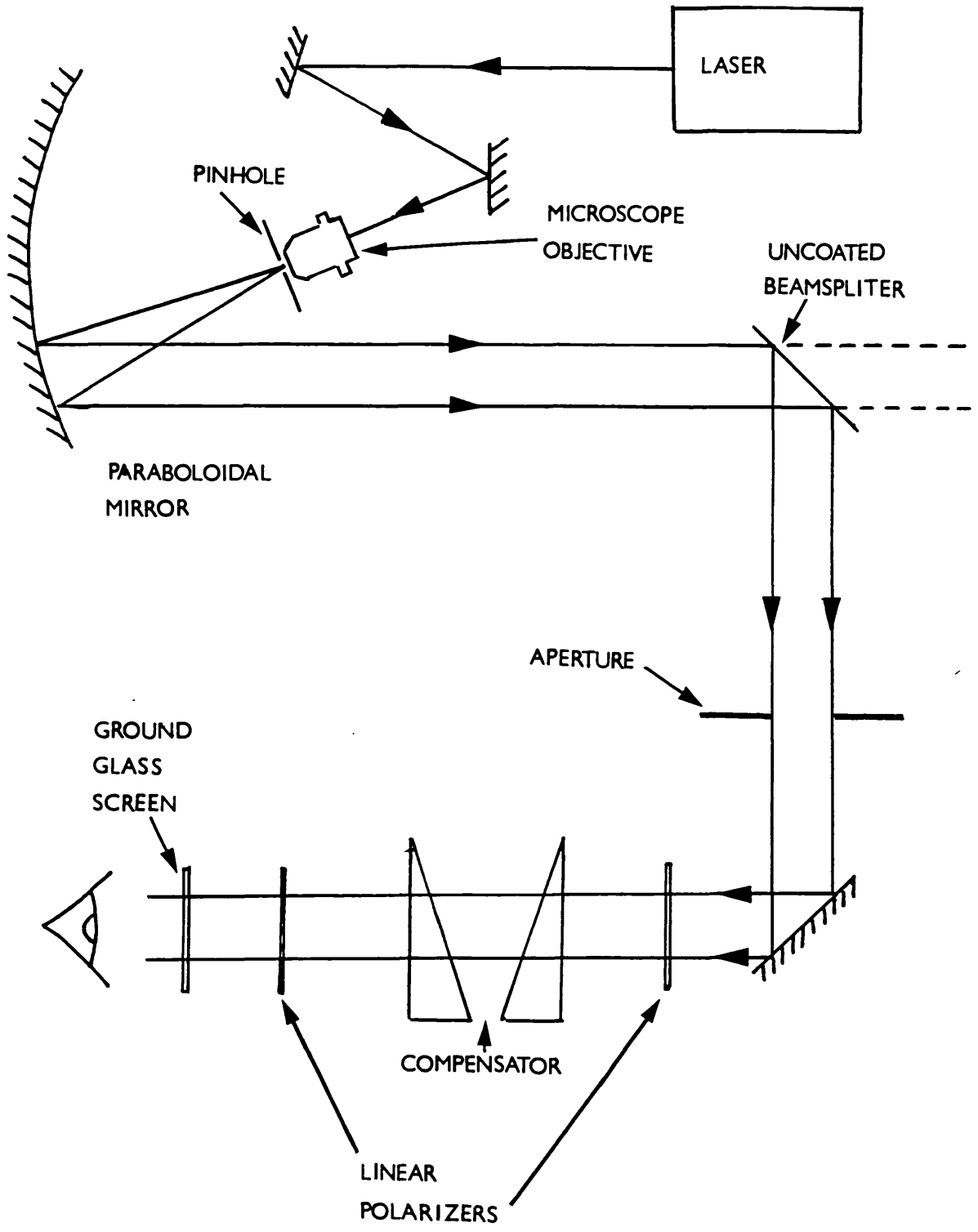

FIG A.3.4

THE EXPERIMENTAL APPARATUS USED TO CALIBRATE THE COMPENSATOR

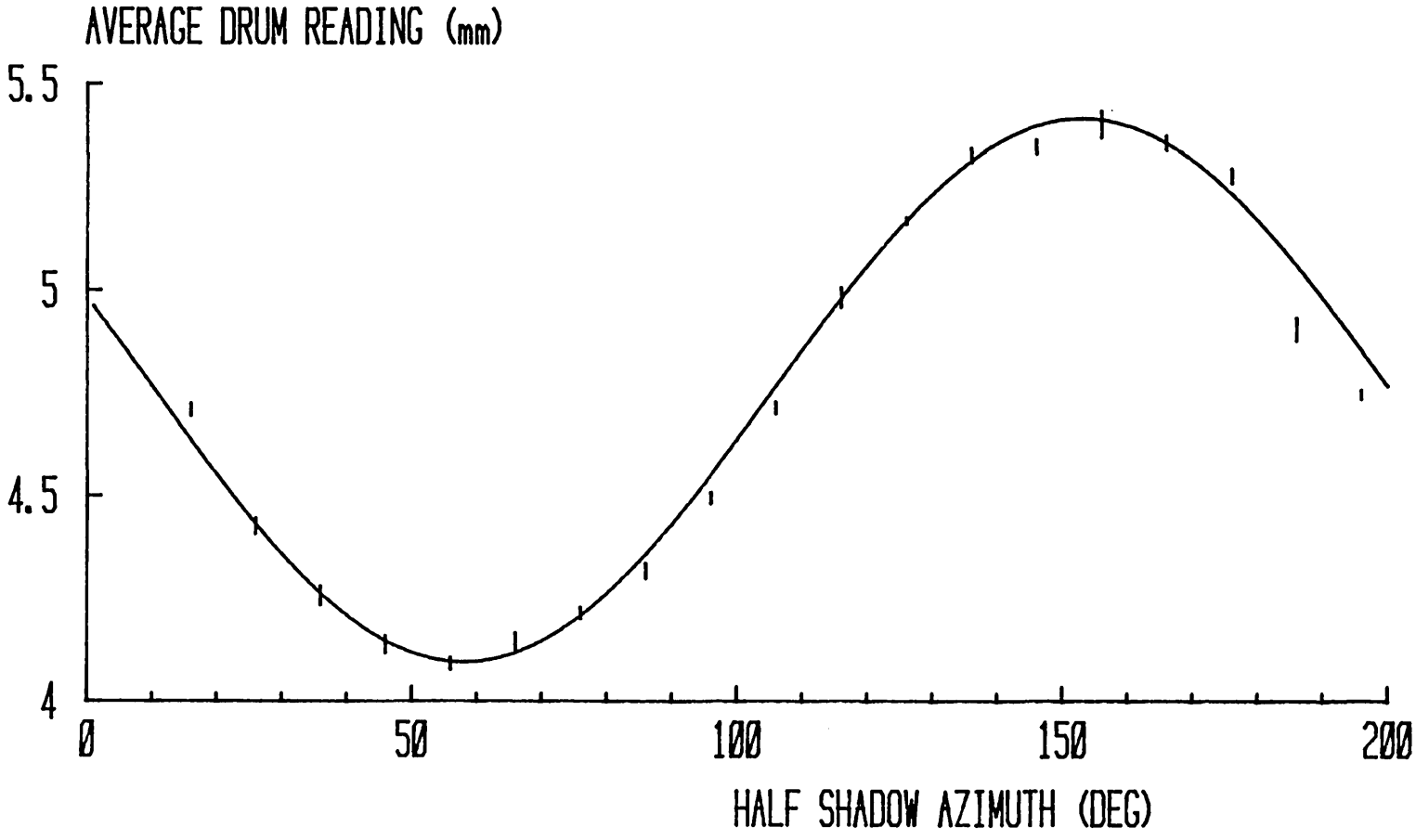

FIG A.3.5
RESULTS FROM THE FIRST PART OF THE CALIBRATION

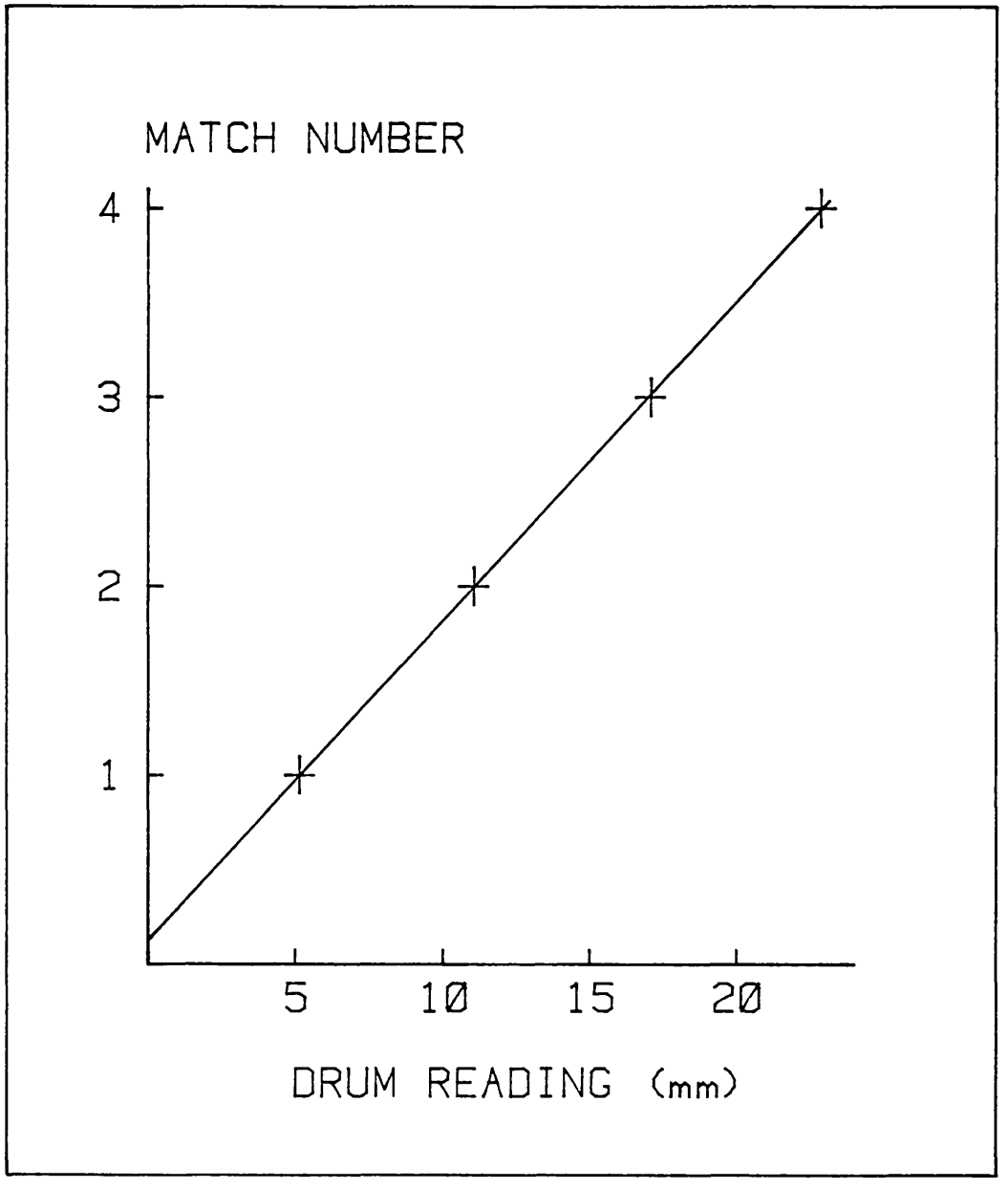

FIG A.3.6
RESULTS FROM THE SECOND PART OF THE CALIBRATION

APPENDIX 4

PROOF OF EQUATION 26 FOR THE BEAM STEERING DEVICE

Proof of equation 26 for the beam steering device

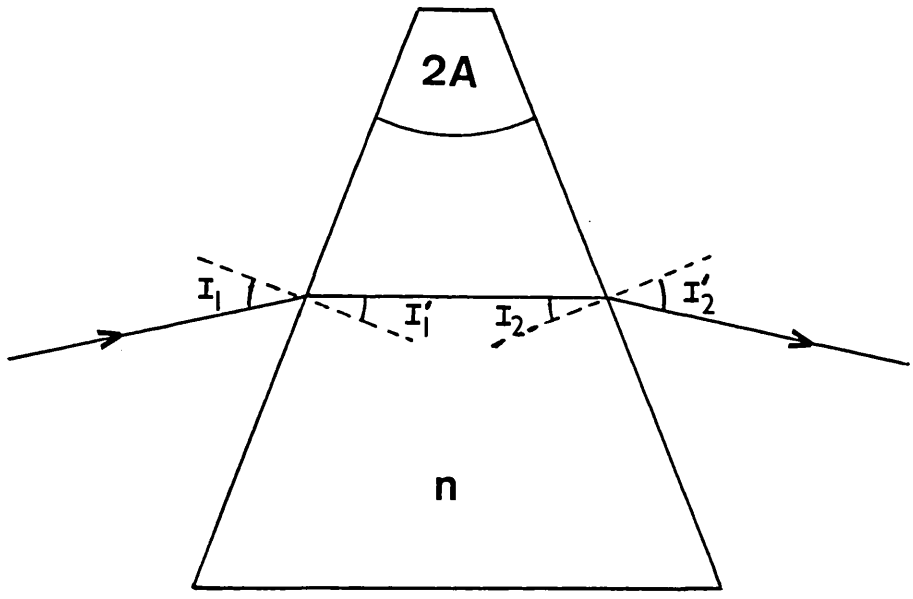

Consider a prism of wedge angle 2A and refractive index n. A light beam incident on the first face at an angle I_1 will pass through the prism with the angles as labelled on the diagram, where:-

$$\sin(I_1) = n \sin(I_1') \qquad \text{(A4.1)}$$

$$I_1' + I_2 = 2A \qquad \text{(A4.2)}$$

$$\sin(I_2') = n \sin(I_2) \qquad \text{(A4.3)}$$

At minimum deviation:—

$$I_1' = I_2 = A \qquad \text{(A4.4)}$$

$$I_1 = I_2' = I_o \qquad \text{(A4.5)}$$

$$\sin(I_o) = n \sin(A) \qquad \text{(A4.6)}$$

If the prism is tilted away from minimum deviation by an angle α, then:—

$$I_1 = I_o + \alpha \qquad \text{(A4.7)}$$

$$I_1' = A + \alpha' \qquad \text{(A4.8)}$$

$$I_2 = A - \alpha' \qquad \text{(A4.9)}$$

$$I_2' = I_o + \alpha'' \qquad \text{(A4.10)}$$

Putting the new values for I_1 and I_1' into (A4.1) gives:—

$$\sin(I_o + \alpha) = n \sin(A + \alpha')$$

$$\sin(I_1) = \sin(I_o + \alpha) = \sin(I_o)\cos(\alpha) + \cos(I_o)\sin(\alpha) \qquad \text{(A4.11)}$$

α is small, therefore:-

$$\sin(I_1) \simeq \sin(I_o)\left(1 - \frac{\alpha^2}{2}\right) + \alpha \cos(I_o) \qquad (A4.12)$$

$$n \sin(I_1') = n \sin(A + \alpha') = n \sin(A)\cos(\alpha') + \cos(A)\sin(\alpha') \qquad (A4.13)$$

$$n \sin(I_1') \simeq n\left[\sin(A)\left(1 - \frac{\alpha'^2}{2}\right) + \alpha' \cos(A)\right] \qquad (A4.14)$$

equating (A4.12) and (A4.14) using (A4.6) we obtain:

$$\alpha \cos(I_o) - \tfrac{1}{2}\alpha^2 \sin(I_o) \simeq n\left[\alpha' \cos(A) - \frac{\alpha'^2}{2}\mathrm{Sin}(A)\right] \qquad (A4.15)$$

Ignoring terms in α'^2 and α^2 gives:

$$\alpha' \simeq \frac{\alpha\, \mathrm{Cos}(I_o)}{n \cos(A)} \qquad (A4.16)$$

which when substituted into (A4.15) gives:

$$n\alpha' \cos(A) \simeq \alpha \cos(I_o) - \tfrac{1}{2}\alpha^2 \sin(I_o) + \frac{n}{2}\sin(A)\left(\frac{\alpha \cos(I_o)}{n \cos(A)}\right)^2 \qquad (A4.17)$$

Rearranging (A4.17) and using (A4.6) gives:

$$\alpha' \simeq \frac{1}{n\cos(A)}\left[\alpha\cos(I_o)+\frac{\alpha^2}{2}\sin(I_o)\left[\frac{\cos^2(I_o)-n^2\cos^2(A)}{n^2\cos^2(A)}\right]\right] \tag{A4.18}$$

now:

$$\cos^2(I_o)-n^2\cos^2(A)=1-\sin^2(I_o)-n^2+n^2\sin^2(A)$$
$$=1-n^2 \tag{A4.19}$$

Therefore:

$$\alpha' \simeq \frac{1}{n\cos(A)}\left[\alpha\cos(I_o)-\frac{\alpha^2}{2}\frac{(n^2-1)\sin(I_o)}{n^2\cos^2(A)}\right] \tag{A4.20}$$

Putting the new values for I_2' and I_2 into (A4.3) gives:

$$\sin(I_o+\alpha'')=n\sin(A-\alpha') \tag{A4.21}$$

Expanding this as before gives:

$$\sin(I_o)\left[1-\frac{\alpha''^2}{2}\right]+\alpha''\cos(I_o)\simeq n\left[\sin(A)\left[1-\frac{\alpha'^2}{2}\right]-\alpha'\cos(A)\right] \tag{A4.22}$$

Rearranging (A4.22) and using (A4.6) gives:

$$\alpha''\cos(I_o)\simeq\frac{\alpha''^2}{2}\sin(I_o)-n\alpha'\cos(A)-\frac{n\alpha'^2}{2}\sin(A) \tag{A4.23}$$

Neglecting terms in α'^2 and α''^2 gives:

$$\alpha'' \simeq - \frac{n \alpha' \cos(A)}{\cos(I_o)} \qquad \text{(A4.24)}$$

Therefore:

$$\alpha'' \simeq \frac{1}{\cos(I_o)} \left[-n \alpha' \cos(A) - \frac{n\alpha'^2 \sin(A)}{2} + \left(\frac{n^2 \alpha'^2 \cos^2(A)}{\cos^2(I_o)} \right) \frac{\sin(I_o)}{2} \right] \qquad \text{(A4.25)}$$

Using (A4.16) and A4.20 to substitute for α' and α'^2 in (A4.25) gives:

$$\alpha'' \simeq -\alpha \frac{-\alpha^2 (n^2-1) \sin(I_o)}{2 n^2 \cos^2(A) \cos(I_o)} + \left(\frac{n^2 \sin(I_o) \cos^2(A)}{2 \cos^2(I_o)} - \frac{n \sin(A)}{2} \right) \frac{\cos(I_o) \alpha^2}{n^2 \cos^2(A)} \qquad \text{(A4.26)}$$

The total deviation, D, is given by:

$$D = -I_1 + I_1' + I_2 - I_2' \qquad \text{(A4.27)}$$

At minimum deviation:

$$D = 2(A - I_o) \qquad \text{(A4.28)}$$

At an angle of incidence α away from minimum deviation:

$$D = 2(A - I_o) - \alpha - \alpha'' \qquad (A4.29)$$

The magnitude of the change in deviation is then:

$$\Delta D = \alpha + \alpha'' \qquad (A4.30)$$

$$\Delta D = \alpha + \alpha'' \simeq \frac{\alpha^2 (n^2-1) \sin(I_o)}{2 n^2 \cos^2(A)\cos(I_o)} - \left(\frac{n^2 \sin(I_o)\cos^2(A)}{\cos^2(I_o)} - n \sin(A)\right) \frac{\cos(I_o)\alpha^2}{2 n^2 \cos^2(A)} \qquad (A4.31)$$

Rearranging this gives:

$$\Delta D \simeq \frac{\alpha^2 (n^2-1) \sin(I_o)}{2 n^2 \cos^2(A)\cos(I_o)} - \left(\frac{n^2 \sin(I_o)\cos^2(A) - \cos^2(I_o) n \sin(A)}{\cos^2(I_o)}\right) \frac{\cos(I_o)\alpha^2}{2 n^2 \cos^2(A)} \qquad (A4.32)$$

which using (A4.19) is:

$$\Delta D \simeq \frac{\alpha^2 \ (n^2-1) \ \sin(I_o)}{n^2 \ \cos^2(A)\cos(I_o)}$$

which is equation 26 in section 2.1.2.

REFERENCES

REFERENCES

M. Abramowitz and I. A. Stegun
Handbook of Mathematical Functions
Dover Publications, New York, 1965

L. M. Ball
Polarization: Blessing and Curse
Electro-Optical Systems Design, p.29, October 1982

M. Banning
Practical Methods of Making and Using Multilayer Filters
JOSA, 37, p. 792, 1947

N. F. Barber
A Diffraction Analysis of a photograph of the Sea
Nature, 164, p.485, 1949

M. E. Barnett and P. R. Harnett
Diffraction Pattern Sampling and its Application to
Directional Enhancement of Geological Image Transparencies
Trans.Inst.Min. and Metal., 84, p.B53, 1975

M. E. Barnett, P. R. Harnett, W. T. Welford and C. G. Wynne
An Interactive Hybrid Processing Facility for Geological
and Geographical Applications
SPIE/OSA, Vol. 74 - Image Processing, p.130, 1976

A. Bauer, A. Fontanel and G. Grau
The Application of Optical Fittering in Coherent Light to the Study of Aerial Photographs of Greenland Glaciers
J. of Glaciology, 6, p.781, 1967

R. Bellerby
Computer Generated Graphics of Representations of Wavefront Aberrations
M.Sc. Report, Imperial College, London, 1981

J. E. Berger and D. Harker
Optical Diffractometer for Production of Fourier Transforms of Electron Micrographs
Rev.Sci.Instrum., 38, p.292, 1967

D. Bertani, M. Cetica and R. Polloni
A Simple Variable-Ratio Beamsplitter for Holography
J.Phys.E:Sci.Instrum., 16, p.602, 1983

K. G. Birch
Spatial Filtering in Optical Data Processing
Rep.Prog.Phys., 35, p.1265, 1972

M. Born and E. Wolf
Principles of Optics, Pergamon Press, 1959

W. W. Buchman, S. J. Holmes and F. J. Woodberry
Single-Wavelength Thin-Film Polarizers
JOSA, 61, p.1604, 1971

K. H. Carnell, M. J. Kidger, A. J. Overill, R. W. Reader,
F. C. Reavell, W. T. Welford and C. G. Wynne
Some Experiments on Precision Lens Centring and Mounting
Optica Acta, 21, p.615, 1974

M. De
A Sensitive Wave-front Tilter
J.Sci.Instrum., 32, p.141, 1955

M. B. Dobrin
Optical Processing in the Earth Sciences
IEEE Spectrum, 5, p.59, 1968

H. B. Dwight
Tables of Integrals and other Mathematical Data
MacMillan Publishing Co., New York, 4th edition, 1961

J. Dyson
Possible Immunities in Interferometer End Mirrors
J.Sci.Instrum., 42, p.823, 1965

J. Dyson
Optics in a Hostile Environment
Appl.Opt., 7, p.569, 1968

J. Dyson
Interferometry as a Measuring Tool
Brighton: Machinery Publishing Co., pp.71-77, 1970

E. B. Felstead
Removal of the Zero Order in Optical Fourier Transformers
Appl.Opt., 10, p.1185, 1971

W. Fink
D. C. Bias Suppression in Diffraction Patterns
Opt.Commun., 5, p.301, 1972

A. K. Ghatak and K. Thyagarajan
Contemporary Optics, Plenum Press, p.241, 1978

J. M. Hammer
In Line Anamorphic Beam Expanders
Appl.Opt., 21, p.2861, 1982

G. Harburn and J. K. Ranniko
Details for an Optical Gate
J.Phys.E:Sci.Instrum., 4, p.394, 1971

P. R. Harnett and M. E. Barnett
Optical Rose Diagrams for Lineament Analysis
Trans.Inst.Min. and Metal., 86, p.B102, 1977

P. R. Harnett, G. D. Mountain and M. E. Barnett
Spatial Filtering Applied to Remote Sensing Imagery
Optica Acta., 25, p.801, 1978

P. R. Harnett
Ph.D. thesis, Imperial College, London, 1980 (in two volumes)

F. S. Harris Jr.
Light Diffraction Patterns
Appl.Opt., 3, p.909, 1964

E. J. Heidecker and T. Supajanya
Simple Optical Method for Routine Analyses of Fracture Traces
Trans.Inst.Min.and Metal., 84, p.B56, 1975

H. G. Jerrard
Optical Compensators for Measurement of Elliptical Polarization
JOSA, 38, p.35, 1948

H. G. Jerrard
Use of a Half-Shadow Plate with Uniform Field Compensators
J.Sci.Instrum., 28, p.10, 1951

H. G. Jerrard
The Examination and Calibration of Soleil Compensators
J.Sci.Instrum., 30, p.65, 1953

D. Joyeux and S. Lowenthal
Optical Fourier Transform: What is the Optimal Setup?
Appl.Opt., 21, p.4368, 1982

V. G. Kulkarni and D. Sen
Holographic Phase Aberration Balancing with an Inexpensive Liquid Gate
Journal of Optics (Calcutta), 12, p.1, 1983

A. P. Lang
Optical Deflector with High and Variable Sensitivity
J.Phys.E:Sci.Instrum., 16, p.1022, 1983

S. H. Lee
Review of Coherent Optical Processing
Appl.Phys., 10, p.203, 1976

R. A. Lessard, W. T. Welford and F. L. Zhang
Sea Wave Detection by Optical Fourier Transforms from Seasat SAR Images
Optica Acta., 28, p.283, 1981

J. P. Machewirth
Laser Polarizers: The Calcite Role
Optical Spectra, December 1979, p.59

G. F. Marshall
Applied Optics and Optical Engineering Vol VI
ed. R. Kingslake and B. J. Thompson
Academic Press, London, pp.248-250, 1980

M. J. McCullagh
Optical Data Processing - A New Geographical Tool
Unpublished report for Kansas Geological Survey
Department of Geography, University of Kansas, 1971

I. D. Nikolov
Fourier Transform Properties of an All-Mirror System
Optica Acta, 29, p.1175, 1982

B. J. Pernick, S. Levinson and C. Bartolotta
Enhancement of Low Spatial Frequency Signals with Optical Aperture Tapering
Appl.Opt., 9, p.1902, 1970

H. J. Pincus and M. B. Dobrin
Geological Applications of Optical Data Processing
J.Geophys.Res., 71, p.4861, 1966

W. A. Shurcliff
Polarized Light: Production and Use
Oxford University Press, 1962

K. Spanner and H. Marth
Precise Positioning with Piezoelectric Translators
Lasers and Applications, August 1983, p.61

H. Stark, W. R. Bennett and M. Arm
Design Considerations in Power Spectra Measurements by
Diffraction of Coherent Light
Appl.Opt., 8, p.2165, 1969

B. J. Thompson
The Information Content of Optical Diffraction Patterns
Optical Information Processing - ed. Y. E. Nesterikhin,
G. W. Stroke and W. E. Kock
US-USSR Science Cooperation Seminar on Optical
Information Processing. Washington, 1975
Plenum Press, New York, p.313, 1976

A. Vander Lugt

A Review of Optical Data-Processing Techniques

Optica Acta, 15, p.1, 1968

V. K. Vats and G. M. Miles

Introduction to Crystal Polarizers : Matching a Type to an Application

Laser Focus, October 1977, p.80

F. T. S. Yu

Optical Information Processing

Wiley, New York, 1983

PUBLICATIONS

J. Phys. E: Sci. Instrum., Vol. 16, 1983. Printed in Great Britain

Optical deflector with high and variable sensitivity

A P Lang
Optics Section, Blackett Laboratory, Imperial College, Prince Consort Road, London SW7 2BZ, UK

Received 14 April 1983

Abstract. With conventional prism beam steering devices, the beam deviation is usually related to the prism movements in a very nonlinear way. Also, the sensitivity is fixed by the wedge angles of the prisms. A new type of device is described with a more linear response than the old types. It has very high resolution which can be varied over several orders of magnitude using the same optical and mechanical components.

1. Introduction

Steering a light beam is most commonly achieved using a plane mirror in an adjustable holder. This method is limited in resolution, and high accuracy mounts tend to be large and expensive.

Prism devices offer higher resolution and more compact mounts, but the usual designs suffer from two main disadvantages. Firstly, the relationship between beam deviation and prism movements is usually very nonlinear (De 1955, Marshall 1980). Secondly, the sensitivity is fixed by the prism wedge angles, and manufacturing tolerances limit the resolution to about an arc second.

The device to be described has a much more linear response than other prism devices. Very high resolution can easily be obtained, and a simple adjustment can vary the sensitivity by several orders of magnitude.

2. Theory

Consider a single prism near minimum deviation. If the prism wedge angle is $2A$, its refractive index is n and the angle of incidence at minimum deviation is I_0, then

$$\sin I_0 = n \sin A. \tag{1}$$

If this prism is turned through a small angle, α, away from minimum deviation, then it can be shown that the deviation increases by

$$\frac{(n^2-1)\sin I_0 \alpha^2}{n^2 \cos^2 A \cos I_0}. \tag{2}$$

Now suppose two prisms, with the same refractive indices and wedge angles are placed almost antiparallel, as in figure 1, with a constant tilt between them of β. The second prism produces a deviation of

$$\frac{-(n^2-1)\sin I_0(\alpha-\beta)^2}{n^2 \cos^2 A \cos I_0}. \tag{3}$$

Hence the total deviation is

$$\frac{(n^2-1)\sin I_0 2\beta\alpha}{n^2 \cos^2 A \cos I_0} + \text{constant} \tag{4}$$

i.e. linear in α, with sensitivity proportional to β.

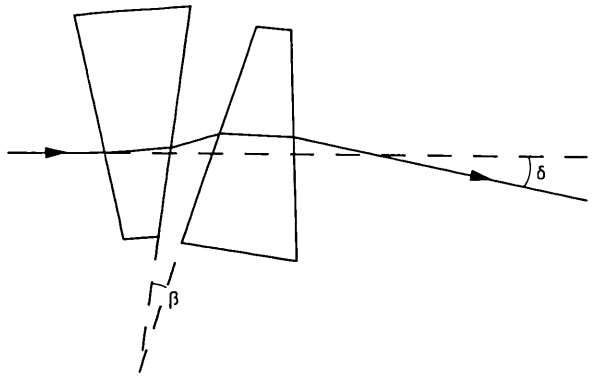

Figure 1. The optical deflector.

3.1. Theoretical results

Computer calculations using an accurate ray trace through the prisms were compared with the results predicted by equation (4), and were found to be in good agreement (within 5%) over a range of incidence angles of about ±20 degrees.

3.2. Experimental results

The device was built using 5° 48′ prisms of BK7 optical glass (refractive index at 633 nm = 1.515), matched to 10 seconds of arc.

It was tested using a laser autocollimator, with an accuracy of about 0.2 arc seconds. Fringe counting techniques were not used due to the limited aperture at large angles of incidence. The prisms were set to the correct orientation and tilt by observing reflections from the four faces, allowing, of course, for the slightly different refraction effects for the various beams.

Figure 2 shows deviation δ against angle of incidence for a tilt of 0.5 degrees. The curve is fairly linear over quite a wide range of incidence angles, and gives a reduction ratio of about 950 to 1. This reduction ratio can be increased to almost any desired value by reducing the wedge angle and the tilt. The main problem is that for tilts less than about 40 times the difference in the wedge angles, the curves become distorted. So for very high sensitivity, the prisms must be accurately matched.

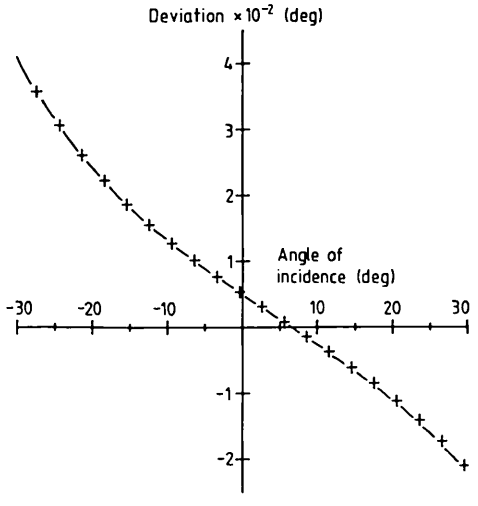

Figure 2. Experimental and theoretical results for 5° 48′ prisms. The crosses are experimental measurements and the full curve is the theoretical result.

4. Other properties of the device

There are two other properties of the device which may be important for some applications. Namely a sideways shift and a phase change of the beam as the prisms are rotated.

For normal-sized devices, the sideways shift will be of a few millimetres, and can be almost eliminated by using the device in a double-pass system. The phase change will be several thousand radians, but this will only be important for a few interferometric uses.

Acknowledgments

The author wishes to thank Professor W T Welford for helpful discussions and the Science and Engineering Research Council for financial support.

References

De M 1955 A sensitive wave-front tilter
J. Sci. Instrum. **32** 141

Marshall G F 1980 *Applied Optics and Optical Engineering* vol. VI ed. R Kingslake and B J Thompson (London: Academic) pp 248–50

6R-524547/TAYFRA/OPTICA/173001

OPTICA ACTA, 1985, VOL. 32, NO. 0, 000–000

Interferometer for DC level removal in optical Fourier transforms

A. P. LANG

Optics Section, The Blackett Laboratory, Imperial College, London SW7 2BZ, England

(*Received 14 September 1984*)

Abstract. Conventional optical Fourier transform systems have speed advantages over digital processors. Unfortunately, undiffracted light forms a very bright spot in the centre of the Fourier transform which corresponds to the average or (DC) transmission level of the object transparency. This tends to mask the low spatial frequency information in the transform, and can damage video cameras and other detectors used to view the transform plane. A high resolution polarization interferometer has been developed to subtract this DC level resulting in improved detectability of low spatial frequency signals. Experimental results are presented.

1. Introduction

In the field of image processing, digital techniques offer the most versatility, but for some applications such as azimuthal or textural classification of images, coherent optical techniques offer higher speeds due to their inherently parallel processing of two dimensional information. One of the problems with conventional optical Fourier transform benches is that there is an intense zero order spot in the middle of the transform plane due to undiffracted light. This tends to mask the low spatial frequency parts of the signal and provides a possible source of damage for any video cameras or photomultipliers used to observe the transform plane.

2. Theory

If an object transparency of complex amplitude transmission $q(x, y)$ is placed in the front focal plane of a lens of focal length f, and illuminated by collimated, coherent light of wavelength λ, then the complex amplitude in the back focal plane of the lens $Q(u, v)$ is given by

$$Q(u, v) = \iint_{-\infty}^{+\infty} q(x, y) \exp\left(-2\pi i(ux + vy)\right) \mathrm{d}x\, \mathrm{d}y, \tag{1}$$

where the actual spatial coordinates in this plane (x', y') are related to the spatial frequency coordinates (u, v) by

$$x' = \lambda f u, \qquad y' = \lambda f v. \tag{2}$$

Equation (1) is a Fourier transform relationship linking $q(x, y)$ and $Q(u, v)$ (see, for example, [1]).

For photographic film, with a circular aperture, $q(x, y)$ is given by

$$q(x, y) = A + Bq'(x, y) \cdot \text{Pill}\,(x, y) \exp i\phi(x, y) \tag{3}$$

where q'(x,y) is the desired signal, A represents the average or DC transmission level of the transparency, B is a scaling constant such that $0 \leqslant q(x, y) \leqslant 1$ and Pill (x, y) is the pill box or top hat function, which defines the aperture and is given by

$$\begin{aligned} \text{Pill}\,(x, y) &= 1, \quad x^2 + y^2 < r^2, \\ &= 0 \quad \text{elsewhere}, \end{aligned} \tag{4}$$

where r is the radius of the aperture. $\exp i\phi(x, y)$ is a phase term due to irregularities in the film thickness, and can be made approximately equal to one by immersing the film in a liquid gate.

Taking the Fourier transform of (3) with $\exp i\phi(x, y) = 1$ gives

$$Q(u, v) = A \cdot \text{Jinc}\,(u, v) + BF\{q'(x, y)\} \otimes \text{Jinc}\,(u, v), \tag{5}$$

where Jinc (u, v) is given by

$$\text{Jinc}\,(u, v) = (2J_1\sqrt{u^2 + v^2})/\sqrt{u^2 + v^2}. \tag{6}$$

F represents the Fourier transform operation, $\otimes$ represents the convolution operation and J_1 is a first order Bessel function of the first kind.

The second term of (5) is the desired signal, but the first term takes the form of a very bright disc surrounded by concentric rings in the centre of the transform plane.

3. Experimental details

3.1. *An example of the problem*

A typical photo of interest is shown in Figure 1, which is an electron microscope view of a sedimentary rock sample. A visual inspection of the negative suggests that there is a directionality present, with dominant spatial frequencies of around four lines per millimetre or less, roughly in the direction A–B. The transform was scanned with a rotating sector disc in front of a photomultiplier to give figure 2. This has been 180° averaged to remove a slight irregularity in the sensitivities of different parts of the photocathode. These results confirm the presence of a directionality which matches that found by a visual inspection of the negative, but its relative strength is not great because of the strong DC signal which takes the form of a circular component of constant radius on the polar diagram.

3.2. *DC level removal*

To get a true idea of the relative strengths of directionalities in photos such as figure 1, the DC level has to be removed or modified. Several workers have attempted this. Stark *et al.* [2] placed a π phase step over half the aperture which gave a modified transform distribution with zero DC level along a direction parallel to the phase step, but at the expense of a slight reduction in resolution along this direction.

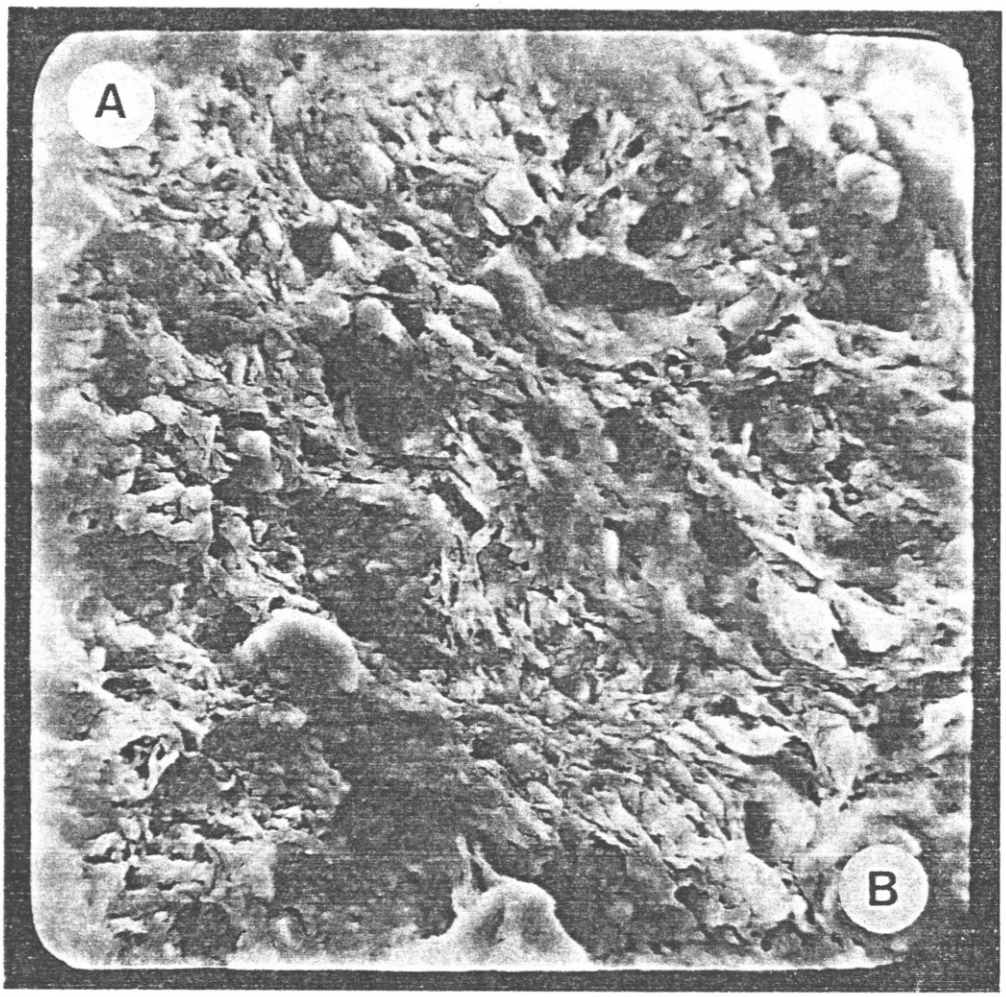

Figure 1. A typical photograph of interest showing a scanning electron microscope view of a sedimentary rock sample.

For two-dimensional inputs, a more complex system must be used. Stark *et al.* [2] suggest the use of apertures with contoured transmission. This was followed by Pernick *et al.* [3] who concluded that such tapers improve the detectability of low spatial frequencies. Unfortunately, this method does not remove the DC, it simply modifies its form to remove the rings at the expense of a wider central peak.

Some of the new incoherent to coherent light valves have MTF curves which are zero for zero spatial frequency, resulting in a transform with zero DC intensity. Unfortunately, these curves do not rise rapidly enough to transmit the low frequency signals of interest. The only viable method of DC removal is by the coherent superposition of the diffraction patterns of the input transparency and a compensating aperture with a transmission equal to the DC transmission of the input transparency. A π phase difference between the two patterns results in cancellation of the DC level. Felstead [4] suggested that this could be achieved using a Mach–Zehnder interferometer, but points out that this would be almost impos-

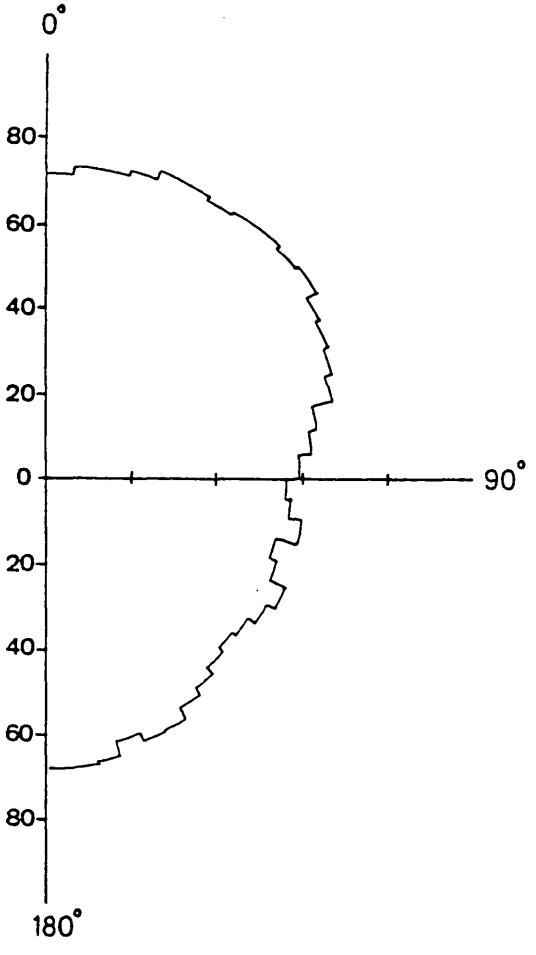

Figure 2. The result of scanning the Fourier transform of figure 1 with a rotating sector disc in front of a photo multiplier. All frequencies below 0·2 lines/mm excluded by a DC stop.

sible to adjust and maintain in the zero fringe position. Fink [5] used a Smith polarization interferometer to successfully remove the DC level but this had a limited aperture and could not readily be adapted for use on the Imperial College Fourier transform bench.

3.3. *Resolution requirements*

Before deciding on the final form of the interferometer it is necessary to calculate the phase, alignment and amplitude resolutions required for the two beams to achieve a given intensity reduction. Computer calculations were performed to find the resolutions required for a DC intensity reduction by a factor of 40 times. Assuming that beam aberrations are negligible, this requires alignment of the two Airy patterns to about 0·1 Rayleigh distances, where the Rayleigh distance is the separation of the peak and the first dark ring for one pattern. For the system in use, with a 700 mm focal length and 25 mm aperture, this is equivalent to a tilt

between the wavefronts of 0·5 arc second, a phase difference within $\pm 5°$ and beam amplitudes matched to within about 2 per cent.

Any aberrations will decrease the cancellation efficiency by modifying the form of the DC pattern. For the Strehl tolerance of the peak of the diffraction pattern to drop by 20 per cent, the wavefront aberration must be $\pm\lambda/14$. For this application, the important thing is the difference in the two diffraction patterns, so $\lambda/14$ can be taken as a rough estimate of the difference tolerance between the two wavefronts. The 20 per cent intensity difference can be partially compensated for by changing the relative amplitude of the beams slightly, at the cost of less efficient cancellation in the rings.

3.4. *Methods of achieving the required resolution*

3.4.1. *Alignment*

In steering a light beam prism devices offer very high resolution and compact mounts, but the usual designs suffer from resolutions limited by manufacturing tolerances to around one arc second and the relationships between beam deviation and prism movements are usually very nonlinear [6, 7]. To achieve the required resolution a new type of prism beam deflector is needed, which was described in an earlier paper [8], and is shown in figure 3. It uses a pair of matched wedge prisms, of wedge angle 2θ and refractive index n, placed almost antiparallel with a small constant tilt between them of β. The beam deviation δ is then approximately given by

$$\delta = -\frac{2(n^2 - 1)\sin I_0 \beta\alpha}{n^2 \cos^2\theta \cos I_0} + \text{constant} \tag{7}$$

where α is the angle between the incident beam and the angle of incidence at minimum deviation for the first prism. A plot of beam deviation δ versus angle of incidence is shown in figure 4.

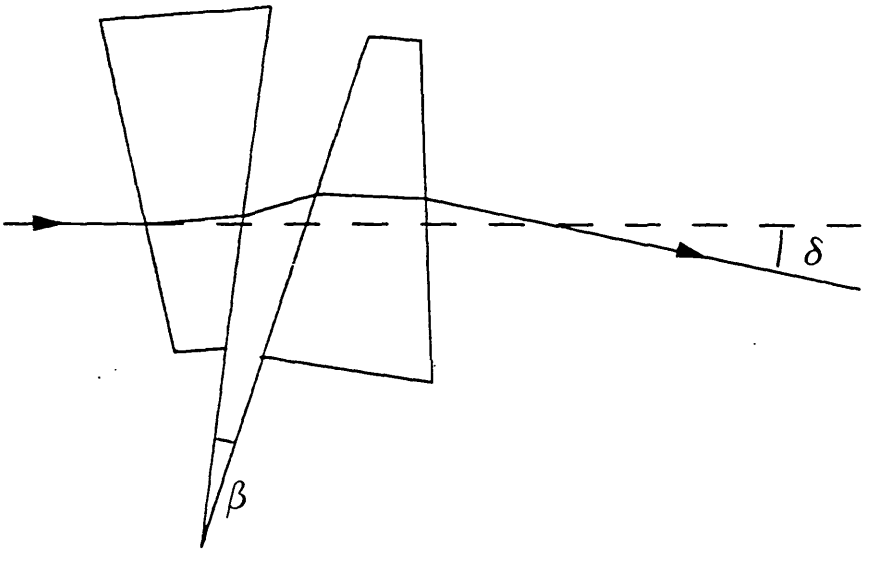

Figure 3. The prism beam steering device; β is the angle or tilt between the almost antiparallel matched wedge prisms, δ is the beam deviation.

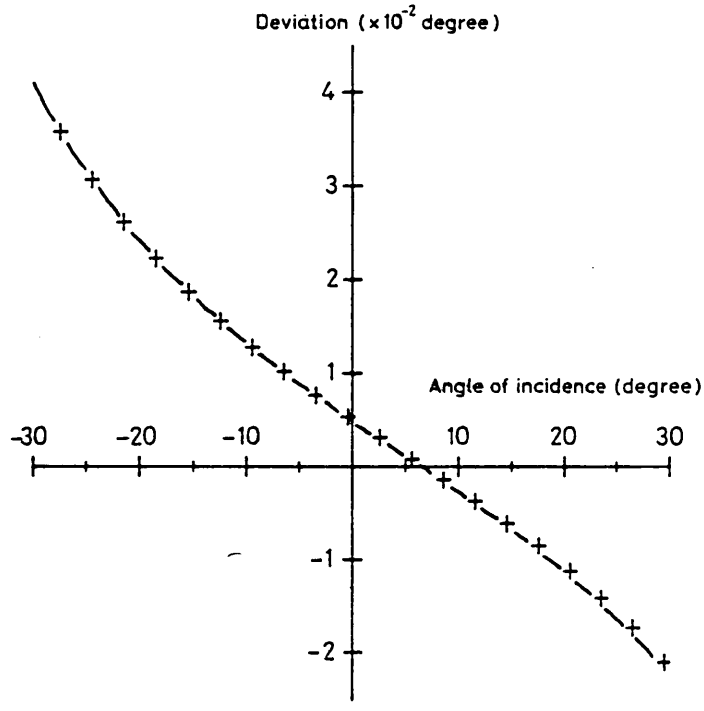

Figure 4. Experimental and theoretical results for prism beam deviation versus angle of incidence for 5°48′ prisms. The crosses are experimental measurements and the full curve is the theoretical result.

3.4.2. *Phase*

Most methods of phase control in interferometry have limited resolution and require components of full interferometric quality which are expensive. However, when polarization interferometers are used, other, more convenient, methods are available. These are based on the fact that the two beams are labelled by their polarization states, and so may be identified and hence manipulated independently of each other outside the interferometer. This is most readily achieved using a variable retarder, such as a uniform field compensator or electro-optic cell, prior to the beams being separated by a polaring beam splitter (see, for example, [9]). Thus the device need not be of full interferometric quality as both beams are affected equally, and stability problems are reduced.

3.4.3. *Amplitude*

As a polarization interferometer is used, the addition of a half wave plate before the polarising beamsplitter will result in a variable ratio beam splitter.

3.5. *The interferometer*

The device had to be built to fit onto the Imperial College spatial filtering bench described by Harnett [10] which imposed a number of restrictions on the design. The final layout is shown in figure 5. Light from an argon ion laser (A)

passed through a halfwave plate (H) and reversed Babinet compensator (R) to provide phase and amplitude control. The two polarizations were then separated by a calcite wedge beamsplitter, and one beam passes through the beam steering prism (S). The prisms are double passed to eliminate the shear. The other beam passes through a second half wave plate to rotate its plane of polarization by 90°. Both beams are then expanded by microscope objectives (E) onto a paraboloidal mirror (P). One beam passes through the input transparency (T) in a liquid gate, whilst the other is deflected by mirror M6 and through the compensating aperture (U). They are then recombined by beamsplitter B2. The lens L1 forms the Fourier transform in plane F which is reimaged and magnified onto the film plane at 0 by lens L2. The transform is also viewed by a video camera (V) via the beamsplitter B3.

3.6. *Monitoring the alignment and phase difference*

Once these resolutions are achievable, methods have to be found to monitor them. Monitoring tilts between plane wavefronts of around half an arc second with a 25 mm aperture poses a number of problems as the fringe spacing is around 200 mm, although observation of the fringes may be used for approximate alignment and electronic detectors could possibly be used for fine tuning.

A simpler technique is to look at the transform plane distribution, which will consist of two overlapping Airy patterns. For separations of about one Rayleigh

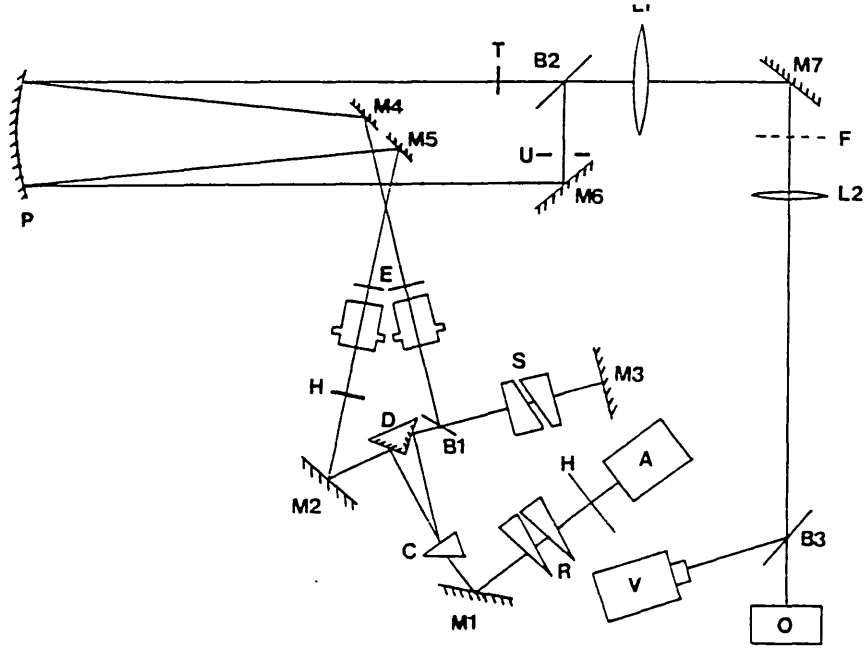

Figure 5. The layout of the interferometer (not to scale), showing A, argon ion laser; H, half wave plate; R, variable retarder; M1, M2, M3, M4, M5, M6, M7, mirrors; C, calcite wedge; B1, B2, B3, beam splitters; D, aluminised prism; S, beam steering prisms; E, microscope objectives + pinholes; P, paraboloidal mirror; L1, Fourier transforming lens; L2, reimaging + magnifying lens; F, Fourier plane; V, video camera; O, 35 mm camera body; T, object transparency; U, compensating aperture.

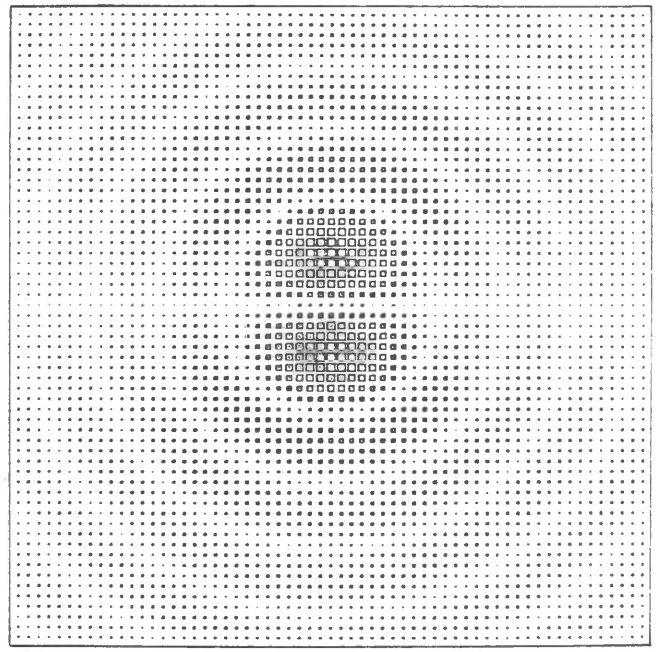

Figure 6. Computed intensity distribution for two Airy patterns with a separation of 0·5 Rayleigh distances and a phase difference of 180°.

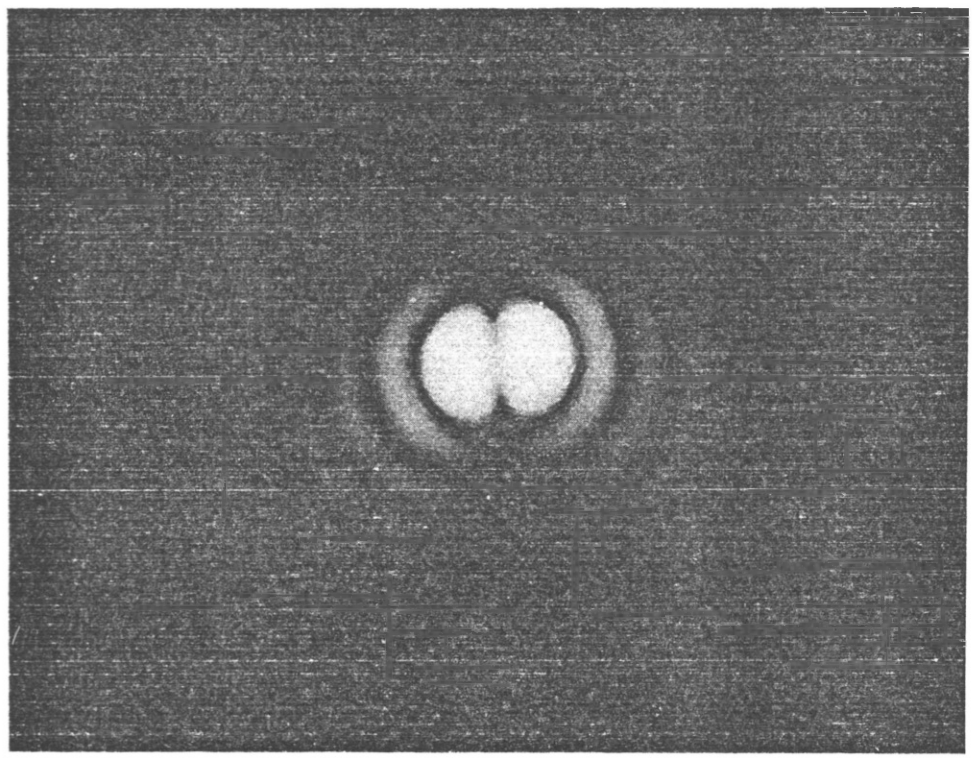

Figure 7. Experimental verification of figure 6.

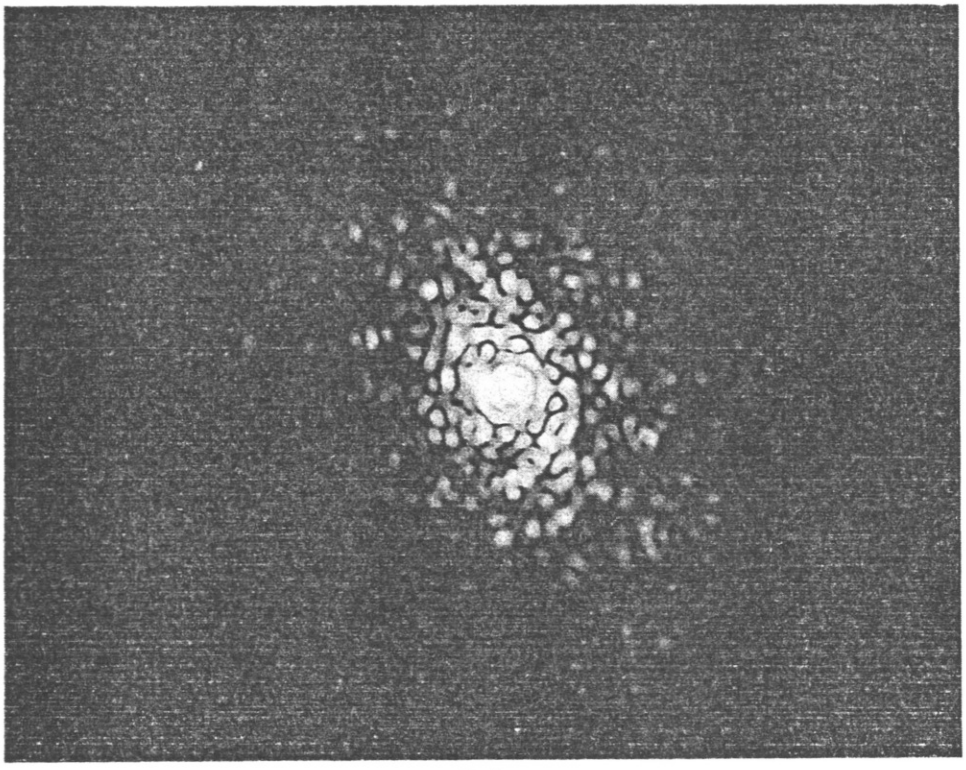

(a)

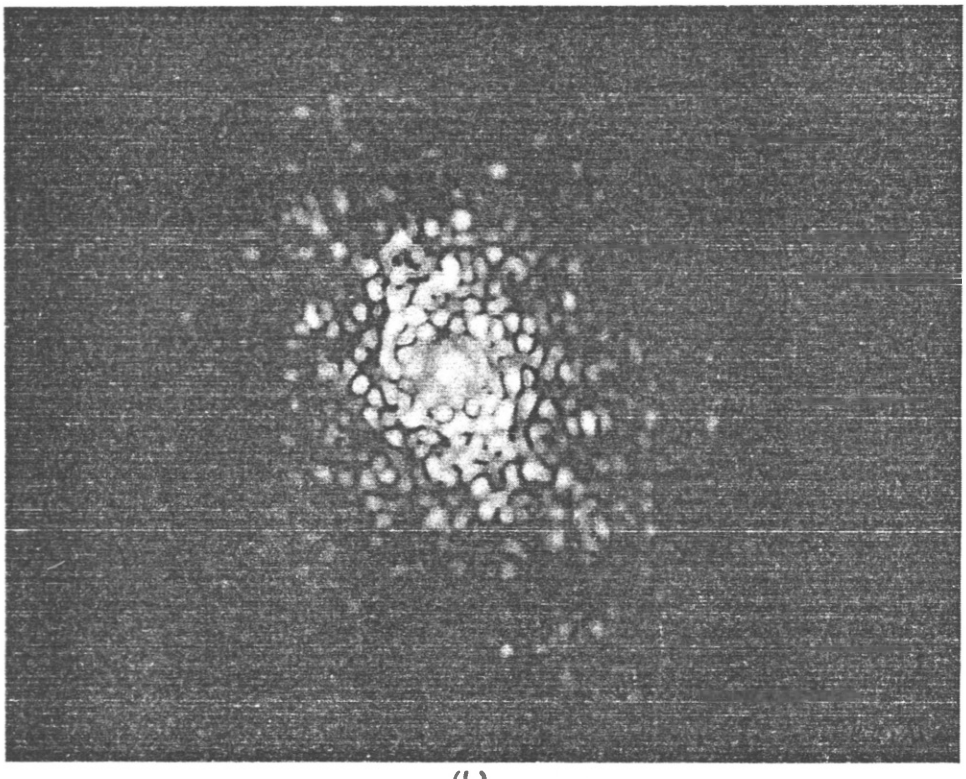

(b)

Figure 8. The optical Fourier transforms of figure 1, with the central Airy disc approximately 35 μm across. In (*b*), the DC level is removed.

distance or less, there are wedge shaped regions of low intensity at right angles to the axis of separation of the two pattern centres. These wedges tend to widen as the separation decreases, and the distance of the wedge axis from the middle of the pattern roughly indicates the phase difference.

Figure 6 shows a computer calculated plot of this pattern, which is verified by the experimental result shown in figure 7. When aligning the interferometer, a highly magnified image of the Fourier plane was viewed through a video camera connected to a density slicer, which was sufficient to monitor to the required resolution.

4. Experimental results

Photographs of the optical Fourier transforms of figure 1 with and without the DC level are shown in figures 8(*a*) and (*b*) respectively. The object transparency was enclosed in a liquid gate, but the laser speckle is still fairly prominent, due to the relatively large magnification of the transform. As a guide to the scale, the Airy disc was approximately 33 μm in diameter in the original transform plane.

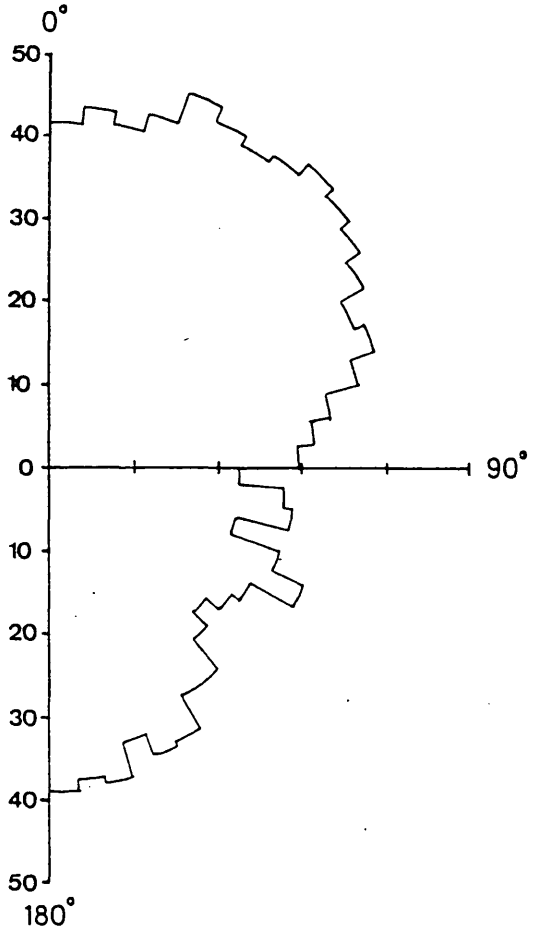

Figure 9. The result of scanning the DC lens transform of figure 1 with a rotating sector disc in front of a photomultiplier, with no DC stop.

The peak intensity reduction is about 30 times, but a photograph cannot show this clearly. The reduction is better shown by the sector scan of the DC-less transform (figure 9) which shows the directionalities more strongly than figure 2, which includes the DC. Figure 9 shows slightly more small fluctuations in the signal—presumably due to small amounts of uncancelled light and slight instabilities of the interferometer. The ratio of the major and minor axes of the scan are similar to those of the transform in the photograph, confirming the view that subtracting the DC pattern results in a more accurate measurement of the directionalities. Various other image processing operations such as image subtraction, contrast reversal and differentiation are possible using this interferometer, and these will be described in a future publication.

5. Conclusions

The measurement of directionalities in photographic transparencies with an optical Fourier transform system is impaired by undiffracted light when the average spatial frequency of the input is low. An interferometer has been constructed to successfully reduce the intensity of this undiffracted light by a factor of approximately 30, giving a more accurate measurement of the directionalities.

Acknowledgments

The author would like to thank Dr. R. W. Smith and Emeritus Professor W. T. Welford for helpful discussions, the Science and Engineering Research Council for financial support and Miss B. King for typing the manuscript.

References

[1] WELFORD, W. T., 1981, *Optics*, second edition (Oxford University Press), pp. 115–116.
[2] STARK, H., BENNETT, W. R., and ARM, M., 1969, *Appl. Optics*, **8**, 2165–2172.
[3] PERNICK, B. J., LEVINSON, S., and BARTOLOTTA, C., 1970, *Appl. Optics*, **9**, 1902–1905.
[4] FELSTEAD, E. B., 1971, *Appl. Optics*, **10**, 1185–1187.
[5] FINK, W., 1972, *Optics Commun.*, **5**, 301–303.
[6] DE, M., 1955, *J. scient. Instrum*, **32**, 141–142.
[7] MARSHALL, G. F., 1980, *Applied Optics and Optical Engineering*, Vol. 6, edited by R. Kingslake and B. J. Thompson (London: Academic Press), pp. 248–250.
[8] LANG, A. P., 1983, *J. Phys. E*, **16**, 1022–1023.
[9] DYSON, J., 1970, *Interferometry as a Measuring Tool* (Brighton: Machinery Publishing Co.), pp. 71–77.
[10] HARNETT, P. R., 1980, PhD Thesis, Vols. 1, 2, Imperial College, London.